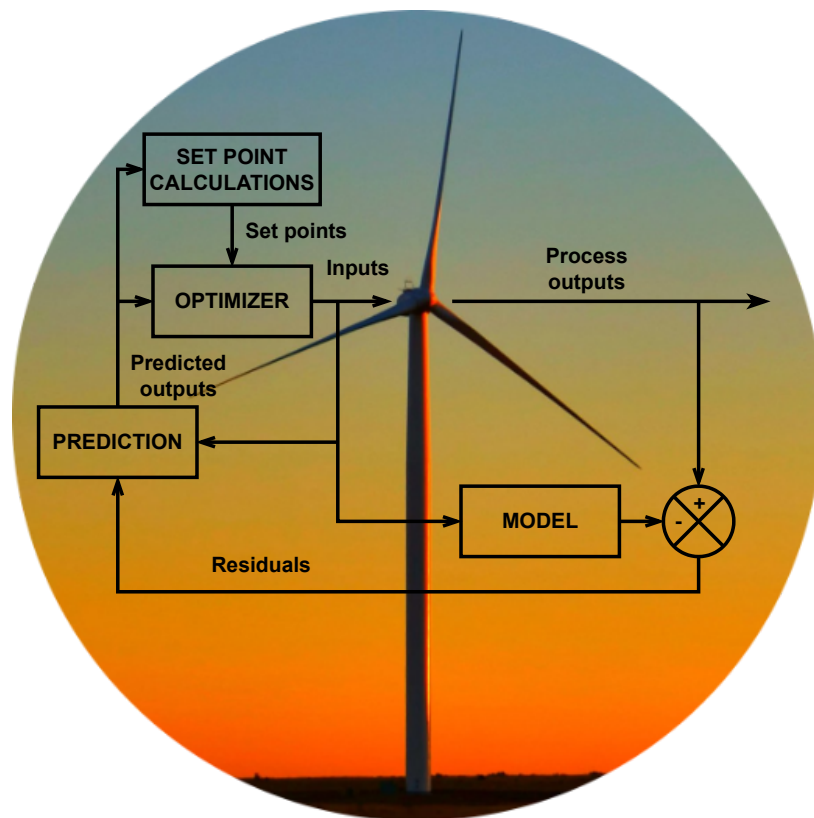

Model Predictive Control of a Wind Turbine

Project Report
CA10-934



Aalborg University
Department of Electronic systems
Fredrik Bajers Vej 7C
DK-9220 Aalborg

Copyright © Aalborg University 2021

The content of this report is freely available, but publication may only be pursued due to agreement with the authors.



AALBORG UNIVERSITY
STUDENT REPORT

MSc in Control and Automation
Department of Electronic systems
Fredrik Bajers Vej 7C
DK-9220 Aalborg
<http://es.aau.dk/>

Title:

Model Predictive Control of a Wind Turbine

Theme:

Control & Automation Master Thesis

Project Period:

Fall semester 2021
Spring semester 2022

Project Group:

CA10-934

Participant(s):

Álvaro Martín Gómez
Oier Ajenjo de Torres
Thomas Haugaard

Supervisor:

Torben Knudsen

Industrial Supervisor:

Michael Melholt Quottrup

Copies:

1

Page Numbers: 142

Date of Completion:

June 1, 2022

Abstract:

In recent times, the wind turbine industry is pushing towards larger and more efficient wind turbines to decrease the cost of energy production. This requires the use of more refined control strategies able to deal with structural load reduction, while optimising power production. In order to consider multiple objectives as well as system constraints, Model Predictive Control (MPC) was selected as control strategy. A non-linear model of the wind turbine was derived, including the dynamics of each blade such that their pitch could be controlled independently. State estimation was performed by means of an Unscented Kalman Filter (UKF) using data from GH Bladed simulation tool as system measurements. It was not possible to obtain acceptable results due to the large mismatch between the model outputs and the data from Bladed, so the first ones were used as virtual measurements by adding typical sensor noise. Afterwards, the MPC was given a prediction model derived by successive linearisation, and designed to account for both partial and full load operation of the wind turbine. The results at the present time are not satisfactory due to not having considered that the states of the linearised model are relative to the operating points in every iteration. It is believed that the results will be promising as soon as this issue is solved.

CONTENTS

ABSTRACT	III
List of Figures	VII
List of Tables	X
PREFACE	1
1 INTRODUCTION	2
1.1 Project Setting	2
1.1.1 Types of wind turbines	3
1.1.2 HAWT components overview	4
1.1.3 Modes of operation	6
1.1.4 Wind turbine control overview	7
1.1.5 Modal analysis	9
1.2 Description of Use Case	11
1.2.1 Mita-Teknik	11
1.2.2 Problem scope	11
1.2.3 Final case description	12
1.3 Problem Formulation	12
1.4 Delimitations	12
1.5 Functional Requirements	13
1.6 Solution Overview	14
2 WIND TURBINE MODELLING	15
2.1 Introduction	15
2.1.1 Degrees of freedom and coordinate systems	16
2.1.2 List of constants and variables	19
2.2 Wind Model	21
2.2.1 Deterministic wind model	21
2.2.2 Stochastic wind model & effective wind speed	26
2.3 Aerodynamic Model	29
2.4 Simple Tower and Blade Models	31
2.4.1 Tower model	32
2.4.2 Tower and blade model	33
2.5 Drive Train Model	35
2.6 Actuator Models	36

2.6.1	Pitch actuator model	37
2.6.2	Generator model	37
2.7	State Estimation With UKF	37
2.7.1	Choosing weights and sigma points	38
2.7.2	Choosing free parameters	39
2.7.3	Procedure	40
2.8	Linearized Model	42
2.9	Linear Model in State Space Representation	48
2.10	Observability	52
3	WIND TURBINE CONTROL	54
3.1	Introduction	54
3.2	Requirement Specification	54
3.2.1	General control objectives	54
3.2.2	Kalman Filter	55
3.2.3	MPC	55
3.3	Control Loops	55
3.4	Below-Rated Wind Speed Proportional Torque Control	56
3.5	MPC Formulation	58
3.6	Solving the Unconstrained Case	63
3.7	Solving the Constrained Case	65
3.8	Mita-Teknik Controller	67
3.8.1	6 m/s mean wind speed test	71
3.8.2	16 m/s mean wind speed test	72
4	IMPLEMENTATION	74
4.1	Introduction	74
4.2	Kalman Filter Implementation	74
4.3	MPC Implementation	77
4.3.1	Horizons	78
4.3.2	Constraints	79
4.3.3	Setpoints	82
4.3.4	Weights	82
4.4	Control Algorithm	84
5	RESULTS AND DISCUSSION	87
5.1	Introduction	87
5.2	Non-linear Simulation	87
5.3	Unscented Kalman Filter	90
5.4	Linear Simulation	91
5.5	MPC	94
5.6	Requirement Fulfilment	97

5.6.1	General control objectives	97
5.6.2	Kalman Filter	98
5.6.3	MPC	98
6	CONCLUSION	99
6.1	Future Work	100
	BIBLIOGRAPHY	100
A	BEM METHOD	105
A.1	Two Dimensional Model of a Blade	105
A.2	One Dimensional Momentum Theory	107
A.3	Blade Element Method	112
A.3.1	Prandtl's tip loss factor	115
A.3.2	Glaurt correction	116
A.4	Coleman Transform-based Control	117
A.5	Softening the Constraints in MPC	118
B	TESTS	120
B.1	Bladed Reference Test	120
B.1.1	6 m/s mean wind speed test	121
B.1.2	16 m/s mean wind speed test	124
B.2	Test of Turbine Model	126
B.3	Test of UKF	129
B.4	Test of Linear Model	132
B.5	Test of MPC	138
C	GITHUB REPOSITORY	142

List of Figures

1.1	Wind turbine types [11].	3
1.2	Main HAWT components [13].	4
1.3	Different wind turbine topologies depending on generator type [15].	5
1.4	Rotational speed and generated power of the wind turbine as functions of wind speed in different operating regions [19].	7
1.5	Wind turbine structural modes [25].	10
1.6	Some of Mita-Teknik competences on the wind industry [26].	11
1.7	Block diagram of the solution	14
2.1	Global system block diagram [19].	15
2.2	Coordinate system for hub loads (a) and for tower loads (b) [29].	16
2.3	DOFs considered for the mathematical modelling [15].	17
2.4	Principal axes (a) and root axes (b) [29].	18
2.5	Wind flow around circular cylinder (black curves), including velocity potentials (white curves) and pressure field (colours), where red indicates high pressure and blue low pressure [31].	22
2.6	Outer diameter of the tower with respect to the height [32].	23
2.7	Tower shadow for different rotor radii R . Mean wind speed $v_m = 10$ m/s. Hub overhang $x_h = 10.93$ m. Tower radius measured at height $h = 31.75$ m corresponding to the tower height minus the blade length.	24
2.8	Wind shear for different rotor radii R . Mean wind speed $v_m = 10$ m/s. Wind shear exponent $\alpha = 0.1$, corresponding to open water.	25
2.9	Wind shear and tower shadow combined effect for different rotor radii R . Mean wind speed $v_m = 10$ m/s. Wind shear exponent $\alpha = 0.1$ (open water). Hub overhang $x_h = 10.93$ m. Tower radius measured at height $h = 31.75$ m corresponding to the tower height minus the blade length.	26
2.10	Stochastic wind speed simulation with $V_{11} = 4/600 \text{ m}^2/\text{s}^3$, $t_i = 0.1$, $\mu_v = 10$ m/s	28
2.11	Tower and blade two mass spring damper models [37].	32
2.12	Drive train model	35
2.13	General block diagram of the Kalman principle	38
2.14	Effects on alpha on the spread of the sigma points [38]	40
3.1	Schematic of the main control loops, with GTC referring to generator torque control, and CPC and IPC to collective and individual pitch control respectively [15, 27].	56

3.2	Power coefficient dependency on tip speed ratio λ and blade pitch angle θ . . .	57
3.3	MPC controller with no constraints and full state measurement [42].	64
3.4	MPC controller with no constraints and state observer [42].	65
3.5	Optimal pitch	67
3.6	Blade performance	68
3.7	C_p curve	68
3.8	Static performance	69
3.9	Loss tables	70
3.10	Bladed simulation results for 6 m/s wind speed.	72
3.11	Bladed simulation results for 16 m/s wind speed.	73
5.1	Simulation of edgewise blade deflection using Euler (a) or 4th order Runge-Kutta (b) discretization method for 20 s. Bladed data has been also added for comparison purposes.	88
5.2	Relative wind speed measured in the nacelle.	88
5.3	Wind speed experienced by each blade in their movement through the rotor plane (a), with zoom into the first 30 s (b).	89
5.4	Generator torque (a) and rotor speed (b).	89
5.5	UKF estimation of mean wind speed measured in the nacelle.	90
5.6	UKF estimation for tower and blade deflection.	91
5.7	Linear model simulation for tower and blade deflection.	92
5.8	Linear model simulation for tower and blade deflection without considering wind shear and tower shadow.	93
5.9	Linear model simulation for tower and blade deflection reducing the sampling time from 0.05 s to 0.01 s.	94
5.10	Mean wind speed (a), rotor speed (b), generator torque (c) and pitch angle of blade 1 (d) responses of the linear and non-linear models applying the control signals computed by the MPC.	96
5.11	Plots for the TSR used by the MPC in comparison to its expected value. . . .	96
5.12	Structural dynamics of the linear and non-linear models applying the control signals computed by the MPC.	97
A.1	Aerofoil of a wind turbine blade [9].	106
A.2	Forces acting on a wind turbine [9].	106
A.3	Relative velocity seen by a section of a blade [9].	108
A.4	Pressure and velocity before and after the rotor plane [9].	109
A.5	Lateral boundary of the control volume [9].	110
A.6	Alternate control volume for a wind turbine [9].	111
A.7	C_p and C_T as functions of the axial induction factor.	112
A.8	Coleman transform-based controller [17].	118
B.1	Bladed simulation plots for a wind speed of 6 m/s	123

B.2	Bladed simulation plots for a wind speed of 16 m/s.	126
B.3	Non-linear model simulation plots.	129
B.4	UKF state estimation plots.	132
B.5	Linear model simulation plots.	135
B.6	Linear model simulation plots not considering wind shear and tower shadow.	138
B.7	Linear and non-linear model simulation using MPC.	141

List of Tables

1.1	Modal analysis of the 15 MW wind turbine Bladed model structure.	9
2.1	Variables	19
2.2	Constants	20
2.3	Different values of α with terrain [33]	24
4.1	Standard deviation for sensor measurement noise	76

List of Acronyms

BEM	Blade Element Momentum Method
CPC	Collective Pitch Control
DOF	Degree of Freedom
DPC	Direct Power Control
EKF	Extended Kalman Filter
FAST	Fatigue, Aerodynamics, Structures and Turbulence
FSWT	Fixed Speed Wind Turbine
FOC	Field Oriented Control
GTC	Generator Torque Control
HAWT	Horizontal Axis Wind Turbine
IPC	Individual Pitch Control
MPC	Model Predictive Control
PID	Proportional Integral Derivative
PMSG	Permanent Magnet Synchronous Generator
SCADA	Supervisory Control And Data Acquisition
SCIG	Squirrel Cage Induction Generators
TSR	Tip Speed Ratio
UKF	Unscented Kalman Filter
UT	Unscented Transform
VAWT	Vertical Axis Wind Turbine
VSWT	Variable Speed Wind Turbine
WRIG	Wound Rotor Induction Generator
WRSG	Wound Rotor Synchronous Generator

PREFACE

This project was made as a long masters' thesis by the last year student group 934 from the Engineering Masters' Degree of Automation and Control at Aalborg University during the fall of 2021 and spring of 2022 from the 2nd of September to the 2nd of June. The supervisors for this project were Torben Knudsen from Department of Electronic Systems and as an external supervisor, Michael Melholt Quottrup. The literature is referenced in the bibliography, and the reference to the literature is a number inside square brackets. Figures and tables are numbered after the section they are in. We would like to thank Mita-Teknik for providing all the necessary resources to proceed with this project.

Aalborg University, June 1, 2022

Signatures

Álvaro Martín Gómez



Signature

Oier Ajenjo de Torres



Signature

Thomas Haugaard



Signature

Chapter 1

INTRODUCTION

Wind power has been used since the Egyptian civilisation started implementing sails on boats to propel them along the Nile river, at around 5000 BC. In the last five millennia, wind-powered machines have grown substantially, starting from the Babylonians and their desire to use the wind for irrigation purposes [1]. Other great examples can include 9th century Iranian, Afghan and Pakistani windmills and wind pumps [2], or traditional Spanish windmills, famously used in literature as the hallucinatory giants fought by Don Quixote.

The first electricity generating wind turbine was discovered by James Blyth, and it was used to power his home town's (Marykirk, Scotland) lights on holidays [3]. The key difference between the two main wind power generators is that wind turbines generate electricity, while windmills are used to generate mechanical energy.

In Denmark, the first small electricity-producing turbines arrived at the hands of physicist Poul La Cour, with a desire to mechanise many manual labours involved in farming. In 1891 he was granted financial support to build a wind turbine to pass electricity through water using electrolysis. That way, he erected the first experimental windmill in Askov [4]. In 1903 La Cour's Danish Wind Power Society started promoting the idea of wind-generated electricity. And, by 1920, even if most Danish windmills were used for mechanical work, the wind turbines provided an equivalent estimation between 120 MW and 150 MW [5].

After World War II, the interest in wind power waned except for some scientists such as Johannes Juul, who worked on a three-bladed, stall-regulated, upwind rotor at Gedser with a span of 24 m. In 1981, a national goal of 1000 MW wind-power was set to increase the contribution of wind to the national electricity up to 10%. In 2001, it provided 16% of the national electricity [5]. By 2020, Denmark's wind share of electric consumption corresponded to 50.4%, or the equivalent of 1.46 TWh [6].

Looking into the future, Denmark as a world leader in wind power will try to reduce CO₂ emissions by 70% by 2030 [7]. One of the solutions in hand, is the construction of two Energy Islands in the North and Baltic seas, equipped with offshore wind turbines [8].

1.1 Project Setting

This section provides an overview of wind turbine technology used nowadays, as well as basic operation and control strategies, in order to provide the necessary background to

properly define the scope of the project.

1.1.1 Types of wind turbines

Modern wind turbines mainly present two different design models depending on the disposition of the blades. If the blades are connected to a vertical shaft, the turbine is called Vertical Axis Wind Turbine (VAWT), while Horizontal Axis Wind Turbine (HAWT) represent the ones that use a horizontal axis [9].

Horizontal axis wind turbines produce the majority of the wind energy nowadays. Some of their advantages are presented below:

- Ability to pitch rotor blades to maximise power generation and minimise structural loads.
- Tall towers allow access to stronger winds.
- Can be placed on uneven terrains or offshore.

Nevertheless, they also present some disadvantages generally related to complicated transportation, operation and maintenance. On the other hand, vertical axis wind turbines present the following advantages [10]:

- Easy maintenance.
- Low transportation and construction cost.
- They are not directional.

Despite the facts presented above, they are overall less efficient, as only the blades facing the wind are driven by it, while the others just follow along. Furthermore, vertical axis rotors present more aerodynamic resistance, and meet a lower and more unstable wind speed as they are installed on ground level.

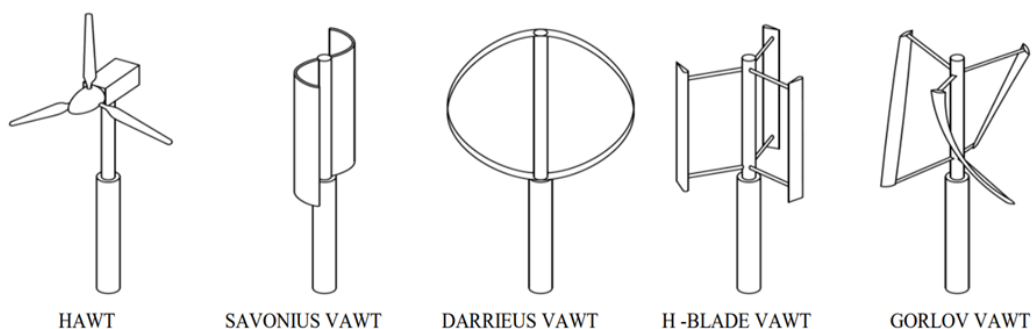


Figure 1.1: Wind turbine types [11].

1.1.2 HAWT components overview

As seen in Fig. 1.2, a modern wind turbine consists of a nacelle located on top of a tower. The nacelle has the hub with the blades attached to it, and contains several key components that serve the purpose of converting wind energy into electrical energy, namely the turbine rotor, the transmission system and the generator. After the generator, there is usually a power electronics interface connected to the grid via a transformer [12].

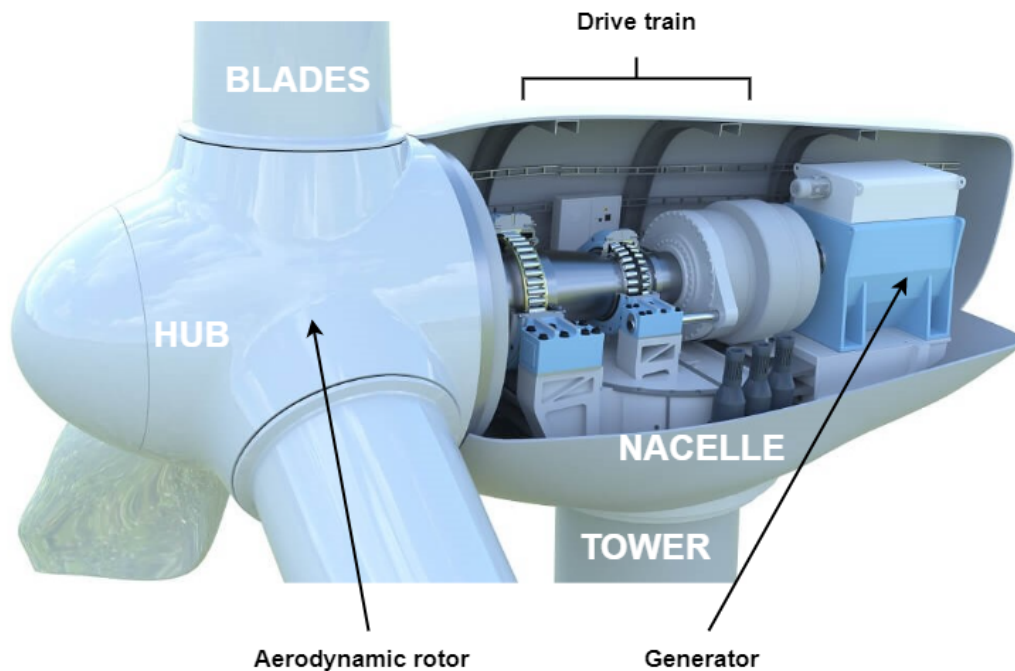


Figure 1.2: Main HAWT components [13].

Aerodynamic rotor

The aerodynamic rotor receives the power from the wind, which causes it to rotate. The rotor mainly consists of the hub, which is attached to the low speed shaft of the wind turbine, and the blades, shaped similarly to an aeroplane wing [12].

Drive train

The drive train is generally composed of the rotor shaft, mechanical brakes and a gearbox. The low speed shaft contains pipes for the hydraulic system to enable the aerodynamic brakes to operate. The gearbox converts the slow high-torque rotation of the aerodynamic rotor into a faster rotation that drives the generator. The high speed shaft is equipped with emergency mechanical brakes, that are used as a backup system for the aerodynamic brakes in case of failure or when the wind turbine is stopped [12].

A relatively new wind turbine topology, which does not present a gearbox, was introduced in 1991 to avoid transmission losses and other issues related to gearbox mechanisms. This technology is known as direct-drive wind turbines [14].

Generator

The generator transforms the mechanical power into electrical power. The most common devices used in the wind turbine industry are synchronous and asynchronous (induction) generators. Synchronous generators are classified into the following types [12]:

- Wound Rotor Synchronous Generator (WRSG).
- Permanent Magnet Synchronous Generator (PMSG).

Asynchronous generators are classified with respect to their rotor design as:

- Squirrel Cage Induction Generators (SCIG).
- Wound Rotor Induction Generator (WRIG).

Figure 1.3 depicts the different types of wind turbine topologies depending on the generator they contain.

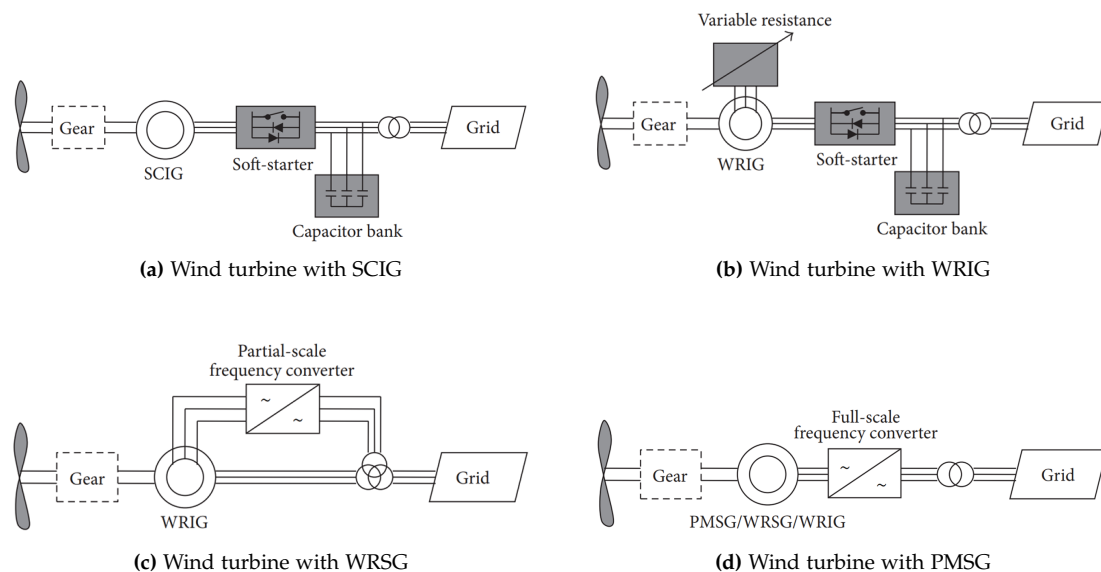


Figure 1.3: Different wind turbine topologies depending on generator type [15].

Power electronics interface

The wind industry comes with the disadvantage of the weather unpredictability, which makes this power source intermittent and unreliable. This has a clear impact on the electrical grid power quality, protection, generation dispatch control and reliability [16]. The

power electronics interface should ensure that the generated power complies with the technical specifications of the grid. The most common power electronics interfaces in the wind turbine industry are the following [12]:

- **Soft starter:** power electrical component used in wind turbines with SCIG to reduce the inrush current to the grid, thereby avoiding large voltage disturbances.
- **Capacitor bank:** electrical component that supplies reactive power to the asynchronous generators of wind turbines.
- **Frequency converter:** power electronic component that facilitates interconnection of two electrical systems with independent frequencies. It is used to control the frequency and voltage of the generator in order to regulate its torque.

1.1.3 Modes of operation

The power available from the wind is given by the following expression [17]:

$$P_{wind}(t) = \frac{1}{2}\rho Av^3(t) \quad (1.1)$$

where:

P_{wind} : power available from the wind	[W]
ρ : air density	[kg/m ³]
A : swept area of the rotor	[m ²]
v : average wind speed in the rotor at hub height	[m/s]

Considering the power coefficient of the wind turbine, which has a theoretical maximum of 0.593 known as the Betz limit [18], the power is more commonly defined as:

$$P(t) = \frac{1}{2}\rho AC_p(\theta, \lambda)v^3(t) \quad (1.2)$$

where C_p refers to the aerodynamic efficiency which depends on the pitch angle of the blades, θ , and the tip speed ratio, λ , this last one assumed for now to be adjusted collectively on the three blades. The tip speed ratio is defined as the ratio between the tangential speed of the blade tip and the wind speed as follows:

$$\lambda(t) = \frac{\omega(t)R}{v(t)} \quad (1.3)$$

where R represents the rotor radius.

Depending on the available wind speed, v , the wind turbine will operate in different modes, as depicted in Fig. 1.4. These regions are delimited by the cut-in, rated and cut-out wind speeds, as well as minimum rotational speed, rated power and rated rotational

speed. At the cut-in wind speed, the wind turbine starts generating power as it starts being economically profitable. If the wind exceeds the cut-out speed, the wind turbine will shut down in order to prevent damage to the mechanical components or the generator. In the region between cut-in and rated wind speed, called partial load region, the wind turbine operates at variable rotor speed to maximise power generation. In the full load region, corresponding to the last region represented in the figure, the power and rotor speed are fixed to their rated values in order to minimise dynamic loads.

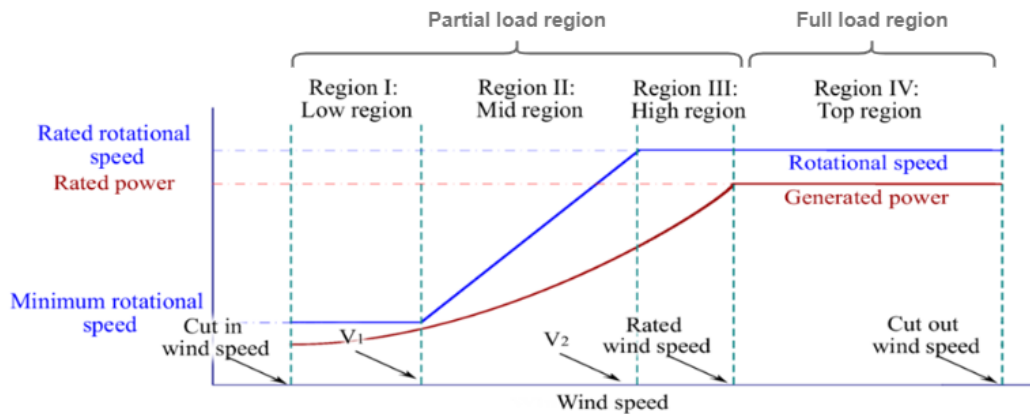


Figure 1.4: Rotational speed and generated power of the wind turbine as functions of wind speed in different operating regions [19].

1.1.4 Wind turbine control overview

Wind turbines can be classified according to the rotational speed of the rotor into Fixed Speed Wind Turbine (FSWT) and Variable Speed Wind Turbine (VSWT) [12, 15]. FSWT rotate at almost constant speed, determined by the gear ratio, grid frequency and number of poles of the generator. They are designed to achieve maximum efficiency only at one given wind speed. They incorporate an SCIG connected directly to the grid, a soft starter, and a capacitor bank for reduction of reactive power consumption. On the other hand, VSWT can adjust the rotor rotational speed according to the wind speed to obtain maximum energy conversion efficiency. It is the most common type of wind turbine used in the wind industry, as it presents advantages regarding efficiency and mechanical stress. However, this comes at the cost of generally requiring more complex control systems and presenting higher costs than their counterpart.

Depending on their operation, wind turbines present different closed-loop control system strategies. The most common are [20]:

- Blade pitch control.
- Stall control.
- Yaw control.

- Generator torque control.

Blade pitch control

The pitch of the blades is changed in order to regulate the power output to the rated value. This control strategy is therefore needed when the turbine is working above-rated wind speed so that design limits are not exceeded. To achieve appropriate load attenuation and power generation, the control system must have a fast response to changing conditions, and thus it should be carefully designed taking into account the turbine dynamics. The control strategy is called Collective Pitch Control (CPC) if the pitch of the three blades is changed collectively by the same amount. In the last decade, there has been an increasing amount of research regarding individual blade pitch regulation for mitigating unsteady loads on the mechanical components of the turbine. These loads are caused by deviations on the estimated mean wind speed due to deterministic effects such as wind shear or tower shadow [21] as well as from turbulence, which presents a more stochastic nature. This strategy is known as Individual Pitch Control (IPC). It can be seen in the literature that both control loops can be designed independently, as the frequency range of the loads considered in each controller is different [17, 20].

Stall control

Some turbines are designed to stall when the wind speed exceeds the design limit, restraining the rotor speed by the generator without utilising any pitch actuation. Subsequently, this method comes with a loss in aerodynamic efficiency [20], which makes it to be generally considered obsolete.

Yaw control

Yaw control must ensure at all times that the nacelle is pointing exactly in the direction of the wind. The corresponding control signal is typically generated using heavily averaged error measurements from a wind vane mounted in the top of the nacelle. Due to the slow response of the yaw control system, a dead-band controller is often adequate enough, turning the nacelle in the appropriate direction when the error exceeds a certain value and stopping it after some time or when a specific angle has been covered [20].

Generator torque control

Variable speed wind turbines present a double fed induction machine or a PMSG. If a frequency converter is situated between the generator and the power grid, the generator speed will be able to vary and the frequency converter could be actively controlled to keep the generator torque at a constant level, by determining the voltage as well as the frequency and phase of the current flowing from the generator [20]. Field Oriented Control (FOC) and Direct Power Control (DPC) are the two typical control strategies applied [22, 23].

1.1.5 Modal analysis

Wind turbines experience several dynamical loads such as aerodynamic loads, variations in wind direction and the effect of gravity. The dynamic behaviour and structural integrity of wind turbines are tested by analysing the structure response to external forces, which could provoke resonance effects. Resonant vibrations are produced when a structure is exposed to a periodical external force taking place close to one or more of its natural frequencies, which depend on its configuration, materials and boundary conditions. At this resonant frequency, the structure will vibrate at higher amplitudes than if the external vibration is applied at any other frequency, compromising the system's integrity. The motion pattern of a system submitted to vibration at its resonant frequency is called normal mode (if the whole system oscillates sinusoidally with the same frequency and fixed phase relation).

Modal analysis is typically used in order to extract the vibrational modes of the structure (represented by their natural frequencies, damping factors and mode shapes) and use them to derive a reliable representation of the dynamics of a system. As the number of modes is the same as the number of Degree of Freedom (DOF)s, let's clarify those first. The structural model in a traditional wind turbine has about 19 to 27 DOFs, which can be classified into:

1. One or two pairs of tower bending modes and one torsional tower mode (3-5 DOFs).
2. Two or three pairs of bending modes and a torsional mode for each blade (15-21 DOFs).
3. One rotor/drive train torsional mode (1 DOFs)

The eigen-frequencies of wind turbine structures lie in the range of 0 to 5 Hz. Table 1.1 shows the results of a modal analysis of a 15-MW wind turbine GH Bladed model considering tower bending and torsion and blade bending modes. All the technicalities of the modal analysis procedure have been skipped; check out the literature for a more in-depth formulation [24, 25]. Some of the different modes are depicted in Fig. 1.5.

Table 1.1: Modal analysis of the 15 MW wind turbine Bladed model structure.

Frequencies [Hz]	Damping ratio	Modal mass [kg]	Modal stiffness [Nm ²]	Mode type
0.541	0.03	2145.8	24763	Blade flapwise normal mode
0.636	0.03	2398.5	38321	Blade edgewise normal mode
1.668	0.03	559.49	61431	Blade flapwise normal mode
2.012	0.03	709.61	113360	Blade edgewise normal mode
0.179	0.005	1804600	2290700	Tower lateral translational attachment mode

Continued on next page

Frequencies [Hz]	Damping ratio	Modal mass [kg]	Modal stiffness [Nm ²]	Mode type
0.180	0.005	1789200	2290700	Tower fore-aft translational attachment mode
0.794	0.005	2.3853×10^8	5.9365×10^9	Tower torsional rotational attachment mode
1.091	0.005	4.1113×10^8	1.9311×10^{10}	Tower lateral rotational attachment mode
1.228	0.005	3.2442×10^8	1.9311×10^{10}	Tower fore-aft rotational attachment mode
2.413	0.005	361680	8.3109×10^7	Tower fore-aft normal mode
2.413	0.005	361680	8.3109×10^7	Tower lateral normal mode

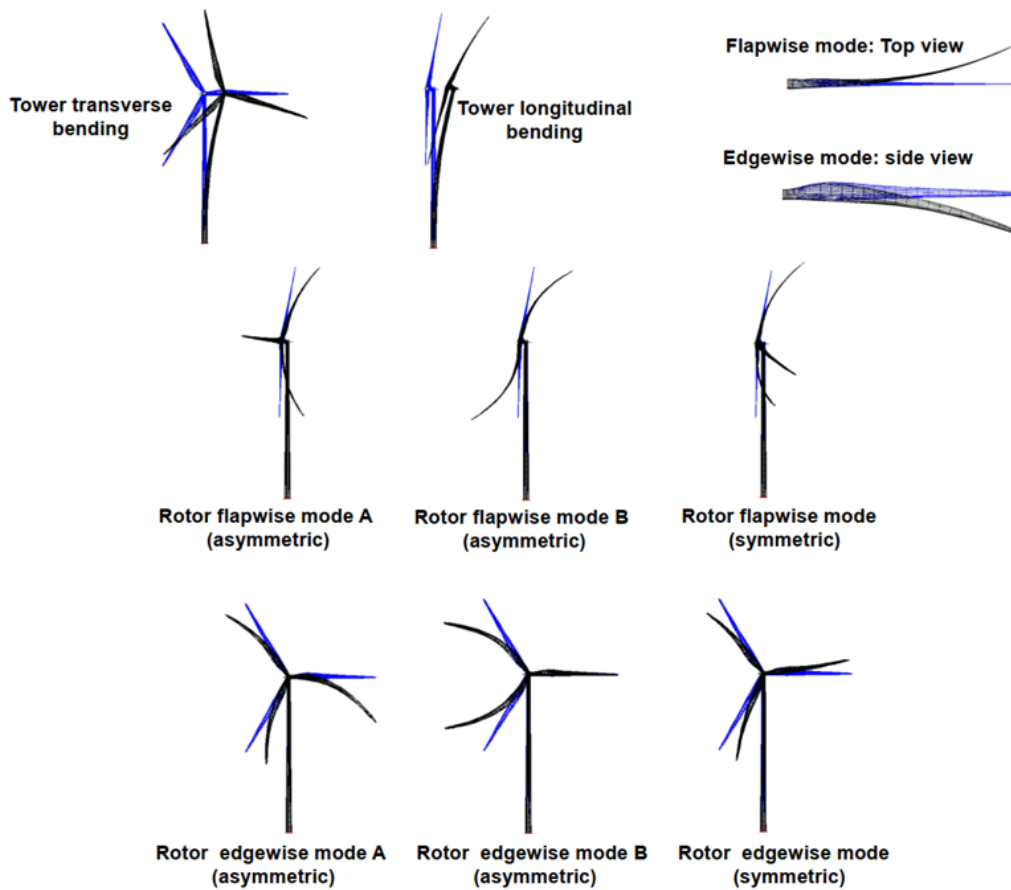


Figure 1.5: Wind turbine structural modes [25].

1.2 Description of Use Case

This section defines more clearly the extent of the project. The manufacturing company that suggested the topic and its delimitations is introduced, and the scope of the task is formulated.

1.2.1 Mita-Teknik

Mita-Teknik is an electrical/electronic manufacturing company that provides wind turbine control solutions to the wind energy industry. It was founded in 1969, and it offers products regarding Turbine Control, Electrical Pitch, Condition Monitoring, Supervisory Control And Data Acquisition (SCADA), Optimization, Retrofit and Customer Partnering. In the field of pitch regulation, they offer CPC and IPC strategies to optimise power generation and ensure minimum structure loads [26].

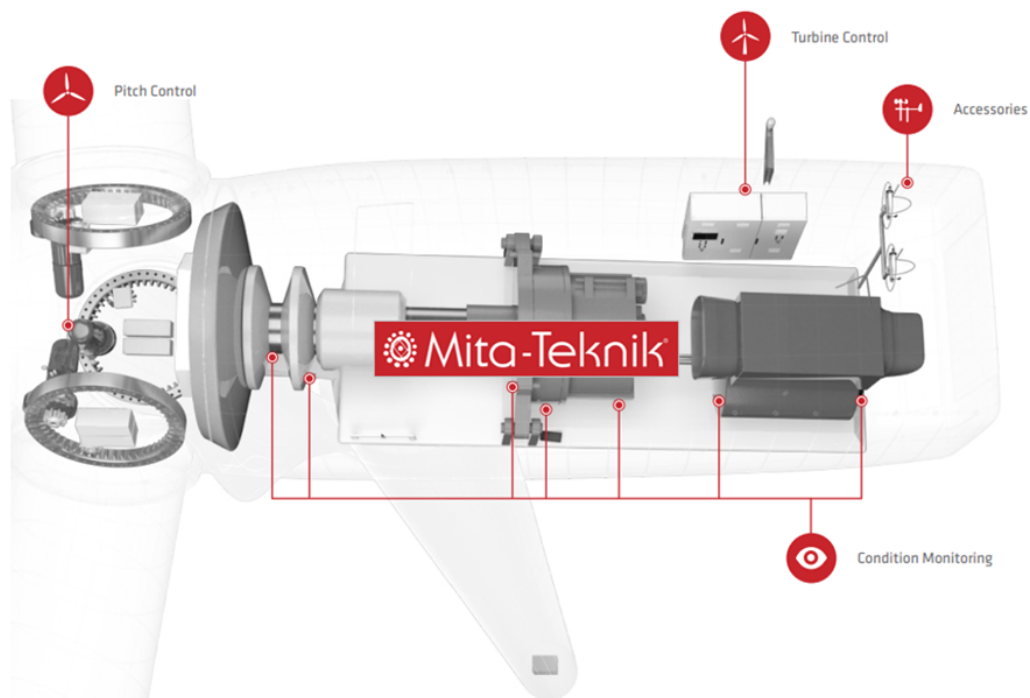


Figure 1.6: Some of Mita-Teknik competences on the wind industry [26].

1.2.2 Problem scope

The power efficiency of a variable-speed variable-pitch wind turbine highly depends on the implemented control algorithms. Conventional methods are not able to consider system constraints, e.g. actuator limitations, constraints in system variables (generator speed, pitch angle, and electrical power), etc. Therefore, it is of interest to study the

performance of MPC strategies in this context, as it allows to tackle several objectives like the previously mentioned ones.

The main goal of this project is then to use MPC to design a control strategy that is able to attenuate structural loads while optimising power production. The present design should cover partial and full load operation of the wind turbine, and some strategy to switch between both operations. Furthermore, the benefits of using individual pitch control to reduce structural loads can also be studied. Finally, the robustness of the presented control strategy could also be addressed.

The designed control strategy can be compared with conventional Proportional Integral Derivative (PID) control methods, provided by Mita-Teknik in the software GH Bladed.

1.2.3 Final case description

The project will comprise the following topics:

- Development of a mathematical model of the variable-speed variable-pitch wind turbine structure for controller synthesis.
- Validation of the mathematical model against the reference GH Bladed model provided by Mita-Teknik.
- Specification of requirements (e.g. constraints) for the MPC.
- Synthesis of the MPC for partial and full load operation.
- Simulation and testing of the designed MPC in Matlab/Simulink, GH Bladed, FAST or another similar tool, and comparison with reference model performance.

1.3 Problem Formulation

The problem formulation forms the foundation for the delimitations and functional requirements, and it will determine the contents of the report.

How can MPC be implemented in a wind turbine to handle multiple system constraints?

1.4 Delimitations

At the time of this project, the 15MW turbine remains a prototype, and the first installation is planned to take place in the second half of 2022 in Østerild national test centre in the second half of 2022 by Vestas. Additionally, in a real life scenario a turbine must be able to handle several scenarios with regards to wind speeds which call for different control strategies. Due to time constraints, not all scenarios can be accounted for. Based on these factors, the following delimitations have been set up:

1. The present design will solely be tested in a simulation environment:
 - Matlab/Simulink
 - GH Bladed
2. The controller will only account for wind speeds from cut-in to cut-out speeds. No mechanism will be designed for stopping the turbine entirely.

1.5 Functional Requirements

Now that the scope of the problem has been defined, a set of functional requirements is specified to define which aspects of the wind turbine behaviour are to be controlled. First, the pitch of the blades should be kept at an optimal value while the rotor speed must be adapted to the wind speed to maximise power capture in partial load conditions. This can be done by adjusting the generator torque, which affects edgewise blade dynamics and drive-train torsion, as well as sideways tower dynamics. In full load conditions, the rotor speed should follow the rated speed, or vary slightly around it. Slow wind speed fluctuations will be tackled by modifying the pitch of the blades collectively, which will reduce the inflow angle as the wind speed increases, thus limiting the captured power. This action affects the thrust, which influences flapwise and edgewise blade dynamics and fore-aft tower dynamics [27].

Additionally, cyclic load variations are caused by the movement of the blades through different altitudes and across the tower as well as by stochastic turbulence. Wind shear and tower shadow cause harmonic bending moment variations in the blades at the angular frequency of the rotor (P) and integers multiples of it, referred to as nP , $n = \{1, 2, 3, \dots\}$. Turbulence provokes stochastic blade load variations with a large frequency content, and peaks centred around nP . A three-bladed rotor will present these load components with a difference in phase of 120° between the three blades, so ideally the structure will only experience the nBP ($B = 3$, $n = \{1, 2, 3, \dots\}$) harmonic content, where the others tend to cancel out. Nevertheless, this assumption become less valid when considering larger wind turbines [28]. Individual pitch control strategies can help reducing these loads.

Therefore, the following requirements have been established:

1. Maximise captured power in partial load conditions by keeping the pitch of the blades at an optimal value and varying the rotor speed.
2. Maintain power production at rated power in full load conditions while keeping the rotor speed at its rated value by varying the pitch of the blades.
3. Reduce blade flapwise and edgewise structural loads.
4. Reduce tower fore-aft and sideways structural loads

1.6 Solution Overview

As the scope of the project is already outlined, an overview to the proposed solution can be proposed at an early stage. The model of the turbine must consider the aerodynamics, mechanics, electrics and actuators. MPC requires an estimate of all internal states at time k in order to both create a set of optimal control inputs over the control horizon and predict the state up to the prediction horizon. As the model will be highly non-linear, the state estimation will be carried out with an UKF. The MPC itself will take state and actuator constraints into account, and will calculate a series of optimal control inputs of which only the first is used, which will then serve as the Kalman filter input at time $k + 1$. A simple block diagram of the proposed solution is shown in Figure 1.7

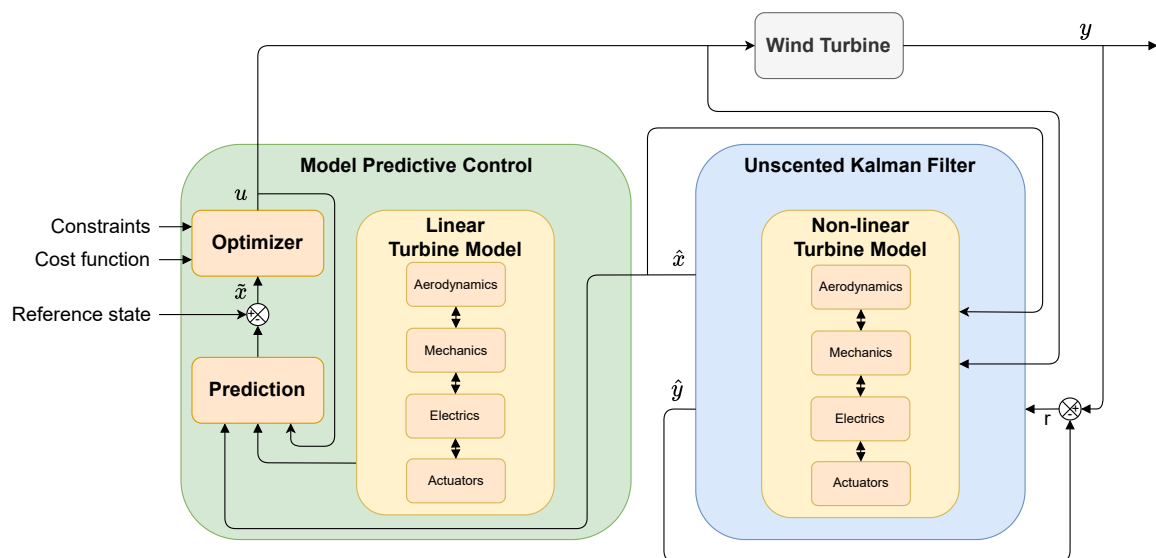


Figure 1.7: Block diagram of the solution

Chapter 2

WIND TURBINE MODELLING

2.1 Introduction

Wind turbine aero-elastic simulation models such as the ones used in the Fatigue, Aerodynamics, Structures and Turbulence (FAST) simulation tool, commonly describe the wind turbine dynamics with around 24 DOF, which is not appropriate for control design purposes due to excessive difficulty and computational cost, which can lead to numerous implementation issues. Therefore, a simpler reduced-order dynamic model including only the essential dynamics will be derived.

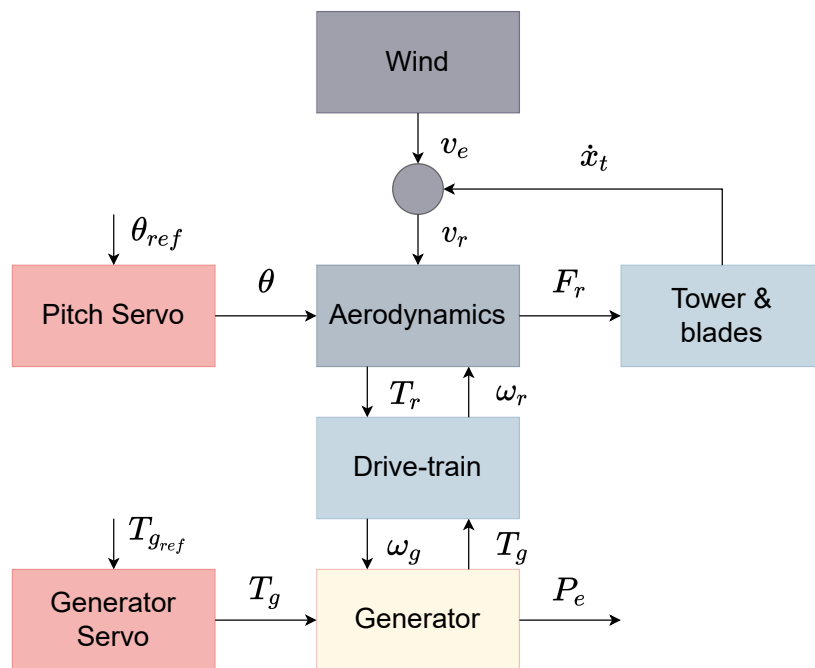


Figure 2.1: Global system block diagram [19].

The wind turbine structure is usually divided into 4 subsystems as can be seen in Fig. 2.1: the aerodynamics, several models for the mechanical structure (drive train, tower and blades), the electrical part (generator and converter) and the actuators (pitch and generator torque). The aerodynamics deal with the transformation of the kinetic energy

of the wind into mechanical torque as a consequence of the aerodynamic shape of the blades. The drive train transfers the rotor torque to the generator, while the tower and blade structures are constantly being deformed by the wind thrust forces. Finally, the generator and converter transform the mechanical energy into electrical energy and the actuators modify their respective control variables when provided with a control signal. The inputs and outputs seen in Fig. 2.1 refer to the effective wind speed, v_e , the relative wind speed measured at the rotor, v_r , the thrust force in the rotor, F_r , the pitch angle, θ , and its reference, θ_{ref} , the rotor aerodynamic torque, T_r , the angular speed of the rotor, ω_r and of the generator, ω_g , the generator torque, T_g , and its reference, T_{gref} , and the generated electrical power, P_e .

2.1.1 Degrees of freedom and coordinate systems

The basic DOF considered are depicted in Fig. 2.3. The coordinate systems used throughout this project are based on the "GL" convention, and are defined hereafter [29].

For hub loads, the reference frame is placed at the centre of the hub as seen in Fig. 2.2a. This frame can be static or rotatory, with the ZN axis aligned with blade 1 axis in the second case. For tower loads, the reference frame is placed at the tower station as seen in Fig. 2.2b.

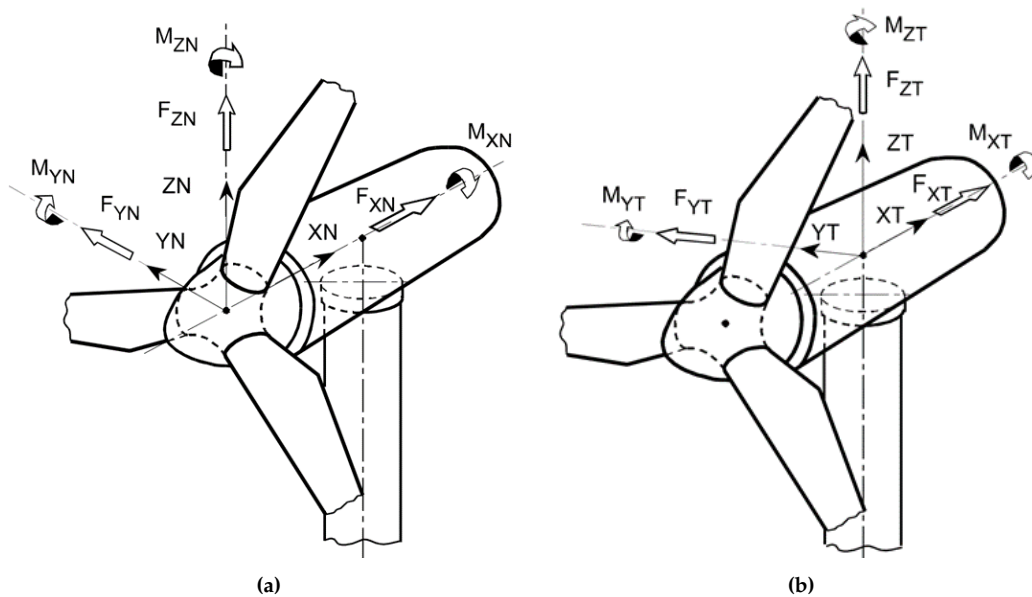


Figure 2.2: Coordinate system for hub loads (a) and for tower loads (b) [29].

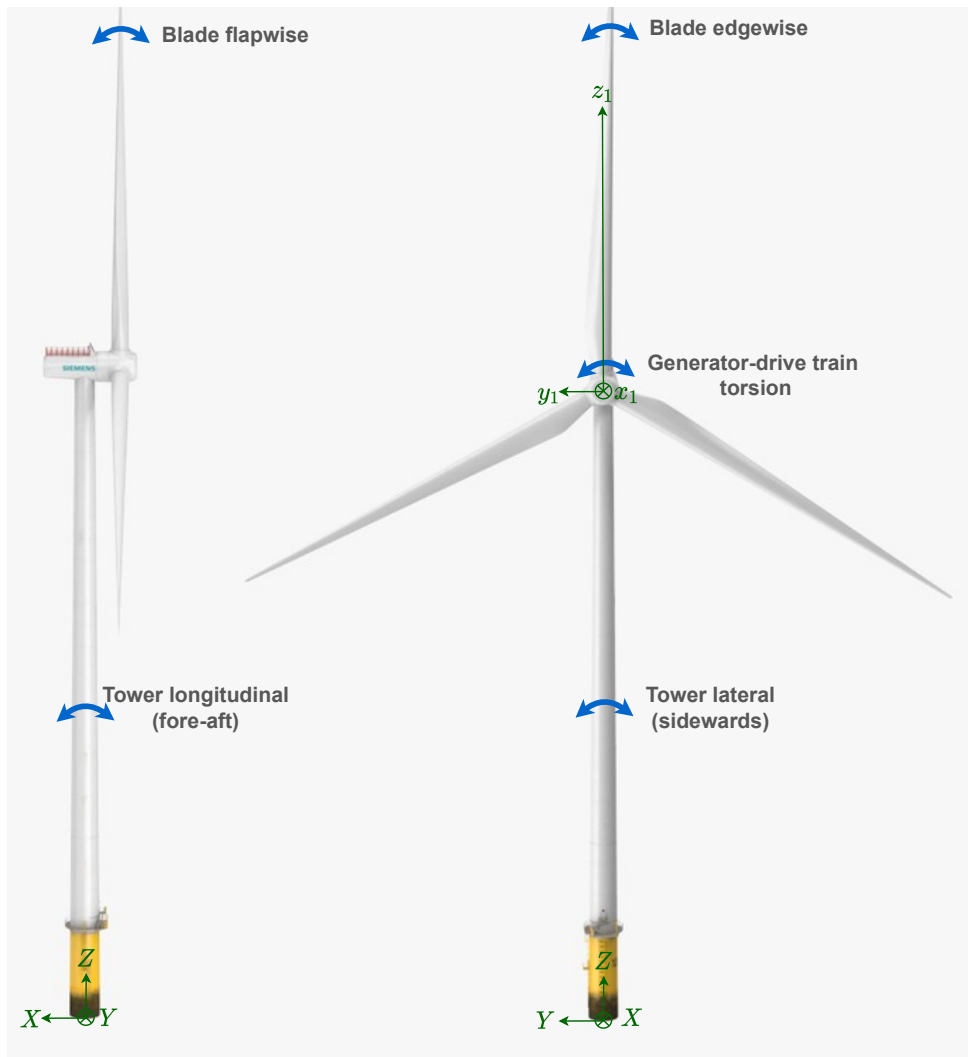


Figure 2.3: DOFs considered for the mathematical modelling [15].

Blade loads can be specified in 4 different coordinate systems: principal axes, root axes, aerodynamic axes and user axes. The GH Bladed model available outputs blade loads in principal axes and root axes.

Regarding the principal axes, the positive z -axis follows the local deflected neutral axis at each blade station towards the blade tip. The positive y -axis is defined by the principal axis orientation, and the positive x -axis is orthogonal to x and y . For output loads, the origin of the axes is located on the neutral axis at each local deflected blade station as seen in Fig. 2.4a.

On the other hand, the orientation of the root axes is fixed to the blade root and does not rotate with blade twist or deflection, but rotates about the z -axis with pitch. For output loads, the origin of the axes is on the neutral axis at each local deflected blade station as

seen in Fig. 2.4b.

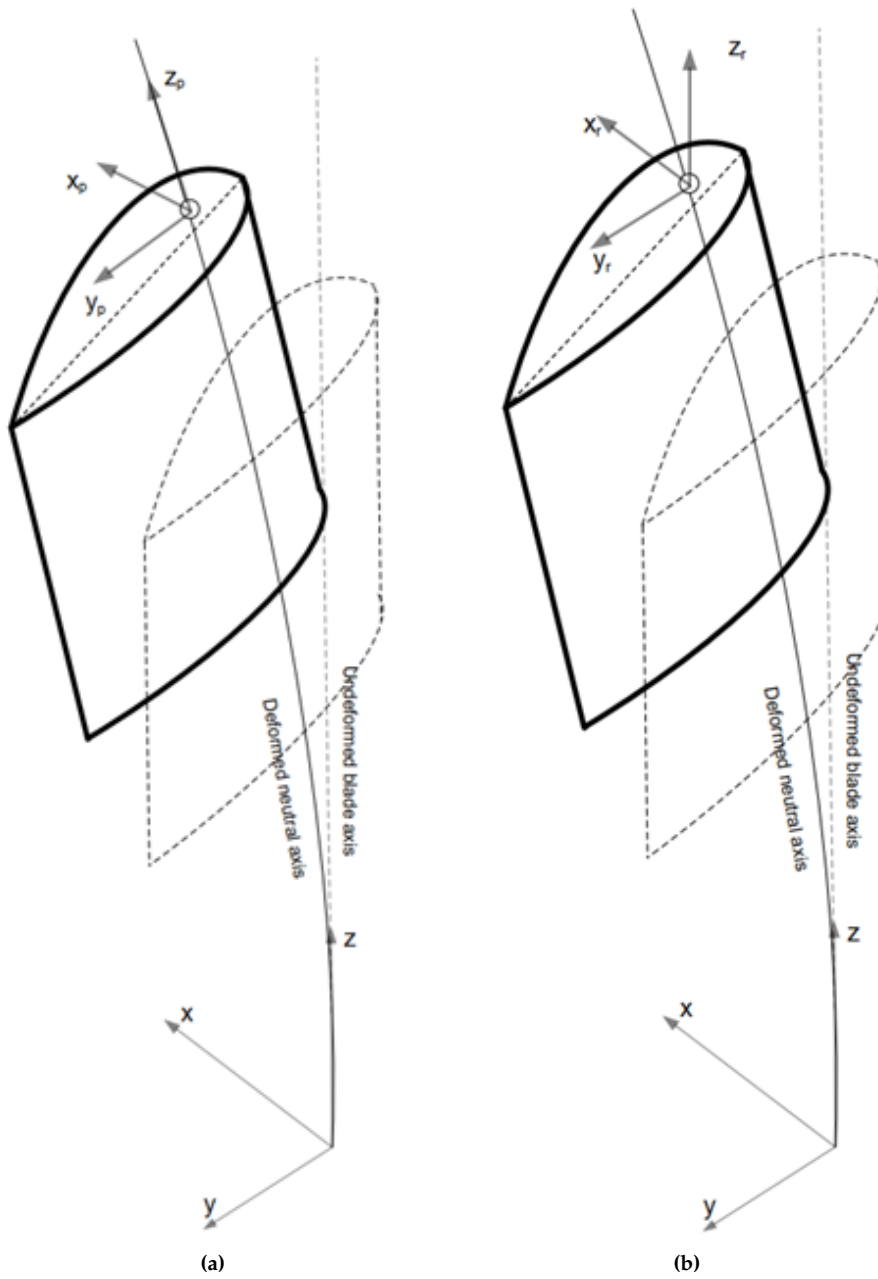


Figure 2.4: Principal axes (a) and root axes (b) [29].

2.1.2 List of constants and variables

Table 2.1: Variables

Variable	Description	Unit
μ_v	Fixed mean wind speed	m/s
v	Wind speed in the x direction in arbitrary point around the tower	m/s
r_t	Tower radius dependant on the height	m
v_m	Mean wind speed	m/s
ψ	Angular position of the rotor	rad
z	Elevation above the surface	m
W_s	Wind share disturbance in wind speed	m/s
v_e	Effective wind speed at hub height	m/s
v_t	Turbulent wind speed	m/s
n_m	White noise mean and variance σ_m^2	.
σ_t	White noise standard deviation of turbulent wind speed	.
C_l	Lift coefficient	.
C_d	Drag coefficient	.
I_b	Blade moment of inertia	kgm ²
I_t	Tower moment of inertia	kgm ²
l	Force of lift per length	N/m
d	Force of drag per length	N/m
α	Local angle of attack	rad
ω_r	Angular velocity of the rotor	rad/s
ϕ	Angle of the incoming flow	rad
θ	Local pitch of the individual blade with respect to the tip	rad
θ_p	Pitch angle of the blade	rad
β	Twist of the blade relative to the rotor plane	rad
V_a	Axial wind velocity	m/s
V_{rot}	Tangential wind velocity	m/s
Δp	The pressure drop over the rotor plane	Pa
v_r	Relative wind velocity seen by the rotor	m/s
x_t	Tower fore-aft top displacement	m
y_t	Tower sideways top displacement	m
x_b	Blade flapwise top displacement	m
y_b	Blade edgewise top displacement	m
ω_g	Angular velocity of the generator	rad/s
T_g	Generator torque	Nm
P_e	Electric power	W
θ_{ref}	Reference pitch actuator angle	rad
θ	Pitch actuator angle	rad

Continued on next page

Variable	Description	Unit
T_{gref}	Reference generator torque	Nm
F_x	Rotor out-of-plane aerodynamic thrust force	N
F_y	Rotor in-plane aerodynamic thrust force	N
T_r	Rotor aerodynamic torque force	Nm
α_b	Blade stiffness tuning parameter	.
λ	Tip Speed Ratio (TSR)	.

Table 2.2: Constants

Constant	Description	Value	Unit
r_{top}	Tower top radius	3.25	m
r_{base}	Tower base radius	5	m
H	Tower height	144.582	m
α	Wind shear exponent for smooth terrain	0.15	.
σ_m^2	White noise variance of mean wind speed	3.333e-4	.
T_s	Sampling time	0.05	s
t_i	Turbulence intensity	0.1	.
ω_p	Peak frequency for the Kaimal spectrum	0.0462	rad/s
ρ	Air density	1.225	kg/m ³
R	Rotor radius	120.998	m
M_t	Tower mass	1,086,002	kg
M_n	Nacelle mass	630,888	kg
m_t	Tower equivalent mass	992,889	kg
k_t	Tower stiffness	1,270,005	N/m
c_t	Tower damping	11,229	Ns/m
f_t	Tower 1 st normal mode frequency	0.18	Hz
ζ_t	Tower damping ratio	0.005	.
l_b	Blade length	117.1836	m
r_b	Blade radius	2.6	m
M_b	Blade mass	65,566	kg
m_b	Blade equivalent mass	6,561	kg
k_{b_x}	Blade stiffness flapwise	82,314	N/m
c_{b_x}	Blade damping flapwise	1,453	Ns/m
k_{b_y}	Blade stiffness edgewise	113,761	N/m
c_{b_y}	Blade damping edgewise	1,708	Ns/m
f_{b_x}	Blade 1 st flapwise normal mode frequency	0.541	Hz
f_{b_y}	Blade 1 st edgewise normal mode frequency	0.636	Hz
ζ_{b_x}	Blade 1 st flapwise normal mode damping ratio	0.03	.
ζ_{b_y}	Blade 1 st edgewise normal mode damping ratio	0.03	.

Continued on next page

Constant	Description	Value	Unit
B	Total number of blades	3	.
J_g	Generator moment of inertia	3,223,000	kgm ²
J_r	Rotor moment of inertia	321,699,000	kgm ²
x_h	Hub overhang	10.93	m
c_d	Drive train damping	0.005	Nms/rad
k_d	Drive train stiffness	1.409e+10	Nm/rad
μ_d	Mechanical loss	0.05	.
η_g	Electrical efficiency	0.93	.
ω_θ	Natural frequency of pitch actuator model	1.2	Hz
ζ_θ	Damping factor of pitch actuator model	0.8	.
τ_g	Generator time constant	0.001	s
A_r	Rotor area	45,995	m ²
θ_{min}	Minimum blade pitch angle	-0.2618	rad
θ_{max}	Maximum blade pitch angle	$\pi/2$	rad
$T_{g,max}$	Maximum generator torque	21,030,000	Nm
$\dot{\theta}_{min}$	Minimum angular velocity of blade pitching	-0.1571	rad/s
$\dot{\theta}_{max}$	Maximum angular velocity of blade pitching	0.1571	rad/s
$\omega_{r,min}$	Minimum angular velocity of the rotor	0.5236	rad/s
$\omega_{r,rat}$	Rated angular velocity of the rotor	0.7917	rad/s
$\omega_{r,max}$	Maximum angular velocity of the rotor	0.8709	rad/s
$P_{e,opt}$	Rated electric power	15	MW
$P_{e,max}$	Electric power	22	MW
λ_{opt}	Optimal TSR	9.0621	.

2.2 Wind Model

The wind affecting a wind turbine has both a deterministic and stochastic nature. Their influence in the wind profile will be analysed hereafter.

2.2.1 Deterministic wind model

Part of the variation of the wind profile over the whole structure of the wind turbine can be described by two deterministic properties, referred to as tower shadow and wind shear [30]. Tower shadow describes the alteration of the wind flow due to the presence of the tower, which is perceived by the blades when they pass in front of it. Wind shear refers to the variation of the wind profile with respect to the height as a result of aerodynamic friction with the ground.

Tower shadow

The presence of the tower cylinder amidst the wind flow generates changes in pressure, and subsequently in the speed of the fluid. Figure 2.5 shows the deformation of the flow lines and the pressure field around the tower section in an aerial view. This will have an impact on the blades when passing in front of the tower, as they will experience minimum wind speed at that point. Using potential flow theory around an infinitely long cylinder, an equation for the wind speed around the tower can be derived [21, 30]:

$$v(x, y, h) = v_m + v_m r_t(h)^2 \frac{y^2 - x^2}{(x^2 + y^2)^2} \quad (2.1)$$

which can be rewritten as a function of the azimuth angle of the rotor ψ , and substituting x by the hub overhang x_h :

$$v(R, \psi, h) = v_m + v_m r_t(h)^2 \frac{(R \sin \psi)^2 - x_h^2}{(x_h^2 + (R \sin \psi)^2)^2} \quad (2.2)$$

where:

v : wind speed in the x direction in an arbitrary point around the tower	[m/s]
v_m : mean wind speed	[m/s]
$r_t(h)$: tower radius dependant on the height	[m]
R : rotor radius	[m]
ψ : angular position of the rotor	[rad]
x_h : hub overhang	[m]

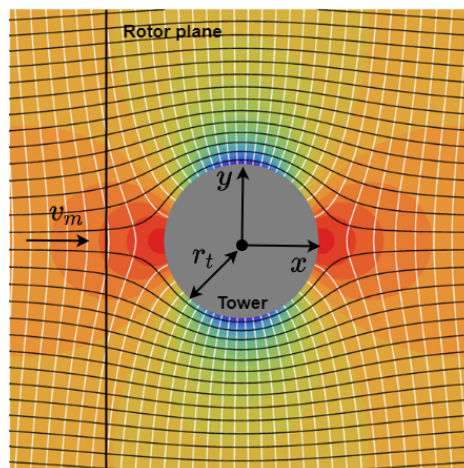


Figure 2.5: Wind flow around circular cylinder (black curves), including velocity potentials (white curves) and pressure field (colours), where red indicates high pressure and blue low pressure [31].

The computed wind speed will not only have a component in the x -axis, but also another in the y -axis that will be disregarded due to its minimal contribution to the rotor torque [30].

Figure 2.6 shows the change in the tower outer radius with respect to its height. For simplicity, it is assumed that the radius varies linearly with the height, and thus its value can be found as follows:

$$r_t(h) = \left(\frac{r_{top} - r_{base}}{H} h \right) + r_{base} \quad (2.3)$$

where:

r_{top}	: tower top radius	[m]
r_{base}	: tower base radius	[m]
H	: hub height	[m]

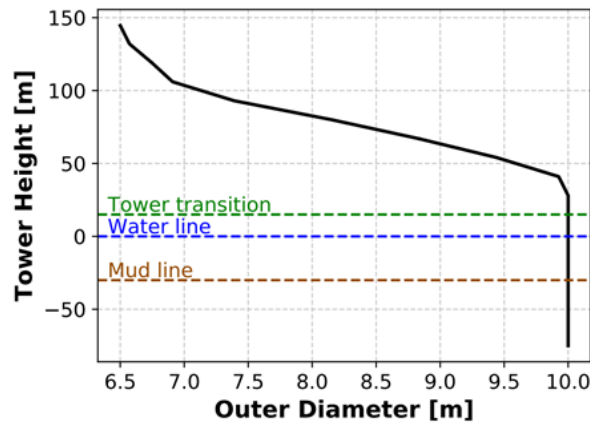


Figure 2.6: Outer diameter of the tower with respect to the height [32].

The wind perturbation produced by the tower shadow with respect to the angular position of the blades is depicted in Fig. 2.7. It can be seen that the wind speed reaches its minimum when the blade is right in front of the tower, and it slightly increases in its vicinity.

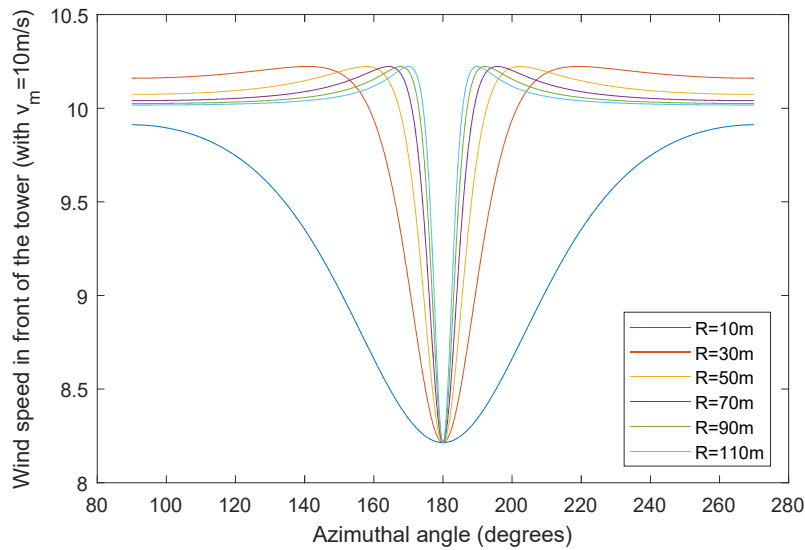


Figure 2.7: Tower shadow for different rotor radii R . Mean wind speed $v_m = 10$ m/s. Hub overhang $x_h = 10.93$ m. Tower radius measured at height $h = 31.75$ m corresponding to the tower height minus the blade length.

Wind shear

Wind shear describes the effect that the friction between the air and the ground has on the wind speed profile. Wind gets slowed down when moving close to the Earth's surface due to the different irregularities that obstruct its flow. Therefore, the blades will experience minimum wind speed when facing downwards. Wind shear can be modelled by [21]:

$$v(z) = v_m \left(\frac{z}{H} \right)^\alpha \quad (2.4)$$

where z represents the elevation above the surface and α refers to the wind shear exponent, which takes into account the type of terrain in which the wind turbine is located. Typical values of α can be seen in Table 2.3.

Table 2.3: Different values of α with terrain [33]

Terrain	α
Open water	0.1
Smooth, level, grass-covered	0.15
Row crops	0.2
Low bushes with a few trees	0.2
Heavy trees	0.25
Several buildings	0.25
Hilly, mountainous terrain	0.25

Writing Eq. 2.4 as a function of the rotor radius R and the blade azimuth angle ψ yields [21]:

$$v(R, \psi) = v_m \left(\frac{R \cos \psi + H}{H} \right)^\alpha \quad (2.5)$$

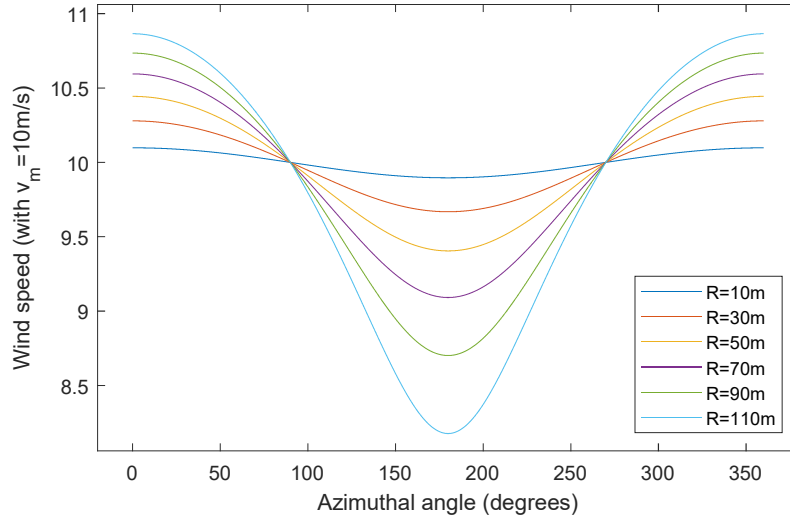


Figure 2.8: Wind shear for different rotor radii R . Mean wind speed $v_m = 10$ m/s. Wind shear exponent $\alpha = 0.1$, corresponding to open water.

Figure 2.8 helps with the visualisation of the effect of the wind shear on the blades with respect to their azimuth angle.

The addition of wind shear and tower shadow effects results in the following expression for wind speed variation with respect to the blades azimuth angle. This is depicted in Fig. 2.9.

$$v(R, \psi) = v_m \left[r_t^2 \frac{(R \sin \psi)^2 - x_h^2}{(x_h^2 + (R \sin \psi)^2)^2} + \left(\frac{R \cos(\psi) + H}{H} \right)^\alpha \right] \quad (2.6)$$

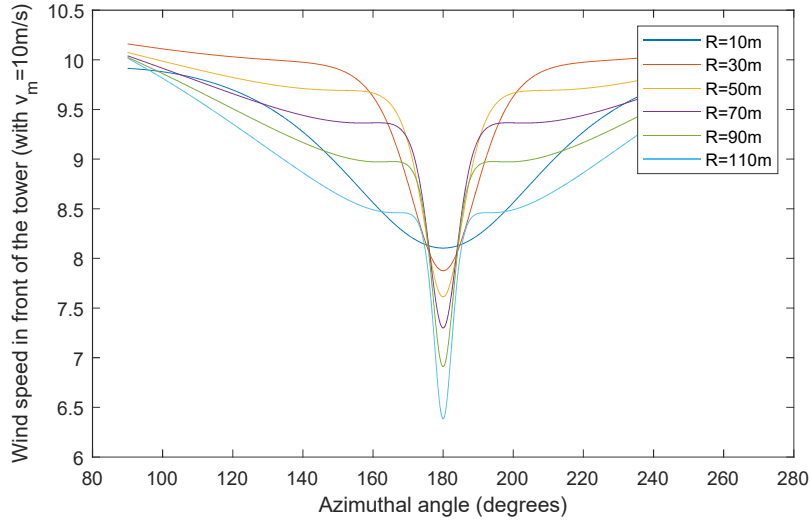


Figure 2.9: Wind shear and tower shadow combined effect for different rotor radii R . Mean wind speed $v_m = 10$ m/s. Wind shear exponent $\alpha = 0.1$ (open water). Hub overhang $x_h = 10.93$ m. Tower radius measured at height $h = 31.75$ m corresponding to the tower height minus the blade length.

2.2.2 Stochastic wind model & effective wind speed

The deterministic wind profile model derived in the previous sections will be used to design the individual pitch controller. This is because the spatial distribution of the wind is needed to try to compensate unbalanced loading on the wind turbine structure. Nevertheless, a stochastic wind model is still needed to properly represent the wind behaviour, and it will be derived for all the rotor area. Therefore, an equivalent value of the wind variation over the entire rotor area needs to be estimated, called effective wind speed.

Effective wind speed, v_e , can be modelled by a mean wind speed, v_m , which varies slowly and can be considered as an average of wind speed measurements in 10 min, and a turbulent term, v_t , as seen in Eq. 2.7.

$$v_e = v_m + v_t \quad (2.7)$$

The fore-aft movement of the nacelle when submitted to wind forces will also be considered in the implementation of the effective wind speed estimation. Lets then define a new variable, v_r , that describes the effective wind speed at the rotor including the tower fore-aft velocity, \dot{x}_t , in its expression:

$$v_r = v_m + v_t - \dot{x}_t \quad (2.8)$$

Mean wind speed

The mean wind speed can be considered as varying slowly from zero to at least 30 m/s. A simple model would be the following random walk:

$$v_m[k] = v_m[k-1] + T_s n_m[k-1]; \quad n_m \in NID(0, \sigma_m^2) \quad (2.9)$$

where n_m represents white noise of zero mean and variance σ_m^2 . This means that the variance of v_m will increase with each time step, reaching a value of $k\sigma_m^2$ after k time steps. Hence, changes over $2\sqrt{k}\sigma_m$ will be unlikely. If it is assumed that the mean wind speed can change approximately 2 m/s in a time lapse of 10 min, then σ_m would be defined as $\sigma_m = \sqrt{\frac{(2\text{m/s})^2}{600\text{s}}}$.

Turbulent part

The turbulent part of the wind speed has zero mean and variance dependent on the mean wind speed. This is expressed with the turbulence intensity, t_i , which is defined as the ratio of standard deviation of fluctuating wind velocity to the mean wind speed (Eq. 2.10) and represents the intensity of wind velocity fluctuation [34]. This parameter is known in statistics as coefficient of variation (CV).

$$t_i = \frac{\sigma_{v_t}}{\mu_v} \quad (2.10)$$

where μ_v refers to a fixed mean wind speed.

The turbulence can be approximated by a first order low pass filter driven by white noise:

$$H(s) = \frac{V_t(s)}{N_t(s)} = \frac{\omega_p}{s + \omega_p} \quad (2.11)$$

where $V_t(s)$ and $N_t(s)$ refer to the turbulent component of the wind and the low pass filter white noise input in the Laplace domain respectively. The frequency ω_p can be chosen to give the same bandwidth as the peak frequency for the Kaimal spectrum [20]:

$$\omega_p = \frac{\mu_v \pi}{2L} \quad (2.12)$$

where $L = 8.1 \cdot \Lambda_1 = 8.1 \cdot 42 = 340.2$ [35]. Reorganising Eq. 2.11 yields:

$$V_t(s)s = -\omega_p V_t(s) + \omega_p N_t(s) \quad (2.13)$$

which can be expressed in the continuous time domain as:

$$\dot{v}_t(t) = -\omega_p v_t(t) + \omega_p n_t(t) \quad (2.14)$$

In order to discretize the previous stochastic differential equation, Euler discretization method is used:

$$\frac{v_t[k] - v_t[k-1]}{T_s} = -\omega_p v_t[k-1] + \omega_p n_t[k-1] \quad (2.15)$$

Rearranging the previous expression yields:

$$v_t[k] = (1 - T_s\omega_p)v_t[k-1] + T_s\omega_p n_t[k-1] \quad (2.16)$$

By defining $a = 1 - T_s\omega_p$, the standard formula for an infinite-impulse response (IIR) low pass filter is obtained:

$$v_t[k] = av_t[k-1] + (1-a)n_t[k-1]; \quad n_t \in NID(0, \sigma_t^2) \quad (2.17)$$

Considering a stationary stochastic process, it is possible to calculate the variance of the previous expression as follows:

$$\text{Var}(v_t) = a^2\text{Var}(v_t) + (1-a)^2\text{Var}(n_t) \quad (2.18)$$

Defining $\text{Var}(n_t) = \sigma_t^2$, $\text{Var}(v_t) = \sigma_{v_t}^2$ and rearranging terms:

$$\sigma_{v_t}^2 = \frac{(1-a)^2}{1-a^2}\sigma_t^2 \quad (2.19)$$

As it was stated before, $\sigma_{v_t}^2 = (t_i\mu_v)^2$, which results in the following:

$$\sigma_t = t_i\mu_v \sqrt{\frac{1-a^2}{(1-a)^2}} \quad (2.20)$$

Figure 2.10 shows a simulation of the two previously derived wind speed components and the effective wind speed as the addition of both.

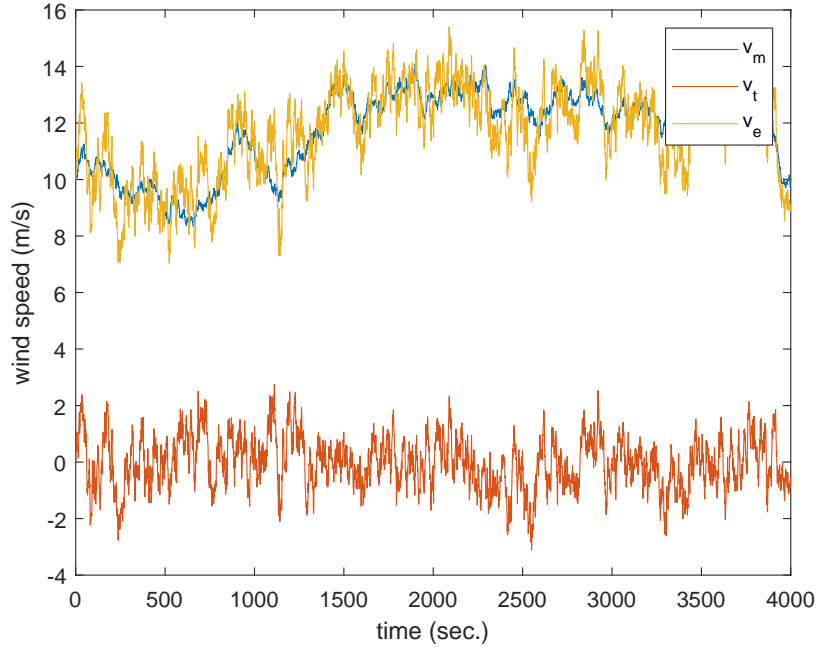


Figure 2.10: Stochastic wind speed simulation with $V_{11} = 4/600 \text{ m}^2/\text{s}^3$, $t_i = 0.1$, $\mu_v = 10 \text{ m/s}$

A non linear model could also be formulated by replacing the fixed mean wind speed μ_v in the turbulent part by the time varying mean wind speed, v_m .

2.3 Aerodynamic Model

The aerodynamic model considers the force applied to the turbine by the wind. Some of the force will be converted into an in-plane torque acting on the rotor based on the pitch of the blades of the turbine. The remainder will be applied as an out-of-plane thrust force applied to the rotor plane. One reliable way to get a detailed look into the aerodynamic forces acting on a turbine is through Blade Element Momentum Method (BEM). BEM involves dividing the rotor area of the turbine into annular elements and determining the thrust and torque acting on each element based on the vortices left in the wake of the rotor plane. A drawback of BEM is that it involves iterative calculations to determine key variables. So while it is well suited for analysing wind turbine performance, it is not well suited for control of a turbine. BEM is derived in Appendix A along with the theoretical background that supports it including a derivation of the Betz limit mentioned in Section 1.1.3. A simpler model will have to be used instead, which considers the total thrust and torque acting on each individual blade based on wind velocity, rotor angular velocity and blade pitch angle. Coefficients are defined for the thrust applied to the blades, as well as the power generated, as functions of blade pitch angle and the ratio between the tip speed and relative wind velocity, seen below:

$$\lambda_i = \frac{\omega_r R - \dot{y}_{b_i}}{v_{r_i} - \dot{x}_{b_i}} \quad (2.21)$$

Note that the tip speed ratio has been modified with respect to the original expression presented in Section 1.1.3 by considering the blade tip sideways and flapwise velocity (\dot{y}_{b_i} and \dot{x}_{b_i} respectively) and the wind speed experienced by each blade, v_{r_i} , defined in Section 2.2, in order to make the expression take into account blade dynamics.

The thrust coefficient describes the relationship between the maximum possible thrust, and the actual thrust generated as seen in Equation 2.22.

$$C_t(\lambda, \theta) = \frac{F_r}{\frac{1}{2}\rho v_r^2 A_r} \quad (2.22)$$

$$C_p(\lambda, \theta) = \frac{P}{\frac{1}{2}\rho v_r^3 A_r} \quad (2.23)$$

where:

C_t : thrust coefficient	[·]
C_p : power coefficient	[·]
F_r : aerodynamic thrust applied to rotor	[N]

P : power obtained from the wind	[W]
ρ : density of the air	[kg/m ³]
v_r : relative wind velocity seen by the rotor	[m/s]
A_r : area of the rotor plane	[m ²]

Isolating F_r and P yields:

$$F_r = \frac{1}{2} \rho v_r^2 A_r C_t(\lambda, \theta) \quad (2.24)$$

$$P = \frac{1}{2} \rho v_r^3 A_r C_p(\lambda, \theta) \quad (2.25)$$

The power coefficient and subsequent derivation of the Betz limit is explained further in Appendix A.2. The power obtained from the wind, P , can be expressed as a function of the angular velocity of the rotor and the torque applied to it as seen in Equation 2.26

$$P = T_r \omega_r \quad (2.26)$$

Inserting the definition of P in Equation 2.26 and isolating the expression for the aerodynamic torque yields:

$$T_r = \frac{1}{2} \rho v_r^3 A C_p(\lambda, \theta) \frac{1}{\omega_r} \quad (2.27)$$

For the purpose of implementing IPC, the in-plane and out-of-plane thrust (F_{y_i} and F_{x_i} in Eqs. 2.28 and 2.29) experienced by each blade will be defined based on the relative wind velocity seen by the individual blades, v_{r_i} , rewritten further down, which will be inserted instead of v_r . The in-plane thrust is derived from the torque applied to the rotor. Taking into account that torque increases with distance from the rotor hub, the point of application of that torque is estimated to be at two thirds the blade length, l_b . To convert the torque into thrust, the torque equation is divided by this length. The out-of-plane thrust will employ the same equation as that for the thrust for the whole rotor. Both in-plane and out-of-plane thrust will be scaled down by dividing the power and thrust coefficients by the amount of blades, B , to account for the force only applying to one blade.

$$F_{y_i} = \frac{1}{2} \rho v_{r_i}^3 A_r \frac{C_p(\lambda_i, \theta_i)}{B} \frac{1}{\omega_r} \frac{3}{2l_b} \quad (2.28)$$

$$F_{x_i} = \frac{1}{2} \rho v_{r_i}^2 A_r \frac{C_t(\lambda_i, \theta_i)}{B} \quad (2.29)$$

where:

$$v_{r_i} = \left(v_t + v_m \left[r_t^2 \frac{(R \sin(\psi_i))^2 - x_h^2}{(x_h^2 + (R \sin(\psi))^2)^2} + \left(\frac{R \cos(\psi) + H}{H} \right)^\alpha \right] - \dot{x}_t - \dot{x}_{b_i} \right) \quad (2.30)$$

$$\psi_i = \psi + i \frac{2\pi}{B} \quad (2.31)$$

C_t and C_p are found by means of a look-up table, where the closest equivalent to the current scenario is chosen [9, 17].

As stated previously, the in-plane thrust force F_{y_i} represents the aerodynamic torque applied to each individual blade. The resulting torque on the rotor can then be written as the summation of the in-plane displacement of each blade y_{b_i} (with negative sign due to the deflection being in the negative y -axis direction) multiplied by the blades sideways stiffness k_{b_y} (found out in Section 2.4) and the distance to the application point of the force as follows:

$$T_r = \sum_i -y_{b_i} k_{b_y} \frac{2l_b}{3} \quad (2.32)$$

with $i \in \{0, 1, 2\}$ and l_b referring to the length of the blades.

2.4 Simple Tower and Blade Models

For control design purposes, a simple mechanical wind turbine model is considered, consisting on five DOF: fore-aft and sideways tower bending, flapwise and edgewise blade bending and rotor rotation.

The tower and blade movement can be expressed as a simple two mass spring damper model as seen in Fig. 2.11. The masses used in this model should be computed as the equivalent mass of the blades, and the equivalent mass of the tower and nacelle, assuming that all the mass is located in a point at a distance l_b and H from the axis of rotation for the blades and the tower/nacelle respectively. This equivalent masses are calculated by using the respective moments of inertia assuming the tower and blades geometry as a cylinder and a cone respectively [36]:

$$I_t = m_n H^2 + \frac{1}{3} m_t H^2 + \frac{1}{4} m_t r_t^2 = m_{t_{eq}} H^2 \rightarrow m_{t_{eq}} = m_n + \frac{1}{3} m_t + \frac{1}{4H^2} m_t r_t^2 \quad (2.33)$$

$$I_b = \frac{1}{10} m_b l_b^2 + \frac{3}{20} m_b r_b^2 = m_{b_{eq}} l_b^2 \rightarrow m_{b_{eq}} = \frac{1}{10} m_b + \frac{3}{20l_b^2} m_b r_b^2 \quad (2.34)$$

where:

I_t : tower and nacelle moment of inertia	[kgm ²]
I_b : blade moment of inertia	[kgm ²]
m_t : tower mass	[kg]
m_n : nacelle mass	[kg]
$m_{t_{eq}}$: tower/nacelle equivalent mass	[kg]
$m_{b_{eq}}$: blade equivalent mass	[kg]
H : tower height	[m]
r_b : blade chord radius	[m]

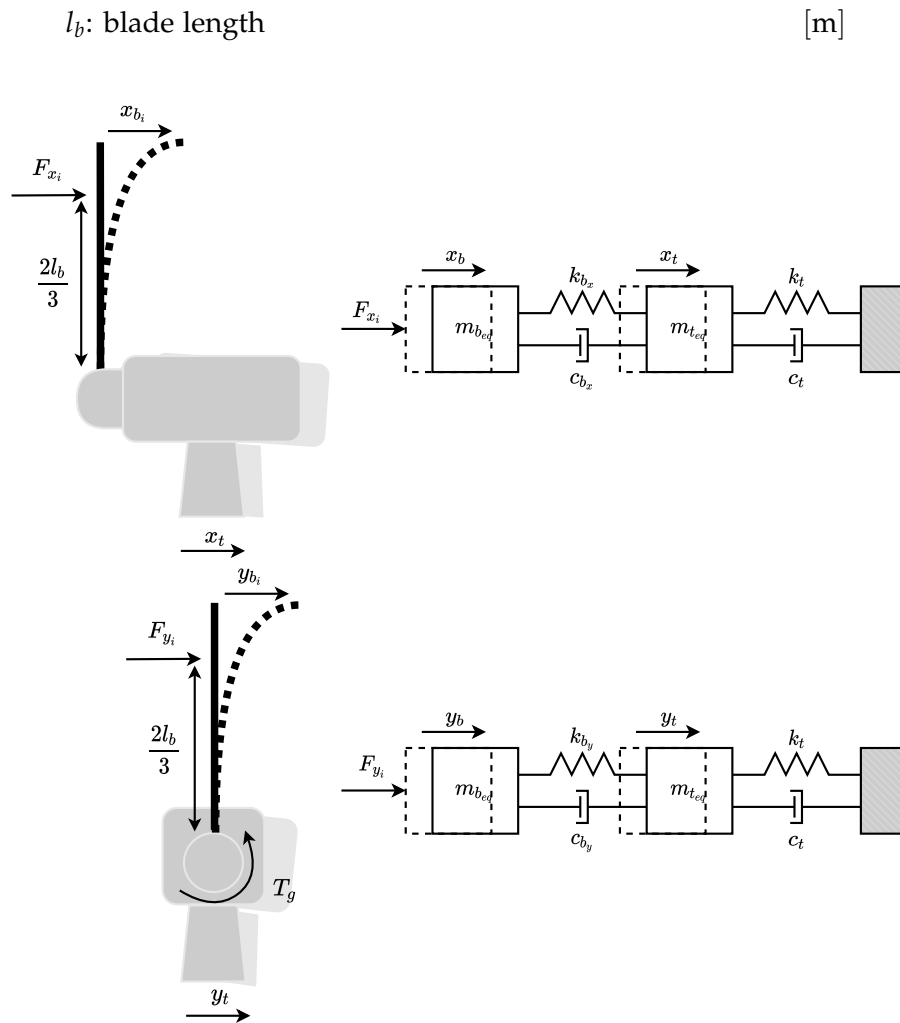


Figure 2.11: Tower and blade two mass spring damper models [37].

2.4.1 Tower model

Focusing solely on the tower for the moment and thus ignoring the effect of blade dynamics would result in the following rigid blade model for the fore-aft and sideways tower bending [17, 27]:

$$m_{t_{eq}} \ddot{x}_t = F_x - \frac{3}{2H} M_{tilt} - c_t \dot{x}_t - k_t x_t \tag{2.35}$$

$$m_{t_{eq}} \ddot{y}_t = -\frac{3}{2H} T_g - c_t \dot{y}_t - k_t y_t \tag{2.36}$$

where:

x_t & y_t : tower fore-aft and sideways top displacement [m]

c_t : tower damping	[N/(m/s)]
k_t : tower stiffness	[N/m]
F_x : rotor out-of-plane thrust force	[N]
M_{tilt} : aerodynamic tilt moment	[Nm]
T_g : generator torque	[Nm]

The term $\frac{3}{2H}$ refers to the ratio between displacement and rotation of the fore-aft tower motion approximated by the motion of a prismatic beam of length H subjected to a bending force load. The aerodynamic tilt moment M_{tilt} is the torque component along the y -axis due to blade asymmetry, found out in Appendix A.4 as a result of applying the Coleman transform to the flapwise blade root bending moments.

The aerodynamic tilt moment M_{tilt} is considered to have a minor effect in comparison with the out-of-plane thrust force F_x , hence, the tower model is rewritten as:

$$m_{teq}\ddot{x}_t = F_x - c_t\dot{x}_t - k_tx_t \quad (2.37)$$

$$m_{teq}\ddot{y}_t = -\frac{3}{2H}T_g - c_t\dot{y}_t - k_ty_t \quad (2.38)$$

2.4.2 Tower and blade model

As the blades are attached to the tower, their dynamics should be considered when describing the tower movement. Apart from the out-of-plane thrust force F_x , which now affects the blade dynamics instead of directly affecting the tower, an in-plane thrust force F_y needs to be included to account for the effect of the wind on each individual blade in the rotor plane. This in-plane thrust force is basically the aerodynamic torque decomposed in three individual forces on each blade, and therefore will only be included when dealing with IPC, as in CPC they would cancel each other.

In CPC, the three blades would be accounted as a single entity with one DOF, and therefore the tower and blade model will be as follows [37]:

$$m_{teq}\ddot{x}_t = Bk_{b_x}(x_b - x_t) + Bc_{b_x}(\dot{x}_b - \dot{x}_t) - k_tx_t - c_t\dot{x}_t \quad (2.39)$$

$$Bm_{beq}\ddot{x}_b = F_x - Bk_{b_x}(x_b - x_t) - Bc_{b_x}(\dot{x}_b - \dot{x}_t) \quad (2.40)$$

$$m_{teq}\ddot{y}_t = -\frac{3}{2H}T_g + Bk_{b_y}(y_b - y_t) + Bc_{b_y}(\dot{y}_b - \dot{y}_t) - k_ty_t - c_t\dot{y}_t \quad (2.41)$$

$$Bm_{beq}\ddot{y}_b = -Bk_{b_y}(y_b - y_t) - Bc_{b_y}(\dot{y}_b - \dot{y}_t) \quad (2.42)$$

where:

x_b & y_b : blade flapwise and edgewise top displacement	[m]
c_{b_x} : blade damping flapwise	[N/(m/s)]
c_{b_y} : blade damping edgewise	[N/(m/s)]

k_{b_x} : blade stiffness flapwise	[N/m]
k_{b_y} : blade stiffness edgewise	[N/m]
B : total number of blades	[·]

If it was desired to use a more precise model, the effect that the centrifugal forces have on the stiffness of the blades could be considered. This creates the following relationship between the angular speed of the rotor ω_r and the blade stiffness parameter k_b :

$$k_b(\omega_r) = \alpha_b m_{b_{eq}} r_b \omega_r^2 \quad (2.43)$$

where:

r_b : distance from the blade root to the blade centre of mass	[m]
α_b : blade stiffness tuning parameter	[·]

It has been decided not to use this relationship for simplification purposes.

In IPC, three DOF should be used to account for the flapwise motion of each individual blade depending on the wind speed they come across at each angular position. In that case, the tower and blade model would be:

$$m_{t_{eq}} \ddot{x}_t = \sum_i [k_{b_x}(x_{b_i} - x_t)] + \sum_i [c_{b_x}(\dot{x}_{b_i} - \dot{x}_t)] - k_t x_t - c_t \dot{x}_t \quad (2.44)$$

$$m_{b_{eq}} \ddot{x}_{b_i} = F_{x_i} - k_{b_x}(x_{b_i} - x_t) - c_{b_x}(\dot{x}_{b_i} - \dot{x}_t) \quad (2.45)$$

$$m_{t_{eq}} \ddot{y}_t = -\frac{3}{2H} T_g + \sum_i [k_{b_y}(y_{b_i} - y_t)] + \sum_i [c_{b_y}(\dot{y}_{b_i} - \dot{y}_t)] - k_t y_t - c_t \dot{y}_t \quad (2.46)$$

$$m_{b_{eq}} \ddot{y}_{b_i} = -F_{y_i} - k_{b_y}(y_{b_i} - y_t) - c_{b_y}(\dot{y}_{b_i} - \dot{y}_t) \quad (2.47)$$

with F_{y_i} referring to the individual blade in-plane thrust force and the subindex $i \in \{0, 1, 2\}$ indicating that the corresponding variable is related to each individual blade.

The values of the stiffness and damping parameters k_{b_x} , k_{b_y} , c_{b_x} and c_{b_y} are found out by using the results of the modal analysis (Table 1.1). The equation of motion for the flapwise and sideways vibration of a viscously damped blade is given by:

$$m_{b_{eq}} \ddot{u} + c_b \dot{u} + k_b u = F \quad (2.48)$$

where F refers to the excitation to the system. Dividing by the mass results in the following:

$$\ddot{u} + 2\zeta_b \omega_b \dot{u} + \omega_b^2 u = \frac{F}{m_{b_{eq}}} \quad (2.49)$$

where ζ_b refers to the damping ratio and ω_b corresponds to the natural pulsation, which are defined as:

$$\zeta_b = \frac{c_b}{2m_{b_{eq}}\omega_b}, \quad \omega_b = \sqrt{\frac{k_b}{m_{b_{eq}}}} \quad (2.50)$$

Using the natural frequencies of the blade flapwise and edgewise normal modes and the corresponding damping ratios extracted from the modal analysis, it is possible to compute the stiffness and damping constants.

Generally, when IPC is being applied to a wind turbine, blade root sensors need to be installed for each blade. The blade root sensors measure the flapwise and edgewise bending moments M_{y_i} and M_{x_i} at the root of each blade, which can be related to the blade displacement by:

$$M_{y_i} = x_{b_i} k_{b_x} \frac{2l_b}{3} \quad (2.51)$$

$$M_{x_i} = y_{b_i} k_{b_y} \frac{2l_b}{3} \quad (2.52)$$

where l_b refers to the blade length and thus, the term $\frac{2l_b}{3}$ refers to the distance from the blade root to the application point of the thrust forces.

2.5 Drive Train Model

The drive train of the wind turbine transfers the rotor's torque to the electrical generator. There are two different kinds of drive train designs; direct- or gearbox-drive. Modelling-wise, the main difference between these two is the gearbox ratio (N_d). For a direct drive train it is considered to be 1, as the synchronous generator is directly powered by the rotor, while for a gearbox drive it depends on the turbines specifications.

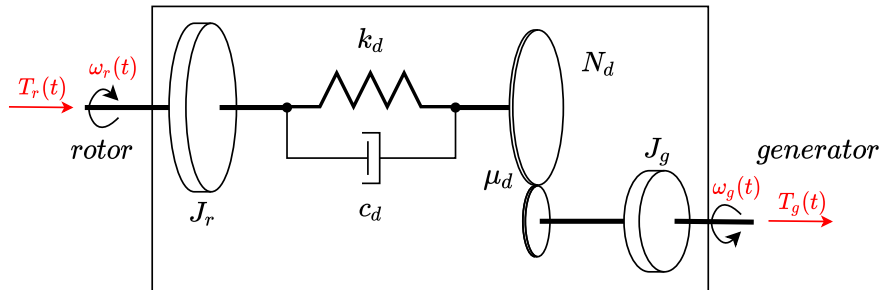


Figure 2.12: Drive train model

For modelling the gearbox drive train, a simple mass-spring-damper will be used for dealing with the drive train torsion DOF, considering this way the model flexibility in the form of stiffness and damping [19].

$$J_r \dot{\omega}_r = (1 - \mu_d) T_r - c_d \dot{\gamma} - k_d \gamma \quad (2.53)$$

$$J_g \dot{\omega}_g = c_d \dot{\gamma} + k_d \gamma - T_g \quad (2.54)$$

$$\dot{\gamma} = \omega_r - \omega_g \quad (2.55)$$

where:

T_r : aerodynamic torque	[Nm]
T_g : generator torque	[Nm]
J_r : rotor inertia	[kgm ²]
J_g : generator inertia	[kgm ²]
N_d : gearbox ratio	[.]
ω_r : rotational speed of the rotor	[rad/s]
ω_g : rotational speed of the generator	[rad/s]
c_d : drive train damping	[Nms/rad]
k_d : drive train stiffness	[Nm/rad]
μ_d : mechanical losses	[.]

Therefore:

$$\ddot{\gamma} = \frac{1}{J_r} [(1 - \mu_d) T_r - c_d \dot{\gamma} - k_d \gamma] - \frac{1}{J_g} (c_d \dot{\gamma} + k_d \gamma - T_g) \quad (2.56)$$

Rearranging the expression:

$$\frac{J_r J_g}{(J_g + J_r)} \ddot{\gamma} = \frac{J_g}{(J_g + J_r)} (1 - \mu_d) T_r - c_d \dot{\gamma} - k_d \gamma + \frac{J_r}{(J_g + J_r)} T_g \quad (2.57)$$

If the wind turbine is considered to be a direct drive wind turbine, the flexibility of the model can be assumed negligible and thus the generator speed, ω_g , would be equal to the rotor speed, ω_r . This rigid model would then be expressed as:

$$(J_r + J_g) \dot{\omega}_r = (1 - \mu_d) T_r - T_g \quad (2.58)$$

If the individual blades are considered for IPC, then the aerodynamic torque can be rewritten as seen in Section 2.3:

$$(J_r + J_g) \dot{\omega}_r = (1 - \mu_d) \sum_i -y_{b_i} k_{b_y} \frac{2l_b}{3} - T_g \quad (2.59)$$

with $i \in \{0, 1, 2\}$.

The generator electrical power can be expressed as:

$$P_e = \eta_g T_g \omega_g \quad (2.60)$$

with η_g referring to the generator efficiency.

2.6 Actuator Models

In order to model the response of the generator counter torque and pitch angle change, a first and second order system are used for each respective actuator.

2.6.1 Pitch actuator model

The pitch of the wind turbine blades can be controlled by an electric or hydraulic servo system. The first type is considered hereafter. Electric pitch actuators are commonly driven by a DC-motor or a vector controlled permanent magnet synchronous machine. For the pitch control design, the basic dynamics can be approximated by a 2nd order system [27]:

$$\ddot{\theta} = \omega_{\theta}^2 \theta_{ref} - 2\omega_{\theta} \zeta_{\theta} \dot{\theta} - \omega_{\theta}^2 \theta \quad (2.61)$$

This model can be expressed in the Laplace domain as follows:

$$\frac{\Theta(s)}{\Theta_{ref}(s)} = \frac{\omega_{\theta}^2}{s^2 + 2\omega_{\theta} \zeta_{\theta} s + \omega_{\theta}^2} \quad (2.62)$$

The undamped natural frequency ω_{θ} has a value of 1.2 Hz, and the damping factor ζ_{θ} is 0.8. The pitch position range goes from 0° to 90° , while the pitch rate limits are $-9^{\circ}/s$ and $9^{\circ}/s$ according to the GH Bladed model.

2.6.2 Generator model

Variable speed wind turbines equipped with a gearbox commonly present an electric conversion system consisting of a double fed asynchronous machine, power electronics and control loops for the desired generator torque and reactive power in the stator of the machine. On the other hand, direct drive wind turbines generally present conversion system based on a permanent magnet synchronous machine. In order to represent the essential dynamics, the model can be approximated by a 1st order system with a certain time constant [27]:

$$\dot{T}_g = \frac{T_{gref} - T_g}{\tau_g} \quad (2.63)$$

which can be written in the Laplace domain as:

$$\frac{T_g(s)}{T_{gref}(s)} = \frac{1}{\tau_g s + 1} \quad (2.64)$$

Based on the data provided by the GH Bladed model, the generator has a time constant of 0.001 s, a minimum demanded torque of 1 Nm and a maximum demanded torque of 2.159×10^7 Nm.

2.7 State Estimation With UKF

An important aspect of implementing MPC is the estimation of the states of the system. Estimation will be done through the use of a Kalman filter. As the turbine model is non-linear, the decision has been made to implement an UKF, as it has similar computational

complexity to the Extended Kalman Filter (EKF), but is either as efficient or potentially better at estimating states in a non-linear system. The UKF uses Unscented Transform (UT), which picks a number of weighted samples, called sigma points, and propagates them through the non-linear state transition and measurement functions to get the *a priori* state and measurement prediction respectively. These are subsequently used to calculate the *a posteriori* state estimate. The noise for both state and measurement will be considered to be additive, as sensor noise is listed in their respective documentation as being stochastic with a constant variance. The Kalman filter has similarities to observer based control in that unknown states have to be estimated based on a series of measurements. Figure 2.13 shows how the error between true output and output estimated based on expected model parameters is used to tweak future state estimates through the Kalman feedback gain, which is also recursively calculated.

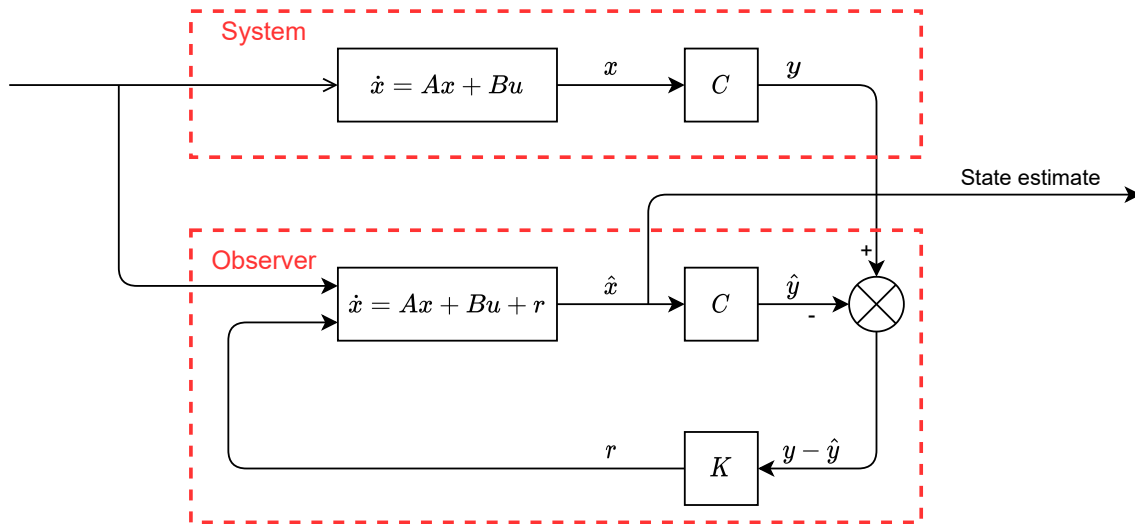


Figure 2.13: General block diagram of the Kalman principle

2.7.1 Choosing weights and sigma points

There are different sampling strategies for choosing the sigma points and weights. The approach used in Scaled Unscented Transform will be outlined here[38]. The first sigma point is defined as $\mathcal{X}_{k-1}^{(0)} = \hat{x}_{k-1}$. The number of sigma points are chosen according to the number of dimensions in the input distribution. For every dimension, two additional points should be added. This means that the total number of sigma points will be $2n + 1$ where n is the number of dimensions. The remaining $2n$ sigma points should be chosen such that they are equally and symmetrically distributed around the mean. The procedure for choosing sigma points is shown below:

$$\mathcal{X}_{k-1}^{(0)} = \hat{x}_{k-1} \quad (2.65)$$

$$\mathcal{X}_{k-1}^{(i)} = \hat{x}_{k-1} + \sqrt{(n + \lambda)} c_i \quad 1 \leq i \leq n \quad (2.66)$$

$$\mathcal{X}_{k-1}^{(n+i)} = \hat{x}_{k-1} - \sqrt{(n + \lambda)} c_i \quad 1 \leq i \leq n \quad (2.67)$$

$$\mathcal{X}_{k-1} = [\mathcal{X}_{k-1}^{(0)} \quad \mathcal{X}_{k-1}^{(i)} \quad \mathcal{X}_{k-1}^{(n+i)}] \quad (2.68)$$

where:

λ : scaling parameter to be defined

c_i : i 'th column of a lower Cholesky factor of P_{k-1}

n : dimension of the state space

$\mathcal{X}_{k-1}^{(i)}$: the i 'th untransformed sigma point

\hat{x}_{k-1} : last iteration's state estimate

P_{k-1} : last iterations *a posteriori* state covariance

Weights will be designated for calculating the mean and covariance of the state and measurement predictions as shown below:

$$W_0^m = \frac{\lambda}{n + \lambda} \quad (2.69)$$

$$W_0^c = W_0^m + (1 - \alpha^2 + \beta) \quad (2.70)$$

$$W_i = \frac{1}{2(n + \lambda)} \quad 1 \leq i \leq 2n \quad (2.71)$$

$$W^c = [W_0^c \quad W_i] \quad (2.72)$$

$$W^m = [W_0^m \quad W_i] \quad (2.73)$$

where:

W^m : additional weight for the estimated state mean

W^c : additional weight for the estimated state covariance

W_i : i 'th weight for the i 'th sigma point

κ, α, β : adjustable scaling parameters

Note that W^c and W^m become vectors of length $2n + 1$.

2.7.2 Choosing free parameters

There is no unique solution to the UKF due to the free parameters α , β and κ . These parameters can be tweaked to adjust the outcome. α is used to scale the spread of the sigma points around the mean. A demonstration for a two-dimensional Gaussian distribution can be seen in Figure 2.14.

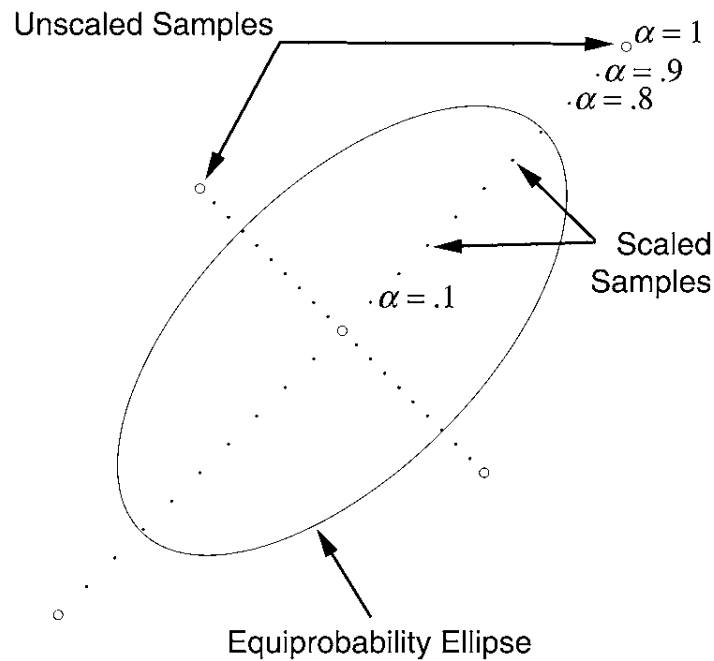


Figure 2.14: Effects on alpha on the spread of the sigma points [38]

The value of κ alters the influence that the state estimate \hat{x} has on calculating the output estimate \hat{y} and covariance P^{yy} . It should be ensured that $\kappa \geq 0$, as otherwise P^{yy} might not be positive definite. β is used to calculate different weights for \hat{y} and P^{yy} . α should be greater than 0 but no larger than 1. α and κ can be combined into one variable λ . Based on [38], the following values are chosen as a starting point:

$$\begin{aligned}\alpha &= 1 \\ \beta &= 2 \\ \kappa &= 0 \\ \lambda &= \alpha^2(n + \kappa) - n\end{aligned}$$

2.7.3 Procedure

For calculating the *a priori* state prediction, the sigma points \mathcal{X}_{k-1} are propagated through the non-linear state transition function to get the transformed sigma points $\mathcal{X}_{k|k-1}$:

$$\mathcal{X}_{k|k-1} = f(\mathcal{X}_{k-1}, u_{k-1}) \quad (2.74)$$

The mean and covariance of the *a priori* state prediction, which are used in calculating the mean and covariance of the *a posteriori* state estimate, can now be calculated with the

weights defined in Equations 2.72 and 2.73 and the transformed sigma points:

$$\hat{x}_{k|k-1} = \sum_{i=1}^{2n+1} W^m(i) \mathcal{X}_{k|k-1}^{(i)} \quad (2.75)$$

$$P_{k|k-1} = Q_{k-1} + \sum_{i=1}^{2n+1} W^c(i) (\mathcal{X}_{k|k-1}^{(i)} - \hat{x}_{k|k-1})(\mathcal{X}_{k|k-1}^{(i)} - \hat{x}_{k|k-1})^T \quad (2.76)$$

where:

Q_{k-1} : process noise covariance

$\hat{x}_{k|k-1}$: mean of *a priori* state prediction

$P_{k|k-1}$: covariance of *a priori* state prediction

The transformed sigma points are then propagated through the measurement function:

$$\psi_{k|k-1} = h(\mathcal{X}_{k|k-1}, u_k) \quad (2.77)$$

The mean and covariance of the *a priori* measurement prediction are then calculated:

$$\hat{y}_{k|k-1} = \sum_{i=1}^{2n+1} W^m(i) \psi_{k|k-1}^{(i)} \quad (2.78)$$

$$P_k^{yy} = R + \sum_{i=1}^{2n+1} W^c(i) (\psi_{k|k-1}^{(i)} - \hat{y}_{k|k-1})(\psi_{k|k-1}^{(i)} - \hat{y}_{k|k-1})^T \quad (2.79)$$

where:

R : measurement noise covariance

$\hat{y}_{k|k-1}$: mean of *a priori* measurement prediction

P_k^{yy} : covariance of *a priori* measurement prediction

Before calculating the Kalman gain, the cross-covariance of the *a priori* state and measurement P_k^{xy} must be calculated:

$$P_k^{xy} = \sum_{i=1}^{2n+1} W^c(i) (\mathcal{X}_{k|k-1}^{(i)} - \hat{x}_{k|k-1})(\psi_{k|k-1}^{(i)} - \hat{y}_{k|k-1})^T \quad (2.80)$$

Calculating the Kalman gain for the *a posteriori* state estimate:

$$K_k = P_k^{xy} (P_k^{yy})^{-1} \quad (2.81)$$

The mean and covariance of the *a posteriori* state estimate can now be updated:

$$\hat{x}_k = \hat{x}_{k|k-1} + K_k (y_k - \hat{y}_{k|k-1}) \quad (2.82)$$

$$P_k = P_{k|k-1} - K_k P_k^{yy} K_k^T \quad (2.83)$$

where:

- \hat{x}_k : mean of *a posteriori* state estimate
- P_k : covariance of *a posteriori* state estimate
- y_k : measurement of true state

The algorithm is run recursively with P_k being used to form next iteration's Cholesky factor [39].

2.8 Linearized Model

There exist multiple versions of MPC depending on the type of model available. In this project it has been decided to implement linear MPC due to its advantages regarding computational efficiency and well addressed stability. However, it is then required to linearise the non-linear model around its operating points, which vary with time. The following derivations detail a Taylor series expansion used to find the linear approximations. It has been decided to use directly the IPC model, as it is the one which would allow the MPC to account for structural load minimisation.

As seen in Section 2.5, the drive train model can be expressed as:

$$(J_r + J_g) \dot{\omega}_r = (1 - \mu_d) T_r - T_g \quad (2.84)$$

Inserting the expression for T_r and rearranging the expression:

$$\dot{\omega}_r = -\frac{(1 - \mu_d) 2k_{b_y} l_b}{3(J_r + J_g)} \sum_i y_{b_i} - \frac{T_g}{J_r + J_g} \quad (2.85)$$

which is linear and thus can be expressed as:

$$\Delta \dot{\omega}_r = -\frac{(1 - \mu_d) 2k_{b_y} l_b}{3(J_r + J_g)} \sum_i \Delta y_{b_i} - \frac{1}{(J_r + J_g)} \Delta T_g \quad (2.86)$$

The tower and blade model was developed in Section 2.4 as:

$$\ddot{x}_t = \frac{k_{b_x}}{m_{t_{eq}}} \sum_i (x_{b_i} - x_t) + \frac{c_{b_x}}{m_{t_{eq}}} \sum_i (\dot{x}_{b_i} - \dot{x}_t) - \frac{k_t}{m_{t_{eq}}} x_t - \frac{c_t}{m_{t_{eq}}} \dot{x}_t \quad (2.87)$$

$$\ddot{x}_{b_i} = \frac{F_{x_i}}{m_{b_{eq}}} - \frac{k_{b_x}}{m_{b_{eq}}} (x_{b_i} - x_t) - \frac{c_{b_x}}{m_{b_{eq}}} (\dot{x}_{b_i} - \dot{x}_t) \quad (2.88)$$

$$\dot{y}_t = -\frac{3}{2Hm_{t_{eq}}} T_g + \frac{k_{b_y}}{m_{t_{eq}}} \sum_i (y_{b_i} - y_t) + \frac{c_{b_y}}{m_{t_{eq}}} \sum_i (\dot{y}_{b_i} - \dot{y}_t) - \frac{k_t}{m_{t_{eq}}} y_t - \frac{c_t}{m_{t_{eq}}} \dot{y}_t \quad (2.89)$$

$$\ddot{y}_{b_i} = -\frac{F_{y_i}}{m_{b_{eq}}} - \frac{k_{b_y}}{m_{b_{eq}}} (y_{b_i} - y_t) - \frac{c_{b_y}}{m_{b_{eq}}} (\dot{y}_{b_i} - \dot{y}_t) \quad (2.90)$$

Equations 2.87 and 2.89 are linear and therefore can be simply rewritten as:

$$\Delta \ddot{x}_t = \frac{k_{b_x}}{m_{t_{eq}}} \sum_i \Delta x_{b_i} + \frac{c_{b_x}}{m_{t_{eq}}} \sum_i \Delta \dot{x}_{b_i} - \left(B \frac{k_{b_x}}{m_{t_{eq}}} + \frac{k_t}{m_{t_{eq}}} \right) \Delta x_t - \left(B \frac{c_{b_x}}{m_{t_{eq}}} + \frac{c_t}{m_{t_{eq}}} \right) \Delta \dot{x}_t \quad (2.91)$$

$$\begin{aligned} \Delta \ddot{y}_t = & -\frac{3}{2Hm_{t_{eq}}} \Delta T_g + \frac{k_{b_y}}{m_{t_{eq}}} \sum_i \Delta y_{b_i} + \frac{c_{b_y}}{m_{t_{eq}}} \sum_i \Delta \dot{y}_{b_i} - \left(B \frac{k_{b_y}}{m_{t_{eq}}} + \frac{k_t}{m_{t_{eq}}} \right) \Delta y_t \\ & - \left(B \frac{c_{b_y}}{m_{t_{eq}}} + \frac{c_t}{m_{t_{eq}}} \right) \Delta \dot{y}_t \end{aligned} \quad (2.92)$$

Conversely, Eqs. 2.88 and 2.90 need to be linearised, which is not straightforward. By substituting v_{r_i} by its expression considering wind shear and tower shadow as seen in Section 2.2, as well as F_{x_i} by the expression derived in Section 2.3, Eq. 2.88 is rewritten as:

$$\begin{aligned} \ddot{x}_{b_i} = & \frac{\rho A_r C_t}{2Bm_{b_{eq}}} \left[v_m r_t^2 \frac{R^2 \sin^2 \psi - x_h^2}{(x_h^2 + R^2 \sin^2 \psi)^2} + v_m \left(\frac{R \cos \psi + H}{H} \right)^\alpha + v_t - \dot{x}_t - \dot{x}_{b_i} \right]^2 \\ & - \frac{k_{b_x}}{m_{b_{eq}}} (x_{b_i} - x_t) - \frac{c_{b_x}}{m_{b_{eq}}} (\dot{x}_{b_i} - \dot{x}_t) \end{aligned} \quad (2.93)$$

Note that the thrust coefficient $C_t(\lambda_i, \theta_i)$ is written as just C_t from now on for simplicity, but always taking into account its dependency on θ_i and λ_i , which in turn depends on ω_r , \dot{y}_{b_i} , v_m , v_t , \dot{x}_t and \dot{x}_{b_i} . The same will be done for the power coefficient, C_p . Furthermore, and due to the complexity of the following expressions, the relative wind speed seen by each blade with all of its variables set in the corresponding operating points will be kept as $v_{r_i}^*$. All in all, the Taylor expansion results in the following:

$$\begin{aligned}
\Delta \ddot{x}_{b_i} = & -\frac{k_{b_x}}{m_{b_{eq}}} \Delta x_{b_i} + \left[\frac{\rho A_r}{2Bm_{b_{eq}}} \left(\frac{\partial C_t}{\partial \dot{x}_{b_i}} \Big|_{eq.} v_{r_i}^{*2} - 2C_t^* v_{r_i}^* \right) - \frac{c_{b_x}}{m_{b_{eq}}} \right] \Delta \dot{x}_{b_i} \\
& + \frac{k_{b_x}}{m_{b_{eq}}} \Delta x_t + \left[\frac{\rho A_r}{2Bm_{b_{eq}}} \left(\frac{\partial C_t}{\partial \dot{x}_t} \Big|_{eq.} v_{r_i}^{*2} - 2C_t^* v_{r_i}^* \right) + \frac{c_{b_x}}{m_{b_{eq}}} \right] \Delta \dot{x}_t \\
& + \frac{\rho A_r}{2Bm_{b_{eq}}} \left[\frac{\partial C_t}{\partial v_m} \Big|_{eq.} v_{r_i}^{*2} + 2C_t^* \left(r_t^2 \frac{R^2 \sin^2 \psi^* - x_h^2}{(x_h^2 + R^2 \sin^2 \psi^*)^2} + \left(\frac{R \cos \psi^* + H}{H} \right)^\alpha \right) v_{r_i}^* \right] \Delta v_m \\
& + \frac{\rho A_r}{2Bm_{b_{eq}}} \left[\frac{\partial C_t}{\partial v_t} \Big|_{eq.} v_{r_i}^{*2} + 2C_t^* v_{r_i}^* \right] \Delta v_t + \frac{\rho v_{r_i}^{*2} A_r}{2Bm_{b_{eq}}} \frac{\partial C_t}{\partial \theta_i} \Big|_{eq.} \Delta \theta_i + \frac{\rho v_{r_i}^{*2} A_r}{2Bm_{b_{eq}}} \frac{\partial C_t}{\partial \dot{y}_{b_i}} \Big|_{eq.} \Delta \dot{y}_{b_i} \\
& + \frac{\rho A_r}{2Bm_{b_{eq}}} \left[C_t^* 2v_m^* \left[r_t^2 \frac{(2R^2 \cos \psi^* \sin \psi^*) (x_h^2 + R^2 \sin^2 \psi^*)^2}{(x_h^2 + R^2 \sin^2 \psi^*)^4} \right. \right. \\
& \left. \left. - r_t^2 \frac{(R^2 \sin^2 \psi^* - x_h^2) 2(2R^2 \cos \psi^* \sin \psi^*) (x_h^2 + R^2 \sin^2 \psi^*)}{(x_h^2 + R^2 \sin^2 \psi^*)^4} \right] \right. \\
& \left. + \alpha \left(\frac{-R \sin \psi^*}{H} \right) \left(\frac{R \cos \psi^* + H}{H} \right)^{\alpha-1} \right] v_{r_i}^* + \frac{\partial C_t}{\partial \psi} \Big|_{eq.} v_{r_i}^{*2} \Big] \Delta \psi + \frac{\rho v_{r_i}^{*2} A_r}{2Bm_{b_{eq}}} \frac{\partial C_t}{\partial \omega_r} \Big|_{eq.} \Delta \omega_r
\end{aligned} \tag{2.94}$$

where:

$$\frac{\partial C_t}{\partial \dot{x}_{b_i}} \Big|_{eq.} = \frac{\partial C_t}{\partial \lambda} \Big|_{eq.} \frac{\partial \lambda}{\partial \dot{x}_{b_i}} \Big|_{eq.} = \frac{\partial C_t}{\partial \lambda} \Big|_{eq.} \frac{\omega_r^* R - \dot{y}_{b_i}^*}{v_{r_i}^{*2}} \tag{2.95}$$

$$\frac{\partial C_t}{\partial \dot{x}_t} \Big|_{eq.} = \frac{\partial C_t}{\partial \lambda} \Big|_{eq.} \frac{\partial \lambda}{\partial \dot{x}_t} \Big|_{eq.} = \frac{\partial C_t}{\partial \lambda} \Big|_{eq.} \frac{\omega_r^* R - \dot{y}_{b_i}^*}{v_{r_i}^{*2}} \tag{2.96}$$

$$\begin{aligned}
\frac{\partial C_t}{\partial v_m} \Big|_{eq.} = \frac{\partial C_t}{\partial \lambda} \Big|_{eq.} \frac{\partial \lambda}{\partial v_m} \Big|_{eq.} = \frac{\partial C_t}{\partial \lambda} \Big|_{eq.} \frac{-(\omega_r^* R - \dot{y}_{b_i}^*)}{v_{r_i}^{*2}} \left(r_t^2 \frac{R^2 \sin^2 \psi^* - x_h^2}{(x_h^2 + R^2 \sin^2 \psi^*)^2} \right. \\
\left. + \left(\frac{R \cos \psi^* + H}{H} \right)^\alpha \right)
\end{aligned} \tag{2.97}$$

$$\frac{\partial C_t}{\partial v_t} \Big|_{eq.} = \frac{\partial C_t}{\partial \lambda} \Big|_{eq.} \frac{\partial \lambda}{\partial v_t} \Big|_{eq.} = \frac{\partial C_t}{\partial \lambda} \Big|_{eq.} \frac{-(\omega_r^* R - \dot{y}_{b_i}^*)}{v_{r_i}^{*2}} \tag{2.98}$$

$$\frac{\partial C_t}{\partial \dot{y}_{b_i}} \Big|_{eq.} = \frac{\partial C_t}{\partial \lambda} \Big|_{eq.} \frac{\partial \lambda}{\partial \dot{y}_{b_i}} \Big|_{eq.} = \frac{\partial C_t}{\partial \lambda} \Big|_{eq.} \frac{-1}{v_{r_i}^*} \tag{2.99}$$

$$\begin{aligned}
\left. \frac{\partial C_t}{\partial \psi} \right|_{eq.} &= \left. \frac{\partial C_t}{\partial \lambda} \right|_{eq.} \left. \frac{\partial \lambda}{\partial \psi} \right|_{eq.} = \left. \frac{\partial C_t}{\partial \lambda} \right|_{eq.} \frac{-(\omega_r^* R - \dot{y}_{b_i}^*)}{v_{r_i}^{*2}} v_m^* \left[r_t^2 \frac{(2R^2 \cos \psi^* \sin \psi^*) (x_h^2 + R^2 \sin^2 \psi^*)^2}{(x_h^2 + R^2 \sin^2 \psi^*)^4} \right. \\
&\quad \left. - r_t^2 \frac{(R^2 \sin^2 \psi^* - x_h^2) 2 (2R^2 \cos \psi^* \sin \psi^*) (x_h^2 + R^2 \sin^2 \psi^*)}{(x_h^2 + R^2 \sin^2 \psi^*)^4} \right. \\
&\quad \left. + \alpha \left(\frac{-R \sin \psi^*}{H} \right) \left(\frac{R \cos \psi^* + H}{H} \right)^{\alpha-1} \right]
\end{aligned} \tag{2.100}$$

$$\left. \frac{\partial C_t}{\partial \omega_r} \right|_{eq.} = \left. \frac{\partial C_t}{\partial \lambda} \right|_{eq.} \left. \frac{\partial \lambda}{\partial \omega_r} \right|_{eq.} = \left. \frac{\partial C_t}{\partial \lambda} \right|_{eq.} \frac{R}{v_{r_i}^*} \tag{2.101}$$

with $\left. \frac{\partial C_t}{\partial \lambda} \right|_{eq.}$ being computed from a lookup table. Note that the Taylor expansion has not been simplified to see more clearly whether each of the terms has been correctly derived from the corresponding partial derivatives.

Eq. 2.90 is also rewritten by substituting v_{r_i} and F_{y_i} by their corresponding expressions as follows:

$$\begin{aligned}
\dot{y}_{b_i} &= -\frac{3\rho A_r C_p}{4B m_{b_{eq}} \omega_r l_b} \left[v_m r_t^2 \frac{R^2 \sin^2 \psi - x_h^2}{(x_h^2 + R^2 \sin^2 \psi)^2} + v_m \left(\frac{R \cos \psi + H}{H} \right)^\alpha + v_t - \dot{x}_t - \dot{x}_{b_i} \right]^3 \\
&\quad - \frac{k_{b_y}}{m_{b_{eq}}} (y_{b_i} - y_t) - \frac{c_{b_y}}{m_{b_{eq}}} (\dot{y}_{b_i} - \dot{y}_t)
\end{aligned} \tag{2.102}$$

and subsequently linearised as:

$$\begin{aligned}
\Delta \dot{y}_{b_i} = & -\frac{k_{b_y}}{m_{b_{eq}}} \Delta y_{b_i} - \left(\frac{3\rho v_{r_i}^{*3} A_r}{4Bm_{b_{eq}} \omega_r^* l_b} \frac{\partial C_p}{\partial \dot{y}_{b_i}} \Big|_{eq.} + \frac{c_{b_y}}{m_{b_{eq}}} \right) \Delta \dot{y}_{b_i} \\
& + \frac{k_{b_y}}{m_{b_{eq}}} \Delta y_t + \frac{c_{b_y}}{m_{b_{eq}}} \Delta \dot{y}_t - \frac{3\rho A_r}{4Bm_{b_{eq}} \omega_r^* l_b} \left[\frac{\partial C_p}{\partial v_m} \Big|_{eq.} v_{r_i}^{*3} \right. \\
& \left. + 3C_p^* \left(r_t^2 \frac{R^2 \sin^2 \psi^* - x_h^2}{(x_h^2 + R^2 \sin^2 \psi^*)^2} + \left(\frac{R \cos \psi^* + H}{H} \right)^\alpha \right) v_{r_i}^{*2} \right] \Delta v_m \\
& - \frac{3\rho A_r}{4Bm_{b_{eq}} \omega_r^* l_b} \left[\frac{\partial C_p}{\partial v_t} \Big|_{eq.} v_{r_i}^{*3} + 3C_p^* v_{r_i}^{*2} \right] \Delta v_t - \frac{3\rho A_r}{4Bm_{b_{eq}} \omega_r^* l_b} \left[\frac{\partial C_p}{\partial \dot{x}_t} \Big|_{eq.} v_{r_i}^{*3} - 3C_p^* v_{r_i}^{*2} \right] \Delta \dot{x}_t \\
& - \frac{3\rho A_r}{4Bm_{b_{eq}} \omega_r^* l_b} \left[\frac{\partial C_p}{\partial \dot{x}_{b_i}} \Big|_{eq.} v_{r_i}^{*3} - 3C_p^* v_{r_i}^{*2} \right] \Delta \dot{x}_{b_i} - \frac{3\rho v_{r_i}^{*3} A_r}{4Bm_{b_{eq}} l_b} \left[\frac{\partial C_p}{\partial \omega_r} \Big|_{eq.} \frac{1}{\omega_r^*} - C_p^* \frac{1}{\omega_r^{*2}} \right] \Delta \omega_r \\
& - \frac{3\rho A_r}{4Bm_{b_{eq}} \omega_r^* l_b} \left[C_p^* 3v_m^* \left[r_t^2 \frac{(2R^2 \cos \psi^* \sin \psi^*) (x_h^2 + R^2 \sin^2 \psi^*)^2}{(x_h^2 + R^2 \sin^2 \psi^*)^4} \right. \right. \\
& \left. \left. - r_t^2 \frac{(R^2 \sin^2 \psi^* - x_h^2) (2R^2 \cos \psi^* \sin \psi^*) (x_h^2 + R^2 \sin^2 \psi^*)}{(x_h^2 + R^2 \sin^2 \psi^*)^4} \right] \right. \\
& \left. + \alpha \left(\frac{-R \sin \psi^*}{H} \right) \left(\frac{R \cos \psi^* + H}{H} \right)^{\alpha-1} \right] v_{r_i}^{*2} + \frac{\partial C_p}{\partial \psi} \Big|_{eq.} v_{r_i}^{*3} \Delta \psi \\
& - \frac{3\rho v_{r_i}^{*3} A_r}{4Bm_{b_{eq}} \omega_r^* l_b} \frac{\partial C_p}{\partial \theta_i} \Big|_{eq.} \Delta \theta_i
\end{aligned} \tag{2.103}$$

where the partial derivatives of C_p with respect of each corresponding variable can be computed analogously to the ones for C_t in the expression for $\Delta \dot{x}_{b_i}$.

The generated power was expressed in Section 2.5 as:

$$P_e = T_g \eta_g \omega_r \tag{2.104}$$

which can be linearised as:

$$\Delta P_e = \eta_g (\omega_r^* \Delta T_g + T_g^* \Delta \omega_r) \tag{2.105}$$

The relationship between blade root moments and blade deflections is already linear, and therefore it can be written as:

$$\Delta M_{y_i} = k_{b_x} \frac{2l_b}{3} \Delta x_{b_i} \tag{2.106}$$

$$\Delta M_{x_i} = k_{b_y} \frac{2l_b}{3} \Delta y_{b_i} \tag{2.107}$$

The turbulent part of the wind model was chosen in Section 2.2 as:

$$\dot{v}_t = -\omega_p v_t + \omega_p n_t \quad (2.108)$$

Using this continuous time formulation requires n_t to be interpreted as generalised continuous time white noise corresponding to a Wiener process with incremental variance σ_t^2 as defined in Section 2.2. For more information on stochastic differential equations and Wiener processes see [40].

Substituting the Kaimal spectrum peak frequency ω_p by its definition and extracting the variance out of the noise due to its dependency on v_m , the following is obtained:

$$\dot{v}_t = -\frac{v_m \pi}{2L} v_t + \frac{v_m \pi}{2L} \sigma_t e_t \quad (2.109)$$

where e_t is (generalised continuous time) white noise with autocorrelation function $\delta(t)$ (Dirac delta function). For simplification purposes, it will be assumed that the Kaimal spectrum frequency and noise variance depends on the constant mean wind speed μ_v instead of depending on the time varying mean wind speed v_m . This directly makes the expression linear:

$$\Delta \dot{v}_t = -\frac{\mu_v \pi}{2L} \Delta v_t \quad (2.110)$$

The mean wind speed was chosen as:

$$\dot{v}_m = n_m \quad (2.111)$$

where n_m is interpreted analogously to n_t , and presents an incremental variance of σ_m^2 , defined in Section 2.2. The previous differential equation has no dependency on the states, hence:

$$\Delta \dot{v}_m = 0 \quad (2.112)$$

The effective wind speed at the rotor measured in the nacelle is simply written as:

$$\Delta v_r = \Delta v_m + \Delta v_t - \Delta \dot{x}_t \quad (2.113)$$

Finally the actuator models are taken into account, starting with the pitch actuator, which is linear and therefore can be written as:

$$\Delta \ddot{\theta}_i = \omega_\theta^2 \Delta \theta_{i_{ref}} - 2\omega_\theta \zeta_\theta \Delta \dot{\theta}_i - \omega_\theta^2 \Delta \theta_i \quad (2.114)$$

and the same for the generator torque:

$$\Delta \dot{T}_g = \frac{\Delta T_{g_{ref}} - \Delta T_g}{\tau_g} \quad (2.115)$$

2.9 Linear Model in State Space Representation

The model has the following states, inputs, measured outputs and outputs to be controlled (see Section 4.3 for a justification on the chosen outputs to be controlled):

$$x = [\omega_r \ x_t \ \dot{x}_t \ y_t \ \dot{y}_t \ x_{b_i} \ \dot{x}_{b_i} \ y_{b_i} \ \dot{y}_{b_i} \ \theta_i \ \dot{\theta}_i \ T_g \ v_t \ v_m \ \psi]^T \quad (2.116)$$

$$u = [\theta_{i_{ref}} \ T_{g_{ref}}]^T \quad (2.117)$$

$$y = [\omega_r \ \dot{x}_t \ \dot{y}_t \ M_{y_i} \ M_{x_i} \ \theta_i \ P_e \ v_r \ \psi]^T \quad (2.118)$$

$$z = [\omega_r \ \dot{x}_t \ \dot{y}_t \ \dot{x}_{b_i} \ \dot{y}_{b_i} \ \lambda \ \theta_i \ \dot{\theta}_i \ P_e]^T \quad (2.119)$$

The model equations can be rearranged in state space form as follows:

$$\dot{x} = Ax + Bu = \begin{bmatrix} A_1 & A_2 \\ A_3 & A_4 \end{bmatrix} x + Bu \quad (2.120)$$

$$y = C_y x \quad (2.121)$$

$$z = C_z x \quad (2.122)$$

It is assumed that the system matrices remain constant throughout the control horizon of the MPC (see Sections 3.5 and 4.3 to find the definition and chosen value of this parameter respectively), and subsequently they are updated by changing the operating points of the linear model for the next iteration of the algorithm. The system matrix is defined as follows:

$$A_1 = \begin{bmatrix} 0 & 0 & 0 & 0 & 0 & 0 & 0 & -a_1 \\ 0 & 0 & 1 & 0 & 0 & 0 & 0 & 0 \\ 0 & -b_3 & -b_4 & 0 & 0 & b_1 & b_2 & 0 \\ 0 & 0 & 0 & 0 & 1 & 0 & 0 & 0 \\ 0 & 0 & 0 & -c_4 & -c_5 & 0 & 0 & c_2 \\ 0 & 0 & 0 & 0 & 0 & 0 & 1 & 0 \\ d_{10} & d_3 & d_4 & 0 & 0 & -d_1 & d_2 & 0 \\ 0 & 0 & 0 & 0 & 0 & 0 & 0 & 0 \end{bmatrix} \quad (2.123)$$

$$A_2 = \begin{bmatrix} 0 & 0 & 0 & -a_2 & 0 & 0 & 0 \\ 0 & 0 & 0 & 0 & 0 & 0 & 0 \\ 0 & 0 & 0 & 0 & 0 & 0 & 0 \\ 0 & 0 & 0 & 0 & 0 & 0 & 0 \\ c_3 & 0 & 0 & -c_1 & 0 & 0 & 0 \\ 0 & 0 & 0 & 0 & 0 & 0 & 0 \\ d_8 & d_7 & 0 & 0 & d_6 & d_5 & d_9 \\ 1 & 0 & 0 & 0 & 0 & 0 & 0 \end{bmatrix} \quad (2.124)$$

$$A_3 = \begin{bmatrix} -e_9 & 0 & -e_7 & e_3 & e_4 & 0 & -e_8 & -e_1 \\ 0 & 0 & 0 & 0 & 0 & 0 & 0 & 0 \\ 0 & 0 & 0 & 0 & 0 & 0 & 0 & 0 \\ 0 & 0 & 0 & 0 & 0 & 0 & 0 & 0 \\ 0 & 0 & 0 & 0 & 0 & 0 & 0 & 0 \\ 0 & 0 & 0 & 0 & 0 & 0 & 0 & 0 \\ 1 & 0 & 0 & 0 & 0 & 0 & 0 & 0 \end{bmatrix} \quad (2.125)$$

$$A_4 = \begin{bmatrix} -e_2 & -e_{11} & 0 & 0 & -e_6 & -e_5 & -e_{10} \\ 0 & 0 & 1 & 0 & 0 & 0 & 0 \\ 0 & -f_1 & -f_2 & 0 & 0 & 0 & 0 \\ 0 & 0 & 0 & -g_1 & 0 & 0 & 0 \\ 0 & 0 & 0 & 0 & -\omega_p & 0 & 0 \\ 0 & 0 & 0 & 0 & 0 & 0 & 0 \\ 0 & 0 & 0 & 0 & 0 & 0 & 0 \end{bmatrix} \quad (2.126)$$

where the constants a_{1-2} , b_{1-4} , c_{1-5} , d_{1-10} , e_{1-11} , f_{1-2} , g_1 represent the expressions shown below:

$$a_1 = \frac{(1 - \mu_d)2k_{b_y}l_b}{3(J_r + J_g)} \quad (2.127)$$

$$a_2 = \frac{1}{J_r + J_g} \quad (2.128)$$

$$b_1 = \frac{k_{b_x}}{m_{t_{eq}}} \quad (2.129)$$

$$b_2 = \frac{c_{b_x}}{m_{t_{eq}}} \quad (2.130)$$

$$b_3 = B \frac{k_{b_x}}{m_{t_{eq}}} + \frac{k_t}{m_{t_{eq}}} \quad (2.131)$$

$$b_4 = B \frac{c_{b_x}}{m_{t_{eq}}} + \frac{c_t}{m_{t_{eq}}} \quad (2.132)$$

$$c_1 = \frac{3}{2Hm_{t_{eq}}} \quad (2.133)$$

$$c_2 = \frac{k_{b_y}}{m_{t_{eq}}} \quad (2.134)$$

$$c_3 = \frac{c_{b_y}}{m_{t_{eq}}} \quad (2.135)$$

$$c_4 = B \frac{k_{b_y}}{m_{t_{eq}}} + \frac{k_t}{m_{t_{eq}}} \quad (2.136)$$

$$c_5 = B \frac{c_{b_y}}{m_{t_{eq}}} + \frac{c_t}{m_{t_{eq}}} \quad (2.137)$$

$$d_1 = \frac{k_{b_x}}{m_{b_{eq}}} \quad (2.138)$$

$$d_2 = \frac{\rho A_r}{2Bm_{b_{eq}}} \left(\left. \frac{\partial C_t}{\partial \dot{x}_{b_i}} \right|_{eq.} v_{r_i}^{*2} - 2C_t^* v_{r_i}^* \right) - \frac{c_{b_x}}{m_{b_{eq}}} \quad (2.139)$$

$$d_3 = \frac{k_{b_x}}{m_{b_{eq}}} \quad (2.140)$$

$$d_4 = \frac{\rho A_r}{2Bm_{b_{eq}}} \left(\left. \frac{\partial C_t}{\partial \dot{x}_t} \right|_{eq.} v_{r_i}^{*2} - 2C_t^* v_{r_i}^* \right) + \frac{c_{b_x}}{m_{b_{eq}}} \quad (2.141)$$

$$d_5 = \frac{\rho A_r}{2Bm_{b_{eq}}} \left[\left. \frac{\partial C_t}{\partial v_m} \right|_{eq.} v_{r_i}^{*2} + 2C_t^* \left(r_t^2 \frac{R^2 \sin \psi^{*2} - x_h^2}{(x_h^2 + R^2 \sin \psi^{*2})^2} + \left(\frac{R \cos \psi^* + H}{H} \right)^\alpha \right) v_{r_i}^* \right] \quad (2.142)$$

$$d_6 = \frac{\rho A_r}{2Bm_{b_{eq}}} \left[\left. \frac{\partial C_t}{\partial v_t} \right|_{eq.} v_{r_i}^{*2} + 2C_t^* v_{r_i}^* \right] \quad (2.143)$$

$$d_7 = \frac{\rho v_{r_i}^{*2} A_r}{2Bm_{b_{eq}}} \left. \frac{\partial C_t}{\partial \theta_i} \right|_{eq.} \quad (2.144)$$

$$d_8 = \frac{\rho v_{r_i}^{*2} A_r}{2Bm_{b_{eq}}} \left. \frac{\partial C_t}{\partial \dot{y}_{b_i}} \right|_{eq.} \quad (2.145)$$

$$d_9 = \frac{\rho A_r}{2Bm_{b_{eq}}} \left[C_t^* 2v_m^* \left[\frac{r_t^2 \left(x_h^2 + R^2 \sin \psi^{*2} \right)^2 (2R^2 \cos \psi^* \sin \psi^*)}{(x_h^2 + R^2 \sin \psi^{*2})^4} - r_t^2 \frac{(R^2 \sin \psi^{*2} - x_h^2) 2 (2R^2 \cos \psi^* \sin \psi^*) (x_h^2 + R^2 \sin \psi^{*2})}{(x_h^2 + R^2 \sin \psi^{*2})^4} + \alpha \left(\frac{-R \sin \psi^*}{H} \right) \left(\frac{R \cos \psi^* + H}{H} \right)^{\alpha-1} \right] v_{r_i}^* + \left. \frac{\partial C_t}{\partial \psi} \right|_{eq.} v_{r_i}^{*2} \right] \quad (2.146)$$

$$d_{10} = \frac{\rho v_{r_i}^{*2} A_r}{2Bm_{b_{eq}}} \left. \frac{\partial C_t}{\partial \omega_r} \right|_{eq.} \quad (2.147)$$

$$e_1 = \frac{k_{b_y}}{m_{b_{eq}}} \quad (2.148)$$

$$e_2 = \frac{3\rho v_{r_i}^{*3} A_r}{4Bm_{b_{eq}} \omega_r^* l_b} \left. \frac{\partial C_p}{\partial \dot{y}_{b_i}} \right|_{eq.} + \frac{c_{b_y}}{m_{b_{eq}}} \quad (2.149)$$

$$e_3 = \frac{k_{b_y}}{m_{b_{eq}}} \quad (2.150)$$

$$e_4 = \frac{c_{b_y}}{m_{b_{eq}}} \quad (2.151)$$

$$e_5 = \frac{3\rho A_r}{4Bm_{beq}\omega_r^*l_b} \left[\left. \frac{\partial C_p}{\partial v_m} \right|_{eq.} v_{r_i}^{*3} + 3C_p^* \left(r_t^2 \frac{R^2 \sin \psi^{*2} - x_h^2}{(x_h^2 + R^2 \sin \psi^{*2})^2} + \left(\frac{R \cos \psi^* + H}{H} \right)^\alpha \right) v_{r_i}^{*2} \right] \quad (2.152)$$

$$e_6 = \frac{3\rho A_r}{4Bm_{beq}\omega_r^*l_b} \left[\left. \frac{\partial C_p}{\partial v_t} \right|_{eq.} v_{r_i}^{*3} + 3C_p^* v_{r_i}^{*2} \right] \quad (2.153)$$

$$e_7 = \frac{3\rho A_r}{4Bm_{beq}\omega_r^*l_b} \left[\left. \frac{\partial C_p}{\partial \dot{x}_t} \right|_{eq.} v_{r_i}^{*3} - 3C_p^* v_{r_i}^{*2} \right] \quad (2.154)$$

$$e_8 = \frac{3\rho A_r}{4Bm_{beq}\omega_r^*l_b} \left[\left. \frac{\partial C_p}{\partial x_{b_i}} \right|_{eq.} v_{r_i}^{*3} - 3C_p^* v_{r_i}^{*2} \right] \quad (2.155)$$

$$e_9 = \frac{3\rho v_{r_i}^{*3} A_r}{4Bm_{beq}l_b} \left[\left. \frac{\partial C_p}{\partial \omega_r} \right|_{eq.} \frac{1}{\omega_r^*} - C_p^* \frac{1}{\omega_r^{*2}} \right] \quad (2.156)$$

$$e_{10} = \frac{3\rho A_r}{4Bm_{beq}\omega_r^*l_b} \left[C_p^* 3v_m^* \left[\frac{r_t^2 \left(x_h^2 + R^2 \sin \psi^{*2} \right)^2 (2R^2 \cos \psi^* \sin \psi^*)^2}{(x_h^2 + R^2 \sin \psi^{*2})^4} \right. \right. \\ \left. \left. - r_t^2 \frac{(R^2 \sin \psi^{*2} - x_h^2) 2(2R^2 \cos \psi^* \sin \psi^*) (x_h^2 + R^2 \sin \psi^{*2})}{(x_h^2 + R^2 \sin \psi^{*2})^4} \right. \right. \\ \left. \left. + \alpha \left(\frac{-R \sin \psi^*}{H} \right) \left(\frac{R \cos \psi^* + H}{H} \right)^{\alpha-1} \right] v_{r_i}^{*2} + \left. \frac{\partial C_t}{\partial \psi} \right|_{eq.} v_{r_i}^{*3} \right] \quad (2.157)$$

$$e_{11} = \frac{3\rho v_{r_i}^{*3} A_r}{4Bm_{beq}\omega_r^*l_b} \left. \frac{\partial C_p}{\partial \theta_i} \right|_{eq.} \quad (2.158)$$

$$f_1 = \omega_\theta^2 \quad (2.159)$$

$$f_2 = 2\omega_\theta \xi_\theta \quad (2.160)$$

$$g_1 = \frac{1}{\tau_g} \quad (2.161)$$

$$\omega_p = \frac{\mu_v \pi}{2L} \quad (2.162)$$

The inputs are included in the system by means of B :

$$B = \begin{bmatrix} 0 & 0 & 0 & 0 & 0 & 0 & 0 & 0 & 0 & 0 & 0 & f_1 & 0 & 0 & 0 & 0 \\ 0 & 0 & 0 & 0 & 0 & 0 & 0 & 0 & 0 & 0 & 0 & 0 & g_1 & 0 & 0 & 0 \end{bmatrix}^T \quad (2.163)$$

The sensor measurements are related to the states using C_y :

$$C_y = \begin{bmatrix} 1 & 0 & 0 & 0 & 0 & 0 & 0 & 0 & 0 & 0 & 0 & 0 & 0 & 0 \\ 0 & -b_3 & -b_4 & 0 & 0 & b_1 & b_2 & 0 & 0 & 0 & 0 & 0 & 0 & 0 \\ 0 & 0 & 0 & -c_4 & -c_5 & 0 & 0 & c_2 & c_3 & 0 & 0 & -c_1 & 0 & 0 \\ 0 & 0 & 0 & 0 & 0 & p_1 & 0 & 0 & 0 & 0 & 0 & 0 & 0 & 0 \\ 0 & 0 & 0 & 0 & 0 & 0 & 0 & p_2 & 0 & 0 & 0 & 0 & 0 & 0 \\ 0 & 0 & 0 & 0 & 0 & 0 & 0 & 0 & 0 & 1 & 0 & 0 & 0 & 0 \\ q_2 & 0 & 0 & 0 & 0 & 0 & 0 & 0 & 0 & 0 & 0 & q_1 & 0 & 0 \\ 0 & 0 & -1 & 0 & 0 & 0 & 0 & 0 & 0 & 0 & 0 & 0 & 1 & 1 \\ 0 & 0 & 0 & 0 & 0 & 0 & 0 & 0 & 0 & 0 & 0 & 0 & 0 & 1 \end{bmatrix} \quad (2.164)$$

where:

$$p_1 = k_{b_x} \frac{2l_b}{3} \quad (2.165)$$

$$p_2 = k_{b_y} \frac{2l_b}{3} \quad (2.166)$$

$$q_1 = \eta_g \omega_r^* \quad (2.167)$$

$$q_2 = \eta_g T_g^* \quad (2.168)$$

Finally, the outputs to be controlled are related to the states using C_z :

$$C_z = \begin{bmatrix} 1 & 0 & 0 & 0 & 0 & 0 & 0 & 0 & 0 & 0 & 0 & 0 & 0 & 0 \\ 0 & 0 & 1 & 0 & 0 & 0 & 0 & 0 & 0 & 0 & 0 & 0 & 0 & 0 \\ 0 & 0 & 0 & 0 & 1 & 0 & 0 & 0 & 0 & 0 & 0 & 0 & 0 & 0 \\ 0 & 0 & 0 & 0 & 0 & 0 & 1 & 0 & 0 & 0 & 0 & 0 & 0 & 0 \\ 0 & 0 & 0 & 0 & 0 & 0 & 0 & 0 & 1 & 0 & 0 & 0 & 0 & 0 \\ r_1 & 0 & r_4 & 0 & 0 & 0 & 0 & 0 & 0 & 0 & 0 & r_3 & r_2 & 0 \\ 0 & 0 & 0 & 0 & 0 & 0 & 0 & 0 & 0 & 1 & 0 & 0 & 0 & 0 \\ 0 & 0 & 0 & 0 & 0 & 0 & 0 & 0 & 0 & 0 & 1 & 0 & 0 & 0 \\ q_2 & 0 & 0 & 0 & 0 & 0 & 0 & 0 & 0 & 0 & 0 & q_1 & 0 & 0 \end{bmatrix} \quad (2.169)$$

where:

$$r_1 = \frac{R}{v_r^*} \quad (2.170)$$

$$r_2 = r_3 = \frac{-\omega_r^* R}{v_r^{*2}} \quad (2.171)$$

$$r_4 = \frac{\omega_r^* R}{v_r^{*2}} \quad (2.172)$$

2.10 Observability

The UKF state estimation will not converge unless the system is observable. Observability evaluates whether a system's internal states can be deduced from the knowledge of

its measurements. More rigorously, a continuous time system:

$$\dot{x}(t) = Ax(t), \quad y(t) = Cx(t) \quad (2.173)$$

is said to be observable if and only if $y(t) \equiv 0 \rightarrow x(t) \equiv 0$.

If the following discrete time system is considered:

$$x(k+1) = Ax(k), \quad y(k) = Cx(k), \quad x(0) = x_0 \quad (2.174)$$

it is possible to iterate in the following way:

$$\begin{aligned} x(0) &= x_0 & y(0) &= Cx_0 \\ x(1) &= Ax_0 & y(1) &= CAx_0 \\ x(2) &= A^2x_0 & y(2) &= CA^2x_0 \\ &\vdots & & \\ x(n-1) &= A^{n-1}x_0 & y(n-1) &= CA^{n-1}x_0 \end{aligned}$$

which can be expressed in matrix form as:

$$\begin{bmatrix} C \\ CA \\ \vdots \\ CA^{n-1} \end{bmatrix} x_0 = \begin{bmatrix} 0 \\ 0 \\ \vdots \\ 0 \end{bmatrix} \quad (2.175)$$

This system of equations with n unknowns has a unique solution if and only if this matrix, called the observability matrix \mathcal{O} , has rank n . Checking this condition in the linear wind turbine model, and using C_y as C matrix, it was found out that the rank of \mathcal{O} is 27, which matches the number of states of our system. Hence, the system is observable.

Chapter 3

WIND TURBINE CONTROL

3.1 Introduction

Wind turbines are large aeroelastic structures subjected to a continuously changing stochastic wind, which require complex control strategies in order to fulfil the functional requirements introduced in Section 1.5. All in all, the designed control methods have the mission of reducing the structural loads in order to increase the lifetime of the wind turbine as well as optimising power production.

Several sensors and actuators are commonly used for control purposes. As stated in Section 2.6, an electric servo system corresponding to the generator torque actuator is available, while blade pitch actuators can be hydraulic or electric servo systems. The structure also comprises blade load sensors, commonly strain sensors or optical fibres used to measure the flapwise and edgewise blade bending moments [17], and accelerometers to determine the sideways and fore-aft tower motion. Furthermore, speed sensors are employed to measure the rotational speed of the generator and rotor, and an anemometer situated in the top of the nacelle provides wind speed measurements at hub-height. Apart from this, LIDAR solutions have been studied in the last decade to explore remote wind measuring, but are not that widely used in real life implementations due to high maintenance costs and thus it has been decided not to use them in this project.

3.2 Requirement Specification

Based on information in Chapter 1 and Chapter 2, a set of requirements can be set up for the various parts of the solution.

3.2.1 General control objectives

Based on the functional requirements, the following general control objectives can be formulated [27]:

1. Regulation of generator counter torque based on rotational speed ω_r for optimal tip speed ratio operation in partial load (obj. 1).
2. Regulation of generator counter torque based on tower sideways loads for their reduction (obj. 4).

3. CPC based on the rotational speed ω_r for rated power operation and reduced fore-aft tower structural loads in full load (obj. 2, 4).
4. IPC based on flapwise blade loads in order to reduce flapwise and edgewise bending loads (obj. 3).

3.2.2 Kalman Filter

The requirements for the state estimator have been defined based on the theory presented in Section 2.7. Specific numbers such as errors have been designated based on subjective self-determined goals rather than any objective metric.

1. The state estimator must be in the form of a UKF.
2. The UKF must be able to estimate states with an average error of less than 5%.

3.2.3 MPC

Goals for the MPC concentrate largely on desired function and control priorities.

1. MPC must be computationally feasible on available hardware.
2. MPC must have control and prediction horizon that ensure stability.
3. MPC must have rotor speed as main priority to avoid physical strain.
4. MPC must have power output as secondary priority to avoid damaging the generator.
5. MPC must have tower and blade loads as tertiary priority to minimise fatigue and extend lifetime.

3.3 Control Loops

The main regulation strategies can be seen in Fig. 3.1. The control loop based on Generator Torque Control (GTC) measures the generator rotational speed ω_g and the side-wards tower displacement acceleration \ddot{y}_t in order to compute a torque reference T_{gref} in order to reduce tower sideways tower bending and drive train torsion. Apart from that, CPC is in charge of generating a global pitch angle reference $\bar{\theta}_{ref}$ using generator speed ω_g and fore-aft tower top acceleration \ddot{x}_t in order to reduce fore-aft tower loads and optimise power production. Furthermore, IPC will reduce blade and nacelle loads using flapwise blade moments and fore-aft tower top acceleration measurements, as well as the blades' azimuth angle [27].

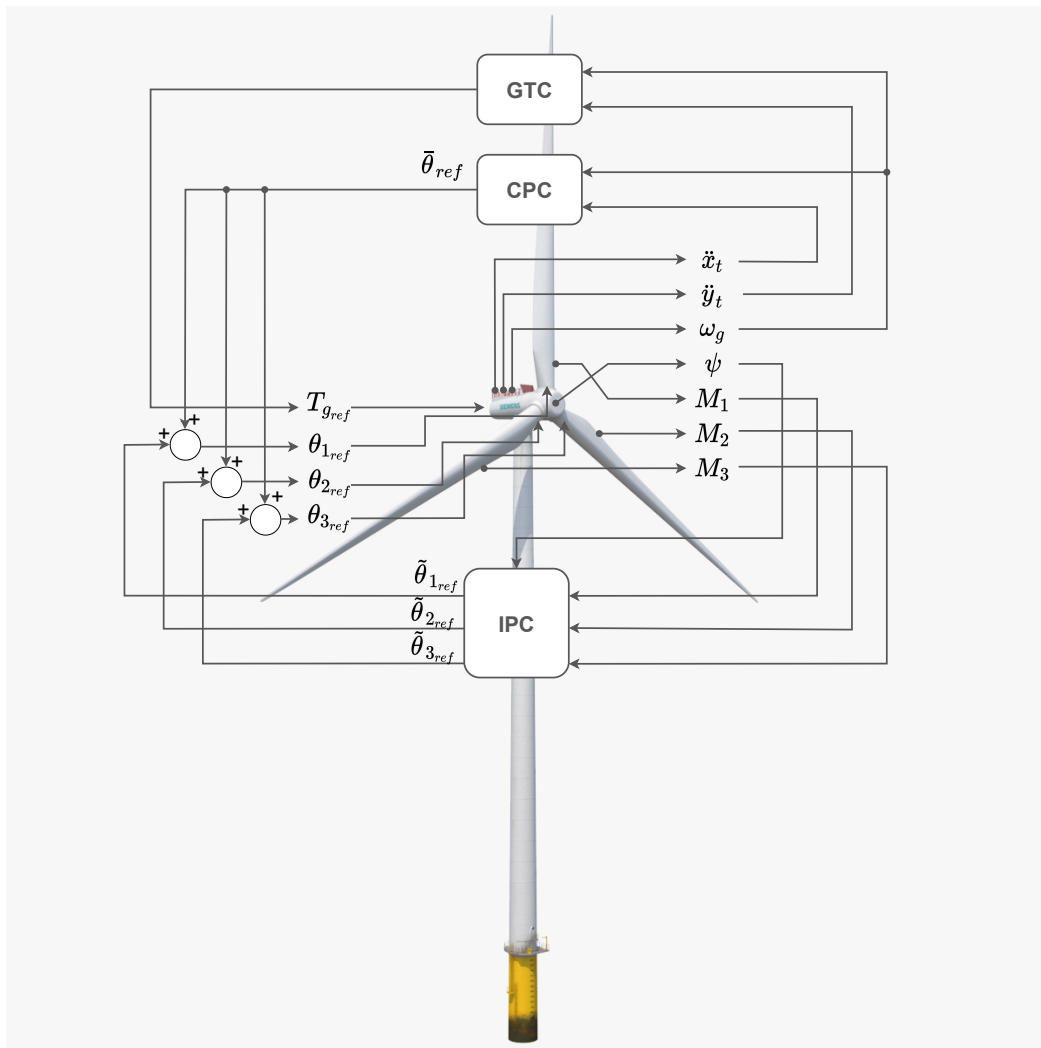


Figure 3.1: Schematic of the main control loops, with GTC referring to generator torque control, and CPC and IPC to collective and individual pitch control respectively [15, 27].

It will not be necessary to design each of these control loops separately, as the cost function of the MPC will be designed to fulfil all control objectives at the same time in an optimal way by making use of its internal linear model derived in Sections 2.8 and 2.9, as explained in Section 3.5.

3.4 Below-Rated Wind Speed Proportional Torque Control

The non-linear model used for UKF state estimation has to follow a pitch and torque reference, which will be generated in an optimal way by the MPC by the end of this project. Nevertheless, the UKF algorithm should be tested prior to the MPC implementation. For

this reason, a basic controller needs to be implemented, which will try to maximise the power production in below-rated wind speed. To accomplish that, the tip speed ratio λ should have an optimum value λ_{opt} , that is, the value at which C_p is maximum as seen in Fig. 3.2. From λ_{opt} , the optimal rotor speed can be computed based on the wind speed measured at each instant (ignoring blade dynamics for simplicity) as [41]:

$$\omega_{opt} = \frac{\lambda_{opt} v_r}{R} \quad (3.1)$$

This method would be feasible if the wind speed measurements were reliable, but disturbances occasioned by the rotor movement as well as the inherent delay due to the anemometers being placed on top of the nacelle and the lack of spatial information provide noisy and unreliable measurements. Hence, the control objective should be achieved in a different way.

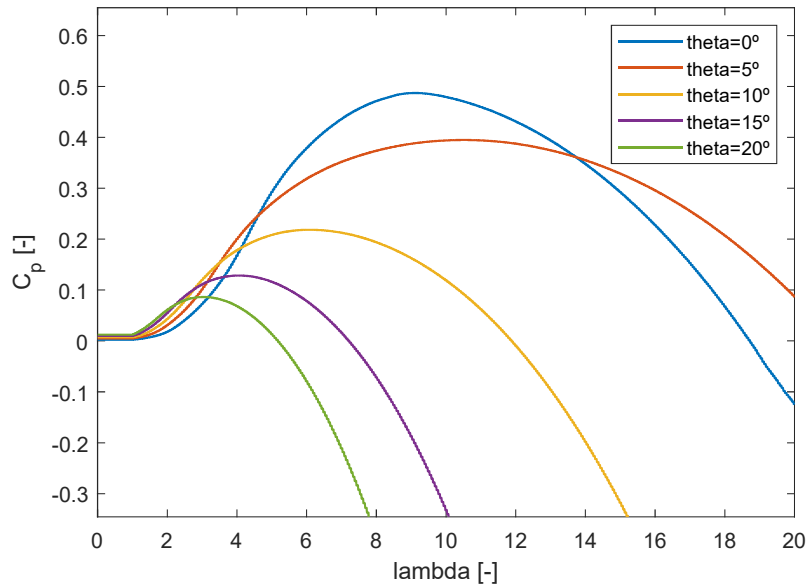


Figure 3.2: Power coefficient dependency on tip speed ratio λ and blade pitch angle θ .

If it is assumed that the rotor speed is following ω_{opt} and that the controller and turbine dynamics are infinitely fast so that the actual rotor speed is equal to this reference, then the aerodynamic torque for this rotor speed would be given by:

$$T_r = \frac{1}{2} \rho v_r^3 A_r C_p(\lambda, \theta) \frac{1}{\omega_r} \quad (3.2)$$

Note that CPC has to be assumed for the design of this controller; otherwise the aerodynamic torque would be expressed taking into account each individual blade as seen in Section 2.3. This approximation should also provide acceptable references in the IPC case.

The previous equation can be rearranged by replacing v_r by its expression isolated from the tip speed ratio:

$$T_r = \frac{1}{2} \frac{\rho R^3 A_r C_p(\lambda, \theta)}{\lambda^3} \omega_r^2 \quad (3.3)$$

which in the optimal case yields:

$$T_r = \frac{1}{2} \frac{\rho R^3 A_r C_{p_{max}}}{\lambda_{opt}^3} \omega_{r_{opt}}^2 \quad (3.4)$$

Eq. 3.4 relates the rotor speed and the aerodynamic torque and can be simply written as:

$$T_r = K \omega_{r_{opt}}^2 \quad (3.5)$$

where:

$$K = \frac{1}{2} \frac{\rho R^3 A_r C_{p_{max}}}{\lambda_{opt}^3} \quad (3.6)$$

As the optimal value for the tip speed ratio does not depend on rotor speed, Eq. 3.5 can be used for any given value of ω_r , resulting in the following optimal aerodynamic torque:

$$T_r = K \omega_r^2 \quad (3.7)$$

In steady state, the generator torque is the aerodynamic torque minus the loss torque. Assuming that these losses are negligible for the derivation of this controller would mean that it would be possible to obtain optimal power production if the generator torque follows Eq. 3.7:

$$T_{g_{ref}} = K \omega_r^2 \quad (3.8)$$

The performance of this controller relies on wind speed variations and rotor inertia, as it has been derived assuming steady state conditions.

3.5 MPC Formulation

This section is mainly based on [42] and gives a theoretic insight on MPC, providing the design procedure needed for its proper implementation.

The objective of MPC is to control a plant in an optimal manner with respect to a given cost function by:

1. Optimising over a certain prediction horizon H_p (that is, H_p samples into the future) to obtain a sequence of predicted optimal control inputs.
2. Applying the 1st sample of the determined predicted optimal inputs to the plant.
3. Moving one sample and repeating the above procedure (receding horizon).

Consider the discrete time linear system [42]:

$$x(k+1) = Ax(k) + Bu(k) \quad (3.9)$$

$$y(k) = C_y x(k) \quad (3.10)$$

$$z(k) = C_z x(k) \quad (3.11)$$

with:

$x \in \mathbb{R}^n$: state vector

$u \in \mathbb{R}^l$: input vector

$y \in \mathbb{R}^{m_y}$: vector of measured outputs

$z \in \mathbb{R}^{m_z}$: vector of outputs to be controlled

The variables y and z typically overlap, so all the controlled outputs will be measured. Also, if $y \equiv z$, the set $m \equiv m_y \equiv m_z$ and $C \equiv C_y \equiv C_z$. At time step k , the sequence of actions will be the following:

1. Obtain measurements $y(k)$.
2. Calculate the optimal plant input $u(k)$.
3. Apply $u(k)$ to the plant.

In order to derive the basic formulation of MPC it should be assumed that the plant model is linear, that the cost function is quadratic and that the constraints are in the form of linear inequalities. Apart from that, the model should be time invariant, and the cost function penalises changes in the input vector $\Delta u(k)$ instead of particular values $u(k)$ in order to introduce integral action and thus avoid steady state error.

To make this formulation realistic, it should not be assumed that the state variables can be measured, so an estimate $\hat{x}(k|k)$ based on the measurements up to time k of the state $x(k)$ will be used. That means the estimate is based on measurements of outputs up to $y(k)$ and inputs up to $u(k-1)$, as the next input $u(k)$ is yet to be determined. The future value of the input u at time $k+i$ is denoted as $\hat{u}(k+i|k)$, while $\hat{x}(k+i|k)$, $\hat{y}(k+i|k)$ and $\hat{z}(k+i|k)$ indicate the predictions made at time k of x , y and z at time $k+i$, supposing that a sequence of inputs $\hat{u}(k+j|k)$ with $j \in [0, 1, \dots, i-1]$ has taken place.

We optimise with respect to the quadratic cost function [42]:

$$V(k) = \sum_{i=H_w}^{H_p} \|\hat{z}(k+i|k) - r(k+i|k)\|_{Q(i)}^2 + \sum_{i=0}^{H_u-1} \|\Delta \hat{u}(k+i|k)\|_{R(i)}^2 \quad (3.12)$$

where:

$$\|w\|_M = \sqrt{w^T M w}$$

$Q(i), R(i) \geq 0$: positive semi-definite weight matrices

$r(k + i|k)$: reference signal

H_p : prediction horizon

H_u : control horizon ($H_p \geq H_u$)

H_w : window parameter ($H_w \geq 1$)

Therefore, the cost function penalises deviations (error vector) on the predicted controlled outputs $\hat{z}(k + i|k)$ from a reference trajectory $r(k + i|k)$. It is important to remark that the prediction horizon has length H_p , but it is not required that we start penalising deviations of z from r immediately (if $H_w > 1$), as there might be some delay between applying an input and observing any effect. It will be always assumed that $H_u \leq H_p$, and the change in input (or control move) will be $\Delta\hat{u}(k + i|k) = \hat{u}(k + i|k) - \hat{u}(k + i - 1|k)$ for $i < H_u$ and $\Delta\hat{u}(k + i|k) = 0$ for $i \geq H_u$ so that $\hat{u}(k + i|k) = \hat{u}(k + H_u - 1|k)$ for all $i \geq H_u$.

The parameters $Q(i), R(i), H_p, H_u, H_w$ are generally tuning parameters.

Constraints on the actuator slew rates (Eq. 3.13), actuator ranges (Eq. 3.14) and controlled variables (Eq. 3.15) can be introduced as follows [42]:

$$E \begin{bmatrix} \Delta\mathcal{U}(k) \\ 1 \end{bmatrix} \leq 0, \quad \Delta\mathcal{U}(k) = [\Delta\hat{u}(k|k)^T \cdots \Delta\hat{u}(k + H_u - 1|k)^T]^T \quad (3.13)$$

$$F \begin{bmatrix} \mathcal{U}(k) \\ 1 \end{bmatrix} \leq 0, \quad \mathcal{U}(k) = [\hat{u}(k|k)^T \cdots \hat{u}(k + H_u - 1|k)^T]^T \quad (3.14)$$

$$G \begin{bmatrix} \mathcal{Z}(k) \\ 1 \end{bmatrix} \leq 0, \quad \mathcal{Z}(k) = [\hat{z}(k + H_w|k)^T \cdots \hat{z}(k + H_p|k)^T]^T \quad (3.15)$$

with E, F and G being matrices of appropriate dimensions.

It is now crucial to find a way of computing the predicted values of the controlled variables $\hat{z}(k + i|k)$ from the estimate of the current state $\hat{x}(k|k)$ and the last input $u(k - 1)$ and the assumed future input changes $\Delta\hat{u}(k + i|k)$. Lets consider a situation in which the whole state vector is measured ($\hat{x}(k|k) = x(k) = y(k)$, so $C_y = I$) and we know nothing about disturbances or measurement noise for simplicity. Then it is possible to predict by iterating the model as follows:

$$\hat{x}(k + 1|k) = Ax(k) + B\hat{u}(k|k) \quad (3.16)$$

$$\hat{x}(k + 2|k) = Ax(k + 1|k) + B\hat{u}(k + 1|k) \quad (3.17)$$

$$= A^2x(k) + AB\hat{u}(k|k) + B\hat{u}(k + 1|k) \quad (3.18)$$

\vdots

$$\hat{x}(k + H_p|k) = A\hat{x}(k + H_p - 1|k) + B\hat{u}(k + H_p - 1|k) \quad (3.19)$$

$$= A^{H_p}x(k) + A^{H_p-1}B\hat{u}(k|k) + \cdots + B\hat{u}(k + H_p - 1|k) \quad (3.20)$$

Note that $\hat{u}(k|k)$ has been used in the 1st line instead of $u(k)$, as we do not know the value of $u(k)$ at the time when we need to calculate the predictions.

As the input was assumed to only vary from time k to $k + H_u - 1$, and remain constant afterwards, $\hat{u}(k + i|k) = \hat{u}(k + H_u - 1)$ for $H_u \leq i \leq H_p - 1$. Furthermore, it is desired to reformulate the inputs $\hat{u}(k + i|k)$ in terms of $\Delta\hat{u}(k + i|k)$ by $\Delta\hat{u}(k + i|k) = \hat{u}(k + i|k) - \hat{u}(k + i - 1|k)$:

$$\hat{u}(k|k) = \Delta\hat{u}(k|k) + u(k-1) \quad (3.21)$$

$$\hat{u}(k+1|k) = \Delta\hat{u}(k+1|k) + \Delta\hat{u}(k|k) + u(k-1) \quad (3.22)$$

$$\vdots$$

$$\hat{u}(k+H_u-1|k) = \Delta\hat{u}(k+H_u-1|k) + \dots + \Delta\hat{u}(k|k) + u(k-1) \quad (3.23)$$

Therefore:

$$\hat{x}(k+1|k) = Ax(k) + B[\Delta\hat{u}(k|k) + u(k-1)] \quad (3.24)$$

$$\begin{aligned} \hat{x}(k+2|k) &= A^2x(k) + AB[\Delta\hat{u}(k|k) + u(k-1)] \\ &\quad + B[\Delta\hat{u}(k+1|k) + \Delta\hat{u}(k|k) + u(k-1)] \end{aligned} \quad (3.25)$$

$$= A^2x(k) + (A+I)B\Delta\hat{u}(k|k) + B\Delta\hat{u}(k+1|k) + (A+I)Bu(k-1) \quad (3.26)$$

$$\vdots$$

$$\begin{aligned} \hat{x}(k+H_u|k) &= A^{H_u}\hat{x}(k|k) + (A^{H_u-1} + \dots + A + I)B\Delta\hat{u}(k|k) + \dots \\ &\quad + B\Delta\hat{u}(k+H_u-1|k) + (A^{H_u-1} + \dots + A + I)Bu(k-1) \end{aligned} \quad (3.27)$$

$$\begin{aligned} \hat{x}(k+H_u+1|k) &= A^{H_u+1}\hat{x}(k|k) + (A^{H_u} + \dots + A + I)B\Delta\hat{u}(k|k) + \dots \\ &\quad + (A+I)B\Delta\hat{u}(k+H_u-1|k) + (A^{H_u} + \dots + A + I)Bu(k-1) \end{aligned} \quad (3.28)$$

$$\vdots$$

$$\begin{aligned} \hat{x}(k+H_p|k) &= A^{H_p}\hat{x}(k|k) + (A^{H_p-1} + \dots + A + I)B\Delta\hat{u}(k|k) + \dots \\ &\quad + (A^{H_p-H_u} + \dots + A + I)B\Delta\hat{u}(k+H_u-1|k) \\ &\quad + (A^{H_p} + \dots + A + I)Bu(k-1) \end{aligned} \quad (3.29)$$

In matrix notation this yields:

$$\mathcal{X}(k) = \mathcal{A}\hat{x}(k|k) + \mathcal{B}_u u(k-1) + \mathcal{B}_{\Delta u} \Delta\mathcal{U}(k) \quad (3.30)$$

where:

$$\mathcal{X}(k) = \begin{bmatrix} \hat{x}(k+1|k) \\ \vdots \\ \hat{x}(k+H_u|k) \\ \hat{x}(k+H_u+1|k) \\ \vdots \\ \hat{x}(k+H_p|k) \end{bmatrix}, \quad \mathcal{A} = \begin{bmatrix} A \\ \vdots \\ A^{H_u} \\ A^{H_u+1} \\ \vdots \\ A^{H_p} \end{bmatrix}, \quad \mathcal{B}_u = \begin{bmatrix} B \\ \vdots \\ \sum_{i=0}^{H_u-1} A^i B \\ \sum_{i=0}^{H_u} A^i B \\ \vdots \\ \sum_{i=0}^{H_p} A^i B \end{bmatrix}$$

$$\mathcal{B}_{\Delta u} = \begin{bmatrix} B & 0 & 0 & \cdots & 0 \\ AB + B & B & 0 & \cdots & 0 \\ \vdots & \ddots & \ddots & & \vdots \\ \sum_{i=0}^{H_u-1} A^i B & \cdots & \cdots & & B \\ \sum_{i=0}^{H_u} A^i B & \cdots & \cdots & & AB + B \\ \vdots & \vdots & \vdots & & \vdots \\ \sum_{i=0}^{H_p} A^i B & \cdots & \cdots & & \sum_{i=0}^{H_p-H_u} A^i B \end{bmatrix}$$

The predictions of z are computed as:

$$\hat{z}(k+1|k) = C_z \hat{x}(k+1|k) \quad (3.31)$$

$$\hat{z}(k+2|k) = C_z \hat{x}(k+2|k) \quad (3.32)$$

$$\vdots \quad (3.33)$$

$$\hat{z}(k+H_p|k) = C_z \hat{x}(k+H_p|k) \quad (3.34)$$

that in matrix notation yields:

$$\mathcal{Z}(k) = \mathcal{C} \mathcal{X}(k) \quad (3.35)$$

with:

$$\mathcal{Z}(k) = \begin{bmatrix} \hat{z}(k+H_w|k) \\ \vdots \\ \hat{z}(k+H_p|k) \end{bmatrix}, \quad \mathcal{C} = \text{diag}(C_z)$$

Substituting $\mathcal{X}(k)$ by the expression derived in Eq. 3.30:

$$\mathcal{Z}(k) = \Psi \hat{x}(k|k) + \Upsilon u(k-1) + \Theta \Delta \mathcal{U}(k) \quad (3.36)$$

where:

$$\Psi = \mathcal{C} \mathcal{A}, \quad \Upsilon = \mathcal{C} \mathcal{B}_u, \quad \Theta = \mathcal{C} \mathcal{B}_{\Delta u}$$

Furthermore, let's define a vector with the difference between the future target trajectory and the response of the system over the prediction horizon if no input changes were made ($\Delta \mathcal{U}(k) = 0$):

$$\mathcal{E}(k) = \mathcal{T}(k) - \Psi \hat{x}(k|k) - \Upsilon u(k-1) \quad (3.37)$$

where:

$$\mathcal{T}(k) = \begin{bmatrix} r(k+H_w|k) \\ \vdots \\ r(k+H_p|k) \end{bmatrix}$$

Now it is possible to reformulate the cost in terms of 'known' signals at time k and $\Delta \mathcal{U}(k)$:

$$V(k) = \sum_{i=H_w}^{H_p} \|\hat{z}(k+i|k) - r(k+i|k)\|_{Q(i)}^2 + \sum_{i=0}^{H_u-1} \|\Delta \hat{u}(k+i|k)\|_{R(i)}^2$$

$$= \|\mathcal{Z}(k) - \mathcal{T}(k)\|_{\mathcal{Q}}^2 + \|\Delta\mathcal{U}(k)\|_{\mathcal{R}}^2 \quad (3.38)$$

$$= \|\Theta\Delta\mathcal{U}(k) - \mathcal{E}(k)\|_{\mathcal{Q}}^2 + \|\Delta\mathcal{U}(k)\|_{\mathcal{R}}^2 \quad (3.39)$$

where the weighting matrices are defined as:

$$\mathcal{Q} = \text{diag}(Q(H_w), \dots, Q(H_p)) \quad (3.40)$$

$$\mathcal{R} = \text{diag}(R(0), \dots, R(H_u - 1)) \quad (3.41)$$

Finally, the cost function is reformulated again for computational reasons:

$$V(k) = \|\Theta\Delta\mathcal{U}(k) - \mathcal{E}(k)\|_{\mathcal{Q}}^2 + \|\Delta\mathcal{U}(k)\|_{\mathcal{R}}^2 \quad (3.42)$$

$$= \mathcal{E}(k)^T \mathcal{Q} \mathcal{E}(k) - 2\Delta\mathcal{U}(k)^T \Theta^T \mathcal{Q} \mathcal{E}(k) + \Delta\mathcal{U}(k)^T [\Theta^T \mathcal{Q} \Theta + \mathcal{R}] \Delta\mathcal{U}(k) \quad (3.43)$$

$$= \text{const} - \Delta\mathcal{U}(k)^T \mathcal{G} + \Delta\mathcal{U}(k)^T \mathcal{H} \Delta\mathcal{U}(k) \quad (3.44)$$

with:

$$\mathcal{G} = 2\Theta^T \mathcal{Q} \mathcal{E}(k), \quad \mathcal{H} = \Theta^T \mathcal{Q} \Theta + \mathcal{R}$$

3.6 Solving the Unconstrained Case

The unconstrained control law can be found by setting the gradient of the cost function $V(k)$ to zero:

$$0 = \nabla_{\Delta\mathcal{U}(k)} V(k) = -\mathcal{G} + 2\mathcal{H}\Delta\mathcal{U}(k) \quad (3.45)$$

and then solve with respect to $\Delta\mathcal{U}(k)$:

$$\Delta\mathcal{U}(k)_{opt} = \frac{1}{2} \mathcal{H}^{-1} \mathcal{G} \quad (3.46)$$

The minimum is guaranteed by differentiating the gradient again with respect to $\Delta\mathcal{U}(k)$ to obtain the Hessian of V :

$$\frac{\partial^2 V}{\partial \Delta\mathcal{U}(k)^2} = 2\mathcal{H} = 2(\Theta^T \mathcal{Q} \Theta + \mathcal{R}) > 0 \quad (3.47)$$

Now, the control move at time k is applied as the first l rows of the vector $\Delta\mathcal{U}(k)_{opt}$:

$$\Delta\hat{u}(k|k)_{opt} = [I_l \quad 0_l \quad \dots \quad 0_l] \Delta\mathcal{U}(k)_{opt} \quad (= \Delta u(k)_{opt}) \quad (3.48)$$

In order to get the controller gain in the same form as the one computed by MATLAB, some rearrangement has to be made. Recalling that:

$$\mathcal{G} = 2\Theta^T \mathcal{Q} \mathcal{E}(k) = 2\Theta^T \mathcal{Q} (\mathcal{T}(k) - \Psi \hat{x}(k|k) - Y u(k-1)) \quad (3.49)$$

$$\mathcal{H} = \Theta^T \mathcal{Q} \Theta + \mathcal{R} \quad (3.50)$$

the following is obtained:

$$\Delta \hat{u}(k|k)_{opt} = [I_l \ 0_l \ \cdots \ 0_l] \frac{1}{2} \mathcal{H}^{-1} \mathcal{G} \quad (3.51)$$

$$= [I_l \ 0_l \ \cdots \ 0_l] (\Theta^T \mathcal{Q} \Theta + \mathcal{R})^{-1} \Theta^T \mathcal{Q} \mathcal{E}(k) \quad (3.52)$$

$$\triangleq K_{MPC} \mathcal{E}(k) \quad (3.53)$$

$$= K_{MPC} (\mathcal{T} - \Psi \hat{x}(k|k) - \Upsilon u(k-1)) \quad (3.54)$$

$$= K_{MPC} [I \ -\Psi \ -\Upsilon] \begin{bmatrix} \mathcal{T} \\ \hat{x}(k|k) \\ u(k-1) \end{bmatrix} \triangleq K_s \begin{bmatrix} \mathcal{T} \\ \hat{x}(k|k) \\ u(k-1) \end{bmatrix} \quad (3.55)$$

with K_{MPC} being the controller gain matrix and K_s the gain computed by "smpccon" MATLAB function. A block diagram of the derived controller can be seen in Fig. 3.3.

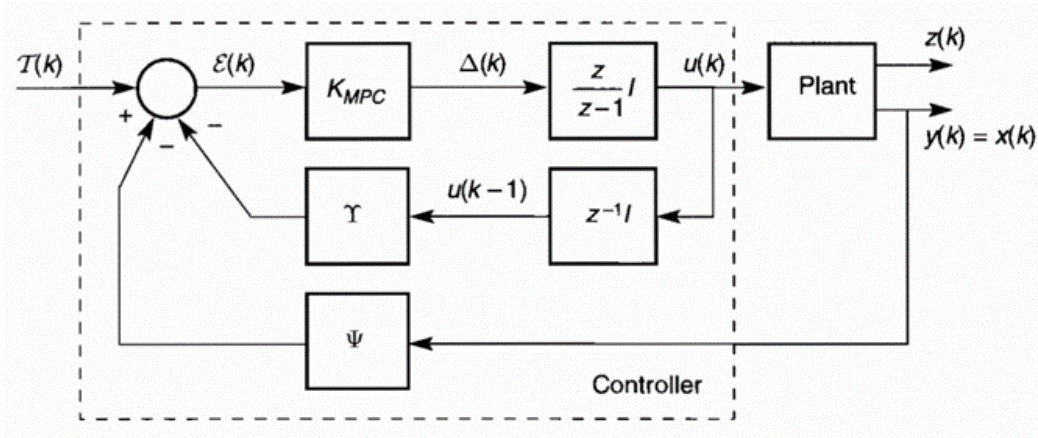


Figure 3.3: MPC controller with no constraints and full state measurement [42].

In a more realistic case, not all the states would be available for measurement, and an observer needs to be used. Hence, the observer will provide the state estimate $\hat{x}(k|k)$ that would replace $x(k)$, as seen in Fig. 3.4.

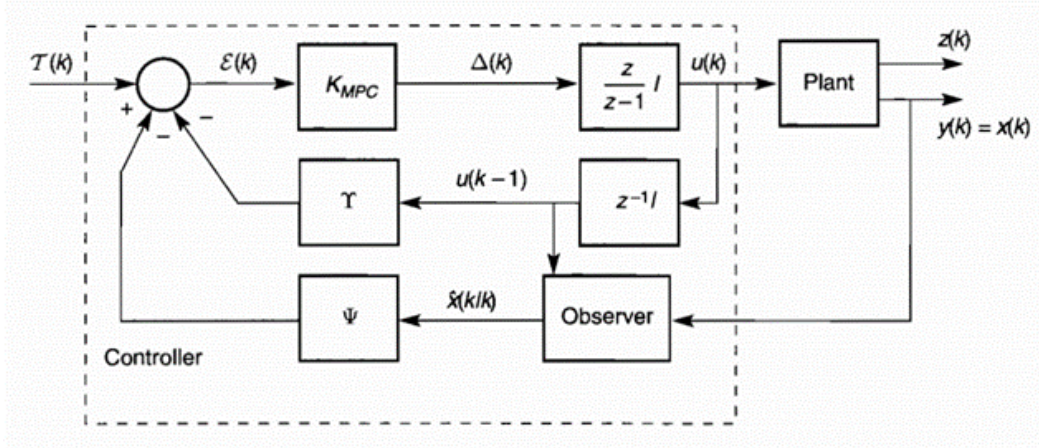


Figure 3.4: MPC controller with no constraints and state observer [42].

Some computational aspects need to be taken into account. First, the following needs to be guaranteed:

$$\mathcal{H} = (\Theta^T Q \Theta + \mathcal{R}) > 0 \quad (3.56)$$

Secondly, the inverse of \mathcal{H} in:

$$\Delta \mathcal{U}(k)_{opt} = \frac{1}{2} \mathcal{H}^{-1} \mathcal{G} \quad (3.57)$$

should never be computed directly, as Θ is often ill conditioned, which can result in \mathcal{H} being ill conditioned. Instead, Cholesky or SVD factorisation of Q and \mathcal{R} should be used to obtain a least squares problem, and then solve it by QR factorisation.

3.7 Solving the Constrained Case

When the control problem incorporates constraints, they should be expressed in terms of $\Delta \mathcal{U}(k)$ and variables known at time k .

For the actuator range constraints:

$$F \begin{bmatrix} \mathcal{U}(k) \\ 1 \end{bmatrix} \leq 0 \quad (3.58)$$

the matrix F is expressed as $F = [F_1 \ \cdots \ F_{H_u}]$ such that:

$$F \begin{bmatrix} \mathcal{U}(k) \\ 1 \end{bmatrix} = \sum_{j=1}^{H_u} F_j \hat{u}(k+j-1|k) + f \leq 0 \quad (3.59)$$

which can be written in terms of $\Delta \hat{u}$ as:

$$\sum_{i=1}^{H_u} \sum_{j=i}^{H_u} F_j \Delta \hat{u}(k+i-1|k) + \sum_{j=1}^{H_u} F_j \hat{u}(k-1) + f \leq 0 \quad (3.60)$$

and then written as a matrix inequality in $\Delta\mathcal{U}$:

$$\mathbf{F}\Delta\mathcal{U}(k) \leq -\mathbf{F}_1 u(k-1) - f \quad (3.61)$$

with $\mathbf{F} = [\mathbf{F}_1 \ \cdots \ \mathbf{F}_{H_u}]$ and $\mathbf{F}_i = \sum_{j=1}^{H_u} F_j$.

For the controlled variable constraints:

$$G \begin{bmatrix} \Delta\mathcal{Z}(k) \\ 1 \end{bmatrix} = G \begin{bmatrix} \Psi\hat{x}(k|k) + Yu(k-1) + \Theta\Delta\mathcal{U}(k) \\ 1 \end{bmatrix} \leq 0 \quad (3.62)$$

it is possible to write $G = [\Gamma \ g]$ to obtain a matrix inequality in $\Delta\mathcal{U}$:

$$\Gamma(\Psi\hat{x}(k|k) + Yu(k-1) + \Theta\Delta\mathcal{U}(k)) + g \leq 0 \quad (3.63)$$

Rearranging the expression:

$$\Gamma\Theta\Delta\mathcal{U}(k) \leq -\Gamma(\Psi\hat{x}(k|k) + Yu(k-1)) - g \quad (3.64)$$

For the actuator slew range constraints:

$$E \begin{bmatrix} \Delta\mathcal{U}(k) \\ 1 \end{bmatrix} \leq 0 \quad (3.65)$$

it is possible to write $E = [W \ w]$ to obtain a matrix inequality in $\Delta\mathcal{U}$:

$$W\Delta\mathcal{U}(k) \leq w \quad (3.66)$$

The constrained MPC problem can now be formulated as:

$$\min_{\Delta\mathcal{U}(k)} V(k) = -\Delta\mathcal{U}(k)^T \mathcal{G} + \Delta\mathcal{U}(k)^T \mathcal{H} \Delta\mathcal{U}(k) \quad (3.67)$$

subject to:

$$\begin{bmatrix} \mathbf{F} \\ \Gamma\Theta \\ W \end{bmatrix} \Delta\mathcal{U}(k) \leq \begin{bmatrix} -\mathbf{F}_1 u(k-1) - f \\ -\Gamma(\Psi\hat{x}(k|k) + Yu(k-1)) - g \\ w \end{bmatrix} \quad (3.68)$$

This has the standard form of a quadratic optimisation algorithm with linear inequality constraints, which is convex due to $\mathcal{H} \geq 0$, and thus there exist standard algorithms to compute its solution.

There exists the possibility of softening the constraints in order to avoid possible infeasibility due to large disturbances, which is briefly explained in Appendix A.5.

3.8 Mita-Teknik Controller

Mita-Teknik has provided a solution in the form of two controllers; a torque controller that follows a rotor speed reference and a pitch controller that follows a collective pitch reference as a function of TSR as seen in Figure 3.5.

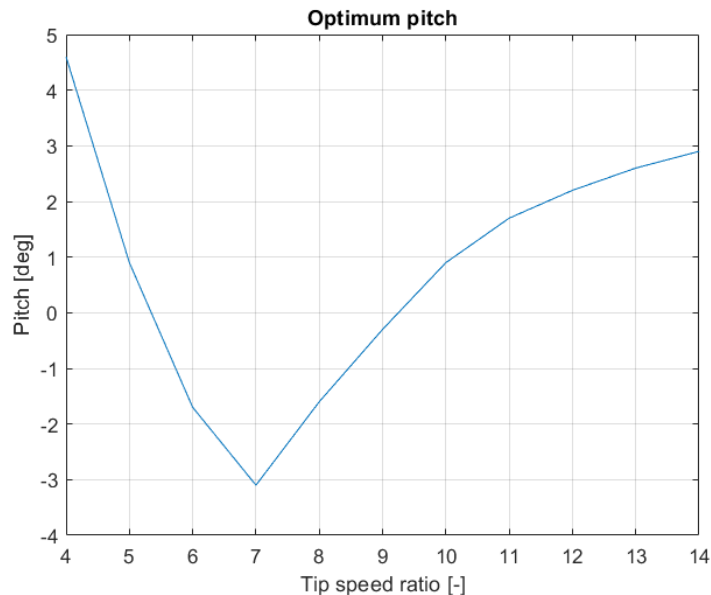


Figure 3.5: Optimal pitch

For below-rated wind speeds, the TSR can be as high as 14 due to the minimum rotor speed of 5 rpm. For rated and above-rated wind speeds, the TSR will instead drop lower than the optimal TSR. For below-rated wind speeds, where possible, the pitch and torque controllers combined will achieve a rotor speed that results in a TSR of 9.0621. This combination maximises the power coefficient, C_p , which determines the amount of energy that is extracted from the wind. Figure 3.6 shows the graph from Figure 3.5 superimposed on a contour map of the power coefficient. This demonstrates how the optimal pitch and TSR combined result in a high power coefficient. The generator torque controller will not be covered here in great detail. For below-rated rotor speeds the generator torque is proportional to the rotor speed. For above-rated rotor speed, the torque will be inversely proportional to keep power production at the rated output.

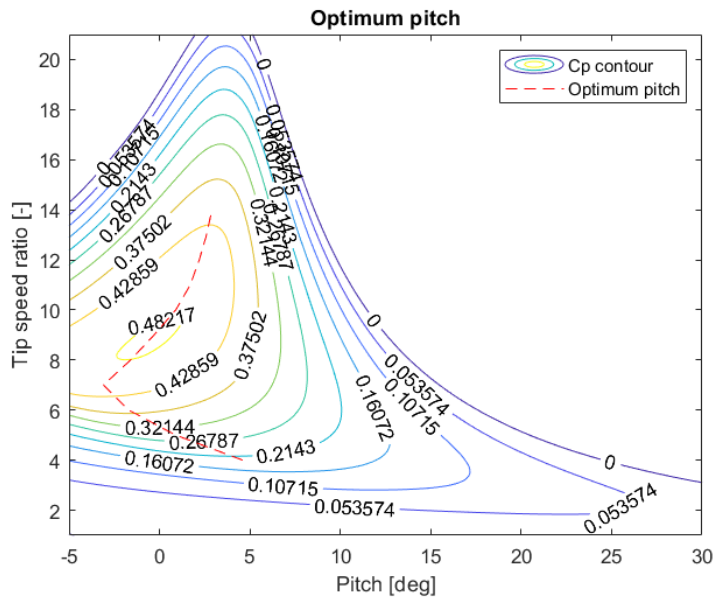


Figure 3.6: Blade performance

As can be seen in Figure 3.6, the highest power coefficient is achieved for a TSR of 9.0621, making this the optimal TSR, and a pitch of 0° . For above-rated wind speeds, the pitch controller must maintain the rated rotor speed of 7.56 rpm. This means that the optimal TSR can no longer be maintained, as it would require the rotor speed to exceed the rated value. This occurs at wind speeds of approximately 10.5 m/s. At this point, the collective pitch reference will be adjusted to keep the rotor speed at its rated speed. As a consequence, there is a drop-off in the power coefficient at wind speeds of 10.5 m/s and above, shown in Figure 3.7, as this energy cannot be utilised.

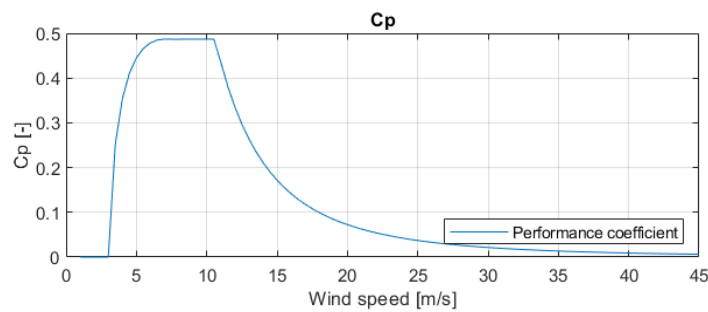


Figure 3.7: C_p curve

The turbine reaches rated power output at 10.5 m/s, corresponding to the point where the rotor reaches rated speed. As wind speeds increase, the pitch increases to reduce the aerodynamic torque acting on the rotor and keeping the rotor speed and generator torque

at rated values. This also reduces the thrust force on the blades, which does not contribute to rotor speed, but acts as a load on the blades. Figure 3.8 shows the pitch, rotor speed, generator power and thrust force for static wind speeds, i.e. without turbulence. Note how the pitch for below-rated wind speeds stays at approximately 0° corresponding to the optimal pitch for the optimal TSR of 9.0621, demonstrating that the controller correctly maximises the power output.

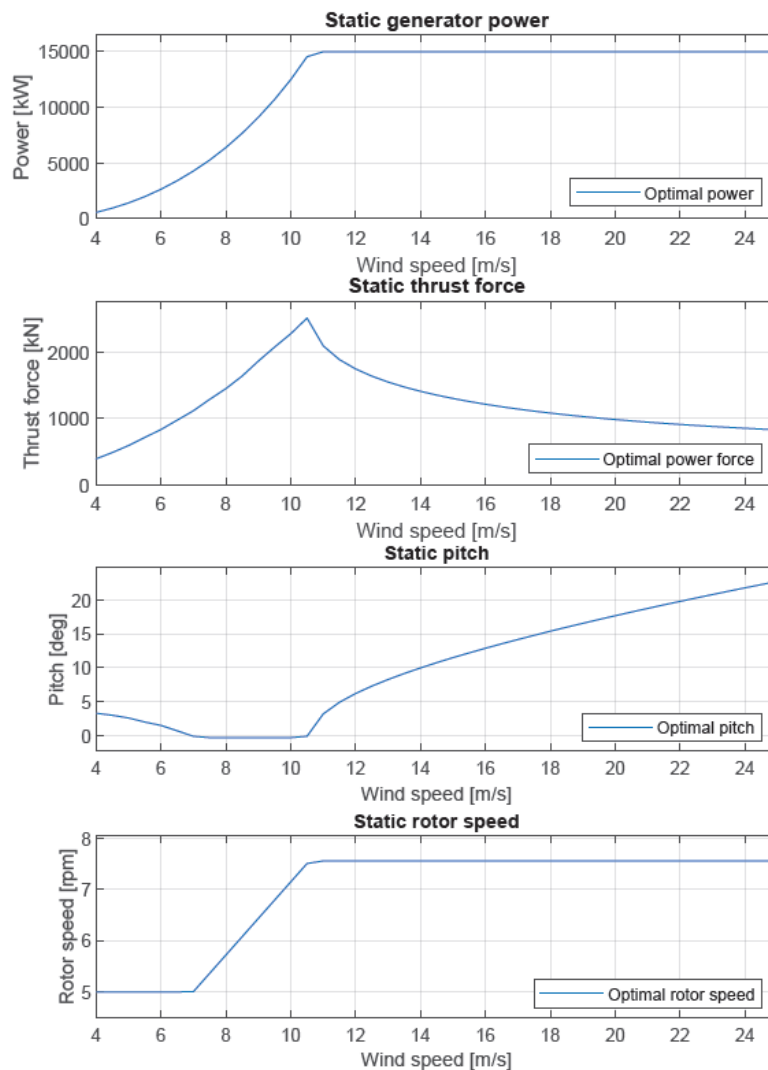


Figure 3.8: Static performance

There are both mechanical and electrical losses in the turbine as a function of aerodynamic torque and generator power respectively. The electrical losses are calculated simply as a scalar value of generator power. The mechanical losses are modelled by an unknown

function. Both electrical and mechanical losses are shown in Figure 3.9. Note that the mechanical function is likely a curve, but is presumably only evaluated for three points and plotted linearly between the points.

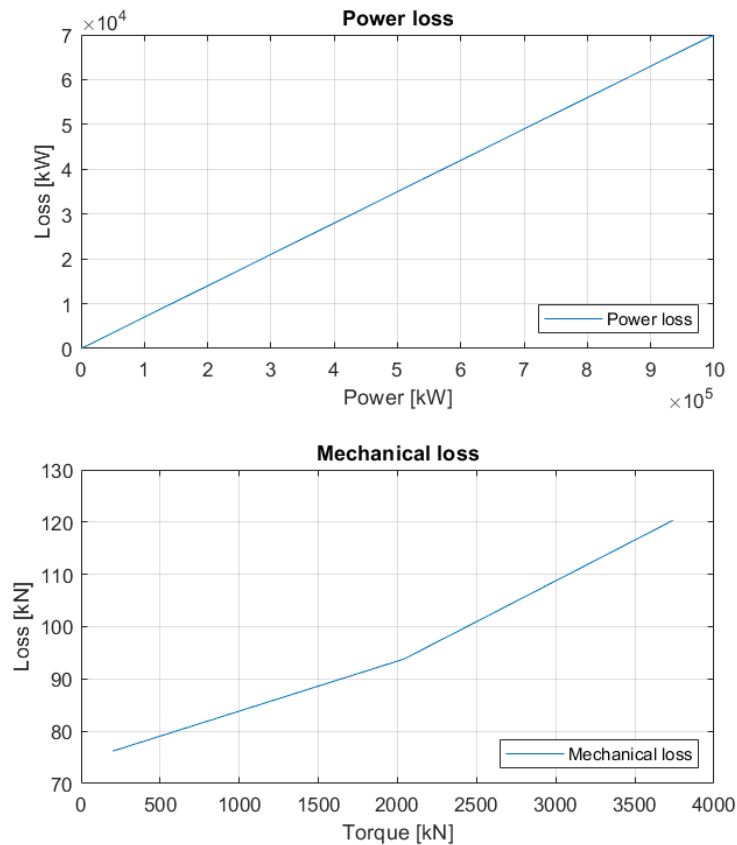
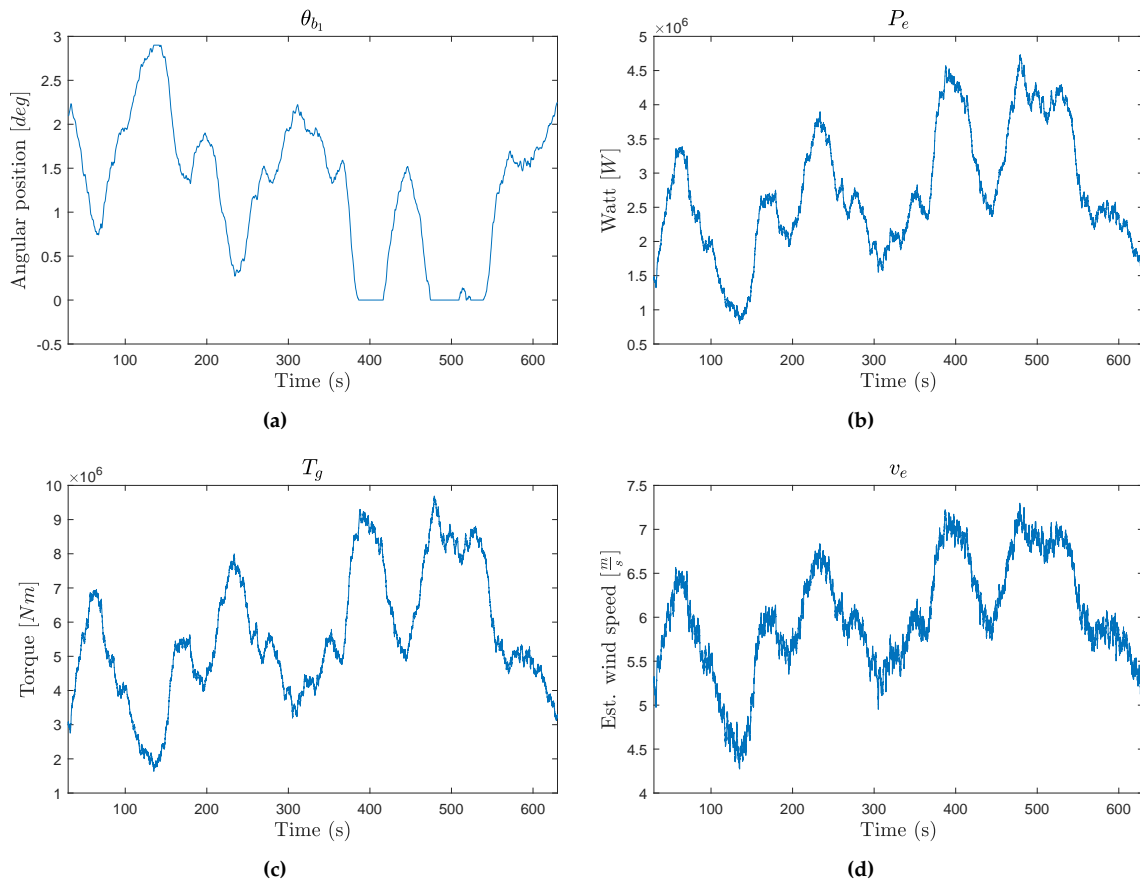


Figure 3.9: Loss tables

Two simulations will be carried out for this controller; one for a mean wind speed of 16 m/s and one for 6 m/s with normal turbulence as defined by the third edition of the IEC 64100-1 standard. These wind speeds represent above-rated and below-rated wind speeds respectively and will demonstrate situational behaviour of the controller. As the controller employs collective pitch control, only one blade will be shown for each scenario as the pitch is the same for all blades. All figures, including tower and blade loads, can be seen in Appendix B.1.

3.8.1 6 m/s mean wind speed test

The following test is carried out for a mean wind speed of 6 m/s. As can be seen in Figures 3.10b to 3.10d, the power generated is proportional to the generator torque and effective wind speed. As the wind speed increases, generator torque also increases which results in a larger power output. The rotor speed seen in Figure 3.10e can be seen to be correlated to wind and generator torque but the relationship is not quite as clear as the torque. The pitch, meanwhile, can be seen to be approximately inversely proportional to the torque, wind and power generated, as power output is greater for lower pitch angles in below-rated production.



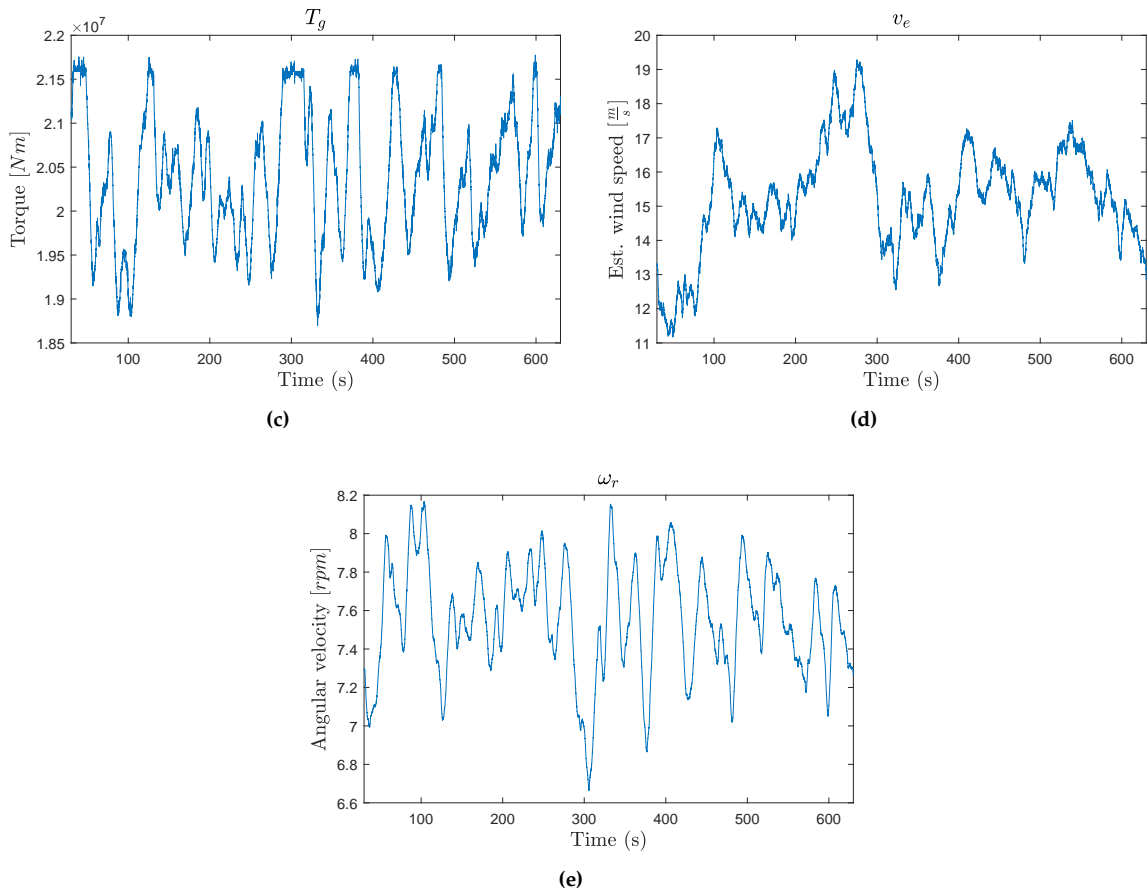


Figure 3.11: Bladed simulation results for 16 m/s wind speed.

Chapter 4

IMPLEMENTATION

4.1 Introduction

In this chapter, all the theory covered in Chapter 2 and Chapter 3 will be implemented. The specific settings used for state estimation will be presented, including variables to be measured and their typical noise associated to them, and parameters such as the prediction and control horizon, weight matrices, lower and upper bounds for variables and reference setpoints will be discussed within the context of MPC. Finally, an overview of the whole estimation and control algorithm will be shown.

4.2 Kalman Filter Implementation

The design of the Kalman filter is explained in Section 2.7. Here, that design is implemented by formulating a set of states, inputs and outputs, and the Kalman filter's effectiveness will be documented.

The states of the system will be the angular velocity of the rotor/generator, the fore-aft and sideways position and velocity of the tower, the flapwise and edgewise position and velocity of each individual blade, as well as their pitch angle and its derivative, the generator torque, the turbulent and mean wind velocity and the blades azimuth angle. The inputs of the system will be the desired pitch of individual blades of the turbine and the desired generator torque. The outputs will be the angular velocity of the rotor/generator, the fore-aft and sideways acceleration of the tower, the flapwise and edgewise root bending moments for each blade, the pitch angle of each blade, the generated power, the relative wind velocity in the rotor and the azimuth angle. The state space system then becomes:

$$x = [\omega_r \ x_t \ \dot{x}_t \ y_t \ \dot{y}_t \ x_{b_i} \ \dot{x}_{b_i} \ y_{b_i} \ \dot{y}_{b_i} \ \theta_i \ \dot{\theta}_i \ T_g \ v_t \ v_m \ \psi]^T \quad (4.1)$$

$$u = [\theta_{i_{ref}} \ T_{g_{ref}}]^T \quad (4.2)$$

$$y = [\omega_r \ \ddot{x}_t \ \ddot{y}_t \ M_{y_i} \ M_{x_i} \ \theta_i \ P_e \ v_r \ \psi]^T \quad (4.3)$$

The state transition functions are as follows:

$$\dot{x}_1 = \frac{(1 - \mu_d)T_r - x_{24}}{J_r + J_g} \quad (4.4)$$

$$\dot{x}_2 = x_3 \quad (4.5)$$

$$\dot{x}_3 = \frac{k_{b_x}}{m_{t_{eq}}} \sum_i (x_{6+i} - x_2) + \frac{c_{b_x}}{m_{t_{eq}}} \sum_i (x_{9+i} - x_3) - \frac{k_t}{m_{t_{eq}}} x_2 - \frac{c_t}{m_{t_{eq}}} x_3 \quad (4.6)$$

$$\dot{x}_4 = x_5 \quad (4.7)$$

$$\dot{x}_5 = \frac{3}{2Hm_{t_{eq}}} x_{24} + \frac{k_{b_y}}{m_{t_{eq}}} \sum_i (x_{12+i} - x_4) + \frac{c_{b_y}}{m_{t_{eq}}} \sum_i (x_{15+i} - x_5) - \frac{k_t}{m_{t_{eq}}} x_4 - \frac{c_t}{m_{t_{eq}}} x_5 \quad (4.8)$$

$$\dot{x}_{6+i} = x_{9+i} \quad (4.9)$$

$$\dot{x}_{9+i} = \frac{F_{x_i}}{m_{b_{eq}}} - \frac{k_{b_x}}{m_{b_{eq}}} (x_{6+i} - x_2) - \frac{c_{b_x}}{m_{b_{eq}}} (x_{9+i} - x_3) \quad (4.10)$$

$$\dot{x}_{12+i} = x_{15+i} \quad (4.11)$$

$$\dot{x}_{15+i} = \frac{F_{y_i}}{m_{b_{eq}}} - \frac{k_{b_y}}{m_{b_{eq}}} (x_{12+i} - x_4) - \frac{c_{b_y}}{m_{b_{eq}}} (x_{15+i} - x_5) \quad (4.12)$$

$$\dot{x}_{18+i} = x_{21+i} \quad (4.13)$$

$$\dot{x}_{21+i} = \omega_\theta^2 u_{1+i} - 2\omega_\theta \zeta_\theta x_{21+i} - \omega_\theta^2 x_{18+i} \quad (4.14)$$

$$\dot{x}_{24} = \frac{u_4 - x_{24}}{\tau_g} \quad (4.15)$$

$$\dot{x}_{25} = -\frac{x_{26}\pi}{2L} x_{25} + \frac{x_{26}\pi}{2L} n_t \quad (4.16)$$

$$\dot{x}_{26} = n_m \quad (4.17)$$

$$\dot{x}_{27} = x_1 \quad (4.18)$$

where:

$$T_r = \sum_i (-x_{12+i}) k_{b_y} \frac{2l_b}{3} \quad (4.19)$$

$$F_{x_i} = \frac{1}{2} \rho v_{r_i}^2 A_r \frac{C_t}{B} \quad (4.20)$$

$$F_{y_i} = \frac{1}{2} \rho v_{r_i}^3 A_r \frac{C_p}{B} \frac{1}{x_1} \frac{3}{2l_b} \quad (4.21)$$

and with v_{r_i} defined as:

$$v_{r_i} = x_{26} \left[r_t^2 \frac{R^2 \sin(x_{27} + \frac{2\pi}{B} i)^2 - x_h^2}{\left(x_h^2 + R^2 \sin(x_{27} + \frac{2\pi}{B} i)^2\right)^2} + \left(\frac{R \cos(x_{27} + \frac{2\pi}{B} i) + H}{H} \right)^\alpha \right] + x_{25} - x_3 - x_{9-11} \quad (4.22)$$

with $i \in \{0, 1, 2\}$.

The measurement functions are as follows:

$$y_1 = x_1 \quad (4.23)$$

$$y_2 = \frac{k_{b_x}}{m_{t_{eq}}} \sum_i (x_{6+i} - x_2) + \frac{c_{b_x}}{m_{t_{eq}}} \sum_i (x_{9+i} - x_3) - \frac{k_t}{m_{t_{eq}}} x_2 - \frac{c_t}{m_{t_{eq}}} x_3 \quad (4.24)$$

$$y_3 = \frac{3}{2Hm_{t_{eq}}} T_g + \frac{k_{b_y}}{m_{t_{eq}}} \sum_i (x_{12+i} - x_4) + \frac{c_{b_y}}{m_{t_{eq}}} \sum_i (x_{15+i} - x_5) - \frac{k_t}{m_{t_{eq}}} x_4 - \frac{c_t}{m_{t_{eq}}} x_5 \quad (4.25)$$

$$y_{4+i} = x_{6+i} k_{b_x} \frac{2l_b}{3} \quad (4.26)$$

$$y_{7+i} = x_{12+i} k_{b_y} \frac{2l_b}{3} \quad (4.27)$$

$$y_{10+i} = x_{18+i} \quad (4.28)$$

$$y_{13} = \eta_g x_{24} x_1 \quad (4.29)$$

$$y_{14} = x_{26} + x_{25} - x_3 \quad (4.30)$$

$$y_{15} = x_{27} \quad (4.31)$$

The process noise covariance matrix is derived from the state space equations above, describing the variance of the stochastic variables seen in Equations 4.16 and 4.17. Equations 4.32 and 4.33 show the variances present in the system.

$$\text{var} \left(\frac{x_{26}\pi}{2L} n_t \right) = \left(\frac{x_{26}\pi}{2L} \right)^2 \sigma_t^2 \quad (4.32)$$

$$\text{var} (n_m) = \sigma_m^2 \quad (4.33)$$

Note that σ_t and σ_m are defined in Section 2.2. The process covariance matrix Q would then present the terms $\left(\frac{x_{26}\pi}{2L} \right)^2 \sigma_t^2$ and σ_m^2 located in the row and column corresponding to the turbulent (x_{25}) and mean wind speed (x_{26}) respectively, and zeros otherwise.

The standard deviation of the noise for all measurements has been chosen by finding out the typical errors for each sensor, which can be seen in Table 4.1.

Table 4.1: Standard deviation for sensor measurement noise

Sensor measurement	σ
Generator speed	0.017
Accelerometer	0.04
Blade root	–
Electrical power	0.035
Wind speed	1
Azimuth angle	–
Pitch angle	0.01

Apart from this, the state covariance P should be, by definition, symmetric positive definite. It was found out that this was not always possible to fulfil. The reasons for it not being positive definite could go from the system being unstable or not observable, both of which do not apply to our case, to having low values of the initial P with respect

to the actual errors or having high model uncertainty. If the Bladed data is taken as measurements, then it makes sense that initialising P with variances of magnitude close to 0.01 does not correctly represent the huge mismatch there is between our model and the one used by the simulation tool (which will be discussed in detail in Chapter 5). To prevent the code from stopping due to this issue, it was decided to implement Higham's method [43], which finds the nearest positive definite approximate of P (minimising the Frobenius norm of the difference) in case there is an iteration in which this condition is not fulfilled.

4.3 MPC Implementation

The theory behind MPC is explained in Section 3.5. Implementation and design choices are outlined here. Key consideration to make are the prediction horizon, control horizon, constraints, and weights. The MPC must be able to pursue two separate objectives depending on the wind speed. At rated and above-rated wind speeds, the objective is to maintain the rated ω_r of 7.56 rpm. In this scenario, the turbine has achieved rated production, and the blades will be pitched to maintain the rotor speed. Below rated wind speed, the blade pitch is fixed at 0° while the controller will maintain a TSR of 9.0621 which maximises the power coefficient. The generator torque will be altered as necessary to achieve this. While each blade has its own tip speed ratio, they are all relative to the rotor speed. As there is only one collective pitch reference, the lambda used will be based on the estimated effective wind velocity at hub height. This means that for below-rated wind speeds, the controller will utilise collective control. For above-rated wind speeds, the controller will utilise individual pitch control to maintain a constant torque on the rotor while compensating for cyclic variations in relative wind speeds seen by individual blades resulting from wind shear and tower shadow. Simultaneously, collective pitch will compensate for overall changes in wind speed. There are no separate setpoints, but both forms are implicit in the MPC control. The approach for individual pitch control should also attenuate the stress placed on the blades resulting fluctuations in loads. Additionally, the MPC should be able to use the turbine model to predict tower loads and minimise those as well. The controlled variables z that are of interest are the angular velocity of the rotor, tower fore-aft and lateral velocities, blade flap-wise and edge-wise velocities, tip speed ratio, pitch rate of the blades, and power generated. The controlled variables then become:

$$z = [\omega_r \quad \dot{x}_t \quad \dot{y}_t \quad \dot{x}_b \quad \dot{y}_b \quad \lambda \quad \theta_i \quad \dot{\theta}_i \quad P_e]^T \quad (4.34)$$

MathWorks [44] provides a simple and comprehensive approach to MPC design, and will serve as the guiding inspiration with the caveat that the guide is designed to be used with MATLAB tools, and will have to be adapted for use in a general case.

4.3.1 Horizons

The window parameter H_w is defined to be equal to 1 as input is assumed to be applied without delay. As a rule of thumb, the prediction horizon should be approximately equivalent to the closed-loop response time such that $T \approx H_p T_s \Leftrightarrow H_p = \frac{T}{T_s}$, though it must also be considered that larger prediction horizons can be computationally infeasible. Since pitch is only a concern for above-rated wind speeds, that is the region that will be considered. As turbulence is modelled as a first order system driven by white noise, large sudden fluctuations will be limited to a few outliers. The largest change in wind velocity seen by individual blades in the span of a few seconds thus happens as a result of the change in azimuth angle. For a given wind speed measured at the hub, the wind speed perceived by individual blades will increase and decrease with changes in altitude relative to the hub, with the lowest speeds additionally being affected by the tower shadow. As such the response time will be considered the time it takes for a blade to undertake the pitch adjustment in order to maintain a constant aerodynamic torque on the rotor in a worst case scenario.

The wind speed that brings about the largest difference in pitch from highest to lowest azimuth angle must be found. Using Equation 2.30, the wind seen by individual blades can be calculated. As the influence on the relative wind velocity caused by the tower fore-aft and blade flapwise movements are tiny compared to the wind itself, their influence on relative wind speed will not be considered, and in any case they amount to high frequency noise that the pitch cannot possibly adjust for. Similarly, the linearised model used for the MPC would not foresee the tower shadow until the blade is inside it due to the model's profound non-linearity, hence the tower shadow will also be disregarded from the relative wind calculation for each blade.

According to the Bladed model, the rated torque is 21,030,000 Nm. Fixing the desired torque for individual blades at $21,030,000/B \text{ Nm} = 7,010,000 \text{ Nm}$, the required power coefficient can be found, and with it the required pitch angle of the blades when the TSR of individual blades is known. Converting the force in Equation 2.28 back to torque and isolating the expression for C_p yields:

$$C_p(\lambda, \theta) = \frac{2BF_y\omega_r}{\rho v_r^3 A_r} \quad (4.35)$$

Testing on all wind speeds from 10.5 m/s to 24 m/s in increments of 0.1 m/s, a wind speed of 12.8 m/s is found to yield the largest pitch range. This gives a power coefficient of 0.4656 and 0.2358 for the lowest and highest azimuth angle respectively, wind speeds of 10.8274 m/s and 13.5843 m/s and local tip speed ratios of 8.8474 and 7.0518. The corresponding pitches are -3.4° and 9.1° . Considering a maximum pitch rate of 9° and disregarding an acceleration period for the pitching, the response time comes out to approximately 1.39 s. As a rule of thumb, the sampling time should be 10% to 25% of the response time. Setting the sample time $T_s = 0.25 \text{ s}$ and padding the response time up to 1.5 s to account for model inaccuracies yields a prediction horizon of $H_p = 6$. It

is generally preferable to have a substantially lower control horizon than prediction horizon, as this promotes faster computation and a more stable controller. For this reason, the control horizon will be set to $H_u = 3$. These values are subject to change following experimentation.

4.3.2 Constraints

For the input increment there are three variables to consider; maximum angular velocity of the blade pitch for each individual blade. Although the inputs are references and do not have limitations on how quickly they can change, experimentation has shown that the MPC is not stable without constraints placed on the slew rates of the blades. From Bladed data it is apparent that the blade pitch can attain a maximum angular velocity of $\pm 9^\circ/\text{s}$, corresponding to approximately $\pm 0.15708 \text{ rad/s}$. Accounting for sampling time, pitch constraints $\theta_{\Delta u, \min} = -0.15708 \cdot T_s \text{ rad}$ and $\theta_{\Delta u, \max} = 0.15708 \cdot T_s \text{ rad}$ are defined. As the generator torque can change virtually instantaneously, no constraint will be imposed on the change in generator torque. The input increment constraints can be defined accordingly:

$$\theta_{\Delta u, \min} \leq \Delta\theta_{i_{\text{ref}}} \leq \theta_{\Delta u, \max} \Leftrightarrow \begin{cases} -\Delta\theta_{i_{\text{ref}}} + \theta_{\Delta u, \min} \leq 0 \\ \Delta\theta_{i_{\text{ref}}} - \theta_{\Delta u, \max} \leq 0 \end{cases} \quad (4.36)$$

The inequality constraints are defined accordingly:

$$E \begin{bmatrix} \Delta\mathcal{U}(k) \\ 1 \end{bmatrix} \leq 0 \quad (4.37)$$

where:

$$E = \begin{bmatrix} -1 & 0 & 0 & 0 & \dots & 0 & \theta_{\Delta u, \min} \\ 1 & 0 & 0 & 0 & \dots & 0 & -\theta_{\Delta u, \max} \\ 0 & -1 & 0 & 0 & \dots & 0 & \theta_{\Delta u, \min} \\ 0 & 1 & 0 & 0 & \dots & 0 & -\theta_{\Delta u, \max} \\ 0 & 0 & -1 & 0 & \dots & 0 & \theta_{\Delta u, \min} \\ 0 & 0 & 1 & 0 & \dots & 0 & -\theta_{\Delta u, \max} \\ 0 & 0 & 0 & 0 & \dots & 0 & 0 \\ 0 & 0 & 0 & 0 & \dots & 0 & 0 \\ \vdots & \vdots & \vdots & \vdots & \ddots & \vdots & \vdots \\ 0 & 0 & 0 & 0 & \dots & 0 & 0 \\ 0 & 0 & 0 & 0 & \dots & 0 & 0 \end{bmatrix}, \quad \begin{bmatrix} \Delta\mathcal{U}(k) \\ 1 \end{bmatrix} = \begin{bmatrix} \Delta\hat{u}_1(k|k) \\ \Delta\hat{u}_2(k|k) \\ \Delta\hat{u}_3(k|k) \\ \Delta\hat{u}_4(k|k) \\ \vdots \\ \Delta\hat{u}_1(k + H_u - 1|k) \\ \Delta\hat{u}_2(k + H_u - 1|k) \\ \Delta\hat{u}_3(k + H_u - 1|k) \\ \Delta\hat{u}_4(k + H_u - 1|k) \\ 1 \end{bmatrix}$$

Constraints on input ranges will be defined according to Bladed data. The pitch reference for all blades as well as the generator torque are considered. The pitch of each blade ranges from -15° to 90° corresponding to -0.2618 rad to $\pi/2 \text{ rad}$. From Bladed data, the

demanded generator torque at above-rated wind velocities is found to be 21,030,000 Nm. For simplicity, the pitch lower and upper boundaries are defined as $\theta_{min} = -0.2618$ rad and $\theta_{max} = \pi/2$ rad and the generator torque upper boundary as $T_{g,max} = 21,030,000$ Nm. The input ranges can be defined accordingly:

$$\theta_{min} \leq \theta_{i_{ref}} \leq \theta_{max} \Leftrightarrow \begin{cases} -\theta_{i_{ref}} + \theta_{min} \leq 0 \\ \theta_{i_{ref}} - \theta_{max} \leq 0 \end{cases} \quad (4.38)$$

$$0 \leq T_{g_{ref}} \leq T_{g,max} \Leftrightarrow \begin{cases} -T_{g_{ref}} \leq 0 \\ T_{g_{ref}} - T_{g,max} \leq 0 \end{cases} \quad (4.39)$$

The inequality constraints are defined accordingly:

$$F \begin{bmatrix} \mathcal{U}(k) \\ 1 \end{bmatrix} \leq 0 \quad (4.40)$$

where:

$$F = \begin{bmatrix} -1 & 0 & 0 & 0 & \dots & 0 & \theta_{min} \\ 1 & 0 & 0 & 0 & \dots & 0 & -\theta_{max} \\ 0 & -1 & 0 & 0 & \dots & 0 & \theta_{min} \\ 0 & 1 & 0 & 0 & \dots & 0 & -\theta_{max} \\ 0 & 0 & -1 & 0 & \dots & 0 & \theta_{min} \\ 0 & 0 & 1 & 0 & \dots & 0 & -\theta_{max} \\ 0 & 0 & 0 & -1 & \dots & 0 & 0 \\ 0 & 0 & 0 & 1 & \dots & 0 & -T_{g,max} \\ \vdots & \vdots & \vdots & \vdots & \ddots & \vdots & \vdots \\ 0 & 0 & 0 & 0 & \dots & -1 & 0 \\ 0 & 0 & 0 & 0 & \dots & 1 & -T_{g,max} \end{bmatrix}, \quad \begin{bmatrix} \mathcal{U}(k) \\ 1 \end{bmatrix} = \begin{bmatrix} \hat{u}_1(k|k) \\ \hat{u}_2(k|k) \\ \hat{u}_3(k|k) \\ \hat{u}_4(k|k) \\ \vdots \\ \hat{u}_1(k + H_u - 1|k) \\ \hat{u}_2(k + H_u - 1|k) \\ \hat{u}_3(k + H_u - 1|k) \\ \hat{u}_4(k + H_u - 1|k) \\ 1 \end{bmatrix}$$

Constraints on controlled variable ranges will be designated according to the Bladed model. These are the rated values and not the true upper boundaries, as there is a safety margin. As a rule of thumb, an additional 10% padding will be added to the rated values to get the upper limits. The rated value of ω_r is 7.56 rpm corresponding to 0.7917 rad/s and the upper boundary then becomes 0.8709 rad/s defined as $\omega_{r,max}$. The minimum value is 5 rpm corresponding to 0.5236 rad/s. However, as the project delimitation limits controller operation to above-rated and below-rated wind speeds, a controller mechanism will not be designed to handle cut-out wind speeds. Due to the stochastic nature of the wind model, a range of mean wind speeds will occasionally produce wind speeds that fall below cut-out speeds. To avoid the MPC crashing due to infeasibility, the lower boundary will not be considered. This is technically not possible in a real life scenario but is necessary due to the limited scope of the project. The optimal TSR will be left unconstrained as it is only followed for rotor speeds of less than 7.56 rpm. According to the Bladed model, the

maximum angular velocity of the blade pitch is limited to $\pm 9^\circ/s$, consequently defining $\dot{\theta}_{min} = -0.1571$ rad/s and $\dot{\theta}_{max} = 0.1571$ rad/s. The constraint on the range of the blade pitch is the same as that defined for the input. The rated power output is 15 MW with the upper limit of $P_{e,max} = 22$ MW. Constraints are not placed on the tower and blade loads as there are no fixed limits to these values. The controlled variable ranges are defined accordingly:

$$\omega_{r,min} \leq \omega_r \leq \omega_{r,max} \Leftrightarrow \begin{cases} -\omega_r + \omega_{r,min} \leq 0 \\ \omega_r - \omega_{r,max} \leq 0 \end{cases} \quad (4.41)$$

$$\theta_{min} \leq \theta \leq \theta_{max} \Leftrightarrow \begin{cases} -\theta + \theta_{min} \leq 0 \\ \theta - \theta_{max} \leq 0 \end{cases} \quad (4.42)$$

$$\dot{\theta}_{min} \leq \dot{\theta} \leq \dot{\theta}_{max} \Leftrightarrow \begin{cases} -\dot{\theta} + \dot{\theta}_{min} \leq 0 \\ \dot{\theta} - \dot{\theta}_{max} \leq 0 \end{cases} \quad (4.43)$$

$$0 \leq P_e \leq P_{e,max} \Leftrightarrow \begin{cases} -P_e \leq 0 \\ P_e - P_{e,max} \leq 0 \end{cases} \quad (4.44)$$

The inequality constraints are defined accordingly:

$$G \begin{bmatrix} \mathcal{Z}(k) \\ 1 \end{bmatrix} \leq 0 \quad (4.45)$$

where:

$$G = \begin{bmatrix} -1 & 0 & 0 & 0 & \dots & 0 & 0 & 0 & 0 & 0 & \omega_{r,min} \\ 1 & 0 & 0 & 0 & \dots & 0 & 0 & 0 & 0 & 0 & -\omega_{r,max} \\ 0 & 0 & 0 & 0 & \dots & 0 & 0 & 0 & 0 & 0 & 0 \\ 0 & 0 & 0 & 0 & \dots & 0 & 0 & 0 & 0 & 0 & 0 \\ 0 & 0 & 0 & 0 & \dots & 0 & 0 & 0 & 0 & 0 & 0 \\ 0 & 0 & 0 & 0 & \dots & 0 & 0 & 0 & 0 & 0 & 0 \\ 0 & 0 & 0 & 0 & \dots & 0 & 0 & 0 & 0 & 0 & 0 \\ 0 & 0 & 0 & 0 & \dots & 0 & 0 & 0 & 0 & 0 & 0 \\ \vdots & \vdots & \vdots & \vdots & \ddots & \vdots & \vdots & \vdots & \vdots & \vdots & \vdots \\ 0 & 0 & 0 & 0 & \dots & 0 & 0 & 0 & 0 & 0 & 0 \\ 0 & 0 & 0 & 0 & \dots & 0 & 0 & 0 & 0 & 0 & 0 \\ 0 & 0 & 0 & 0 & \dots & 0 & 0 & -1 & 0 & 0 & \theta_{min} \\ 0 & 0 & 0 & 0 & \dots & 0 & 0 & 1 & 0 & 0 & -\theta_{max} \\ 0 & 0 & 0 & 0 & \dots & 0 & 0 & 0 & -1 & 0 & \dot{\theta}_{min} \\ 0 & 0 & 0 & 0 & \dots & 0 & 0 & 0 & 1 & 0 & -\dot{\theta}_{max} \\ 0 & 0 & 0 & 0 & \dots & 0 & 0 & 0 & 0 & -1 & 0 \\ 0 & 0 & 0 & 0 & \dots & 0 & 0 & 0 & 0 & 1 & -P_{e,max} \end{bmatrix}, \quad \begin{bmatrix} \mathcal{Z}(k) \\ 1 \end{bmatrix} = \begin{bmatrix} \hat{z}_1(k+1|k) \\ \hat{z}_2(k+1|k) \\ \hat{z}_3(k+1|k) \\ \hat{z}_4(k+1|k) \\ \vdots \\ \hat{z}_5(k+H_p|k) \\ \hat{z}_6(k+H_p|k) \\ \hat{z}_7(k+H_p|k) \\ \hat{z}_8(k+H_p|k) \\ \hat{z}_9(k+H_p|k) \\ 1 \end{bmatrix}$$

4.3.3 Setpoints

The setpoints will combine with the weights to calculate the cost function in the MPC. Not all setpoints will be active depending on the wind speed. This will be solved by setting their respective weights to 0. The rated rotor speed ω_r will follow a setpoint of 0.7917 rad/s at above-rated wind speeds. All of the tower and blade loads will follow a setpoint of 0. λ will follow the optimal TSR of 9.0621 at below-rated wind speeds. The blade pitch angles will follow a setpoint of 0° at below-rated wind speeds, and the power output will follow a setpoint of 15 MW at above-rated wind speeds. The blade pitch rates have no setpoint as they only exist as controlled variables to be constrained.

4.3.4 Weights

Before determining weights, scaling parameters will be defined for all the input increment and output variables. The scaling parameters will be defined according to the full span of their respective variables. The variables will be divided by their respective parameter, which achieves a normalising effect. This is especially important as variables differ by several orders of magnitude. The benefit of scaling parameters is that it allows for a choice of weights that only have to factor in the importance of tracking a given variable without having to consider the magnitude of said variable. The span of variables will not consider the additional 10% added to the constraints of ω_r and P_e as this additional range is never intentionally entered. λ ranges from 21.12 at the cut-in wind speed of 3 m/s to 3.99 at the cut-out wind speed of 24 m/s. From the Bladed model and pre-existing simulation data for wind velocities of approximately 24 m/s, the following scaling parameters have been chosen for the remaining variables:

$$\Delta r_s = [1.8326 \quad 21,030,000]^T \quad (4.46)$$

$$q_s = [1.0472 \quad 0.4 \quad 0.3 \quad 18.7 \quad 12 \quad 17.12 \quad 1.8326 \quad 0.3142 \quad 22,022,564]^T \quad (4.47)$$

Where the entries of q_s correspond to those of Equation 4.34 and the entries of r_s correspond to the increments of Equation 4.2. Model uncertainties can result in large input increments to correct for unpredictable deviations. Larger weights result in smaller input increments due to penalising the input, which makes the controller more robust when dealing with flaws in the model prediction at the cost of reducing tracking performance. There is a substantial possibility of inaccuracies given the complexity of the turbine model. However, it is important to note that the pitch and pitch rate have both been constrained to within their physical operating limits. For this reason there is not much concern about large input increments, and a default value of 0.1 for both input increments is chosen in order to prioritise reference tracking. The weight matrix R is defined accordingly:

$$R = \begin{bmatrix} 0.1 & 0 \\ 0 & 0.1 \end{bmatrix} \quad (4.48)$$

The weights for the controlled variables will be designated according to the importance of tracking the corresponding variable and how large a tracking error is considered acceptable, with lower weights being lower priority. The following weights will be considered:

- 0 - Setpoint does not apply
- 0.05 - Low priority; Large tracking error acceptable
- 0.2 - Below-average priority
- 1 - Average priority; Default value
- 5 - Above average priority
- 20 - High priority; Small tracking error desired

The tower loads are unavoidable, but it is still desirable to minimise them. Their weights are all set to 1. Regardless of wind speed, the pitch rate has no reference and as such will not have a weight.

For above-rated wind speeds, the main priority is to ensure that ω_r maintains the rated value of 0.7917 rad/s and does not go over that value to avoid straining the turbine, and the secondary priority is to maximise power output P_e . For this reason, ω_r will be given a weight of 20. This weight alone will not maximise the power output as there are two degrees of freedom in the generator torque and blade pitch, and a sub-optimal combination could be chosen which does not maximise power output. For this reason the power output will receive a weight of 5 to ensure it is given greater importance than the loads such that the generator torque will be maximised without doing so at the expense of ω_r . The blade pitch angle is left with a weight of 0 as the remaining degree of freedom for the MPC to alter to minimise the cost function. The weight for λ will also be set to 0 as the optimal TSR is not of interest here.

For below-rated wind speeds, the weights for λ and θ_i will be set to 20. This ensures a maximisation of the power coefficient. The weight for ω_r will be set to 0 as it is not desirable to reach the rated rotor speed for below-rated winds. The MPC will automatically apply the generator torque that accomplishes this, effectively maximising power output without needing to apply a weight. To avoid penalising the below-rated power output, P_e will be given a weight of 0 as it is not possible to reach the 15 MW setpoint. Two tracking error weight matrices Q_1 and Q_2 are defined according to whether the rated ω_r or optimal

TSR is pursued respectively:

$$Q_1 = \begin{bmatrix} 20 & 0 & 0 & 0 & 0 & 0 & 0 & 0 & 0 \\ 0 & 1 & 0 & 0 & 0 & 0 & 0 & 0 & 0 \\ 0 & 0 & 1 & 0 & 0 & 0 & 0 & 0 & 0 \\ 0 & 0 & 0 & 1 & 0 & 0 & 0 & 0 & 0 \\ 0 & 0 & 0 & 0 & 1 & 0 & 0 & 0 & 0 \\ 0 & 0 & 0 & 0 & 0 & 0 & 0 & 0 & 0 \\ 0 & 0 & 0 & 0 & 0 & 0 & 0 & 0 & 0 \\ 0 & 0 & 0 & 0 & 0 & 0 & 0 & 0 & 0 \\ 0 & 0 & 0 & 0 & 0 & 0 & 0 & 0 & 20 \end{bmatrix}, Q_2 = \begin{bmatrix} 0 & 0 & 0 & 0 & 0 & 0 & 0 & 0 & 0 \\ 0 & 1 & 0 & 0 & 0 & 0 & 0 & 0 & 0 \\ 0 & 0 & 1 & 0 & 0 & 0 & 0 & 0 & 0 \\ 0 & 0 & 0 & 1 & 0 & 0 & 0 & 0 & 0 \\ 0 & 0 & 0 & 0 & 1 & 0 & 0 & 0 & 0 \\ 0 & 0 & 0 & 0 & 0 & 20 & 0 & 0 & 0 \\ 0 & 0 & 0 & 0 & 0 & 0 & 20 & 0 & 0 \\ 0 & 0 & 0 & 0 & 0 & 0 & 0 & 0 & 0 \\ 0 & 0 & 0 & 0 & 0 & 0 & 0 & 0 & 0 \end{bmatrix} \quad (4.49)$$

4.4 Control Algorithm

The developed MATLAB code comprising the whole state estimation and control procedure follows the structure presented in Algorithm 1. The explanation of functions is included when those functions have been implemented, that is, when they are not built-in in MATLAB or taken from a third party.

Algorithm 1 Estimation and control procedure

```

1:  $f(x), h(x)$  ▷ Define non-linear model
2:  $x_{tv_0} \leftarrow x_i$  ▷ Initialize true values, state estimations and inputs with initial conditions
3:  $y_{tv_0} \leftarrow y_i$ 
4:  $\hat{x}_0 \leftarrow x_i$ 
5:  $u_{prev} \leftarrow u_i$ 
6:  $z_{ref} \leftarrow$  Desired reference ▷ Define reference values for the MPC
7:  $x_{op} \leftarrow x_i$  ▷ Initialize operating point for the MPC linear model
8:  $Q, R$  ▷ Define process and measurement noise matrices
9:  $P_0 \leftarrow P_i$  ▷ Initialize error covariance matrix
10: for  $k = 0 \rightarrow N$  do
11:    $\hat{u}_k \leftarrow \text{MPC}(\hat{x}_k, x_{op}, u_{prev}, z_{ref_{k:k+H_p}})$  ▷ Compute optimal control signal
12:    $u_{prev} \leftarrow \hat{u}_k$ 
13:    $[x_{tv_{k+1}}, y_{tv_{k+1}}] \leftarrow \text{NONLINEARSIM}(x_{tv_k}, \hat{u}_k, Q, R)$  ▷ Simulate non-linear system
14:    $y_{me_{k+1}} \leftarrow$  Sensor measurements (Bladed)
15:    $[\hat{x}_{k+1}, P_{k+1}] \leftarrow \text{UKF}(\hat{x}_k, y_{me_{k+1}}, u_{prev}, f(x), h(x), Q_k, R, P_k)$  ▷ Perform state estimation
(if real measurements cannot be used, replace  $y_{me}$  by  $y_{tv}$ )
16:    $x_{op} \leftarrow \hat{x}_{k+1}$  ▷ If  $y_{tv}$  is used in UKF,  $x_{tv}$  can replace  $\hat{x}$ 
17: end for

18: function  $\text{UKF}(\hat{x}_k, y_{me_{k+1}}, \hat{u}_k, f(x), h(x), Q_k, R, P_k)$ 
19:    $\alpha, \beta, \kappa \leftarrow$  Tuning values
20:   if  $P_k \leq 0$  then
21:      $P_k \leftarrow \text{NEARESTSPV}(P_k)$  ▷ If  $P_k \leq 0$ , find nearest symmetric positive definite
matrix using Higham's algorithm
22:   end if
23:    $c_i \leftarrow \text{CHOL}(P_k)$  ▷  $i^{\text{th}}$  column of a lower Cholesky factorization of  $P_k$ 
24:    $\lambda = \alpha^2(n + \kappa) - n$ 
25:    $\mathcal{X}_k = [\hat{x}_k \quad \hat{x}_k + \sqrt{(n + \lambda)}c_i \quad \hat{x}_k - \sqrt{(n + \lambda)}c_i]$   $1 \leq i \leq n$  ▷ Define sigma points
26:    $W^{(i)} = \frac{1}{2(n + \lambda)}$   $1 \leq i \leq 2n$ 
27:    $W_c = \begin{bmatrix} \frac{\lambda}{n + \lambda} & W^{(i)} \end{bmatrix}$  ▷ Weight for transformed covariance
28:    $W_m = \begin{bmatrix} \frac{\lambda}{n + \lambda} + (1 - \alpha^2 + \beta) & W^{(i)} \end{bmatrix}$  ▷ Weight for transformed mean
29:    $\mathcal{X}_{k+1|k} \leftarrow \text{RK4}(f(x), h(x), \mathcal{X}_k, \hat{u}_k, n, v)$  ▷ Prediction transformation
30:    $\hat{x}_{k+1|k} = \sum_{i=1}^{2n+1} W_m^{(i)} \mathcal{X}_{k+1|k}^{(i)}$  ▷ Mean of predicted state
31:    $P_{k+1|k} = Q_k + \sum_{i=1}^{2n+1} W_c^{(i)} \left( \mathcal{X}_{k+1|k}^{(i)} - \hat{x}_{k+1|k} \right) \left( \mathcal{X}_{k+1|k}^{(i)} - \hat{x}_{k+1|k} \right)^T$  ▷ Covariance of
predicted state
32:    $\psi_{k+1|k} = h(\mathcal{X}_{k+1|k}, u_{prev})$  ▷ Observation transformation
33:    $\hat{y}_{k+1|k} = \sum_{i=1}^{2n+1} W_m^{(i)} \psi_{k+1|k}^{(i)}$  ▷ Mean of predicted output

```

```

34:    $P_{k+1}^{yy} = R + \sum_{i=1}^{2n+1} W_c^{(i)} \left( \psi_{k+1|k}^{(i)} - \hat{y}_{k+1|k} \right) \left( \psi_{k+1|k}^{(i)} - \hat{y}_{k+1|k} \right)^T$    ▷ Covariance of
      predicted output
35:    $P_{k+1}^{xy} = \sum_{i=1}^{2n+1} W_c^{(i)} \left( \mathcal{X}_{k+1|k}^{(i)} - \hat{x}_{k+1|k} \right) \left( \psi_{k+1|k}^{(i)} - \hat{y}_{k+1|k} \right)^T$    ▷ Cross-covariance between
      state and output
36:    $K_{k+1} = P_{k+1}^{xy} \left( P_{k+1}^{yy} \right)^{-1}$    ▷ Kalman gain
37:    $\hat{x}_{k+1} = \hat{x}_{k+1|k} + K_{k+1} (y_{me_{k+1}} - \hat{y}_{k+1|k})$    ▷ Update state estimate
38:    $P_{k+1} = P_{k+1|k} - K_{k+1} P_{k+1}^{yy} K_{k+1}^T$    ▷ Update covariance estimate
39:   return  $\hat{x}_{k+1}, P_{k+1}$ 
40: end function

41: function NONLINEARSIM( $x_{tv_k}, \hat{u}_k, Q, R$ )
42:    $n = \sqrt{Q} \cdot N(0, 1)$    ▷ Process noise
43:    $v = \sqrt{R} \cdot N(0, 1)$    ▷ Measurement noise
44:    $[x_{tv_{k+1}}, y_{tv_{k+1}}] \leftarrow \text{RK4}(f(x), h(x), x_{tv_k}, \hat{u}_k, n_k, v_k)$    ▷ 4th order Runge-Kutta
45:   return  $x_{tv_{k+1}}, y_{tv_{k+1}}$ 
46: end function

47: function MPC( $\hat{x}_k, x_{op}, u_{prev}, z_{ref_{k:k+H_p}}$ )
48:    $A, B, C, D$    ▷ Define linear model
49:    $Q, R$    ▷ Define weight matrices
50:    $H_p, H_u, H_w$    ▷ Define prediction and control horizon, and window parameter
51:    $\mathcal{A}, \mathcal{B}_u, \mathcal{B}_{\Delta u}, \mathcal{C}, \mathcal{Q}, \mathcal{R}$    ▷ Lifting procedure
52:    $\mathcal{U} = [\hat{u}_k^T \dots \hat{u}_{k+H_u-1}^T]^T$    ▷ Vector comprising control signals to be computed
53:    $\Delta \mathcal{U} = [\Delta \hat{u}_k^T \dots \Delta \hat{u}_{k+H_u-1}^T]^T$    ▷ Vector comprising change in control signals
54:    $\mathcal{X} = \mathcal{A} \hat{x}_k + \mathcal{B}_u u_{prev} + \mathcal{B}_{\Delta u} \Delta \mathcal{U}$    ▷ State predictions
55:    $\Psi = \mathcal{C} \mathcal{A}, \mathcal{Y} = \mathcal{C} \mathcal{B}_u, \Theta = \mathcal{C} \mathcal{B}_{\Delta u}$ 
56:    $\mathcal{Z} = \Psi \hat{x}_k + \mathcal{Y} u_{prev} + \Theta \Delta \mathcal{U}$    ▷ Predictions for controlled outputs

57:    $\mathcal{T} = \begin{bmatrix} z_{ref_{k+H_w}} \\ \vdots \\ z_{ref_{k+H_p}} \end{bmatrix}$    ▷ Vector comprising reference values
58:    $\mathcal{E} = \mathcal{T} - \Psi \hat{x}_k - \mathcal{Y} u_{prev}$    ▷ Difference between reference trajectory and predicted
      controlled outputs with  $\Delta \mathcal{U} = 0$ 
59:    $\mathcal{G} = 2\Theta^T \mathcal{Q} \mathcal{E}, \mathcal{H} = \Theta^T \mathcal{Q} \Theta + \mathcal{R}$ 
60:    $V = \mathcal{E}^T \mathcal{Q} \mathcal{E} - \Delta \mathcal{U}^T \mathcal{G} + \Delta \mathcal{U}^T \mathcal{H} \Delta \mathcal{U}$    ▷ Cost function
61:    $F, E, G$    ▷ Define constraint matrices
62:   Constraints  $\leftarrow F \begin{bmatrix} \mathcal{U} \\ 1 \end{bmatrix} \leq 0, E \begin{bmatrix} \Delta \mathcal{U} \\ 1 \end{bmatrix} \leq 0, G \begin{bmatrix} \mathcal{Z} \\ 1 \end{bmatrix} \leq 0,$ 
63:    $[\hat{u}_{k:k+H_u-1}, x_{MPC_{k+1:k+H_p}}] \leftarrow \text{MPCOBJ}(\text{Constraints}, V, \hat{x}_k, x_{op}, u_{prev}, z_{ref_{k:k+H_p}})$    ▷ Solve
      using YALMIP-Mosek
64:   return  $\hat{u}_k$ 
65: end function

```

Chapter 5

RESULTS AND DISCUSSION

5.1 Introduction

The main results obtained will be presented in this chapter, followed by a discussion regarding their correctness, stability and reliability, among other properties. All in all, the feasibility of the estimation and control procedure derived to this point will be tested.

5.2 Non-linear Simulation

In order to simulate the non-linear model derived in Sections 2.2 to 2.6 and rewritten in state space form in Section 4.2, it is necessary to discretize the model, and to provide it with control inputs in each time step. The control inputs have been computed for a below-rated power production scenario using the simple torque control derived in Section 3.4, which sets the pitch angle of the blades to 0° while computing the torque reference as the constant K times the rotor speed squared.

Initially, Euler's method was chosen as the discretisation procedure due to its simplicity, but it was found out to be not precise enough for our system, as it gave an unstable response. The dynamics of the different mechanical components were analysed independently, finding out that the poles of the linearised blade dynamics were particularly close to the imaginary axis. This caused the poles of the discretised linear system to lie slightly outside the unit circle, thus provoking instability. For this reason, a more precise approach such as 4th order Runge-Kutta was chosen. A comparison of the edgewise blade deflection using both Euler's method and 4th order Runge-Kutta can be seen in Figs. 5.1a and 5.1b.

It is important to remark the apparent difference in oscillation frequency between the Bladed signal and our model's signal, noticeable in Fig. 5.1b. The high frequency oscillations represent the blade dynamics, while the low frequency oscillations are induced by the tower dynamics. The amplitude of the low frequency oscillations is much more prominent in the Bladed simulation due to differences in the model that remain unknown, although it is believed to be caused by the effect of gravity, as this mismatch is exclusively seen in the edgewise blade dynamics. It is difficult to see these oscillations in the simulation of our model, but as soon as the signal approaches steady state it becomes more clear (in Appendix B see Fig. B.3k to find the plot for all the simulation time). Besides, a larger amplitude can be observed in the high frequency oscillations during the signal transient

of the simulation of our model, which is perfectly normal.

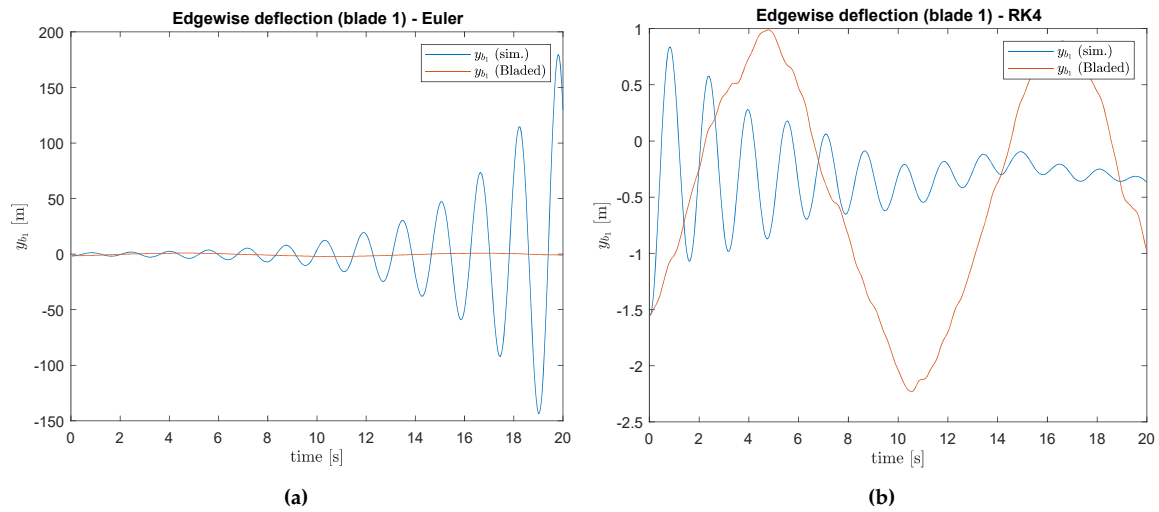


Figure 5.1: Simulation of edgewise blade deflection using Euler (a) or 4th order Runge-Kutta (b) discretization method for 20 s. Bladed data has been also added for comparison purposes.

The wind speed has an important randomness associated to it which makes it vary differently in both Bladed and our simulation. The plot seen in Fig. 5.2 shows that they present similar characteristics regarding mean and perhaps a slightly larger turbulent intensity in the wind from Bladed. Regardless, the wind model used seems adequate.

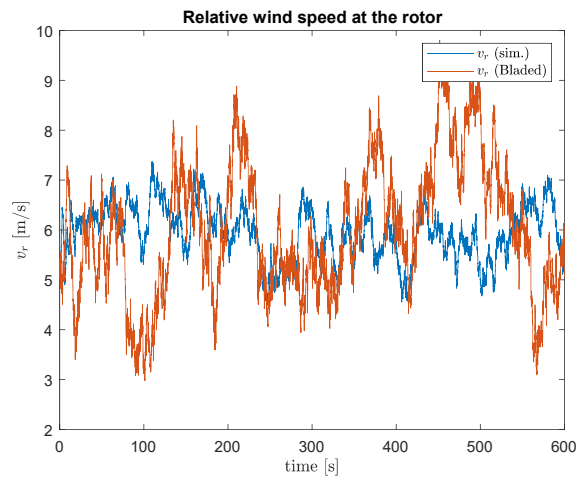


Figure 5.2: Relative wind speed measured in the nacelle.

Apart from that, the wind speed experienced by each individual blade including the effect of wind shear and tower shadow is plotted in Figs. 5.3a and 5.3b. The graphs shows the characteristic periodic oscillations that had been previously depicted in Fig. 2.9.

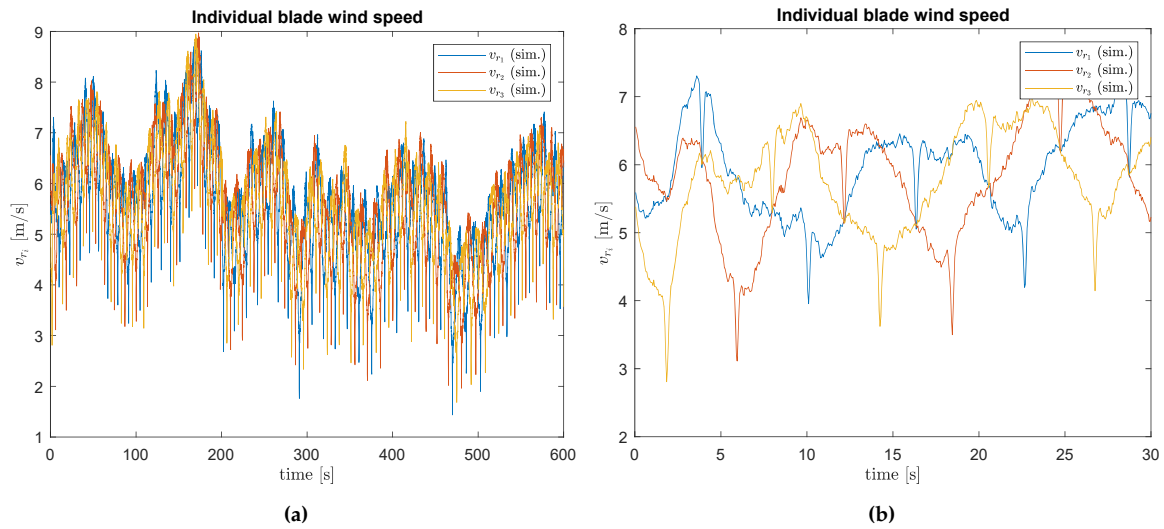


Figure 5.3: Wind speed experienced by each blade in their movement through the rotor plane (a), with zoom into the first 30s (b).

The mismatch in wind speed leads to different driving torque and thrust forces, which will influence the generator's reaction torque and the angular speed of the rotor, apart from the structural dynamics. This can be observed in Figs. 5.4a and 5.4b. Besides, the rotor speed is much more stable in the simulation from Bladed, which is explained by the more sophisticated control used by the simulation tool.

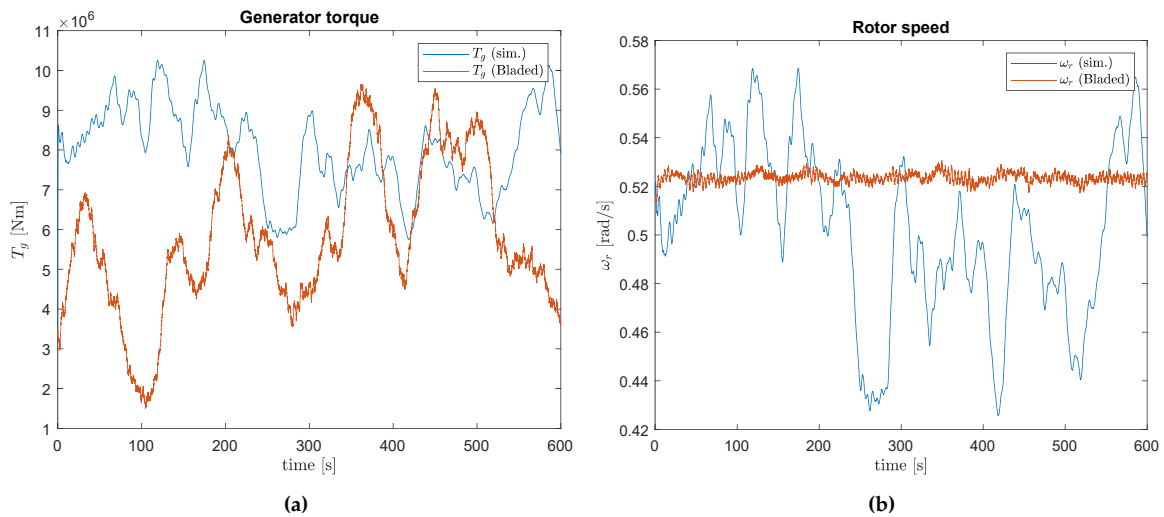


Figure 5.4: Generator torque (a) and rotor speed (b).

To check the plots for the rest of the system states, including structural dynamics, in comparison with the simulation data from Bladed, see Fig. B.3 in Appendix B.

5.3 Unscented Kalman Filter

The performance of the UKF seems to be greatly affected by the large mismatch between the model outputs and the Bladed data. For this reason, it has not been possible to obtain acceptable results combining both simulation data, as the estimations soon tend towards infinity. The problem was tackled by selecting the states or functions of states that could be measured in real life from the non-linear simulation and adding noise to simulate the typical inaccuracy of real sensor measurements. This way, the measurements are closely related to the states and the previous large mismatch disappears. This solution is not ideal at all, as it means that the designed estimation and control algorithm would have problems when being implemented in a real life scenario, and shows the importance of using an accurate model to represent the system. Applying this change, the UKF was able to accurately estimate the states with an error lower than 4.5%. The noise with largest variance was applied to the wind speed to represent the inaccuracy of anemometer measurements at the nacelle, and its UKF estimation can be seen in Fig. 5.5.

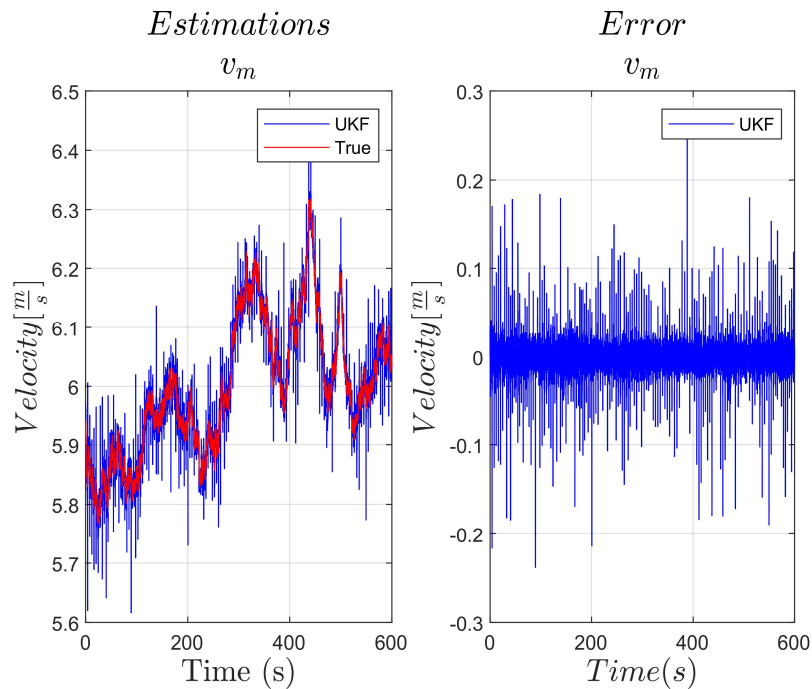


Figure 5.5: UKF estimation of mean wind speed measured in the nacelle.

The estimated tower and blade deflections are shown in Fig. 5.6 as an example of the UKF performance in some of the other states. To check the rest of the plots, see Fig. B.4 in Appendix B.

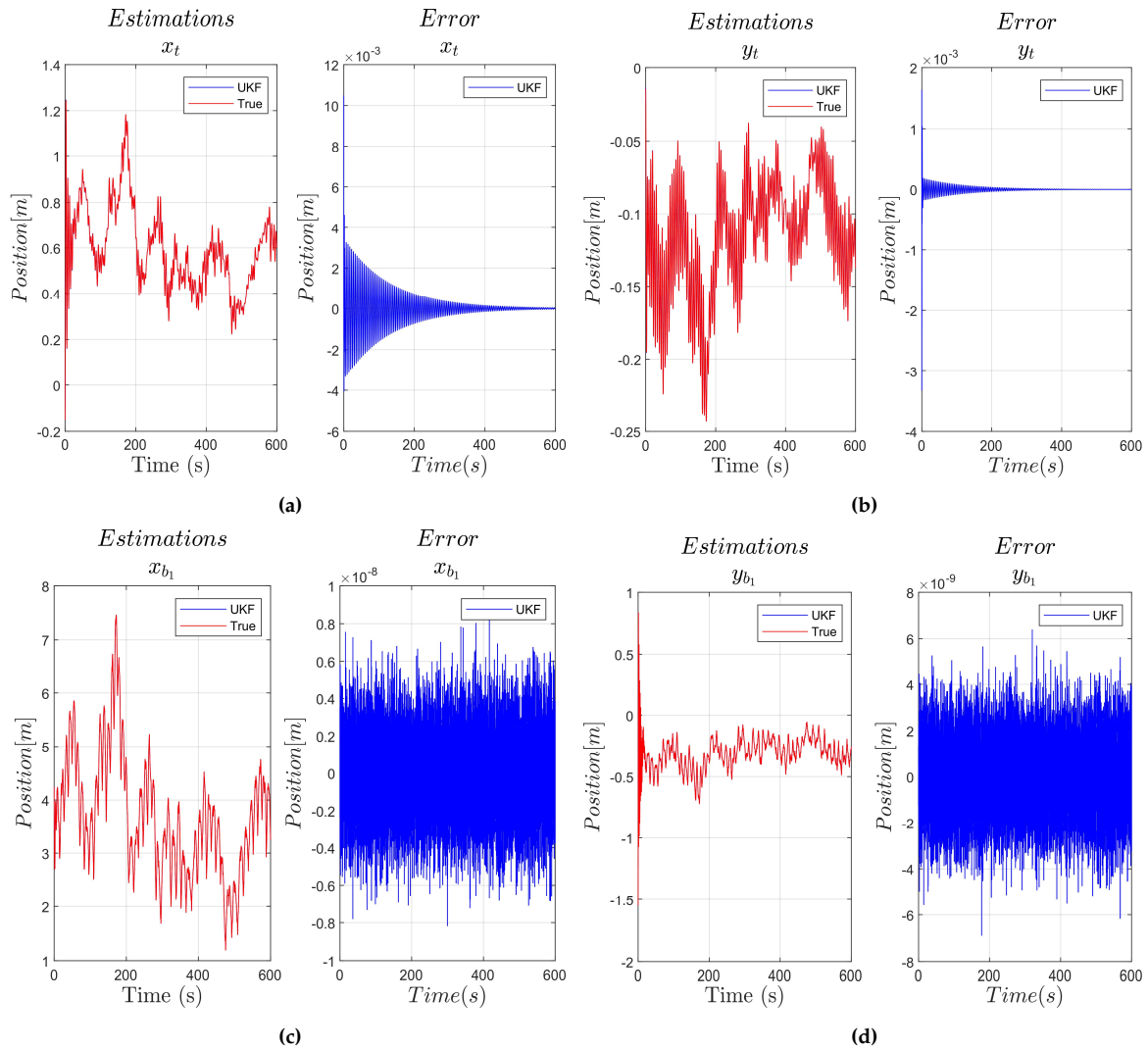


Figure 5.6: UKF estimation for tower and blade deflection.

5.4 Linear Simulation

The linear prediction model used in the MPC is simulated separately using the same torque controller that was previously used to simulate the non-linear model. The linearisation has been performed around certain operating points that change with time, which means that the system matrices must change with each time step. Besides, 4th order Runge-Kutta has also been chosen as discretisation method for the reasons stated in Section 5.2.

The structural dynamics shown in Fig. 5.7 exhibit high oscillations and considerable instability. The oscillations are mainly induced by the partial derivatives of the blade

flapwise and edgewise dynamics with respect to the azimuth angle, as they deal with highly non-linear terms corresponding to the wind shear and tower shadow effects, that are very dependent on the operating point of the azimuth angle, which at the same time varies significantly with each iteration.

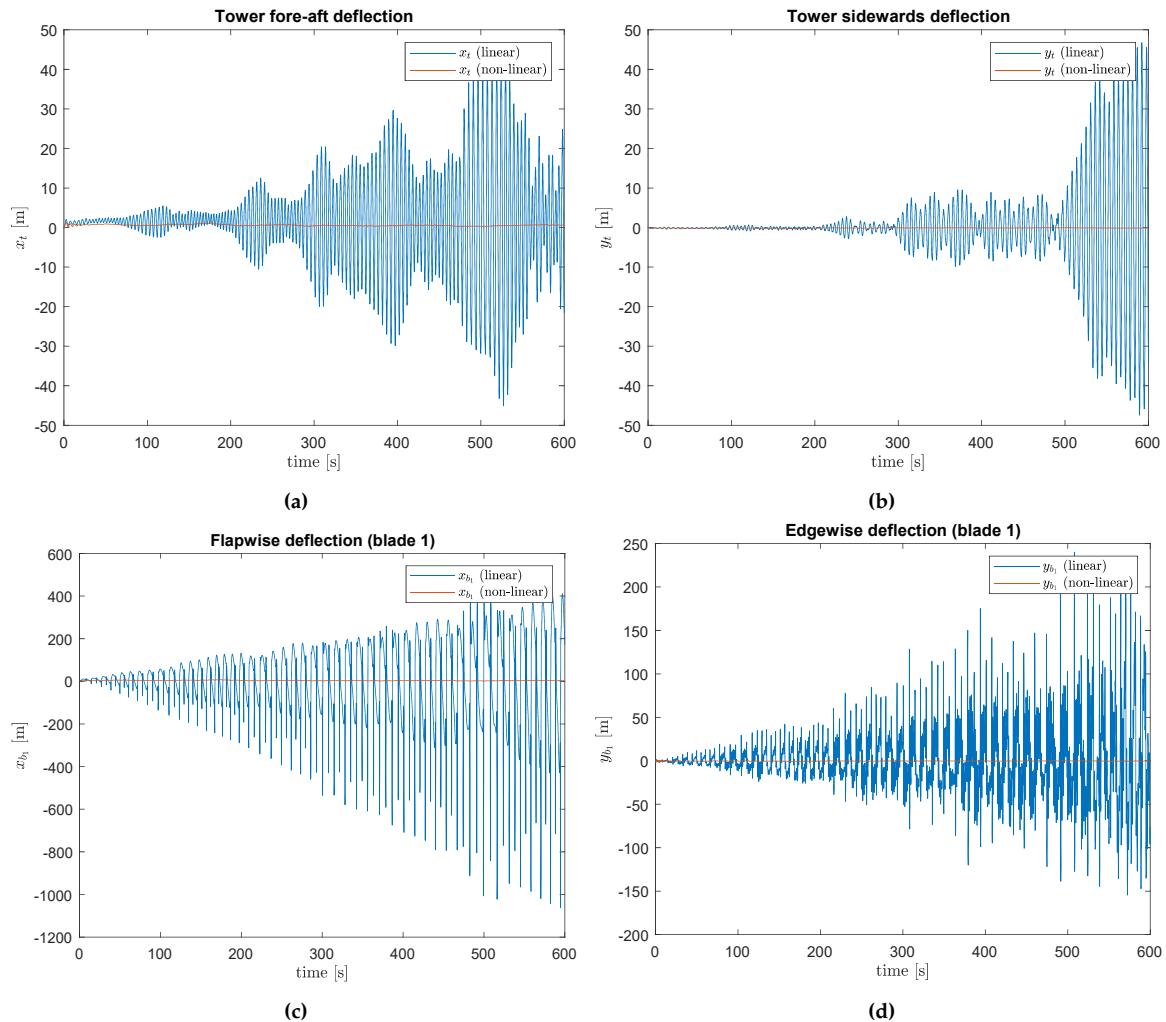


Figure 5.7: Linear model simulation for tower and blade deflection.

Another simulation was performed removing the wind shear and tower shadow expressions from the system in order to check if it gives stable and more accurate responses, and also to simplify the linearisation process, making it easier to detect any possible error. This gave the results shown in Fig. 5.8, which exhibit much more acceptable responses. No error was found in the linearisation process, although a certain offset can be observed in some of the states, namely the out-of-plane blade and tower dynamics, now that there are no large oscillations overshadowing it. Its cause remains unknown, as the maths behind

the derivation of the linear model seem to be correct (see Section 2.8).

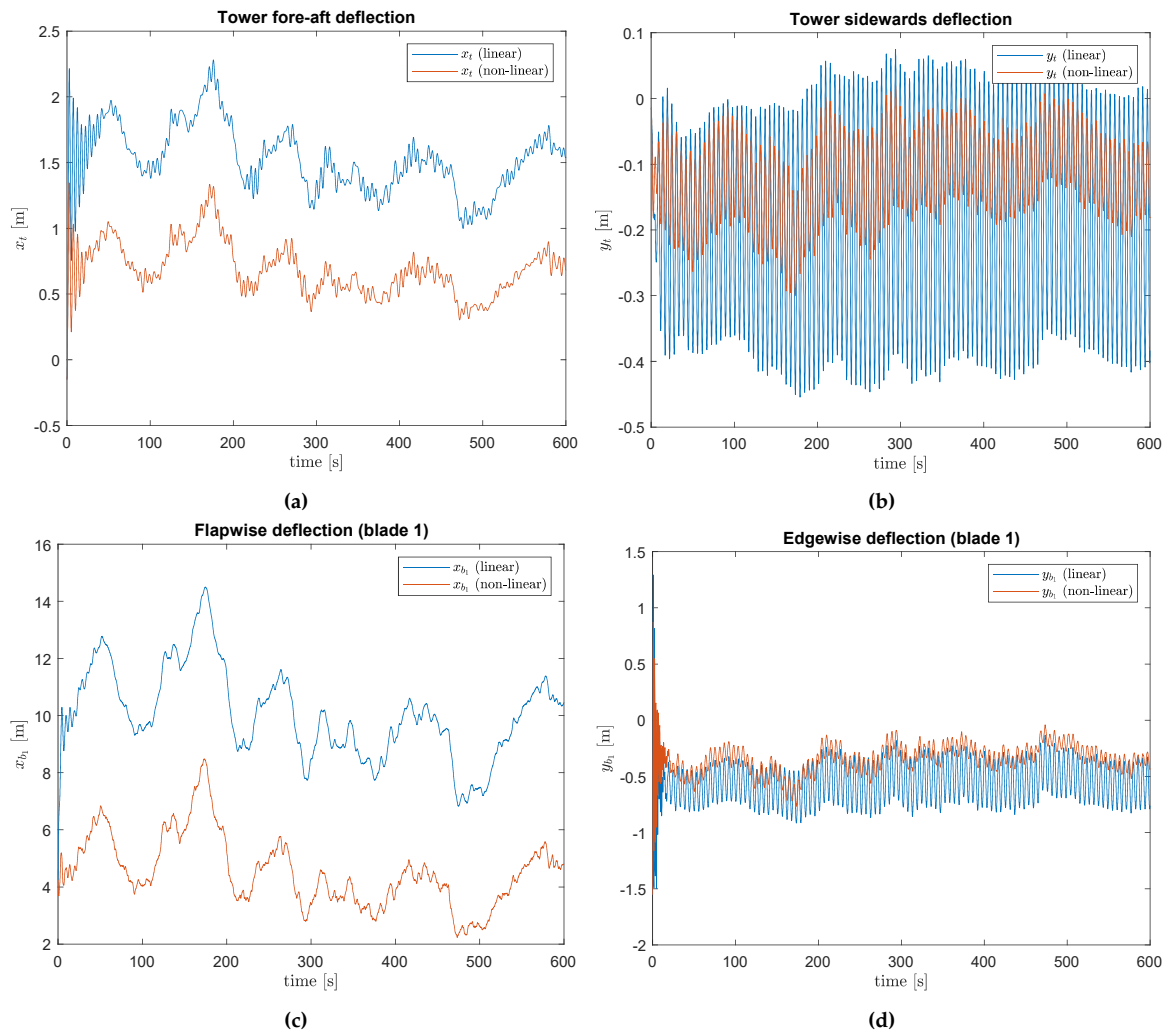


Figure 5.8: Linear model simulation for tower and blade deflection without considering wind shear and tower shadow.

As a last attempt to try to improve the linear system's performance (including wind shear and tower shadow), it was decided to reduce the sample time from 0.05 s to 0.01 s. Figure 5.9 shows a less unstable behaviour in exchange of presenting oscillations of even larger amplitude than in Fig. 5.7, which incline us to think that there is no way of obtaining a more acceptable linear system response by using the simple torque controller derived in Section 3.4 along with the non-linear model considered. Hence, it remains the job of the MPC to try to change this.

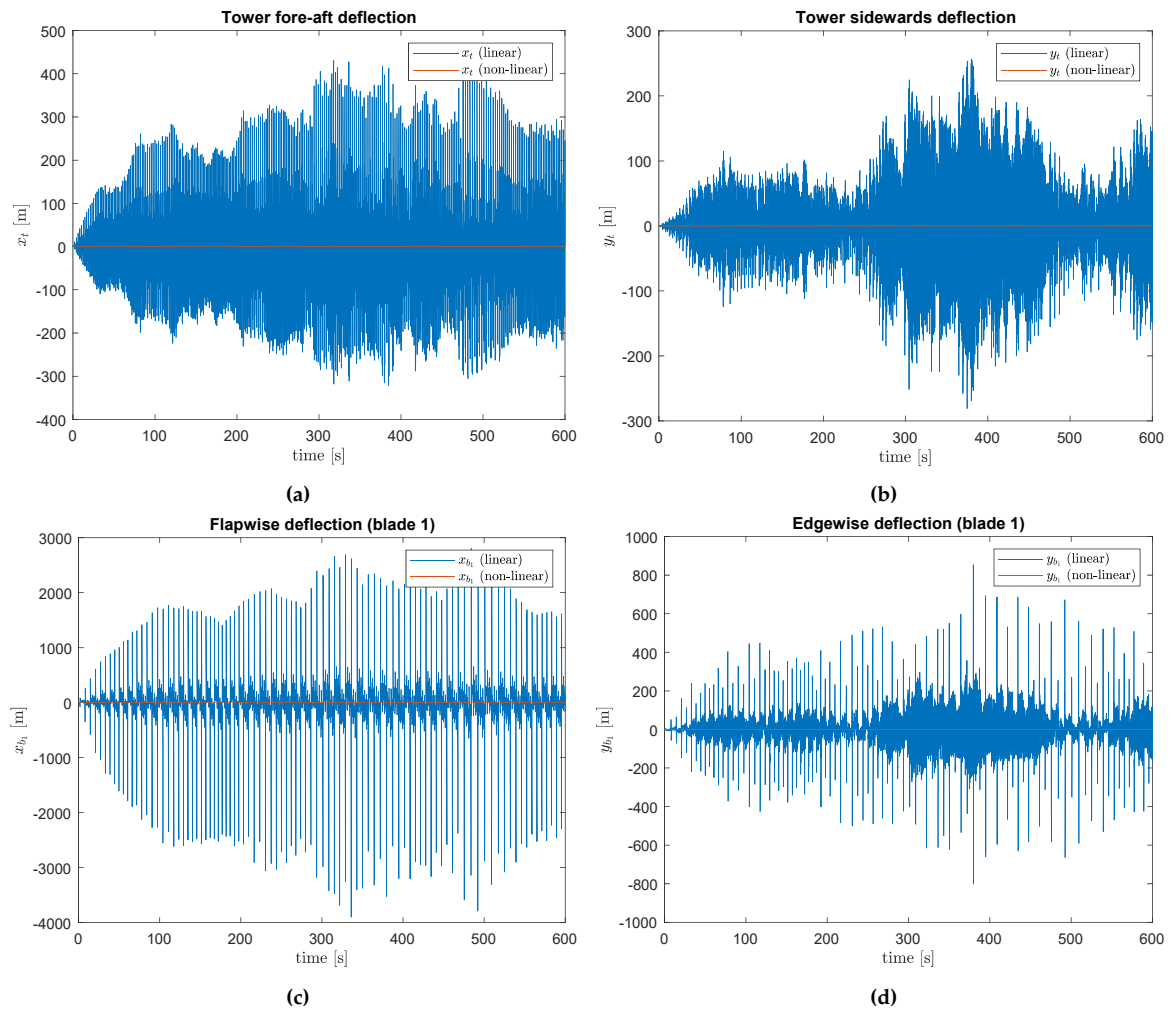


Figure 5.9: Linear model simulation for tower and blade deflection reducing the sampling time from 0.05 s to 0.01 s.

5.5 MPC

It was possible to obtain results using the MPC with the following settings: wind speed of 6 m/s to simulate below-rated power production; wind shear and tower shadow removed from the model and no constraints on the controlled variable ranges, as considering both causes the optimisation algorithm to become infeasible after some iterations. This is believed to be caused by the way the incremental variables of the linearised system have been used. Lets recall the way the linearised system is really defined, which can be seen in Section 5.5, in contrast with how it is expressed in Eq. 2.120. This means that all the variables are referenced to the corresponding operating point of the current iteration,

something that was mistakenly ignored.

$$\Delta\dot{x} = A\Delta x + B\Delta u \quad (5.1)$$

$$\Delta y = C_y \Delta x \quad (5.2)$$

$$\Delta z = C_z \Delta x \quad (5.3)$$

Taking this into account, a new term would appear by grouping the constant terms (Section 5.5), which would have to be considered in the lifting procedure of the MPC [45].

$$\dot{x} - \dot{x}_{op} = A(x - x_{op}) + B(u - u_{op}) \rightarrow \dot{x} = Ax + Bu + K \quad (5.4)$$

$$y = C_y x \quad (5.5)$$

$$z = C_z x \quad (5.6)$$

Anyways, the erroneous results obtained to this point will be analysed hereafter, leaving the mentioned change to be implemented after hand in due to time constraints.

Taking into account that the data from Bladed uses a sampling time of 0.05 s, which has been used to simulate the non-linear model, UKF and linearised model, and that the last one already exhibits a highly oscillatory behaviour, it is believed that using the sampling time of 0.25 s chosen in Section 4.3 would only worsen the performance. In addition to this, prediction and control horizons were both set to 10. These values are, however, not in accordance with the approach outlined by MathWorks.

With the settings considered, it is clear that performing IPC will not be possible, as the deterministic cyclic loads produced by wind shear and tower shadow have been removed. Still, as this simulation concerns below-rated power production, the control objectives require that the pitch of the blades is kept at 0 rad while the TSR is kept at its optimal value by regulating rotor speed through the generator torque.

The graphs shown below compare the performance of both the linear system and the non-linear system using the control signals generated by the MPC. Fig. 5.10d shows that the pitch is approximately kept in 0 rad. At the same time, the generator torque gradually decreases until none is applied (Fig. 5.10c), which makes the rotor speed rise above not only the rated, but also the maximum rotor speed (Fig. 5.10b). This would have violated the constraints if they had been added to the optimiser. The reason for this behaviour is that the MPC is trying to keep the TSR at the optimal value of 9.0621, but due to the issue stated previously, its value is much lower than it should, which can be seen in Fig. 5.11 (around 0.1). Hence, the MPC tries to correct this by increasing the rotor speed, reducing the generator torque. But it is easily seen that, in reality, the value of the TSR greatly surpasses its optimal (as an example, the value of λ using the wind and rotor speed taken after 100 s would be around 17, which can be also checked in Fig. 5.11).

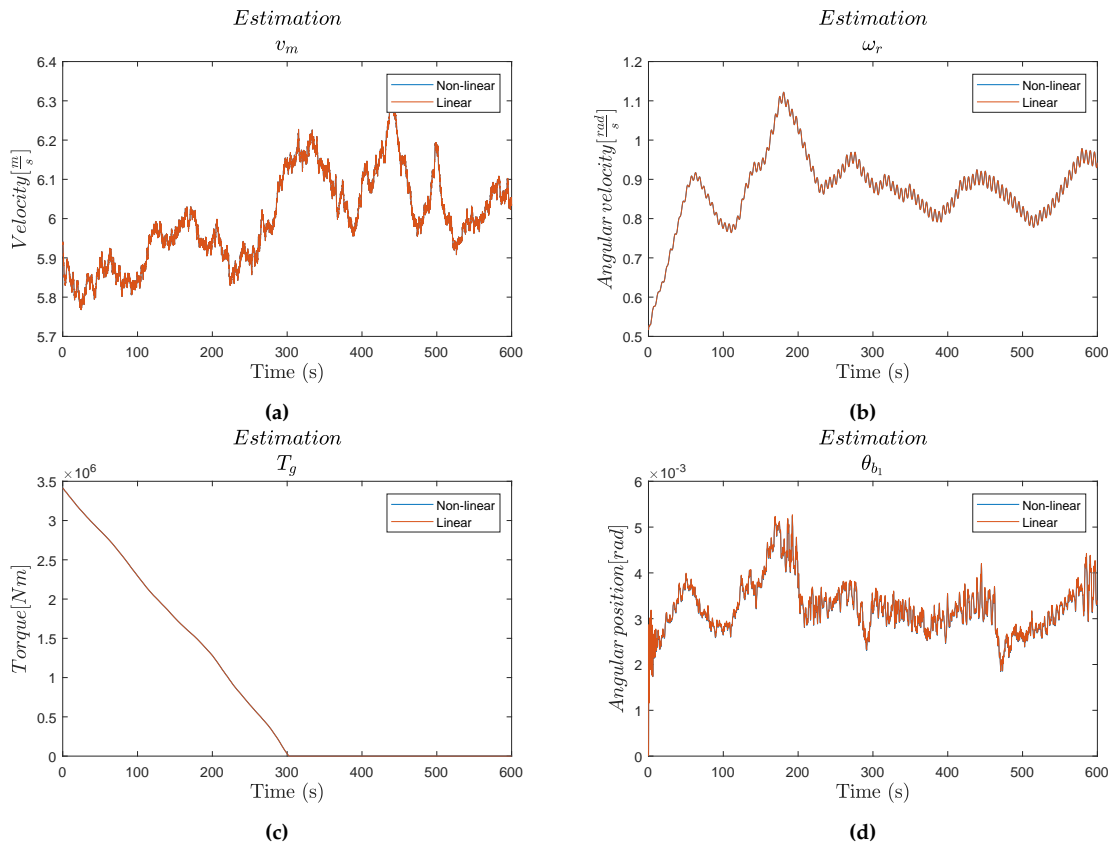


Figure 5.10: Mean wind speed (a), rotor speed (b), generator torque (c) and pitch angle of blade 1 (d) responses of the linear and non-linear models applying the control signals computed by the MPC.

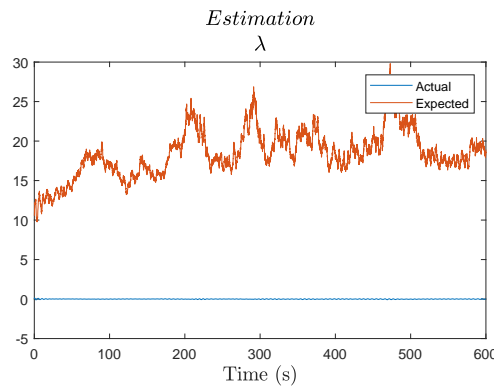


Figure 5.11: Plots for the TSR used by the MPC in comparison to its expected value.

Apart from that, the structural dynamics show an acceptable behaviour, as seen in Fig. 5.12. This is due to the fact that its not part of the below-rated control objective to reduce structural loads, but maximising power production. Hence, the tower and blade

deflections look the same as the ones plotted in Section 5.4 with no wind shear or tower shadow.

At the present time, it was not possible to perform a simulation for above-rated wind speed. It is expected that solving the issue regarding the incremental variables will allow the simulation to be performed and provide acceptable results.

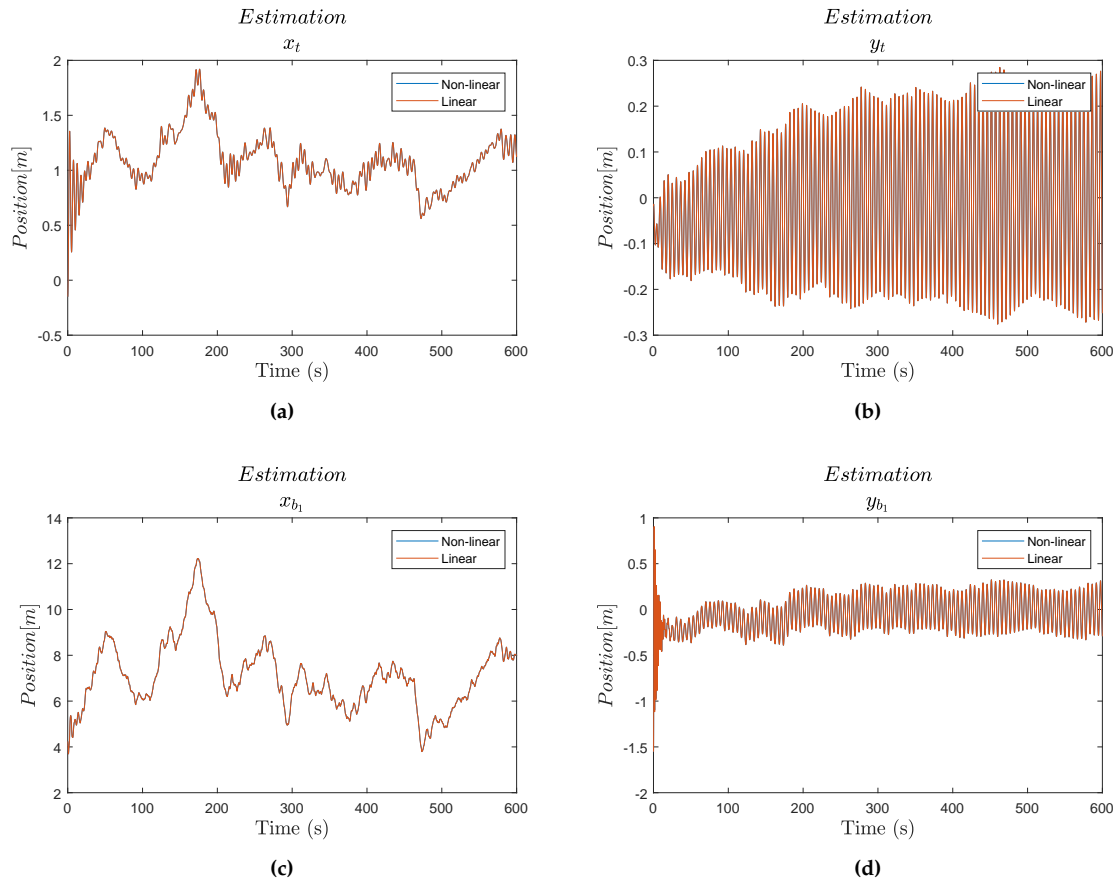


Figure 5.12: Structural dynamics of the linear and non-linear models applying the control signals computed by the MPC.

5.6 Requirement Fulfilment

This section will clarify if the requirements specified in Section 3.2 have been fulfilled or not.

5.6.1 General control objectives

- × Regulation of generator counter torque based on rotational speed ω_r for optimal tip speed ratio operation in partial load (obj. 1).

- × Regulation of generator counter torque based on tower sideways loads for their reduction (obj. 4).
- × CPC based on the rotational speed ω_r for rated power operation and reduced fore-aft tower structural loads in full load (obj. 2, 4).
- × IPC based on flapwise blade loads in order to reduce flapwise and edgewise bending loads (obj. 3).

As specified in Section 5.5, the MPC did not consider that the states of the linearised system are perturbations around the operating point, and thus the results do not fulfil the requirements.

5.6.2 Kalman Filter

- ✓ The state estimator must be in the form of a UKF.
- ✓ The UKF must be able to estimate states with an average error of less than 5%.
 - As stated in Section 5.3, the estimation error is lower than 4.5%

5.6.3 MPC

- ✓ × MPC must be computationally feasible on available hardware.
 - The code has run in a laptop with an Intel Core i7-8750H processor and 16 GB of RAM, and each iteration requires around 0.1 s. If the sampling time is set to 0.25 s, the requirement would be fulfilled in this hardware. Nevertheless, if the sampling time is changed to 0.05 s, it would not be fulfilled.
- ✓ MPC must have control and prediction horizon that ensure stability.
- ✓ MPC must have rotor speed as main priority to avoid physical strain.
- ✓ MPC must have power output as secondary priority to avoid damaging the generator.
- ✓ MPC must have tower and blade loads as tertiary priority to minimise fatigue and extend lifetime.

Chapter 6

CONCLUSION

This project explores the possibility of controlling a 15 MW wind turbine by means of an MPC in order to consider multiple objectives and acknowledge system constraints. A simulation tool, GH Bladed, was provided by Mita-Teknik to simulate the behaviour of the wind turbine in a detailed and accurate way. This way, the obtained data could be used as measurements from the "real" system, and help evaluate and improve the correctness of the model derived. The control objectives were defined to account for both partial and full load operation of the wind turbine. In partial load, the pitch of the blades should be kept constant while the rotor speed is regulated by the generator counter torque such that power capture is maximised. Conversely, the rotor speed should follow its rated value in full load conditions to limit the power generated, which is done by changing the pitch of the blades collectively. Besides, cyclic loads produced by the wind shear and tower shadow effects should be mitigated by pitching the blades independently based on their azimuth angle. Hence, a non-linear model was designed to fulfil the control purposes, including the wind, the aerodynamics, the mechanical structure using five DOF, the generator and the corresponding actuators. Discretisation was achieved by making use of 4th order Runge-Kutta, as Euler's method was not precise enough to ensure the stability of the discretised system. State estimation was performed using a UKF due to the non-linear property of the model as well as the potential superiority in comparison with EKF. It was found out that the large mismatch between the model outputs and Bladed data prevented the UKF from converging, and thus it was decided to use the model outputs as system measurements by adding typical sensor noise. Afterwards, the tuning parameters of the MPC were chosen based on a structured approach and modified based on experimentation, namely the prediction and control horizons, and the constraints for the system variables and weights were defined. The MPC was provided with an adaptive linear model based on successive linearisations of the original non-linear model around the current operating point in order to compute its predictions. These local linear models were found out to be particularly oscillatory when simulated separately due to the highly non-linear nature of the original model. The results obtained using the MPC show the crucial importance of taking into account that the linearised system states are perturbations around the operating points and not absolute variables themselves, which gave rise to erroneous performance when the optimiser tried to fulfil an apparently unattainable objective. It is expected to acquire successful results as soon as this is taken into consideration.

6.1 Future Work

First of all, some more work should be done regarding the non-linear model. For instance, the fact that the rotor and nacelle centre of mass are situated at a certain distance from the tower centre of mass has an influence in the tower top bending which could be taken into account if the structural dynamics were defined as torque equations instead of force equations. Furthermore, the effect of gravity could be considered to try to make the blade edgewise dynamics resemble more the data taken from Bladed. The blade moment of inertia could also be defined in a more precise way such that the equivalent mass of the blades is more exact. Finally, the effect of centrifugal forces on the blade stiffness could be considered.

In order to reduce the computational complexity of the successive linearisation of the model, there is the possibility of applying model reduction based on the dominant eigenvalues of the system [46], ignoring the evolution of the fast modes in the calculations.

It would also be of interest to consider using soft constraints in the MPC due to advantages regarding potential infeasibility when a large disturbance occurs, which is a possibility when the prediction model differs substantially from the real plant.

Lastly, it could be of interest to compare the performance of the proposed control strategy with that of a non-linear MPC to check if it provides more accurate results, but taking into account that the computation of the future control moves can be non-convex and thus exhibit several optima, apart from the remarkably higher computational cost.

Bibliography

- [1] Mathew Sathyajith. *Wind energy. Fundamentals, resource analysis and economics*. July 2006. DOI: 10.1007/3-540-30906-3.
- [2] Ahmad Y. Hasan and Donald R. Hill. *Islamic technology: an illustrated history*. Cambridge University Press; Unesco Cambridge [Cambridgeshire], 1986.
- [3] Trevor J. Price. "Blyth, James (1839–1906), electrical engineer and university teacher". In: *Oxford University Press* (Sept. 2017). DOI: 10.1093/ref:odnb/100957.
- [4] Peter Karnøe. *Dansk vindmølleindustri: en overraskende international success: om innovationer, industriudvikling og teknologipolitik*. Samfundslitteratur, 1991.
- [5] Martin J. Pasqualetti, Robert Righter, and Paul Gipe. "Wind Energy, History of". In: *Encyclopedia of Energy*. Ed. by Cutler J. Cleveland. New York: Elsevier, 2004, pp. 419–433. ISBN: 978-0-12-176480-7. DOI: <https://doi.org/10.1016/B0-12-176480-X/00045-0>.
- [6] Renewable Energy News. *Denmark close to wind output record in 2020*. Jan. 2021. URL: <https://renews.biz/65510/denmark-close-to-wind-output-record-in-2020>. (accessed: 29.10.2021).
- [7] Richard Orange. *Denmarks climate policies insufficient to meet 2030 emissions target*. Feb. 2021. URL: <https://www.theguardian.com/world/2021/feb/28/denmark-climate-policies-insufficient-to-meet-2030-emissions-target>. (accessed: 28.10.2021).
- [8] Energistyrelsen (Danish Energy Agency). *Denmarks Energy Islands*. Mar. 2021. URL: <https://ens.dk/en/our-responsibilities/wind-power/energy-islands/denmarks-energy-islands>. (accessed: 11.10.2021).
- [9] Martin O. L. Hansen. *Aerodynamics of wind turbines*. Routledge, 2015.
- [10] Erich Hau and Horst Renouard. *Fundamentals*. Heidelberg: Springer Berlin, 2006. DOI: 10.1007/3-540-29284-5.
- [11] Marco Casini. "Small vertical axis wind turbines for energy efficiency of buildings". In: *Journal of Clean Energy Technologies* 4.1 (2016), pp. 56–65.
- [12] Trevor M. Letcher. *Wind energy engineering: A handbook for onshore and offshore wind turbines*. Academic Press, 2017.
- [13] Paul Dvorak. *How large offshore wind turbines are challenging bearing designs*. 2018. URL: <https://www.windpowerengineering.com/large-offshore-wind-turbines-challenging-bearing-designs/>. (accessed: 11.10.2021).

- [14] Edis Osmanbasic. *The Future of Wind Turbines: Comparing Direct Drive and Gearbox*. 2020. URL: <https://www.engineering.com/story/the-future-of-wind-turbines-comparing-direct-drive-and-gearbox>. (accessed: 23.05.2022).
- [15] Luis Arturo Soriano, Wen Yu, and Jose de Jesus Rubio. "Modeling and control of wind turbine". In: *Mathematical Problems in Engineering* 2013 (2013).
- [16] S. Shivashankar et al. "Mitigating methods of power fluctuation of photovoltaic (PV) sources – A review". In: *Renewable and Sustainable Energy Reviews* 59 (2016), pp. 1170–1184.
- [17] Wai Hou Alan Lio. *Blade-pitch control for wind turbine load reductions*. Springer, 2018.
- [18] Albert Betz. *Introduction to the theory of flow machines*. Elsevier, 2014.
- [19] Mahmood Mirzaei. *Wind Turbine Control: Robust Model Based Approach*. English. IMM-PHD-2012 281. Technical University of Denmark, 2012.
- [20] Tony Burton et al. *Wind energy handbook*. John Wiley & Sons, 2011.
- [21] Swagata Das, Neeraj Karnik, and Surya Santoso. "Time-domain modeling of tower shadow and wind shear in wind turbines". In: *International Scholarly Research Notices* 2011 (2011).
- [22] Youcef Djeriri et al. "A comparative study between field oriented control strategy and direct power control strategy for DFIG". In: *Journal of Electrical Engineering* 14.2 (June 2014), pp. 169–178.
- [23] Mehdi Allagui, Othman Bk Hasnaoui, and Jamel Belhadj. "A 2MW direct drive wind turbine; vector control and direct torque control techniques comparison". In: *Journal of Energy in Southern Africa* 25.2 (2014), pp. 117–126.
- [24] Takwa Sellami et al. "Modal and harmonic analysis of three-dimensional wind turbine models". In: *Wind Engineering* 40.6 (2016), pp. 518–527.
- [25] Jayanth R Ramamurthy. *Wind plant interaction with series-compensated power systems*. Michigan Technological University, 2011.
- [26] Mita-Teknik. *Complete Solutions*. URL: https://www.mita-teknik.com/media/2499/mt_concept-overview_brochure_en_r6_0.pdf. (accessed: 06.10.2021).
- [27] H Markou et al. "Morphological study of aeroelastic control concepts for wind turbines". In: *ECN Report* (2006).
- [28] Ervin A. Bossanyi. "Individual blade pitch control for load reduction". In: *Wind Energy: An International Journal for Progress and Applications in Wind Power Conversion Technology* 6.2 (2003), pp. 119–128.
- [29] GL Garrard Hassan. "Bladed user manual V4.3". In: *Garrard Hassan & Partners Ltd., Bristol, England* (2012).

- [30] Allan Juul Larsen and Thomas Stampe Mogensen. "Individuel pitchregulering af vindmølle". MA thesis. Technical University of Denmark, DTU, DK-2800 Kgs. Lyngby, Denmark, 2006.
- [31] Johan Hoffman, Johan Jansson, and Claes Johnson. "New theory of flight". In: *Journal of Mathematical Fluid Mechanics* 18.2 (2016), pp. 219–241.
- [32] E. Gaertner et al. *Definition of the IEA wind 15-megawatt offshore reference wind turbine Tech. Rep.* 2020.
- [33] "Engineering ToolBox. Wind Shear". 2008. URL: https://www.engineeringtoolbox.com/wind-shear-d_1215.html. (accessed: 22.09.2021).
- [34] Alessio Pipinato. *Innovative bridge design handbook: Construction, rehabilitation and maintenance*. Butterworth-Heinemann, 2015.
- [35] International Electrotechnical Commission. *International Standard IEC 61400-1. Wind Turbines*. Tech. rep. Aug. 2005.
- [36] omar1810 (<https://math.stackexchange.com/users/160232/omar1810>). *Moment of inertia of a solid cone about a diameter of the base as axis*. 2014. URL: <https://math.stackexchange.com/q/1082670>. (accessed: 17.03.2022).
- [37] Silvio Simani. "Overview of modelling and advanced control strategies for wind turbine systems". In: *Energies* 8.12 (2015), pp. 13395–13418.
- [38] Mohinder S. Grewal and Angus P. Andrews. *Kalman Filtering Theory and Practice using MATLAB*. John Wiley & Sons, 2008.
- [39] Matthew Rhudy and Yu Gu. *Understanding Nonlinear Kalman Filters, Part II: An Implementation Guide*. 2004.
- [40] Athanasios Papoulis and S. Unnikrishna Pillai. *Probability, random variables, and stochastic processes*. Tata McGraw-Hill Education, 2002.
- [41] Mate Jelavic, Vlaho Petrovic, and Nedjeljko Peric. "Individual pitch control of wind turbine based on loads estimation". In: *2008 34th Annual Conference of IEEE Industrial Electronics*. IEEE. 2008, pp. 228–234.
- [42] Jan Marian Maciejowski. *Predictive control: with constraints*. Pearson education, 2002.
- [43] Nicholas J Higham. "Computing a nearest symmetric positive semidefinite matrix". In: *Linear algebra and its applications* 103 (1988), pp. 103–118.
- [44] MathWorks. *Tune Weights*. 2022. URL: <https://se.mathworks.com/help/mpc/ug/tuning-weights.html>. (accessed: 22.03.2022).
- [45] Altay Zhakatayev et al. "Successive linearization based model predictive control of variable stiffness actuated robots". In: *2017 IEEE international conference on advanced intelligent mechatronics (AIM)*. IEEE. 2017, pp. 1774–1779.

- [46] Ioannis Bonis, Weiguo Xie, and Constantinos Theodoropoulos. “A linear model predictive control algorithm for nonlinear large-scale distributed parameter systems”. In: *AIChE Journal* 58.3 (2012), pp. 801–811.

Appendix A

BEM METHOD

This section will explain BEM. Some aspects of the derivations will be glanced over. This is to avoid dragging on at length, as the topic is quite extensive. The topic will be split up into three parts: one part explaining the aerodynamics of individual blades, one part examining one-dimensional momentum theory that leads to equations for thrust and force coefficients, and finally the classical BEM which will be used to analyse the aerodynamics of a wind turbine. While the iterative approach outlined in Appendix A.3 makes BEM unsuitable for control, it can still be used in wind turbine analysis, as well as deriving some factors used in actual control synthesis, such as the Betz limit and the power coefficient used in determining the torque acting on the rotor. Note that the variables in this section do not necessarily conform to the rest of the report, and have all been defined where they appear.

A.1 Two Dimensional Model of a Blade

The blades of a wind turbine are long and slender, and their design can be compared to the wings of a plane in that their shape is meant to generate lift using the flow of air. As the wind moving across the blade has far more velocity streamwise than it does spanwise, an assumption is made that the flow at any given point is two-dimensional. Subsequently, the aerofoil seen in Fig. A.1 can be considered.

The aerofoil assumes a blade of infinite span, as otherwise it would have to consider different diameters as different sections of the blade are considered. Additionally, for a more true representation, it is necessary to correct for vortices behind the blades which act as disturbances for the angle of attack α . While difficult to realise, this approach is still of interest as it allows for modelling the forces acting on individual segments of the blade as seen in Fig. A.2.

The wind flow V_∞ denotes the freestream velocity, which is the air far upstream from the wind turbine before it is affected by changes in pressure and velocity caused by the rotor. The wind flow has an angle of attack, which plays a large role in the direction of the resulting force F . This force can be broken down into lift, L , and drag, D . The torque on the rotor should be maximised in order to best exploit the wind. The lift coefficient, C_l ,

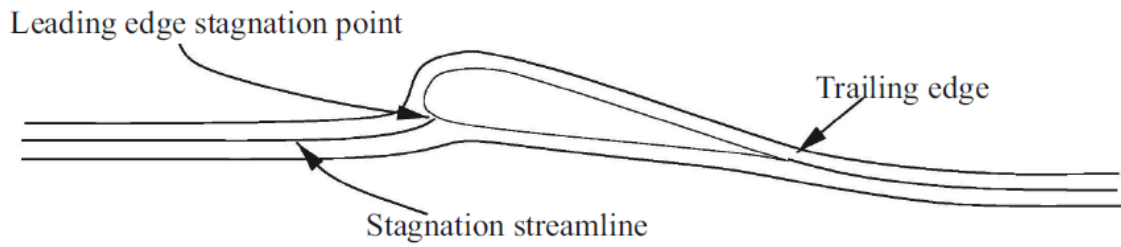


Figure A.1: Aerofoil of a wind turbine blade [9].

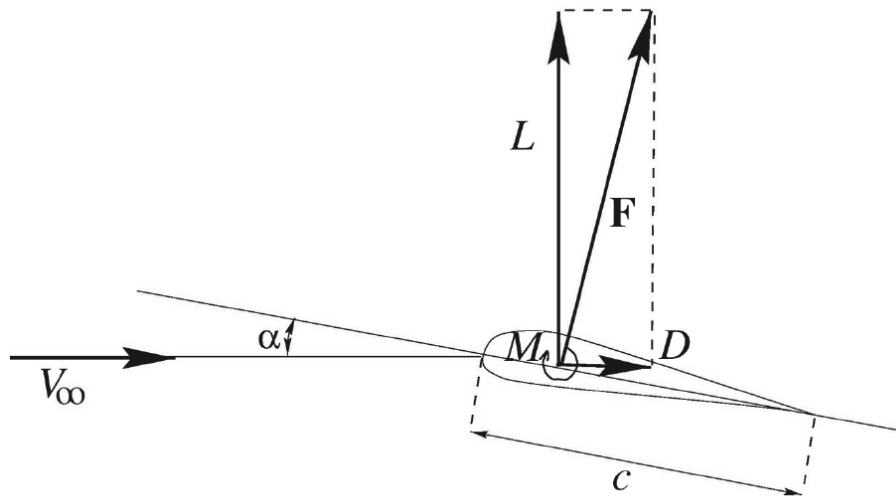


Figure A.2: Forces acting on a wind turbine [9].

and drag coefficient, C_d , are defined as follows:

$$C_l = \frac{l}{\frac{1}{2}\rho V_\infty^2 c} \quad (\text{A.1})$$

$$C_d = \frac{d}{\frac{1}{2}\rho V_\infty^2 c} \quad (\text{A.2})$$

Where:

ρ : density of the air	$[\text{kg}/\text{m}^3]$
c : length of the aerofoil, often called the chord	$[\text{m}]$
l : force of lift per length	$[\text{N}/\text{m}]$
d : force of drag per length	$[\text{N}/\text{m}]$

In practise, however, the lift and drag coefficients are usually found by looking up values in tables rather than calculation. Lift is generated by the way air flows around the aerofoil. The shape of the aerofoil results in lower pressure above it, which generates lift. Both C_l and C_d depend on α . C_l increases linearly with α until a certain value, after which the aerofoil stalls and C_l decreases quickly. After stalling, C_d begins to increase rapidly. The actual points where stalling occurs depends on the shape of the aerofoil. Thin-nosed aerofoils stall much more abruptly than thick-nosed ones [9].

A.2 One Dimensional Momentum Theory

The momentum theory examines the forces acting on the wind turbine which generates mechanical energy from the kinetic energy in the wind, as well as how the wind speed and pressure is affected by the wind turbine. Here it is assumed that the rotor is a permeable disk that allows air flow to pass through while also acting as a drag device. It is also assumed that it is ideal, i.e. being frictionless and having no rotational velocity component in the wake. These assumptions require some adjustments to be made in order to correct for some shortcomings, but these will be discussed in Appendix A.3.

As the blades of the wind turbine rotate, they create a system of vortices in the wake. This wake can be simply described by an axial induction factor a and a tangential induction factor a' . Here, a represents the induced velocity factor in the axial direction opposite the direction of the wind; essentially the reduction of wind velocity in the rotor plane. The factor a' represents the rotational wind velocity opposite the rotation of the blades. In the rotor plane and wake, this is given by $a'\omega r$ and $2a'\omega r$ respectively where ω is the angular velocity of the rotor and r is the radius from the centre of the rotor at a given point of examination. If both a and a' are known, the local angle of attack can be calculated by Equation A.3.

$$\alpha = \phi - \theta \quad (\text{A.3})$$

$$\tan(\phi) = \frac{V_a}{V_{rot}} \quad (\text{A.4})$$

$$\theta = \theta_p + \beta \quad (\text{A.5})$$

$$V_a = (1 - a)V_o \quad (\text{A.6})$$

$$V_{rot} = (1 + a')\omega r \quad (\text{A.7})$$

where:

α : local angle of attack	[rad]
θ : local pitch of the individual blade with respect to the tip	[rad]
θ_p : pitch angle of the blade	[rad]
β : twist of the blade relative to the rotor plane	[rad]
ϕ : angle of the incoming flow	[rad]

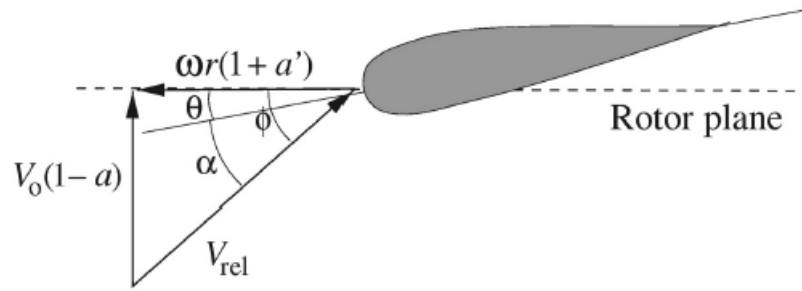


Figure A.3: Relative velocity seen by a section of a blade [9].

V_a : axial wind velocity	[m/s]
V_{rot} : tangential wind velocity	[m/s]
ω_r : angular velocity of the rotor	[rad/s]
r : radius of the rotor	[m]

The pitch angle is measured relative to the rotor plane. The pitch is calculated locally as the blades of a wind turbine are not completely stiff, and the pitch at one part of the blade will not necessarily match that of another part of the blade due to the forces acting on it. How the blades are divided into sections will be explained further in Appendix A.3. Figure A.3 shows the velocities seen by a section of an individual blade. As can be seen, V_{rel} is a combination of the axial and tangential velocity at the rotor plane.

Figure A.4 shows how the wind speed and pressure are affected by the wind turbine.

The wind speed and pressure start at V_0 and p_0 coming in from a great distance from the wind turbine. The disruption to the wind speed occurs some distance from the rotor plane as the wind drops from V_0 to u at the rotor plane to u_1 in the wake. From the ideal properties of the rotor, the thrust T can be found:

$$T = \Delta p A \quad (\text{A.8})$$

where:

Δp : the pressure drop over the rotor plane	[Pa]
A : the area of the rotor	[m ²]
T : thrust	[N]

Applying Bernoulli's principle in regards to fluid dynamics, Δp is found to be:

$$\Delta p = \frac{1}{2} \rho (V_0^2 - u_1^2) \quad (\text{A.9})$$

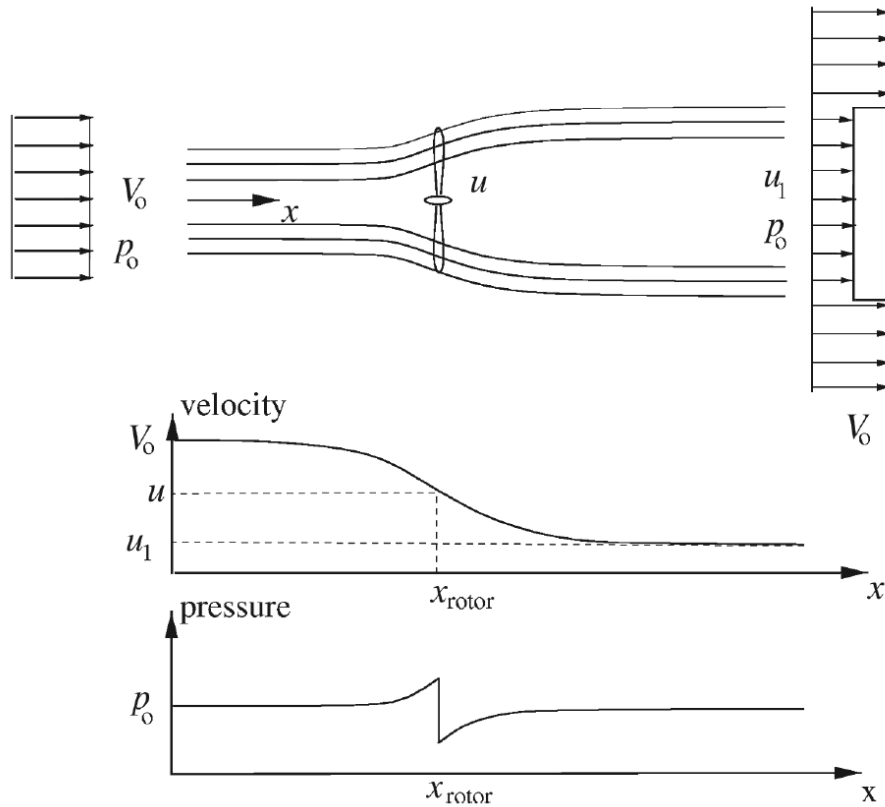


Figure A.4: Pressure and velocity before and after the rotor plane [9].

Applying the axial momentum equation on integral form with the cross-sectional area A_{cv} yields [9]:

$$\frac{\partial}{\partial t} \iiint_{cv} \rho u(x, y, z) dx dy dz + \iint_{cs} u(x, y, z) \rho V \cdot dA = F_{ext} + F_{pres} \quad (\text{A.10})$$

where:

ρ : density of the fluid	[kg/m ³]
u : velocity of fluid particles with respect to a reference system	[m/s]
V : velocity of the particles with respect to the surface that they cross	[m/s]
dA : normal of the surface of the control volume	[·]
F_{pres} : forces acting on the control volume in the axial direction	[N]
F_{ext} : external force not along the axial direction	[N]

The first term in Equation A.10 is zero as the flow is assumed to be stationary. Additionally, since the pressure is the same on either end of the control volume (V_0 and u_1 in

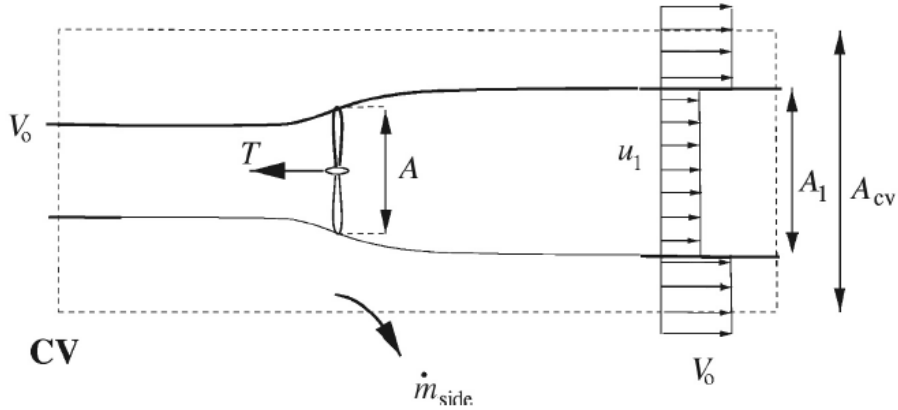


Figure A.5: Lateral boundary of the control volume [9].

Figure A.4) F_{pres} is also zero. Figure A.5 shows the lateral boundary of the control volume where \dot{m}_{side} is used in Equation A.11 and Equation A.12.

Using the assumptions of an ideal wind turbine, the thrust T can be found to be:

$$-T = \rho u_1^2 A_l + \rho V_o^2 (A_{cv} - A_l) + \dot{m}_{side} V_o - \rho V_o^2 A_{cv} \quad (\text{A.11})$$

$$\dot{m}_{side} = \rho A_l (V_o - u_1) \quad (\text{A.12})$$

where:

A_l : area of the cross-section of the wake [m²]

A_{cv} : area of the cross-section of the control volume [m²]

\dot{m}_{side} : the mass flow through the lateral boundary of the control volume [kg/s]

Note that the flow of mass was found by considering the conservation of mass, which can also be used to find the relationship between A and A_l :

$$\dot{m} = \rho u A = \rho u_l A_l \quad (\text{A.13})$$

where:

\dot{m} : flow of mass through the wake [kg/s]

A : area swept by the rotor [m²]

Combining Equations A.10 to A.12 gives:

$$T = \rho u A (V_o - u_l) = \dot{m} (V_o - u_l) \quad (\text{A.14})$$

Substituting Equation A.8 for T and Equation A.9 for Δp demonstrates that the velocity in the rotor plane is the mean of the undisturbed wind velocity and the final velocity in the wake as seen in Equation A.15.

$$u = \frac{1}{2} (V_o + u_l) \quad (\text{A.15})$$

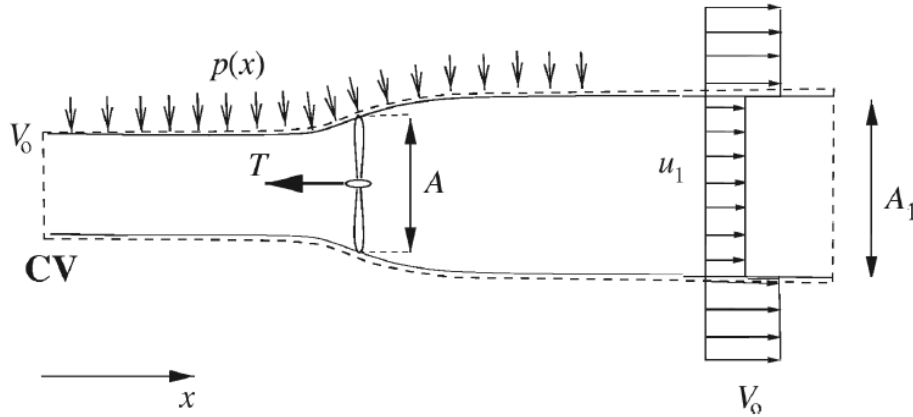


Figure A.6: Alternate control volume for a wind turbine [9].

Figure A.6 shows an alternate control volume which can be used to find the shaft power P . The flow is assumed to be frictionless and there is no change in the energy between the inlet and outlet of the control volume. The shaft power can be found from the control volume in Figure A.6 using the integral energy equation.

$$P = \dot{m} \left(\frac{1}{2} V_0^2 + \frac{p_o}{\rho} - \frac{1}{2} u_1^2 - \frac{p_o}{\rho} \right) \quad (\text{A.16})$$

$$= \rho u A \left(\frac{1}{2} V_0^2 + \frac{p_o}{\rho} - \frac{1}{2} u_1^2 - \frac{p_o}{\rho} \right) \quad (\text{A.17})$$

$$= \frac{1}{2} \rho u A (V_0^2 - u_1^2) \quad (\text{A.18})$$

The velocity in the rotor plane, u , can also be defined based on the axial induction factor a as seen in Equation A.19.

$$u = (1 - a) V_0 \quad (\text{A.19})$$

Combining Equation A.15 and Equation A.19 results in Equation A.20.

$$u_1 = (1 - 2a) V_0 \quad (\text{A.20})$$

Substituting Equation A.20 in Equations A.14 and A.18 allows for defining T and P based on the axial induction factor in Equations A.21 and A.22 respectively.

$$T = 2\rho V_0^2 a(1 - a)A \quad (\text{A.21})$$

$$P = 2\rho V_0^3 a(1 - a)^2 A \quad (\text{A.22})$$

Both thrust and power are frequently used to define a thrust and power coefficient, the latter can be used to find the maximum power that can be extracted from the wind.

$$C_P = \frac{P}{\frac{1}{2} \rho V_0^3 A} \quad (\text{A.23})$$

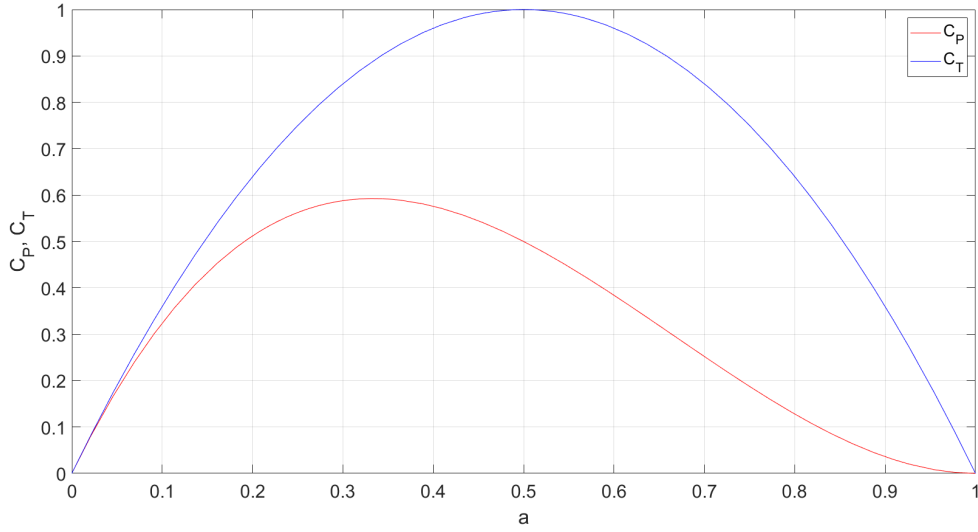


Figure A.7: C_P and C_T as functions of the axial induction factor.

$$C_T = \frac{T}{\frac{1}{2}\rho V_0^2 A} \quad (\text{A.24})$$

Inserting Equations A.21 and A.22 in place of T and P gives:

$$C_P = 4a(1 - a)^2 \quad (\text{A.25})$$

$$C_T = 4a(1 - a) \quad (\text{A.26})$$

Plotting Equations A.25 and A.26 as functions of the axial induction factor a in Figure A.7 gives an insight into how much power can be extracted from the wind.

Taking the derivative of C_P with respect to a results in Equation A.27

$$\frac{dC_P}{da} = 4(1 - a)(1 - 3a) \quad (\text{A.27})$$

From Equation A.27 it can be seen that the maximum value of C_P is attained for $a = 1/3$, corresponding to a value of $C_P = 16/27 \approx 59.26\%$. This means that the theoretical maximum of available energy that can be used is 59.26%. This is what's known as the Betz limit. This approach is, however, only valid for values of a under approximately 0.3 to 0.4. An indication of this can be seen in Equation A.20, where the wind velocity in the wake would be negative for $a > 0.5$, implying that the ideal model falls apart beyond a certain limit [9].

A.3 Blade Element Method

The ideal wind turbine model allows for easy derivation of a usable model but as mentioned, the equation for the thrust coefficient is invalid for a certain range of values

for the axial induction factor. BEM assumes an infinite number of blades, which results in a different vortex system in the wake, and additionally it represents the wake as a symmetric and ideal streamtube that does not exist in reality. The problem of the axial induction factor can be solved using the Glauert correction. The assumption of infinite blades can be corrected by applying Prandtl's tip loss factor. These corrections will be introduced where they are applicable. BEM draws heavily upon one-dimensional momentum theory. The streamtubes seen in Figure A.4 and Figure A.5 are used, but are now discretised into a set amount of annular elements. An assumption is made that there is no flow across the boundaries, and as such, the forces acting on each element of the blades can be considered independently of each other. An additional assumption is made that the force applied from the blade of each element on the flow is constant across the element, i.e. an infinite number of blades is assumed. The thrust of the blades on the flow as well as the torque on the annular element are calculated in Equation A.28 and Equation A.29 respectively.

$$dT = 2\pi r \rho u (V_o - u_i) dr \quad (\text{A.28})$$

$$dM = 2\pi r^2 \rho u C_\theta dr \quad (\text{A.29})$$

$$C_\theta = 2a' \omega r \quad (\text{A.30})$$

where:

dT : thrust applied by the blades on the flow	[N]
dM : torque on the annular element	[Nm]
dr : height of the annular element	[m]
C_θ : rotational tangential velocity in the wake	[m/s]

Substituting Equations A.19, A.20 and A.30 for their respective variables in Equations A.28 and A.29 gives Equations A.31 and A.32

$$dT = 4\pi r \rho V_o^2 a(1-a) dr \quad (\text{A.31})$$

$$dM = 4\pi r^3 \rho V_o \omega (1-a) a' dr \quad (\text{A.32})$$

If the lift and drag coefficients from Equations A.1 and A.2 are known, the lift and drag can be isolated by replacing the freestream velocity by the relative velocity seen at a given section of the blade, as this is what determines lift and drag generated by that section.

$$l = \frac{1}{2} \rho V_{rel}^2 c C_l \quad (\text{A.33})$$

$$d = \frac{1}{2} \rho V_{rel}^2 c C_d \quad (\text{A.34})$$

The lift and drag must subsequently be projected onto the rotor plane as it is the forces relative to that plane which are of interest.

$$P_N = l \cos(\phi) + d \sin(\phi) \quad (\text{A.35})$$

$$P_T = l \sin(\phi) - d \cos(\phi) \quad (\text{A.36})$$

where:

P_N : force normal to rotor plane

P_T : force tangential to rotor plane

Equations A.35 and A.36 can be normalized with respect to $\frac{1}{2}\rho V_{rel}^2 c$, such that l and d are replaced with C_l and C_d respectively, leading to Equations A.37 and A.39.

$$C_n = C_l \cos(\phi) + C_d \sin(\phi) \quad (\text{A.37})$$

$$= \frac{P_N}{\frac{1}{2}\rho V_{rel}^2 c} \quad (\text{A.38})$$

$$C_t = C_l \sin(\phi) - C_d \cos(\phi) \quad (\text{A.39})$$

$$= \frac{P_T}{\frac{1}{2}\rho V_{rel}^2 c} \quad (\text{A.40})$$

From Figure A.3 it can be seen that V_{rel} can be found geometrically both by considering the axial and tangential velocity.

$$V_{rel} \sin(\phi) = V_o(1 - a) \quad (\text{A.41})$$

$$V_{rel} \cos(\phi) = \omega r(1 + a') \quad (\text{A.42})$$

A "solidity" variable σ is introduced, which defines the area of the control volume which is covered by the blades of the wind turbine.

$$\sigma(r) = \frac{c(r)B}{2\pi r} \quad (\text{A.43})$$

where:

σ : proportion of annular volume covered by blades

c : chord length at radius r

B : number of blades

r : radius measured at the control volume

Since P_N and P_T are forces per length, dT and dM can be defined based on those.

$$dT = BP_N dr \quad (\text{A.44})$$

$$dM = rBP_T dr \quad (\text{A.45})$$

Inserting the definition of V_{rel} that can be isolated from Equation A.41 into Equation A.38, and then inserting the subsequent isolated definition of P_N into Equation A.44

yields a new definition for dT . The same can be done for Equation A.45 by using the two definitions of V_{rel} from Equations A.41 and A.42 in Equation A.40. As a result, dT and dM then become:

$$dT = \frac{1}{2}\rho B \frac{V_o^2(1-a)^2}{\sin^2(\phi)} c_{C_n} dr \quad (\text{A.46})$$

$$dM = \frac{1}{2}\rho B \frac{V_o(1-a)\omega r(1+a')}{\sin(\phi)\cos(\phi)} c_{C_t} r dr \quad (\text{A.47})$$

However, dT and dM are calculated based on the assumption of infinite blades, which must be addressed [9].

A.3.1 Prandtl's tip loss factor

Here, Prandtl's tip loss factor is introduced. The tip loss factor corrects the assumption of infinite blades. The factor is valid as long as the loads are equally distributed azimuthally, that is, the blades are all evenly distributed in the rotor plane, which is the case for the wind turbine. Using Prandtl's correction yields a result that should be very close to the real world scenario for a set number of blades. Equations A.31 and A.32 can be rewritten to include the correction factor F :

$$dT = 4\pi r \rho V_o^2 a(1-a) F dr \quad (\text{A.48})$$

$$dM = 4\pi r^3 \rho V_o \omega (1-a) a' F dr \quad (\text{A.49})$$

$$F = \frac{2}{\pi} \cos^{-1}(e^{-f}) \quad (\text{A.50})$$

$$f = \frac{B}{2} \frac{R-r}{r \sin(\phi)} \quad (\text{A.51})$$

where:

$$R = \text{total radius of the rotor} \quad [\text{m}]$$

Using this correction, Equations A.46 and A.47 can be set equal to Equations A.48 and A.49 respectively. Applying σ as a scalar value to the normalised thrust, a new definition of a can be isolated from the first equation while a new definition of a' can be isolated from the second equation.

$$a = \frac{1}{\frac{4F\sin^2(\phi)}{\sigma C_n} - 1} \quad (\text{A.52})$$

$$a' = \frac{1}{\frac{4F\sin(\phi)\cos(\phi)}{\sigma C_t} - 1} \quad (\text{A.53})$$

These variables are of fundamental importance in BEM, but as mentioned earlier, there are shortcomings in this approach that must be corrected [9].

A.3.2 Glauert correction

It is now time to introduce Glauert correction for high values of a . Essentially, once a passes a defined limit, a new equation for calculating it will be used. There is no single way to define this limit, but in accordance with the source material, the limit $a_c = 0.2$ will be used. Based on the value of a , the two equations seen in Equation A.54 can be used to find the thrust coefficient.

$$C_T = \begin{cases} 4a(1-a)F & a \leq a_c \\ 4(a_c^2 + (1-2a_c)a)F & a > a_c \end{cases} \quad (\text{A.54})$$

Equation A.24 gives the definition for the thrust coefficient. Adapting it to be used on the control volume by replacing A with $2\pi r dr$, it instead becomes:

$$C_T = \frac{dT}{\frac{1}{2}\rho V_0^2 2\pi r dr} \quad (\text{A.55})$$

$$(\text{A.56})$$

Using Equation A.46 as dT results in Equation A.57.

$$C_T = \frac{(1-a)^2 \sigma C_n}{\sin^2(\phi)} \quad (\text{A.57})$$

This equation for C_T can be equated to the two scenarios seen in Equation A.54.

$$4a(1-a)F = \frac{(1-a)^2 \sigma C_n}{\sin^2(\phi)} \quad (\text{A.58})$$

$$4(a_c^2 + (1-2a_c)a)F = \frac{(1-a)^2 \sigma C_n}{\sin^2(\phi)} \quad (\text{A.59})$$

For each of these scenarios, a new equation for a is defined:

$$a = \frac{1}{\frac{4F \sin^2(\phi)}{\sigma C_n} - 1} \quad (\text{A.60})$$

$$a = \frac{1}{2} \left[2 + K(1-2a_c) - \sqrt{(K(1-2a_c) + 2)^2 + 4(Ka_c^2 - 1)} \right] \quad (\text{A.61})$$

$$K = \frac{4F \sin^2(\phi)}{\sigma C_n} \quad (\text{A.62})$$

Equation A.60 is the original definition of the axial induction factor whereas Equation A.61 is the new one to be defined if a is found to be greater than a_c , in this case 0.2 [9].

BEM process

The steps for BEM can now be outlined.

1. Set $a=a'=0$
2. Compute flow angle according to Equation A.4
3. Compute local angle of attack according to Equation A.3
4. Look up C_l and C_d for the given angle of attack
5. Calculate C_n and C_t according to Equations A.37 and A.39
6. Calculate a according to either Equation A.60 or Equation A.61 depending on the value of a given in Equation A.60.
7. If a and a' has changed beyond a designated tolerance, start from step 2 again. Otherwise continue to the last step.
8. Compute dT and dM on the annular control volume according to Equations A.48 and A.49.

Each annular control volume must run through this calculation. It remains to be decided how high each annular element must be, and consequently how many of them there must be. For the purpose of implementing MPC, it must also be decided how many iterations ahead BEM should be calculated. The resulting number of equations could potentially be computationally heavy [9].

A.4 Coleman Transform-based Control

The flapwise blade root bending moments M_i are defined in the coordinate system that rotates with the blades, and thus there is a phase shift of 120° between them. In order to compute these loads in the fixed reference frame it is necessary to apply the Coleman transform, which is a matrix that depends on the rotor azimuth angle and therefore varies with time as can be seen below:

$$\begin{bmatrix} \bar{M} \\ M_{tilt} \\ M_{yaw} \end{bmatrix} = \begin{bmatrix} \frac{1}{3} & & \\ \frac{2}{3} \sin \psi(t) & \frac{2}{3} \sin \psi(t) + \frac{2\pi}{3} & \frac{2}{3} \sin \psi(t) + \frac{4\pi}{3} \\ \frac{2}{3} \cos \psi(t) & \frac{2}{3} \cos \psi(t) + \frac{2\pi}{3} & \frac{2}{3} \cos \psi(t) + \frac{4\pi}{3} \end{bmatrix} \begin{bmatrix} M_1 \\ M_2 \\ M_3 \end{bmatrix} \quad (\text{A.63})$$

where the average flapwise blade bending moment \bar{M} can be interpreted in terms of hub loadings, but is typically not considered.

Subsequently, the tilt and yaw flapwise root bending moments M_{tilt} and M_{yaw} are used to generate tilt and yaw pitch control signals θ_{tilt} and θ_{yaw} , which are then projected back to

the rotatory reference frame to obtain the individual pitch signals for each blade (Eq. A.64), as depicted in Fig. A.8.

$$\begin{bmatrix} \theta_{ref_1} \\ \theta_{ref_2} \\ \theta_{ref_3} \end{bmatrix} = \begin{bmatrix} 1 & \sin \psi(t) & \cos \psi(t) \\ 1 & \sin \psi(t) + \frac{2\pi}{3} & \cos \psi(t) + \frac{2\pi}{3} \\ 1 & \sin \psi(t) + \frac{4\pi}{3} & \cos \psi(t) + \frac{4\pi}{3} \end{bmatrix} \begin{bmatrix} \bar{\theta} \\ \theta_{tilt} \\ \theta_{yaw} \end{bmatrix} \quad (\text{A.64})$$

with $\bar{\theta}$ referring to the averaged blade pitch signal.

To decouple the IPC actions from those of CPC, the blade moments and the pitch control signals are redefined as seen in Eq. A.65. Fig. A.8 depicts the whole process.

$$\begin{bmatrix} \theta_{ref_1} \\ \theta_{ref_2} \\ \theta_{ref_3} \end{bmatrix} := \begin{bmatrix} \bar{\theta}_{ref} + \tilde{\theta}_{ref_1} \\ \bar{\theta}_{ref} + \tilde{\theta}_{ref_2} \\ \bar{\theta}_{ref} + \tilde{\theta}_{ref_3} \end{bmatrix}, \quad \begin{bmatrix} M_1 \\ M_2 \\ M_3 \end{bmatrix} := \begin{bmatrix} \tilde{M} + \tilde{M}_1 \\ \tilde{M} + \tilde{M}_2 \\ \tilde{M} + \tilde{M}_3 \end{bmatrix} \quad (\text{A.65})$$

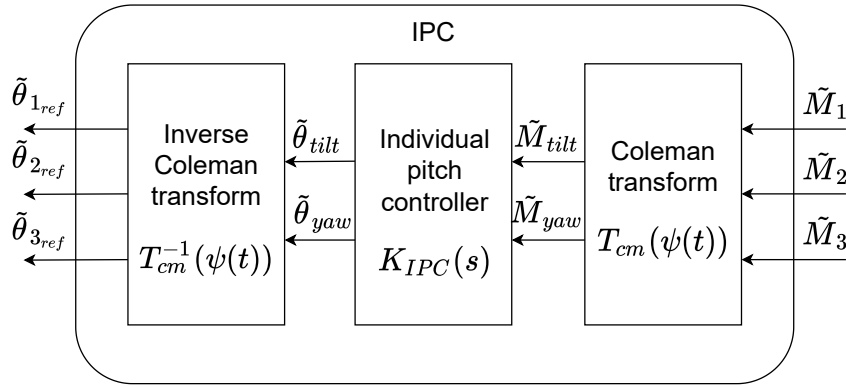


Figure A.8: Coleman transform-based controller [17].

A.5 Softening the Constraints in MPC

The optimisation problem could become infeasible when adding constraints. This can happen due to an unexpectedly large disturbance, such that the plant is not able to be restricted within the constraints, or due to differences between the plant and the internal model, which could be interpreted by the controller as large disturbances and eventually provoke the same outcome.

This can be circumvented by *ad hock* measures such as applying the same control signal $\hat{u}(k|k)$ as in the previous step, or the one computed as $\hat{u}(k+1|k)$ or $\hat{u}(k+2|k)$ last step, or by "constraint management" strategies, in which the least important constraints are relaxed to obtain feasibility.

One systematic strategy consists in softening the constraints, that is, allowing them to be crossed if necessary. Input constraints are normally not softened, as actuators have physical limitations that cannot be surpassed, not like output constraints.

One way to soften the constraints is to add "slack variables" defined such that they are non-zero only if the constraints are violated, and which values are strongly penalised by the cost function in order to motivate the optimiser to keep them at zero as long as it is possible. The slack variables are introduced in the form of a vector ϵ and a scalar $\rho \geq 0$ as follows:

$$\min_{\Delta\mathcal{U}(k), \epsilon} V(k) = -\Delta\mathcal{U}(k)^T \mathcal{G} + \Delta\mathcal{U}(k)^T \mathcal{H} \Delta\mathcal{U}(k) + \rho \|\epsilon\| \quad (\text{A.66})$$

subject to

$$\begin{bmatrix} \mathbf{F} \\ \Gamma\Theta \\ W \end{bmatrix} \Delta\mathcal{U}(k) \leq \begin{bmatrix} -\mathbf{F}_1 u(k-1) - f \\ -\Gamma(\Psi \hat{x}(k|k) + Y u(k-1)) - g \\ w \end{bmatrix} + \epsilon \quad (\text{A.67})$$

$$\epsilon \geq 0 \quad (\text{A.68})$$

If $\rho = 0$ the problem becomes unconstrained, while as $\rho \rightarrow \infty$ the original constrained problem is recovered. A disadvantage of this formulation is that the original constraints can be violated even if it is not necessary. An alternative would be to penalise the 1-norm (sum of violations) or the ∞ -norm (maximum violation) of the constraint violations.

Appendix B

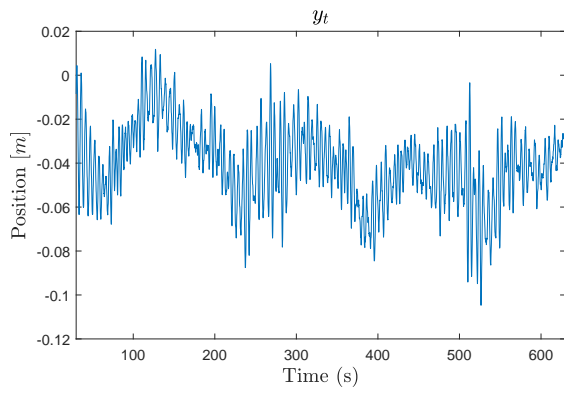
TESTS

This chapter will outline the simulations carried out in the GH Bladed simulation tool for different scenarios as well as the tests of the components of the system in order to document functionality and integration of said components into one system. Due to the interdependent nature of the components, the testing will be carried out in the form of a sequential integration starting with the non-linear model of the wind turbine, then adding the UKF for an accurate estimation of the states of the model, the linear prediction model used within MPC, and finally the MPC using the estimated states to test its functionality and verify the effectiveness of the cost function.

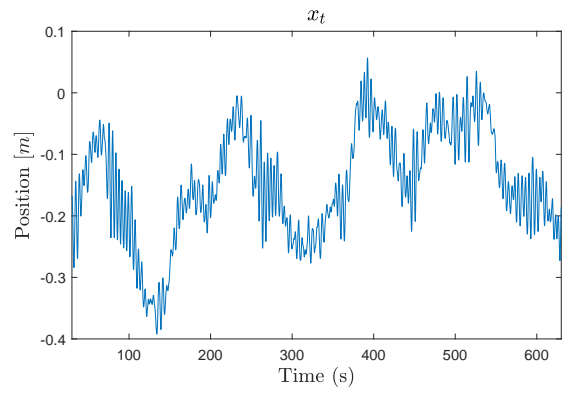
B.1 Bladed Reference Test

For comparison purposes, a test of Mita-Teknik's own controller will be tested. Two tests will be carried out for two mean wind speeds of 6 m/s and 16 m/s with normal turbulence as defined by the third edition of the IEC 61400-1 standard. These mean wind speeds are chosen as they represent below-rated and above-rated wind speeds and will show the two controllers pursuing an optimal pitch for both scenarios.

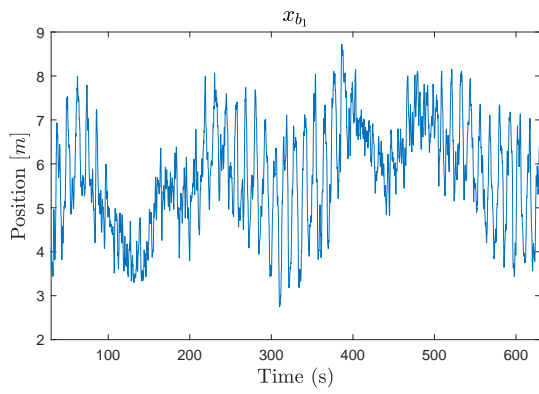
B.1.1 6 m/s mean wind speed test



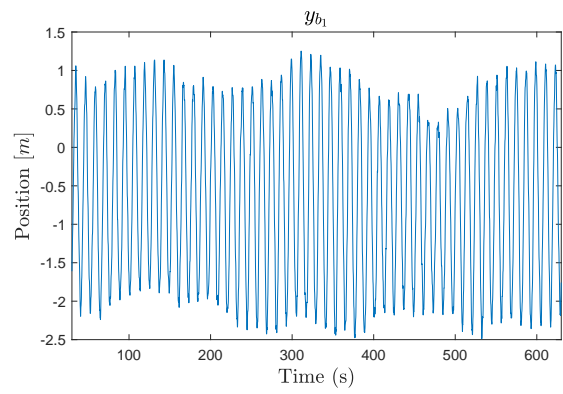
(a)



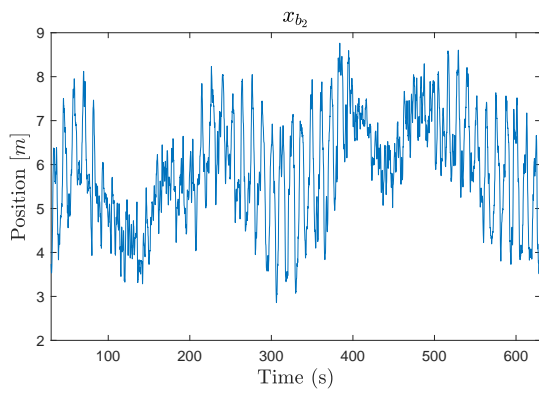
(b)



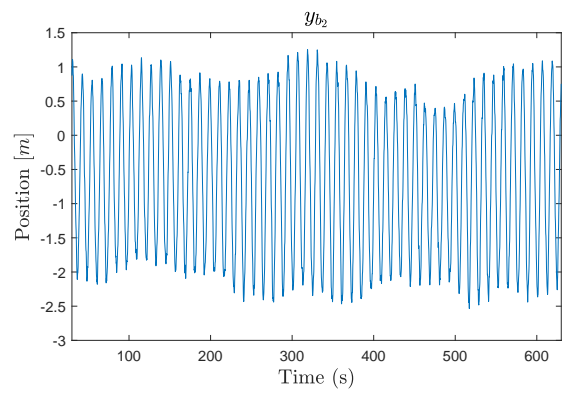
(c)



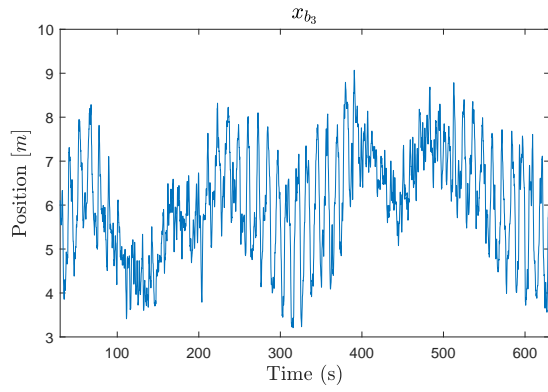
(d)



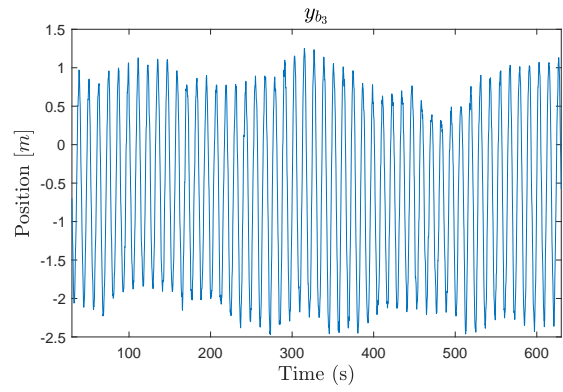
(e)



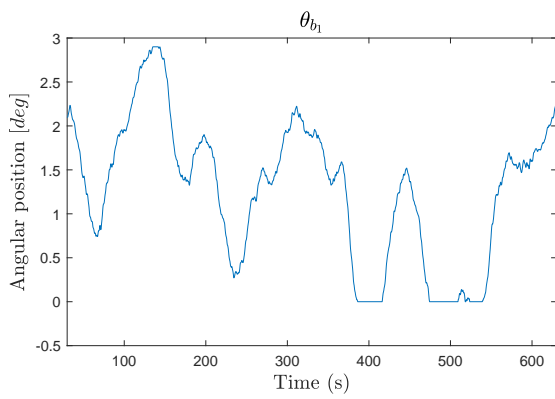
(f)



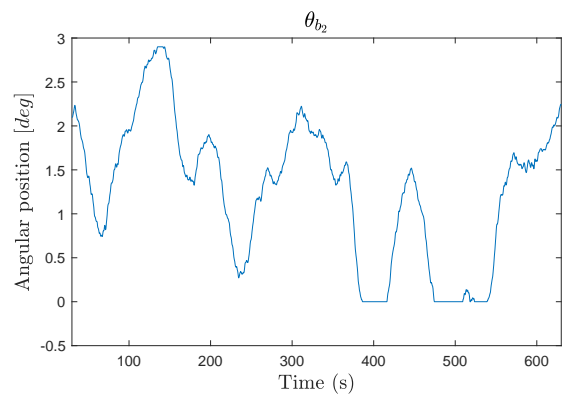
(g)



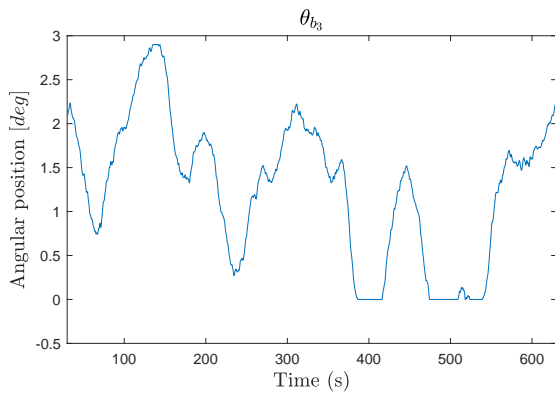
(h)



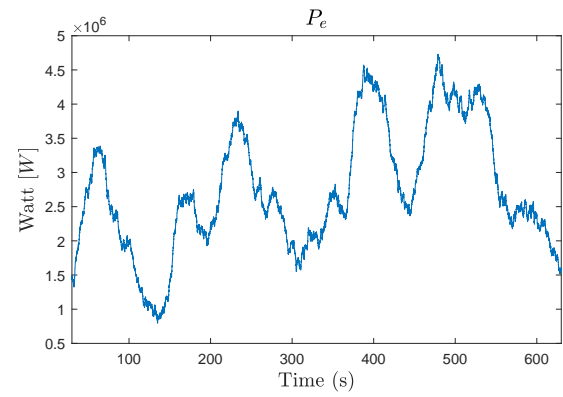
(i)



(j)



(k)



(l)

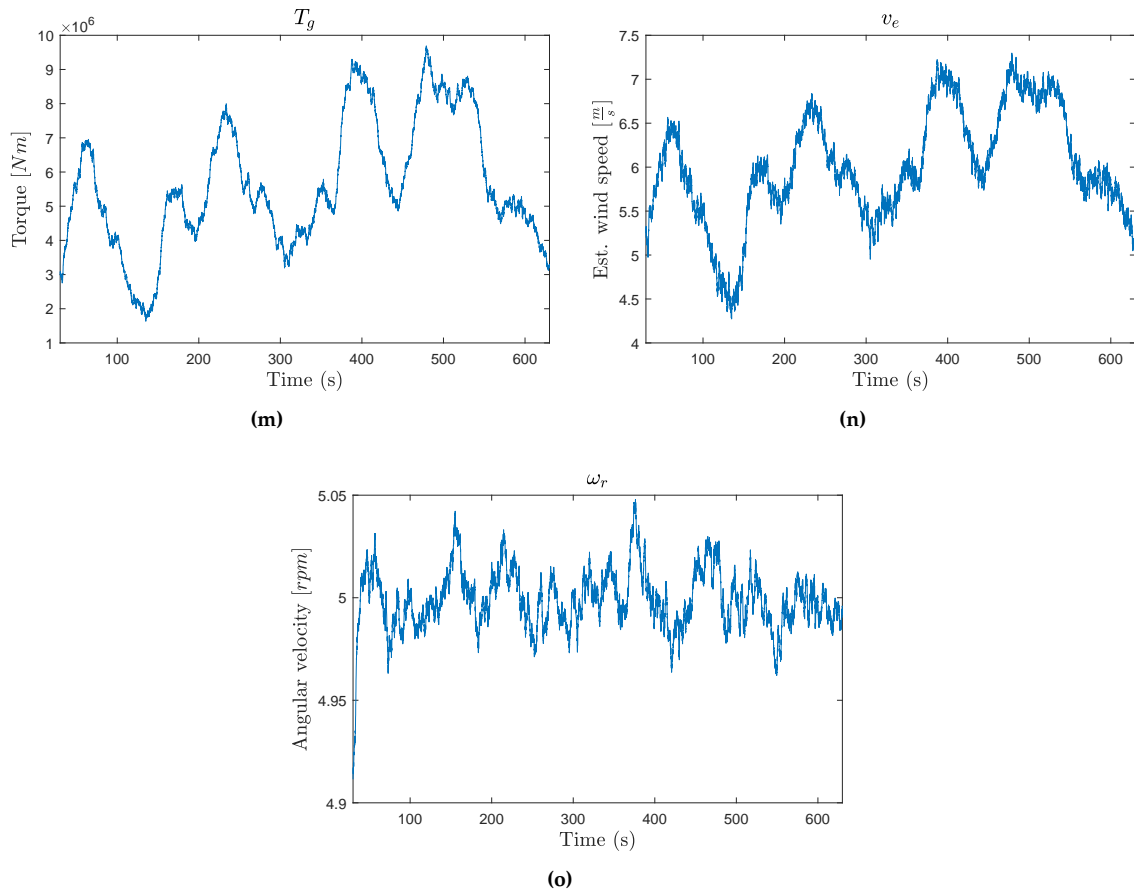
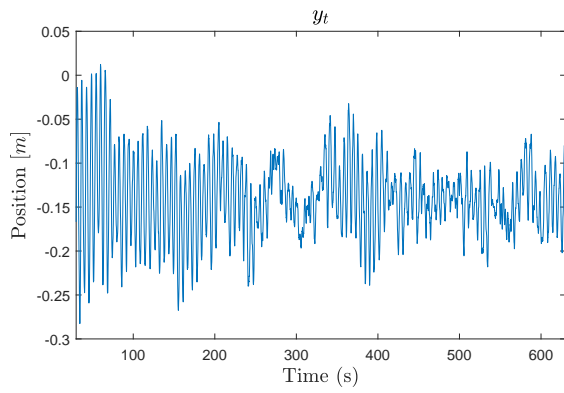
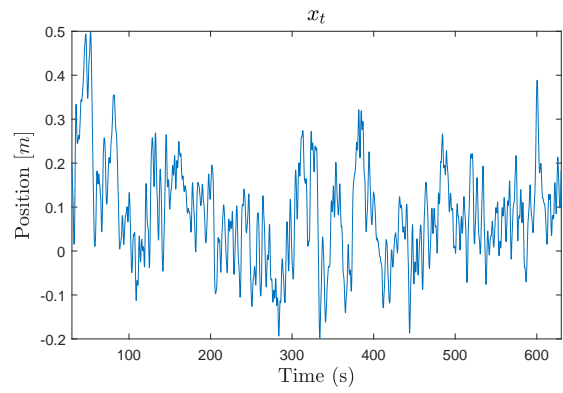


Figure B.1: Bladed simulation plots for a wind speed of 6 m/s

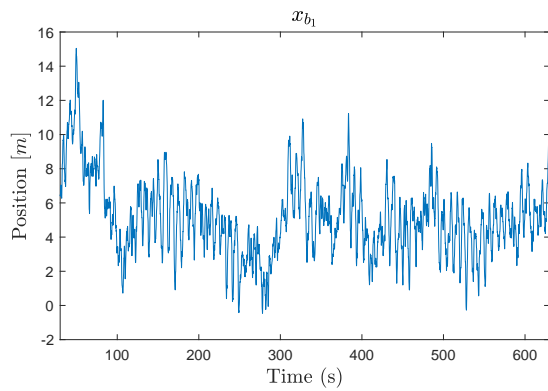
B.1.2 16 m/s mean wind speed test



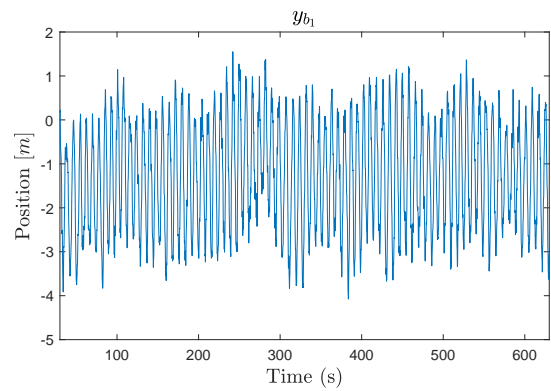
(a)



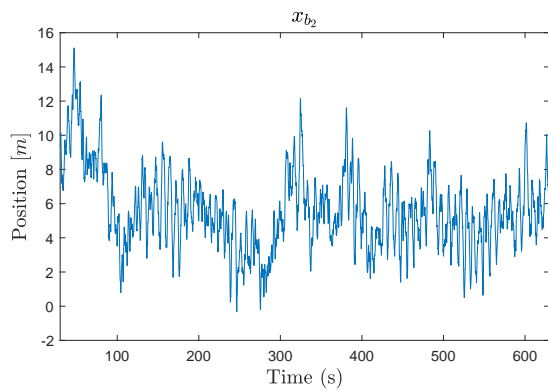
(b)



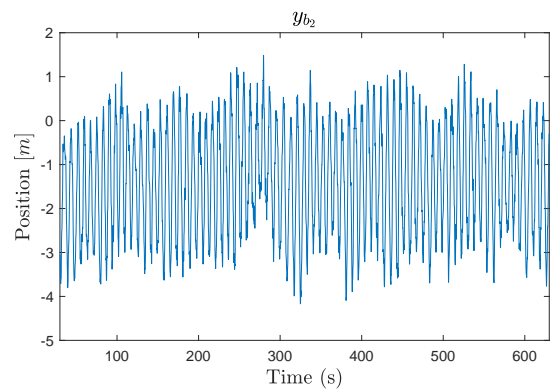
(c)



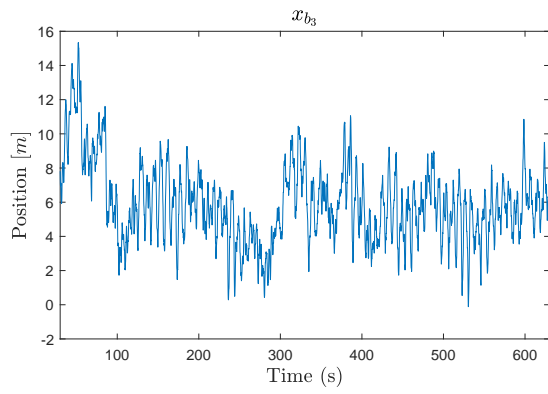
(d)



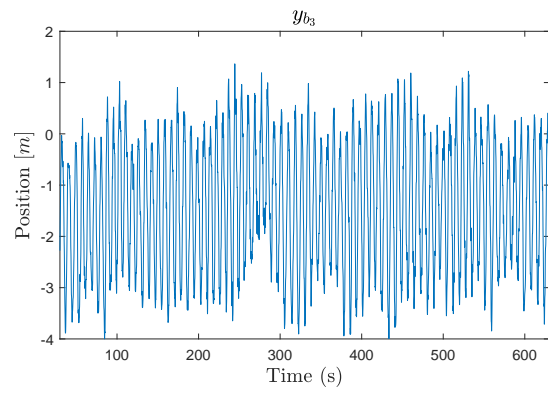
(e)



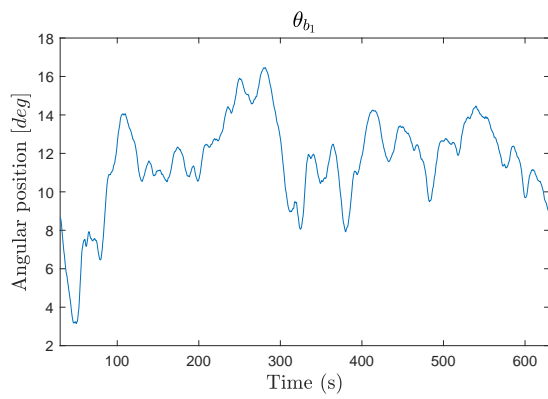
(f)



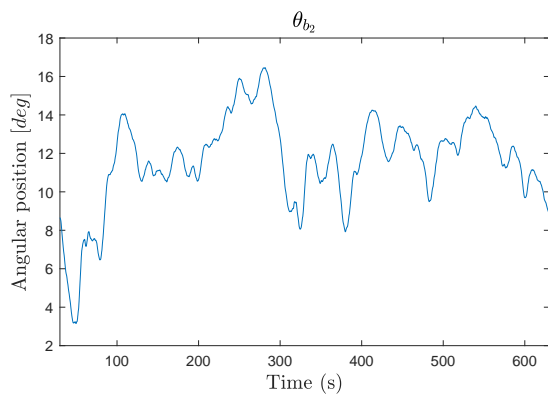
(g)



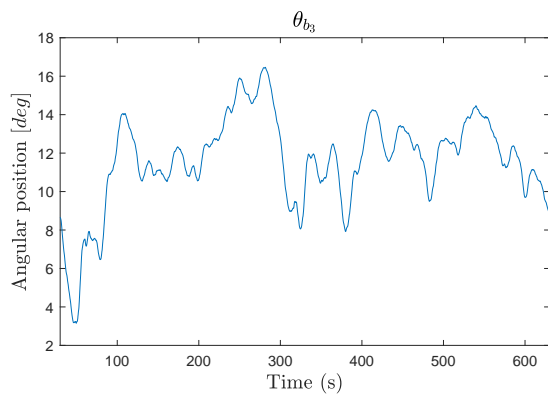
(h)



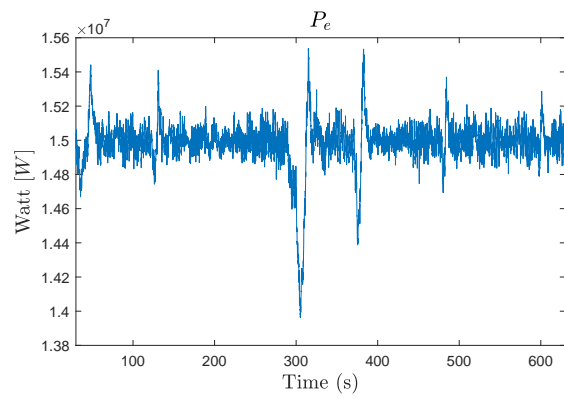
(i)



(j)



(k)



(l)

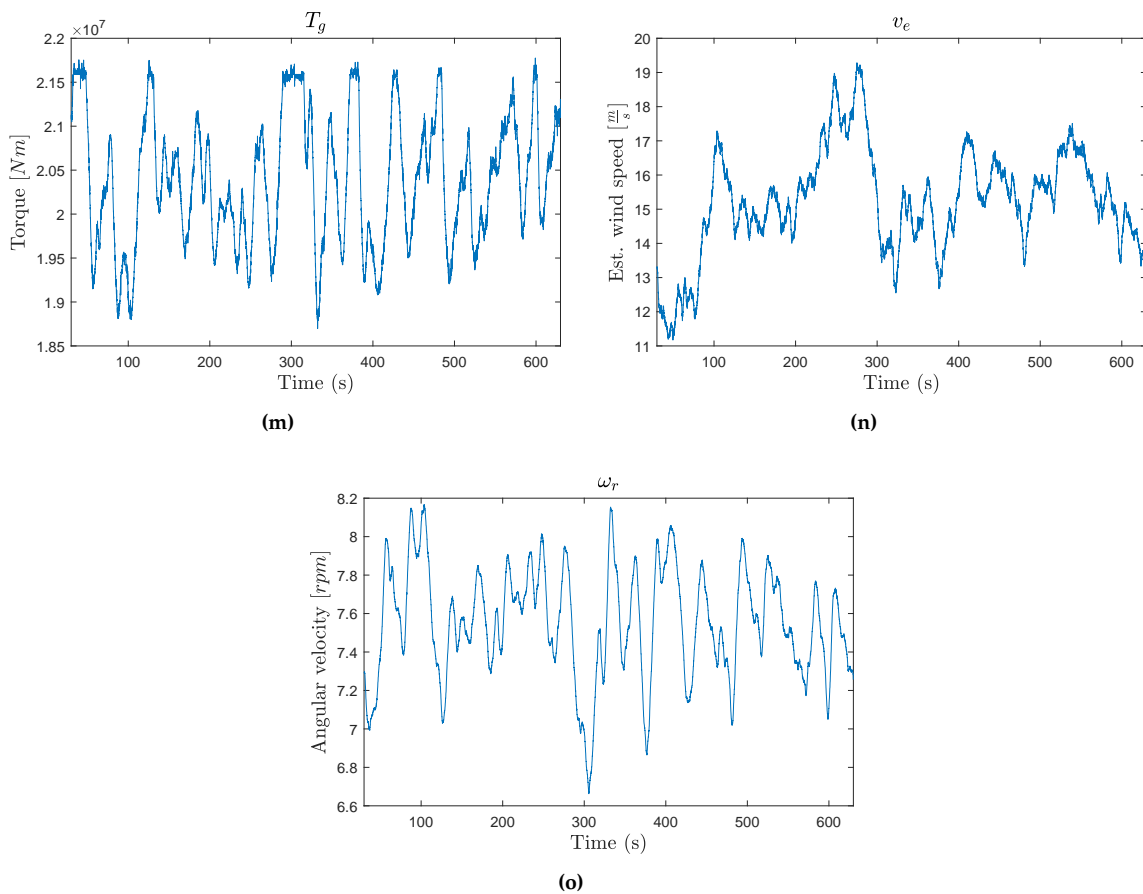
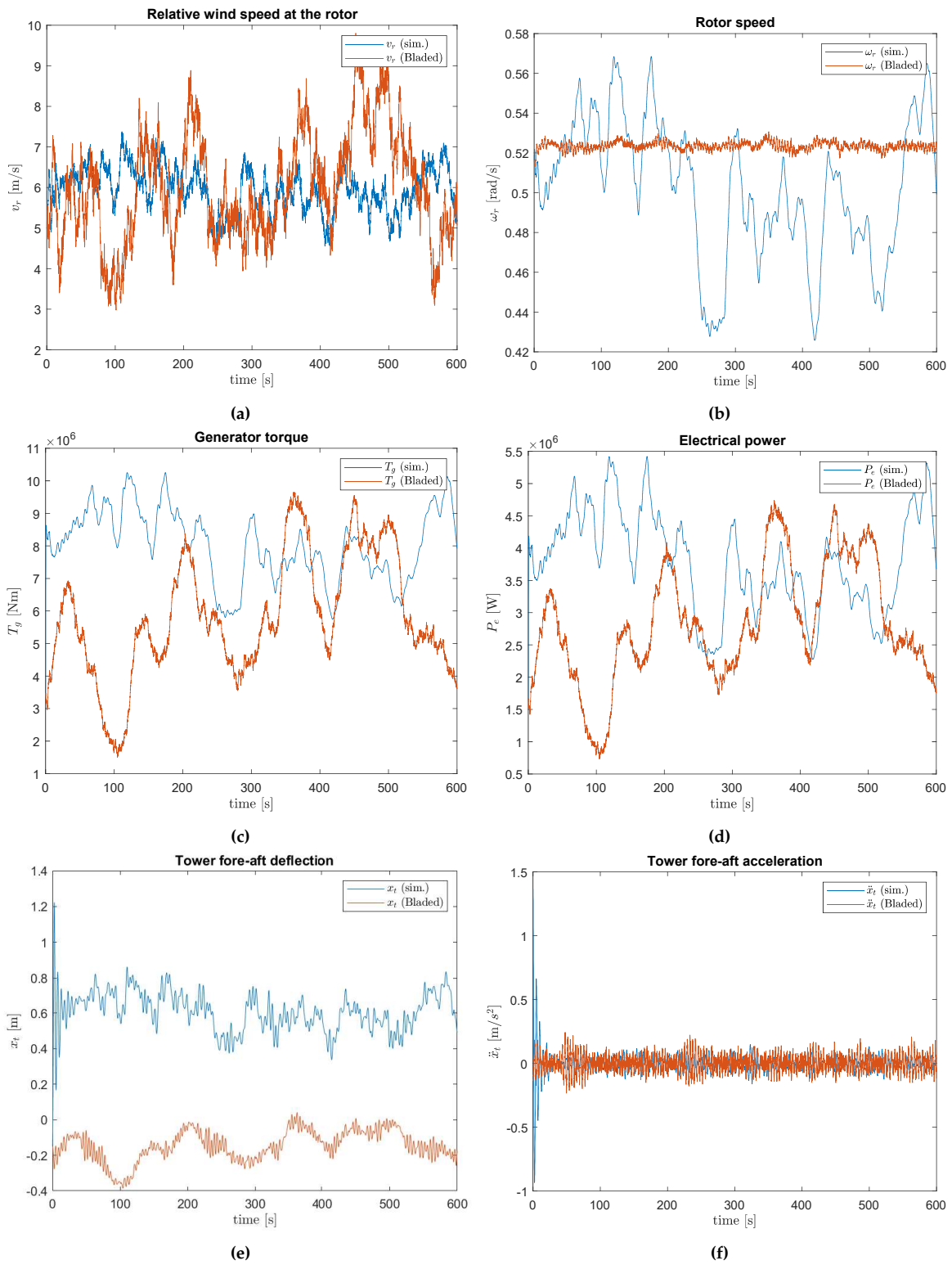


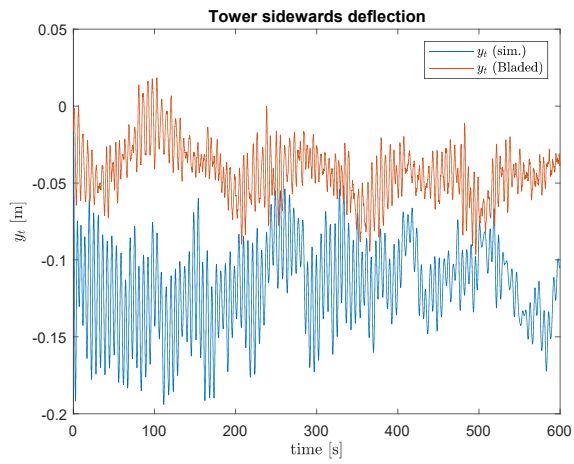
Figure B.2: Bladed simulation plots for a wind speed of 16 m/s.

B.2 Test of Turbine Model

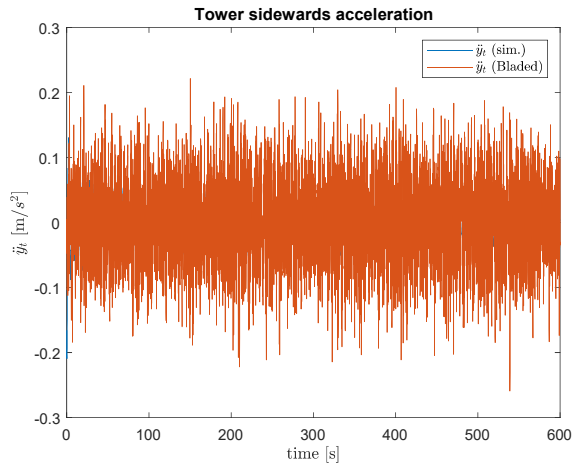
The test of the turbine model must demonstrate the stability of the model using a simple torque-based controller to create a closed-loop system. Furthermore, the values of the state variables obtained from the simulation should be compared with the Bladed data to check its accuracy. The reference pitch angle of the blades is set to 0° to simulate below-rated power generating scenario, using a mean wind speed of 6 m/s. The generator torque reference is subsequently computed as the constant K derived in Section 3.4 times the rotor speed squared.

Even though the discretization of the model differential equations was initially done using Euler's method, it was found out that it was not accurate enough for this model, as the poles of some subsystems, in particular the blade flapwise and edgewise dynamics, were very close to the imaginary axis. Hence, it was decided to use 4th order Runge-Kutta, which lead to the results seen in Fig. B.3.

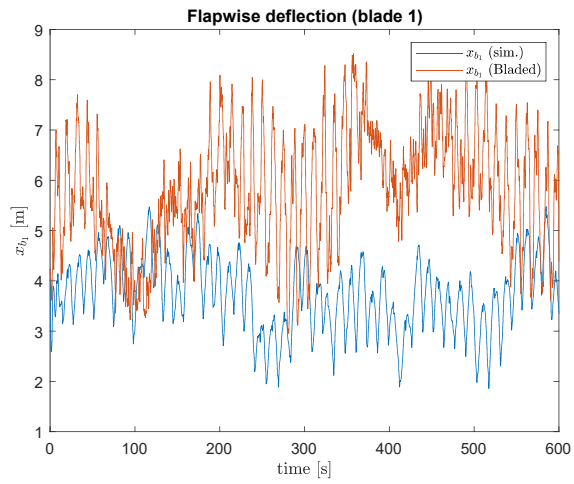




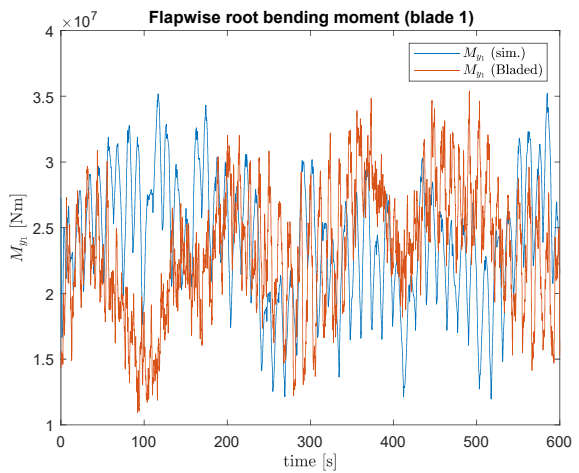
(g)



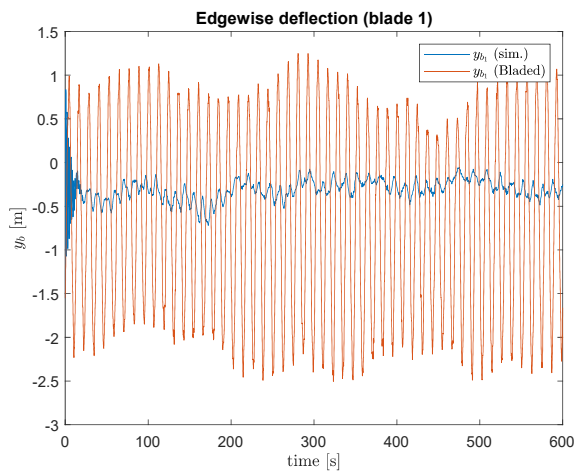
(h)



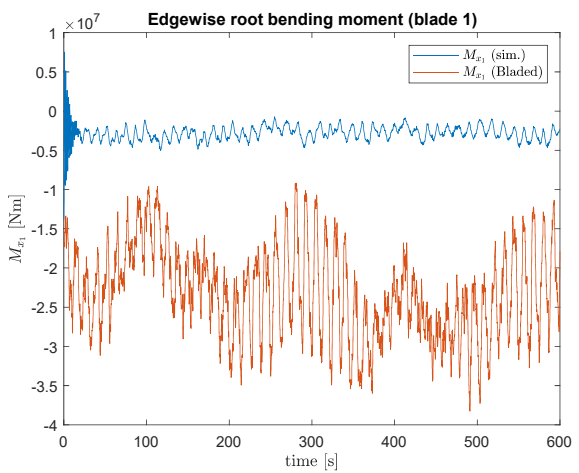
(i)



(j)



(k)



(l)

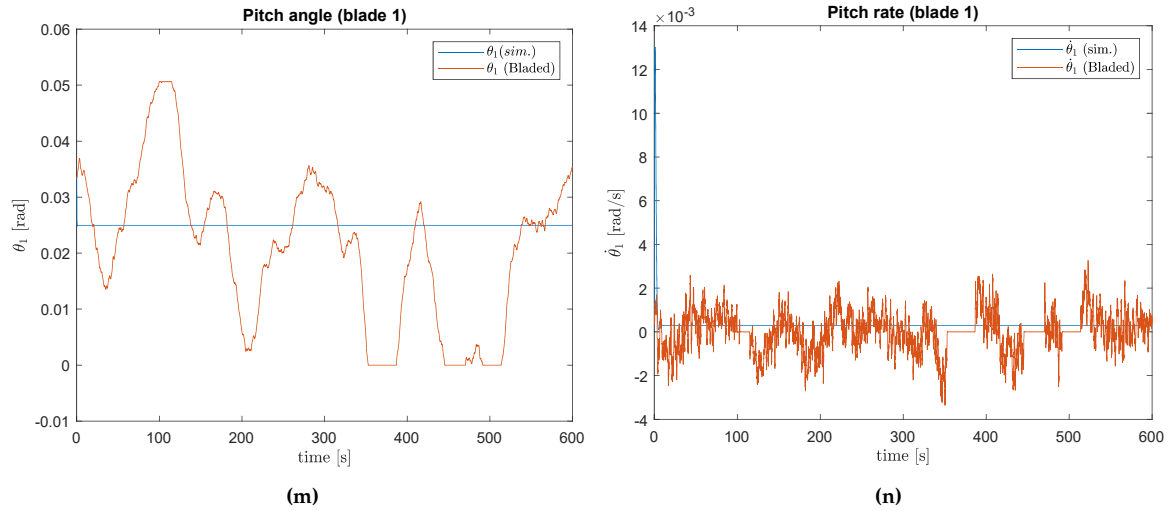


Figure B.3: Non-linear model simulation plots.

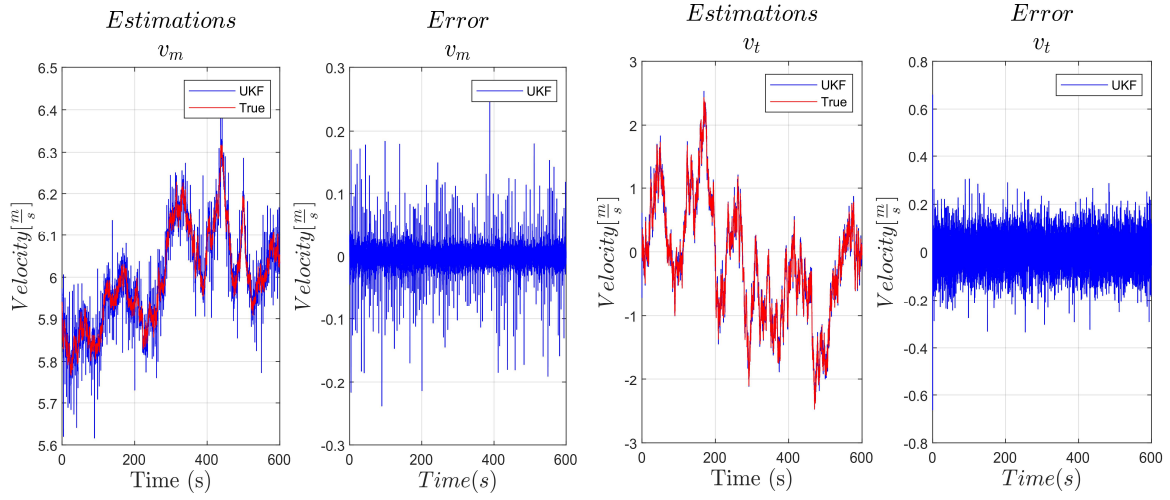
First, it can be seen that the wind speed varies slightly different in our model with respect to Bladed model, as it is a stochastic variable defined differently, perhaps with a larger turbulence intensity. Apart from this, the Bladed model uses a much more complex control algorithm than the simple torque control used to simulate our model, which provides a much more stable rotor speed regulated using the blade pitch angles.

A particularly noticeable deviation can be observed in the tower fore-aft deflection graph (e). This is due to the fact that our model does not consider the hub overhang torque, which affects the top of the tower by deflecting it around 0.8 m from its expected position.

The Bladed data also shows considerably higher oscillations in the blade edgewise deflection (k) in comparison with our simulation. The reason for this has not yet been found out, but it is believed to be due to the effect of gravity on the blades depending on their azimuth position. This mismatch leads to high deviations in the blade edgewise root bending moments.

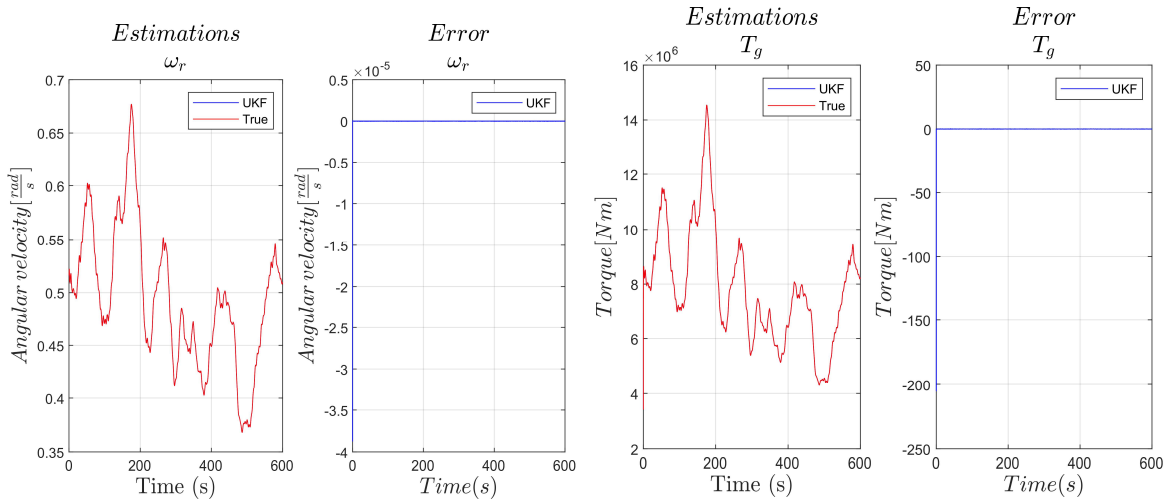
B.3 Test of UKF

The test of the Kalman Filter must demonstrate the filter's ability to precisely estimate the states of the turbine model. Using the data obtained from Bladed as system measurements makes the filter unable to converge, due to the large mismatch between the outputs of the system derived in this project and the outputs from Bladed simulation model. For this reason, it was necessary to use some of the simulated true states of our model (adding the corresponding sensor noise) as measurements. This gave the results shown in Fig. B.4. It can be seen that the states are accurately estimated by the filter, as expected.



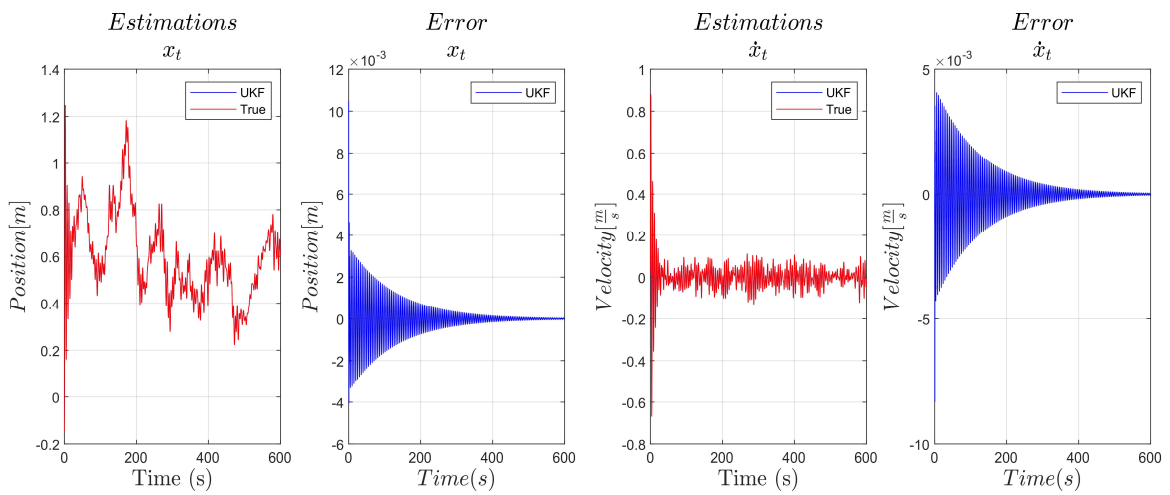
(a)

(b)



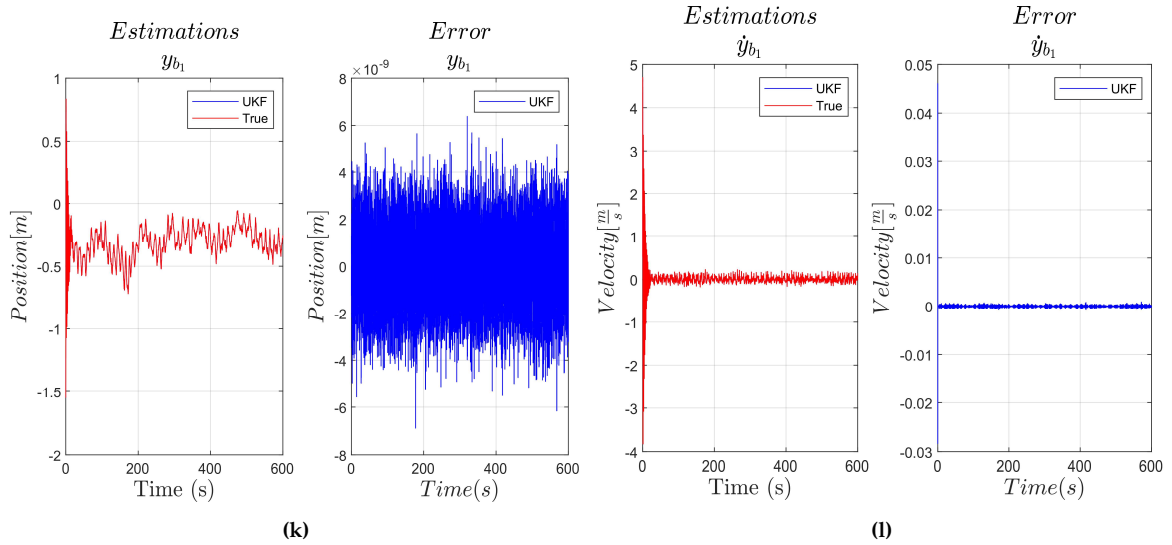
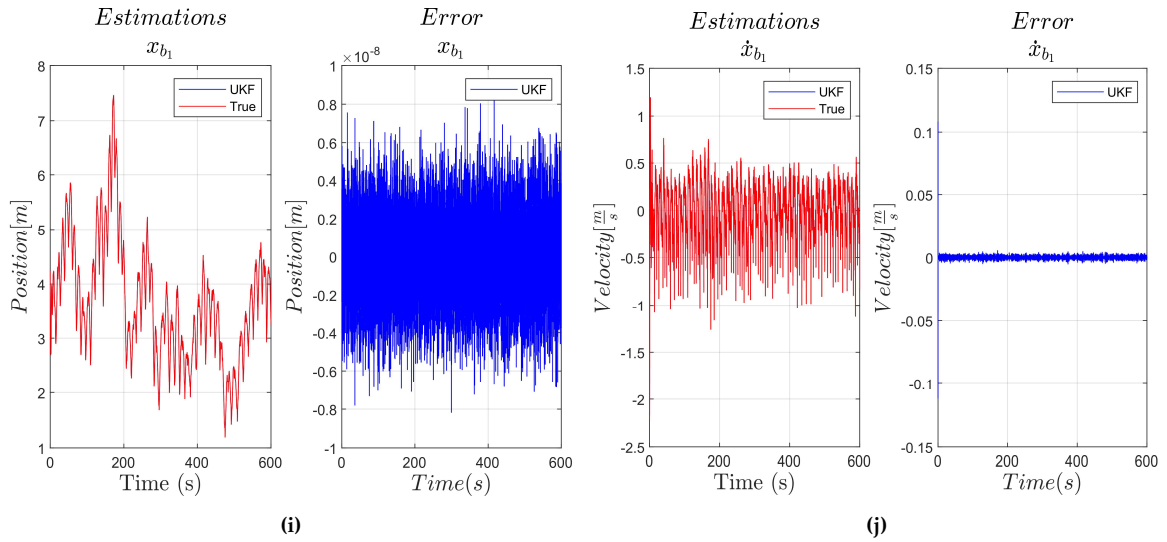
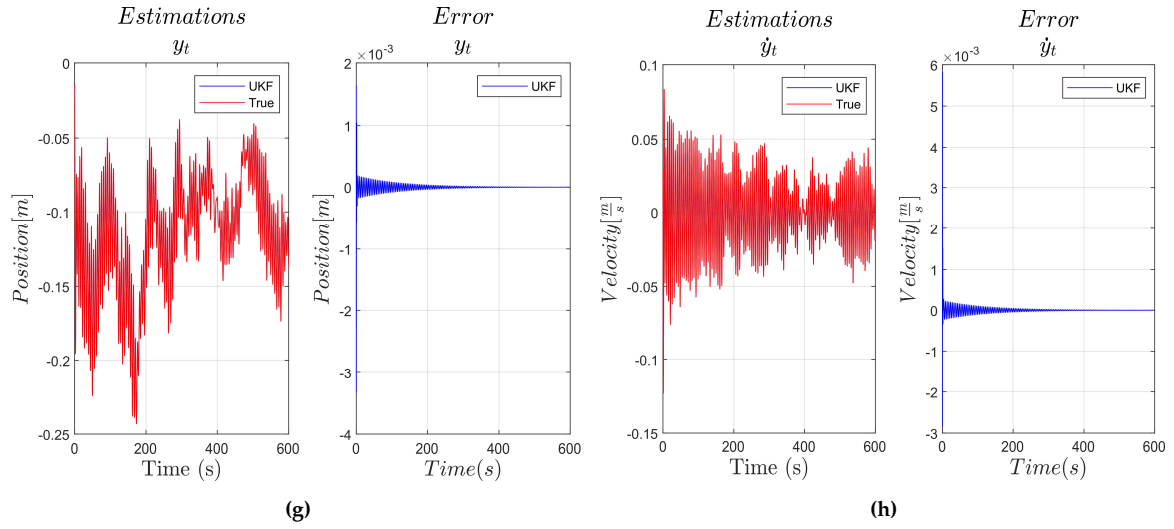
(c)

(d)



(e)

(f)



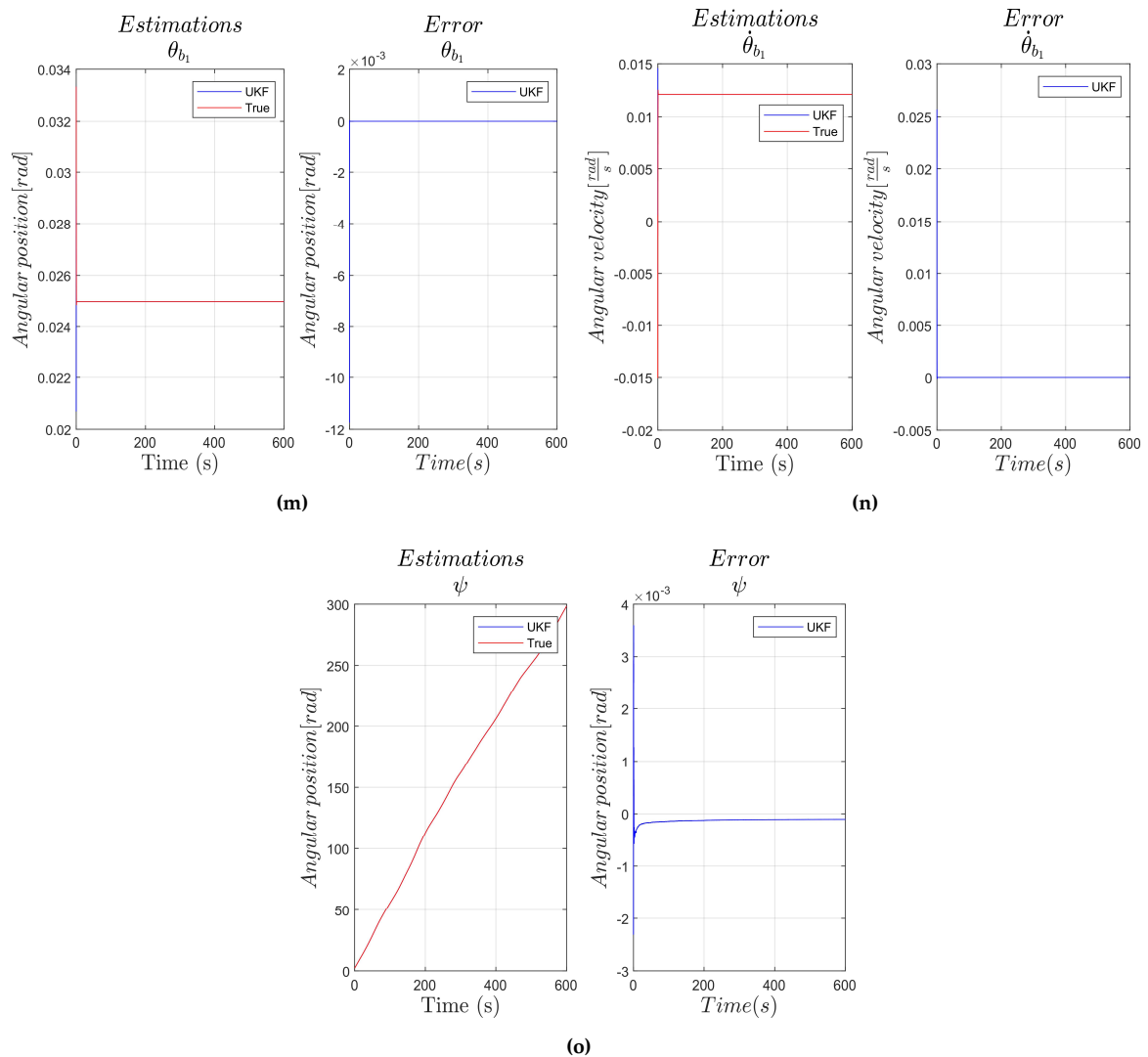
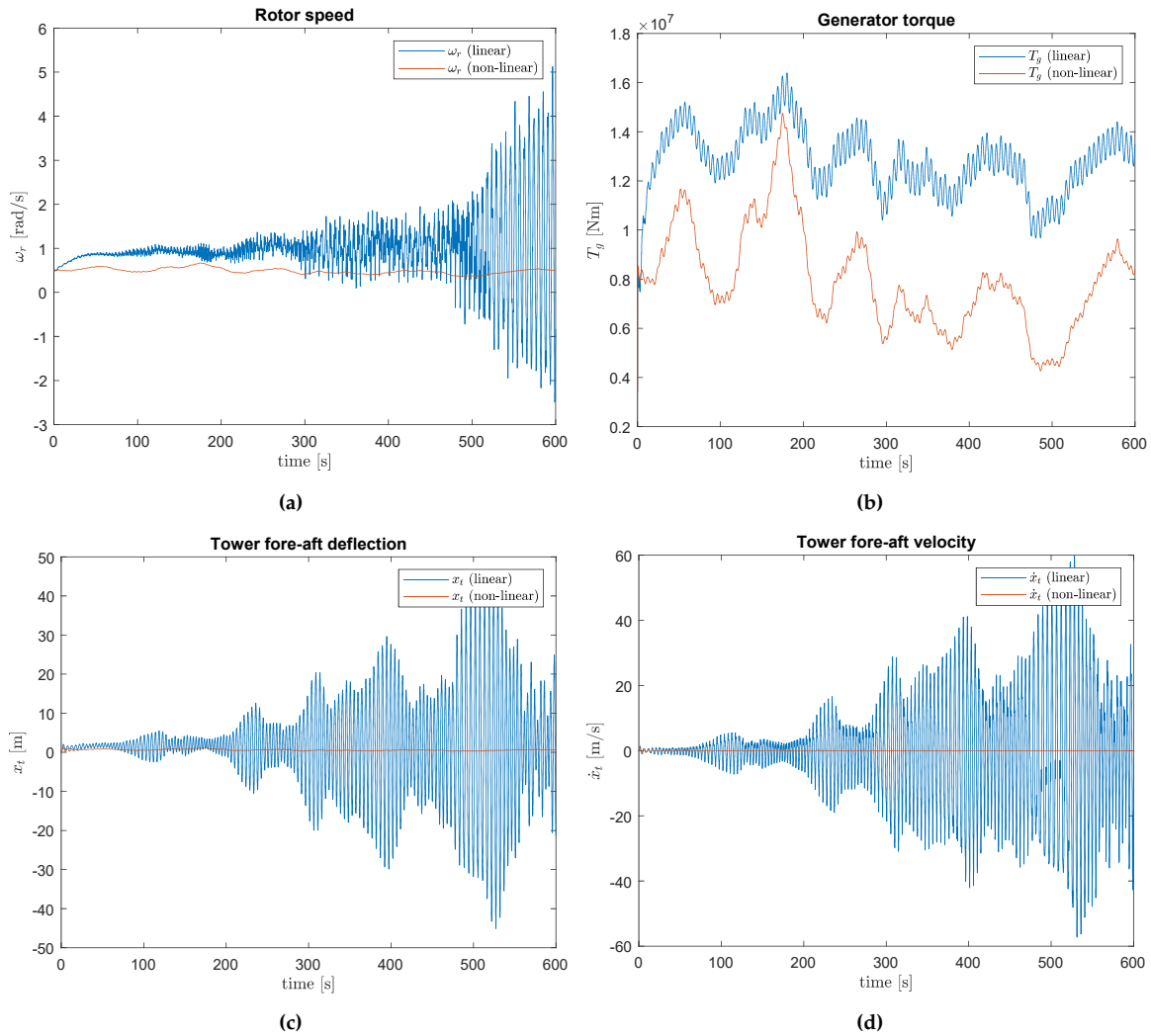


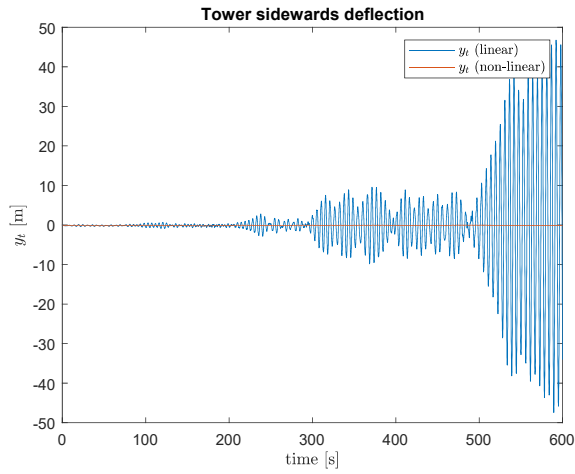
Figure B.4: UKF state estimation plots.

B.4 Test of Linear Model

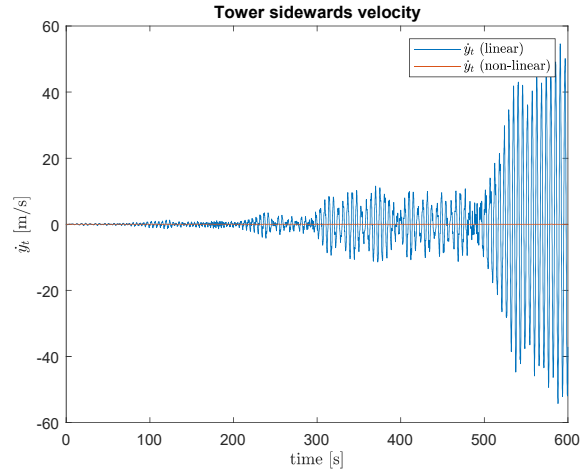
The linearised model was tested using the basic torque controller also implemented in the testing of the non-linear model. The operating points of the system are taken from the non-linear model simulation and thus changed in every iteration. Besides, 4th order Runge Kutta has also been used as discretization method instead of Euler's method, as the instability issues observed in the simulation of the non-linear model are still present or even augmented by the linearization. The graphs obtained can be seen in Fig. B.5. Note that some of the plotted states are not the same as the ones plotted in the linear model due to their usefulness; for example, the tower acceleration plots have been substituted

by the tower velocities, as they represent more clearly the structural loads (the tower fore-aft and sideways velocity were chosen in the MPC as variables to be controlled for that reason). Furthermore, it would not have been very useful to show the tower velocities in the non-linear model test as there is no Bladed measurement to compare to. The same can be said for the blade root moments, which have now been substituted by the blade velocities in each direction. The wind speed has not been plotted, as it is just a constant after the linearization.

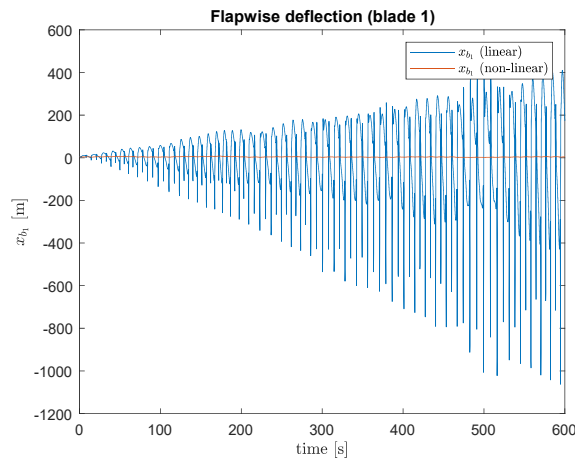




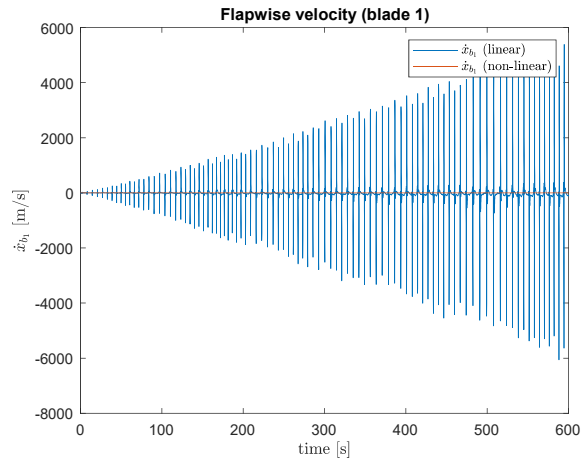
(e)



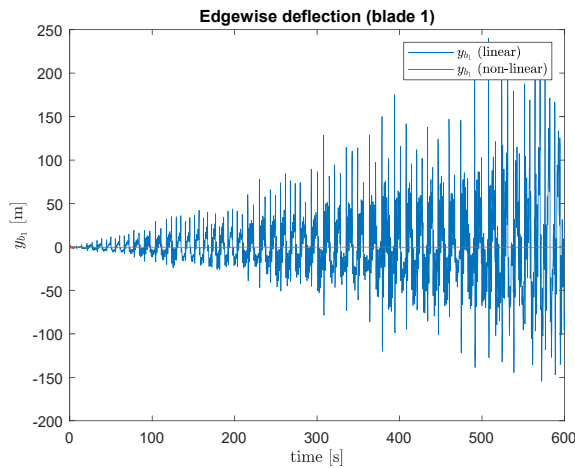
(f)



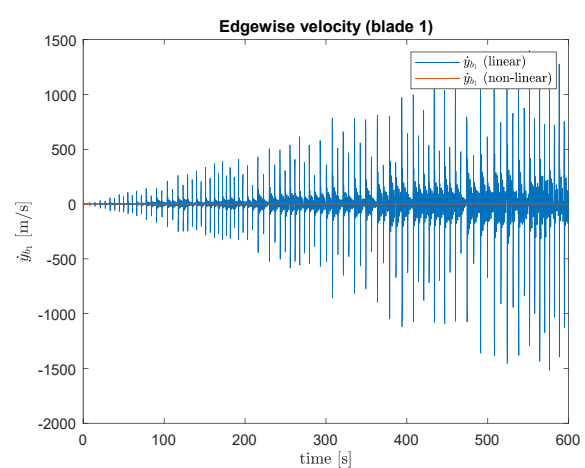
(g)



(h)



(i)



(j)

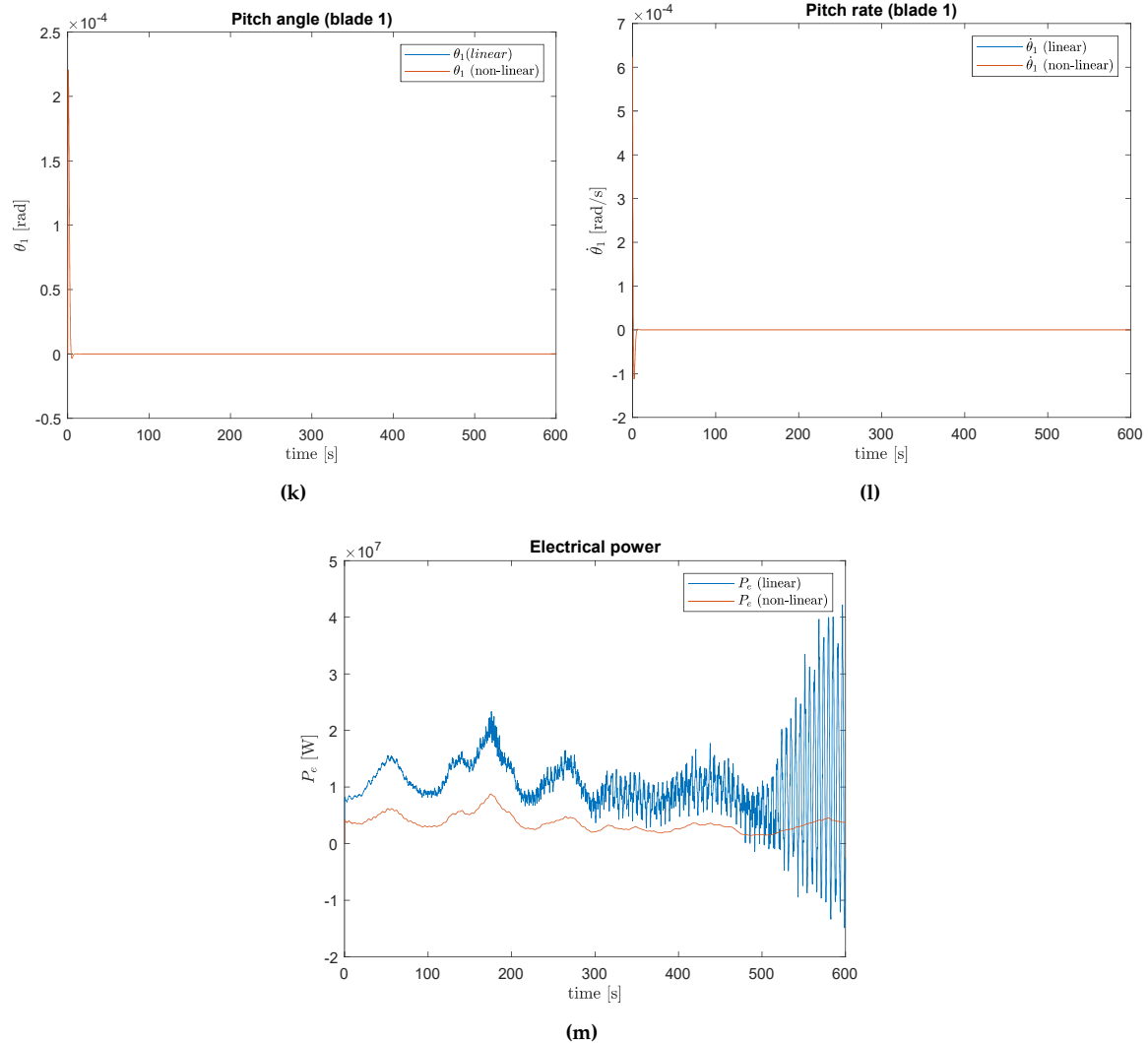
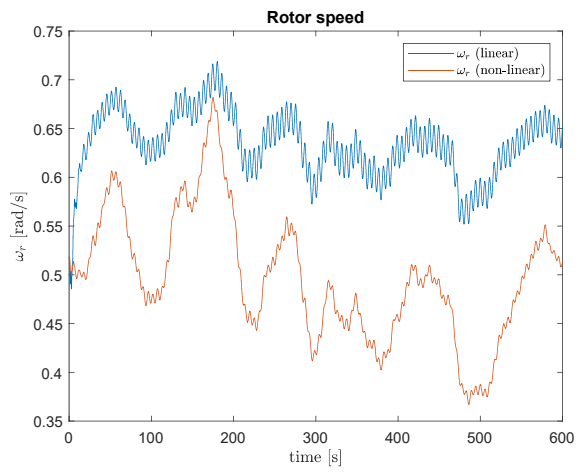
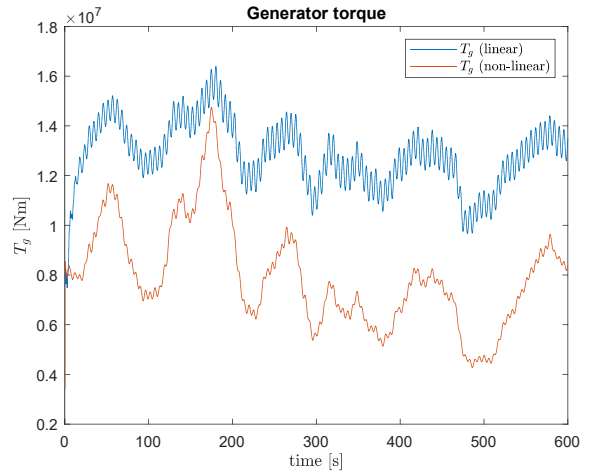


Figure B.5: Linear model simulation plots.

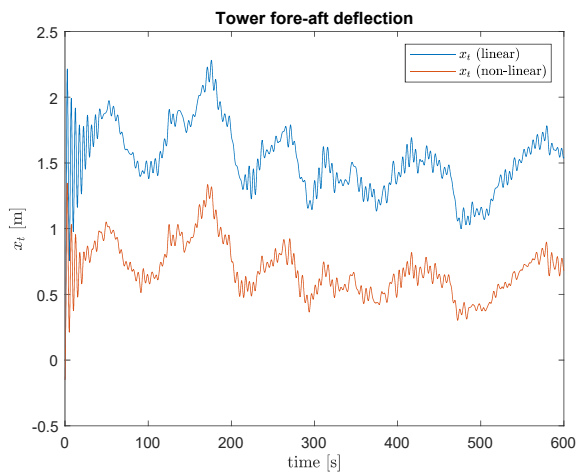
It can be seen that the oscillations in the tower and blade dynamics increase with time, provoking an effect on the rotor speed, generator torque and electrical power. These results do not provide a satisfactory representation of the wind turbine's dynamics. In order to discard the possibility of an error in the linearisation, the wind shear and tower shadow terms were removed from the non-linear system so that it becomes much easier to carry out the procedure. The results obtained are shown in Fig. B.6, which still show slight instability, suggest that a better controller is needed to obtain a more acceptable response.



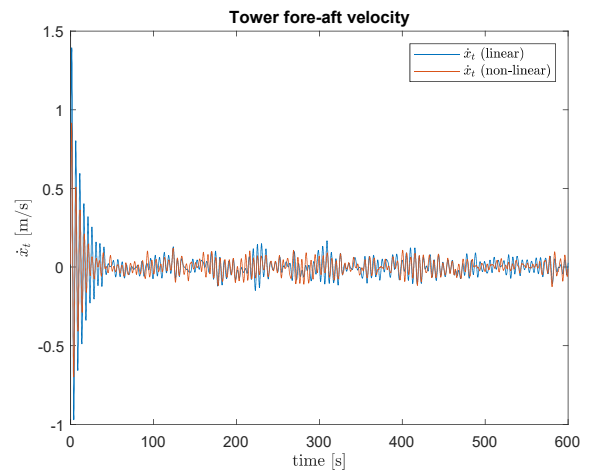
(a)



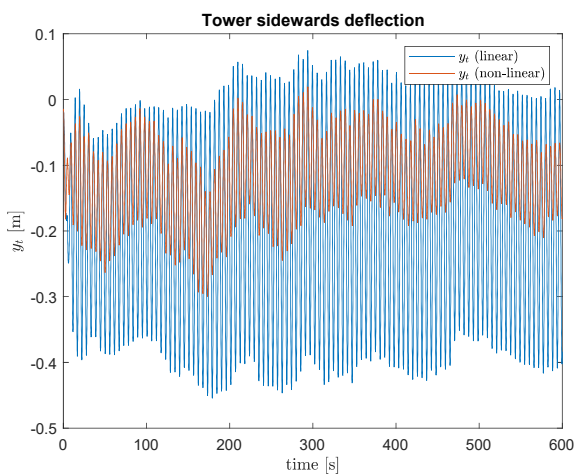
(b)



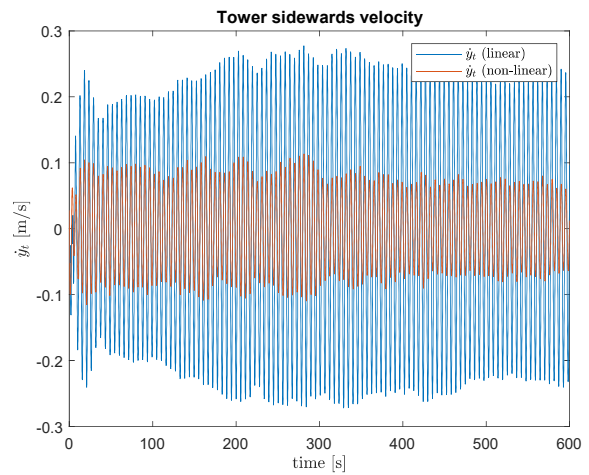
(c)



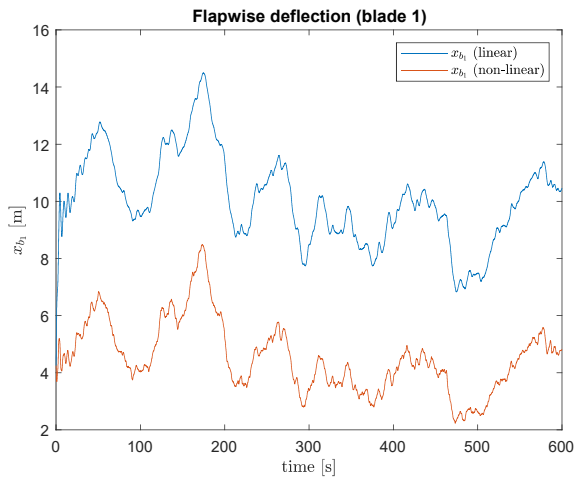
(d)



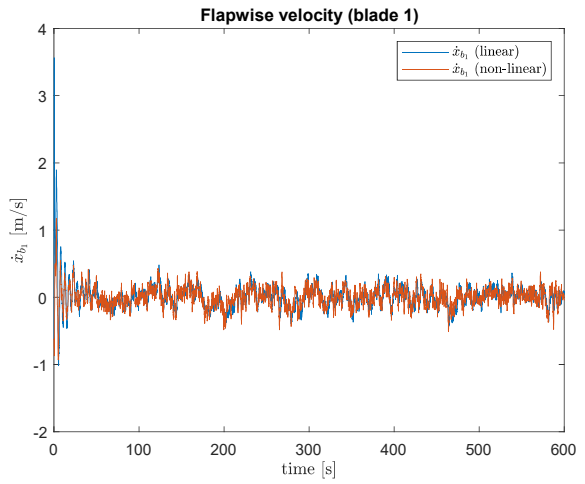
(e)



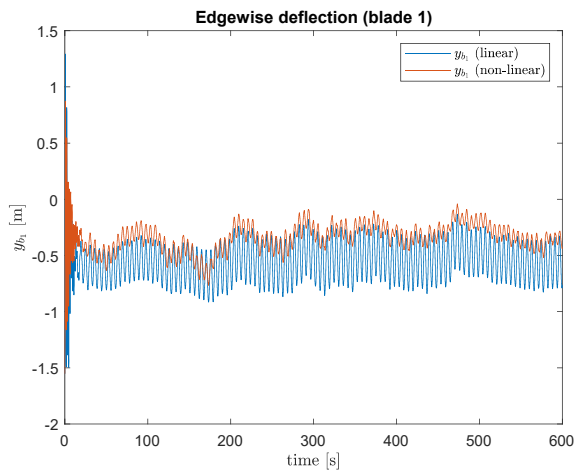
(f)



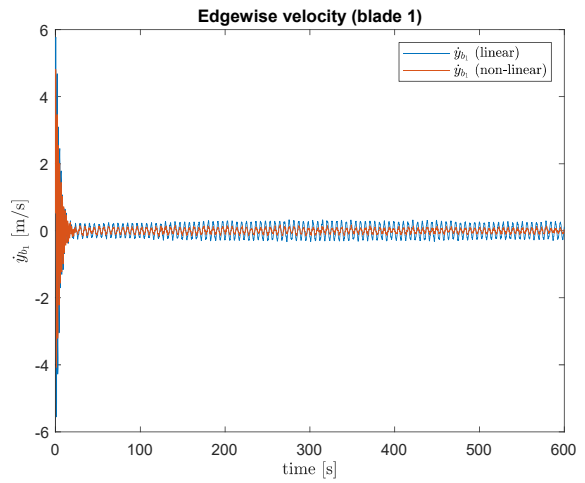
(g)



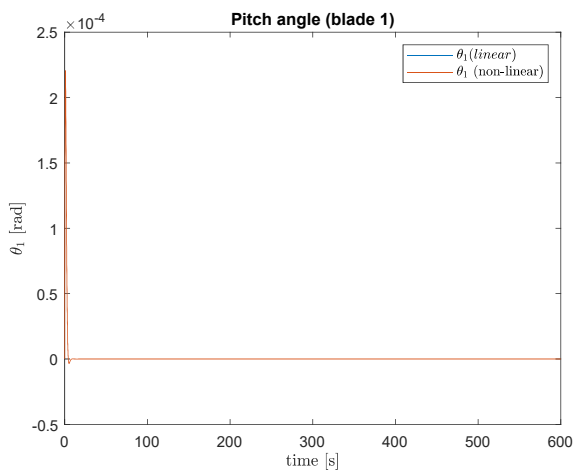
(h)



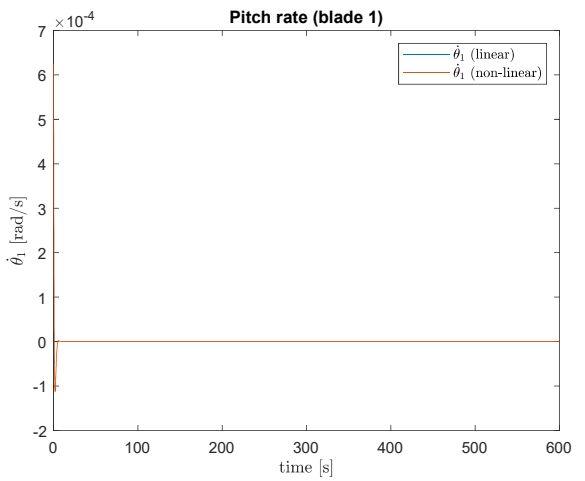
(i)



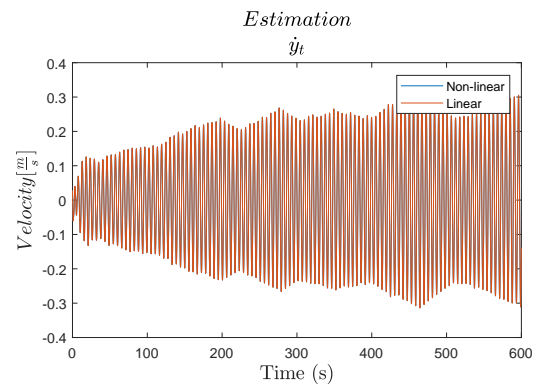
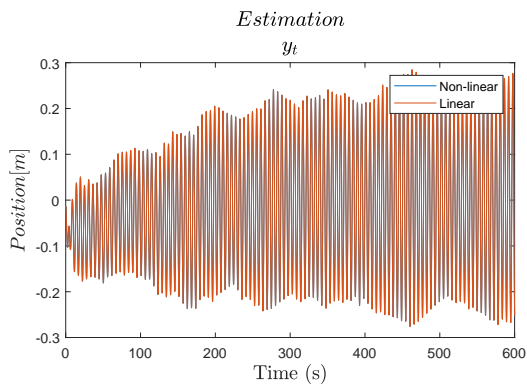
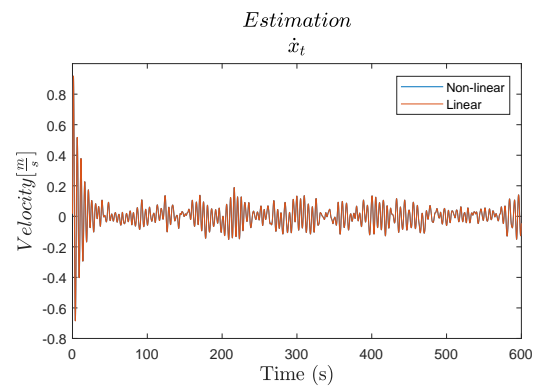
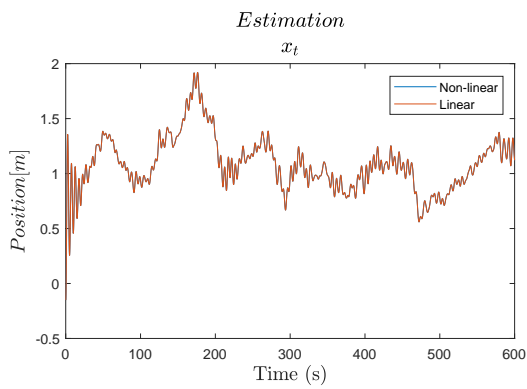
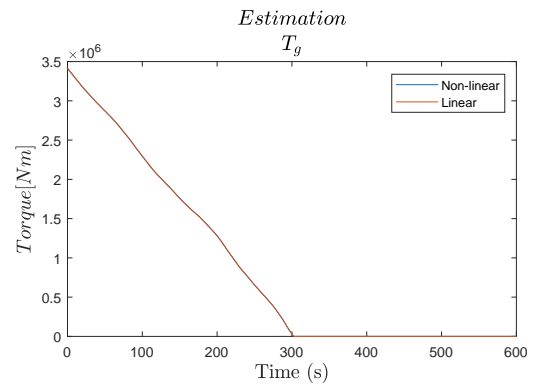
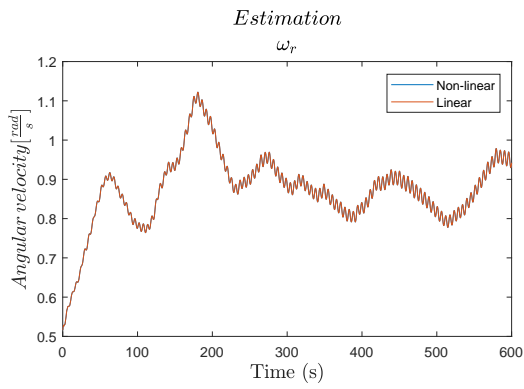
(j)

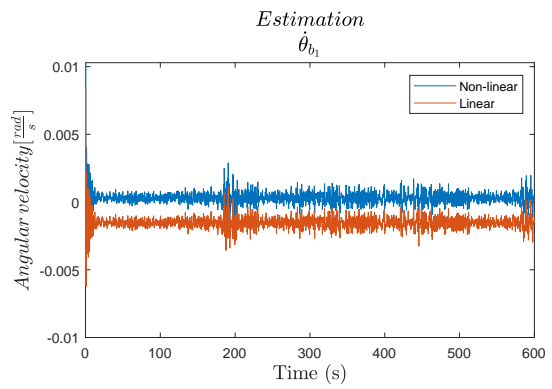
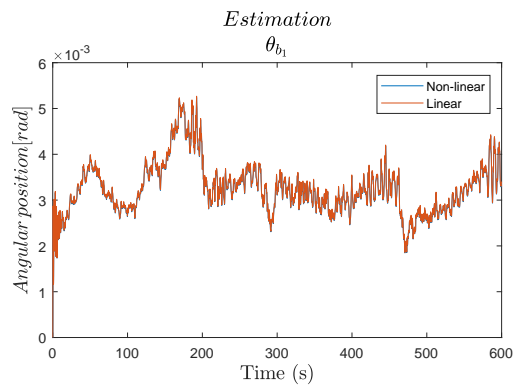
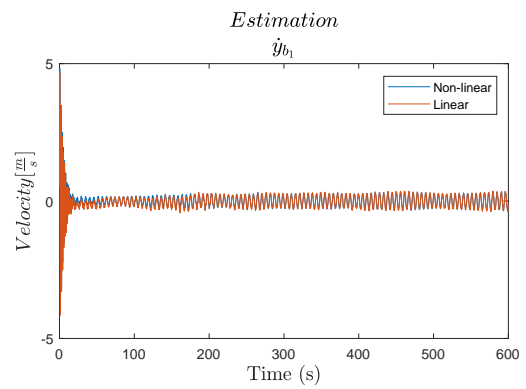
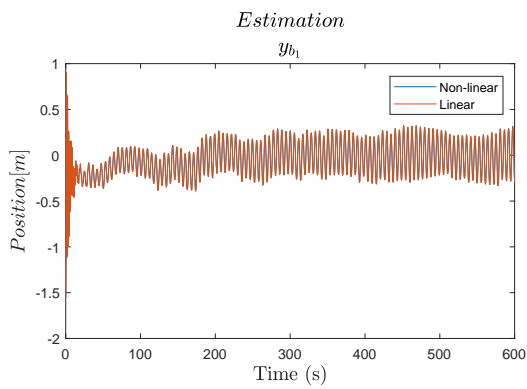
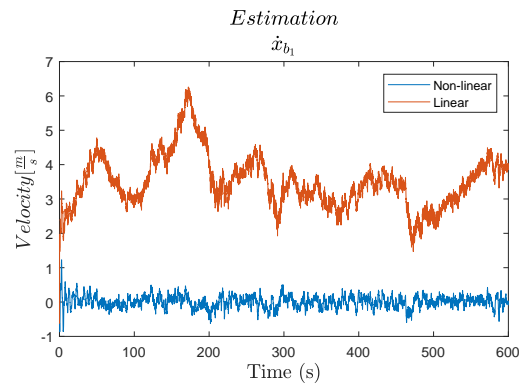
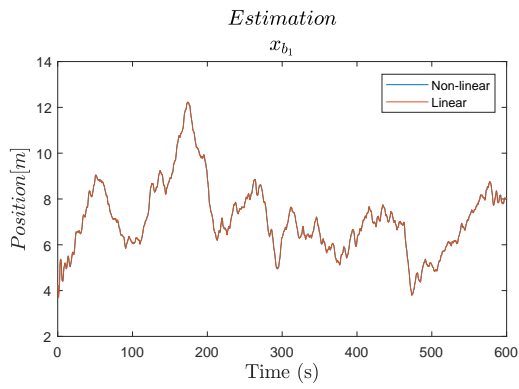


(k)



(l)





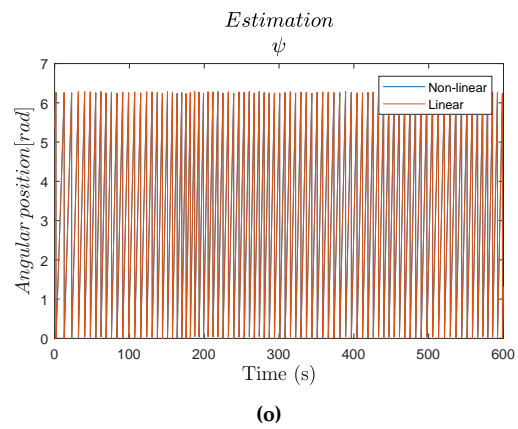


Figure B.7: Linear and non-linear model simulation using MPC.

Appendix C

GITHUB REPOSITORY

The MATLAB code can be found in the following GitHub repository:

